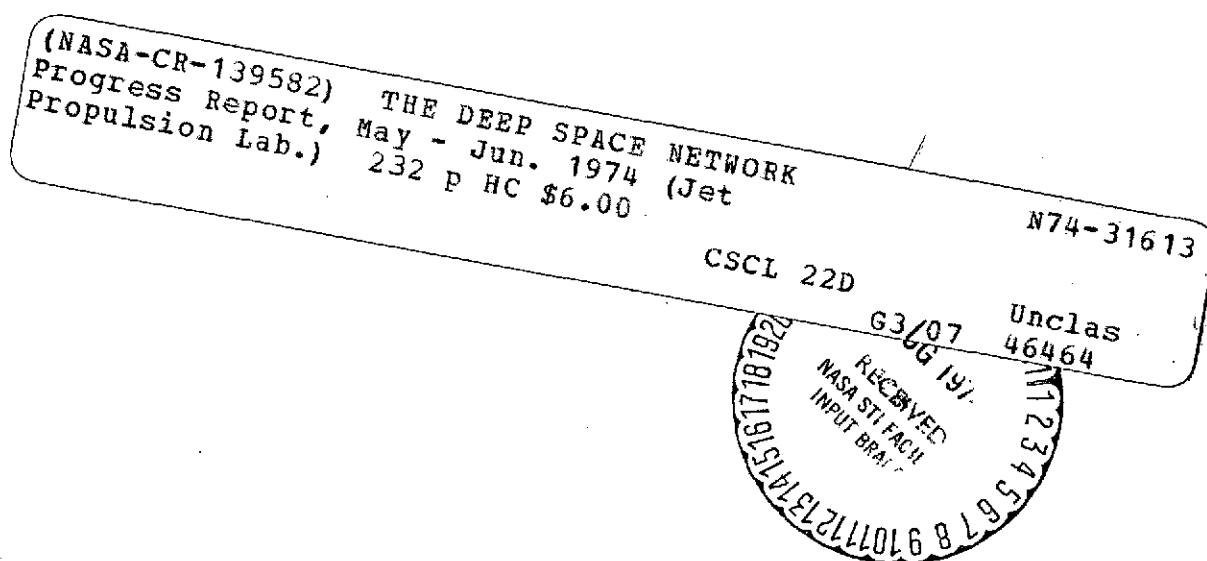


NATIONAL AERONAUTICS AND SPACE ADMINISTRATION

*The Deep Space Network
Progress Report 42-22*

May and June 1974



JET PROPULSION LABORATORY
CALIFORNIA INSTITUTE OF TECHNOLOGY
PASADENA, CALIFORNIA

August 15, 1974

Prepared Under Contract No. NAS 7-100
National Aeronautics and Space Administration

Preface

Beginning with Volume XX, the Deep Space Network Progress Report changed from the Technical Report 32- series to the Progress Report 42- series. The volume number continues the sequence of the preceding issues. Thus, Progress Report 42-20 is the twentieth volume of the Deep Space Network series, and is an uninterrupted follow-on to Technical Report 32-1526, Volume XIX.

This report presents DSN progress in flight project support, tracking and data acquisition (TDA) research and technology, network engineering, hardware and software implementation, and operations. Each issue presents material in some, but not all, of the following categories in the order indicated:

Description of the DSN

Mission Support

- Ongoing Planetary/Interplanetary Flight Projects
- Advanced Flight Projects

Radio Science

- Radio Science Support
- Special Projects

Supporting Research and Technology

- Tracking and Ground-Based Navigation
- Communications—Spacecraft/Ground
- Station Control and Operations Technology
- Network Control and Data Processing

Network Engineering and Implementation

- Network Control System
- Ground Communications
- Deep Space Stations

Operations

- Network Operations
- Network Control System Operations
- Ground Communications
- Deep Space Stations

Planning and Facilities

- TDA Planning
- Facility Engineering

In each issue, the part entitled "Description of the DSN" describes the functions and facilities of the DSN and may report the current configuration of one of the five DSN systems (Tracking, Telemetry, Command, Monitor and Control, and Test and Training).

The work described in this report series is either performed or managed by the Tracking and Data Acquisition organization of JPL for NASA.

Page intentionally left blank

Contents

DESCRIPTION OF THE DSN

DSN Functions and Facilities	1
N. A. Renzetti	

MISSION SUPPORT

Ongoing Planetary/Interplanetary Flight Projects

Viking Mission Support	5
D. J. Mudgway NASA Code 311-03-21-70	
Pioneer 10 and 11 Mission Support	11
R. B. Miller NASA Code 311-03-21-20	
Helios Mission Support	16
P. S. Goodwin NASA Code 311-03-21-50	

SUPPORTING RESEARCH AND TECHNOLOGY

Tracking and Ground-Based Navigation

The Measurement of Dispersive Effects Using the Mariner 10 S- and X-Band Spacecraft to Station Link	22
G. A. Madrid NASA Code 310-10-60-52	
DSN-MVM'73 S/X Dual-Frequency Doppler Demonstration	28
F. B. Winn, K. W. Yip, and S. J. Reinbold NASA Code 310-10-60-62	
Dual-Spacecraft Radio Metric Tracking	51
R. A. Preston NASA Code 310-10-60-51	
An Evaluation of QVLBI OD Analysis of Pioneer 10 Encounter Data in the Presence of Unmodeled Satellite Accelerations	66
B. D. O'Reilly and C. C. Chao NASA Code 310-10-60-50	

Contents (contd)

Communications—Spacecraft/Ground

The Ultimate Limits of Binary Coding for a Wideband Gaussian Channel	78
S. A. Butman and R. J. McEliece	
NASA Code 310-20-67-08	
S/X Experiment: DSS 14 Pre- and Post-Track Ranging Calibrations for Mariner 10 Tracking Passes and Associated Problems	81
T. Y. Otoshi	
NASA Code 310-20-66-06	
S/X Experiment: DSS 14 S/X Ground System Ranging Tests	90
T. Y. Otoshi and P. D. Batelaan	
NASA Code 310-20-66-06	
A Dual Hybrid Mode Feedhorn for DSN Antenna Performance Enhancement	101
R. F. Thomas and D. A. Bathker	
NASA Code 310-20-65-03	

Station Control and Operations Technology

DSN Research and Technology Support	109
E. B. Jackson	
NASA Code 310-30-69-02	

Network Control and Data Processing

Forward Error Correction for the Ground Communications Facility?	114
O. H. Adeyemi and R. J. McEliece	
NASA Code 310-40-70-02	
Observations on Microprocessors and Computing Efficiency	118
C. C. Klimasauskas and J. W. Layland	
NASA Code 310-40-72-02	
Simulation Study of a GCF Retransmission Scheme	125
L. R. Welch	
NASA Code 310-40-70-02	
GCF Wideband Switch Subassembly—Application Techniques	129
E. F. Bird	
NASA Code 310-40-74-03	
Control-Restrictive Instructions for Structured Programming (CRISP) . .	134
R. C. Tausworthe	
NASA Code 310-40-72-05	

Contents (contd)

NETWORK ENGINEERING AND IMPLEMENTATION

Network Control System

NCS Minicomputer Systems Status Report	152
R. G. Petrie	
NASA Code 311-03-32-40	

Network Control System Block I and Block II Software	160
S. E. Friesema	
NASA Code 311-03-32-40	

Deep Space Stations

Faraday Rotation Experiment	170
A. L. Price	
NASA Code 311-03-14-64	

Waveguide Inspection Techniques	176
J. R. Loreman	
NASA Code 311-03-14-21	

Telemetry and Command Multiple-Mission Software (Model C)	180
V. D. Jones	
NASA Code 311-03-42-53	

An Interrupt Timing Simulation	183
V. D. Jones and R. L. Schwartz	
NASA Code 311-03-42-53	

OPERATIONS

Network Operations

S-Band/X-Band Doppler Two-Way Nonlinear Jitter Analysis Using Simplified Series-Expansion Techniques	190
R. C. Bunce	
NASA Code 311-03-14-52	

A Re-Examination of the AGC Calibration Procedure	197
G. L. Stevens	
NASA Code 311-03-14-52	

Tracking Operations During the Mariner 10 Mercury Encounter	202
A. L. Berman and G. L. Spradlin	
NASA Code 311-03-12-40	

Bibliography	212
-------------------------------	------------

DSN Functions and Facilities

N. A. Renzetti
Office of Tracking and Data Acquisition

The objectives, functions, and organization of the Deep Space Network are summarized. Deep space station, ground communication, and network operations control capabilities are described.

The Deep Space Network (DSN), established by the National Aeronautics and Space Administration (NASA) Office of Tracking and Data Acquisition (OTDA) under the system management and technical direction of the Jet Propulsion Laboratory (JPL), is designed for two-way communications with unmanned spacecraft traveling approximately 16,000 km (10,000 mi) from Earth to the farthest planets of our solar system. It has provided tracking and data acquisition support for the following NASA deep space exploration projects, for which JPL has been responsible for the project management, development of the spacecraft, and conduct of mission operations:

- (1) Ranger.
- (2) Surveyor.
- (3) Mariner Venus 1962.

- (4) Mariner Mars 1964.
- (5) Mariner Venus 1967.
- (6) Mariner Mars 1969.
- (7) Mariner Mars 1971.
- (8) Mariner Venus/Mercury 1973.

The DSN has also provided tracking and data acquisition support for the following projects:

- (1) Lunar Orbiter, for which the Langley Research Center carried out the project management, spacecraft development, and mission operations functions.

- (2) Pioneer, for which the Ames Research Center carried out the project management, spacecraft development, and mission operations functions.
- (3) Apollo, for which the Lyndon B. Johnson Space Center was the project center and the Deep Space Network supplemented the Spaceflight Tracking and Data Network (STDN), which is managed by the Goddard Space Flight Center (GSFC).
- (4) Helios, a joint United States/West Germany project.
- (5) Viking, for which the Langley Research Center provides the project management and Lander spacecraft, and conducts mission operations, and for which JPL provides the Orbiter spacecraft.

The Deep Space Network is one of two NASA networks. The other, the Spaceflight Tracking and Data Network, is under the system management and technical direction of the Goddard Space Flight Center. Its function is to support manned and unmanned Earth-orbiting and lunar scientific and advanced technology satellites. Although the DSN was concerned with unmanned lunar spacecraft in its early years, its primary objective now and into the future is to continue its support of planetary and interplanetary flight projects.

A development objective has been to keep the network capability at the state of the art of telecommunications and data handling and to support as many flight projects as possible with a minimum of mission-dependent hardware and software. The DSN provides direct support to each flight project through that project's tracking and data systems. This management element is responsible for the design and operation of the hardware and software in the DSN which are required for the conduct of flight operations.

As of July 1972, NASA undertook a change in the interface between the network and the flight projects. Since January 1, 1964, the network, in addition to consisting of the Deep Space Stations and the Ground Communications Facility, had also included the Mission Control and Computing Facility and had provided the equipment in the mission support areas for the conduct of mission operations. The latter facilities were housed in a building at JPL known as the Space Flight Operations Facility (SFOF). The interface change was to accommodate a hardware interface between the network operations control functions and the mission control and computing functions. This resulted in the flight project's picking up

the cognizance of the large general-purpose digital computers, which were used for network processing as well as mission data processing. It also assumed cognizance of all of the equipment in the flight operations facility for display and communications necessary for the conduct of mission operations. The network has already undertaken the development of hardware and computer software necessary to do its network operations control and monitor functions in separate computers. This activity became known as the Network Control System implementation. A characteristic of the new interface is that the network provides direct data flow to and from the stations via appropriate ground communications equipment to Mission Operations Centers, wherever they may be; namely, metric data, science and engineering telemetry, and such network monitor data as are useful to the flight project. It accepts command data from the flight project directly into the ground communications equipment for transmission to the station and thence to the spacecraft in a standardized format.

In carrying out its functions, the network activities can be divided into two general areas. The first includes those functions which are associated with the in-flight support and in tracking the spacecraft; its configuration can be characterized as follows:

- (1) *DSN Tracking System.* Generates radio metric data; i.e., angles, one- and two-way doppler and range, and transmits raw data to mission control.
- (2) *DSN Telemetry System.* Receives, decodes, records, and retransmits engineering and scientific data generated in the spacecraft to Mission Control.
- (3) *DSN Command System.* Accepts coded signals from Mission Control via the Ground Communications Facility (GCF) and transmits them to the spacecraft in order to initiate spacecraft functions in flight.

The second category of activity supports testing, training, and network operations control functions and is configured as follows:

- (1) *DSN Monitor and Control System.* Instruments, transmits, records, and displays those parameters of the DSN necessary to verify configuration and validate the network. Provides operational direction and configuration control of the network and primary interface with flight project mission control personnel.

- (2) *DSN Test and Training System*. Generates and controls simulated data to support development, test, training, and fault isolation within the DSN. Participates in mission simulation with flight projects.

The capabilities needed to carry out the above functions have evolved in three technical areas:

- (1) The Deep Space Stations that are distributed around Earth and which, prior to 1964, formed part of the Deep Space Instrumentation Facility. The technology involved in equipping these stations is strongly related to the state of the art of telecommunications and flight/ground design considerations and is almost completely multimission in character. Table 1 gives a description of the Deep Space Stations and the Deep Space Communications Complexes (DSCCs) they comprise.
- (2) Ground communications. This technology supports the Earth-based point-to-point voice and data communications from the stations to the Network Operations Control Area at JPL, Pasadena, and to the Mission Operations Centers, wherever they may be. It is based largely on the capabilities of the common carriers throughout the world which are engineered into an integrated system by the Goddard Space Flight Center for support of all NASA programs. The term "Ground Communications Facility" is used for the sets of hardware and software needed to carry out the functions.

The Network Operations Control Center is the functional entity for centralized operational control of the network and interfaces with the users. It has two separable functional elements; namely, Network Operations Control and Network Data Processing.

The functions of the Network Operations Control Center are:

- (1) Control and coordination of network support to meet commitments to network users.
- (2) Utilization of the network data processing computing capability to generate all standards and limits required for network operations.
- (3) Utilization of network data processing computing capability to analyze and validate the performance of all network systems.

The personnel who carry out the above functions are on the first floor of Building 230, wherein mission operations functions are carried out by certain flight projects. Network personnel are directed by an Operations Control Chief. The functions of the Network Data Processing are:

- (1) Processing of data used by Network Operations Control for the control and analysis of the network.
- (2) Display in Network Operations Control Area of data processed in Network Data Processing Area.
- (3) Interface with communications circuits for input to and output from Network Data Processing Area.
- (4) Data logging and production of the intermediate data records.

The personnel who carry out these functions are located in Building 202, which is approximately 200 m from Building 230. The equipment consists of minicomputers for real-time data system monitoring, two XDS Sigma 5's, display, magnetic tape recorders, and appropriate interface equipment with the ground data communications.

Table 1. Tracking and data acquisition stations of the DSN

DSCC	Location	DSS	DSS serial designation	Antenna		Year of initial operation
				Diameter, m (ft)	Type of mounting	
Goldstone	California	Pioneer	11	26(85)	Polar	1958
		Echo	12	26(85)	Polar	1962
		(Venus) ^a	13	26(85)	Az-El	1962
		Mars	14	64(210)	Az-El	1966
Tidbinbilla	Australia	Weemala	42	26(85)	Polar	1965
		Ballima	43	64(210)	Az-El	1973
—	Australia	Honeysuckle Creek	44	26(85)	X-Y	1973
—	South Africa	Hartebeesthoek	51	26(85)	Polar	1961
Madrid	Spain	Robledo	61	26(85)	Polar	1965
		Cebreros	62	26(85)	Polar	1967
		Robledo	63	64(210)	Az-El	1973

^aA maintenance facility. Besides the 26-m (85-ft) diam Az-El mounted antenna, DSS 13 has a 9-m (30-ft) diam Az-El mounted antenna that is used for interstation time correlation using lunar reflection techniques, for testing the design of new equipment, and for support of ground-based radio science.

Viking Mission Support

D. J. Mudgway
DSN Systems Engineering

D. W. Johnston
Network Operations

As part of the activity for preparing the Deep Space Network for support of the Viking mission, it is planned to conduct a series of tests in which multiple data streams are passed between the Deep Space Stations (DSSs) and the Viking Mission Control and Computing Center (VMCCC).

The data streams simulate real data types and data rates and are handled by all the hardware and software in the DSS and VMCCC in exactly the same way as the real data. The performance of the DSN and VMCCC in generating, handling, and processing these data is a measure of the readiness of the entire Ground Data System to enter live mission support.

The first series of these tests has recently been run between the Compatibility Test Area (CTA 21) and the VMCCC and the results are reported in this article.

I. DSN-VMCCC System Integration Tests

A. Interfaces

Organizationally the Viking Project is structured into six systems as follows:

- (1) Viking Orbiter System (VOS).
- (2) Viking Lander System (VLS).
- (3) Launch and Flight Operations System (LFOS).

- (4) Launch Vehicle System (LVS).
- (5) Viking Mission Control and Computing Center System (VMCCCS).
- (6) Tracking and Data System (TDS).

It is a matter of Project policy that the interfaces between adjacent systems shall be formally documented and tested as a prerequisite to any Project prelaunch testing. This policy is given in Ref. 1.

In the case of the interface between the VMCCC and the Deep Space Network (DSN) portion of the TDS, Ref. 2 formally describes and controls the VMCCC to DSN interface for Viking. To accomplish this purpose, it is necessary to describe (1) the media by which the information is transferred between the systems, (2) the intrasystem constraints, which include the functional relationship between each portion of a particular system in the DSN and in the MCCC, and (3) the data formats which will provide the framework for data interchange.

B. Testing

The plan by which these interfaces will be tested is given in Ref. 3. These series of tests are called System Integration Tests (SITs); separate SITs are planned between the VMCCC and each tracking station or test facility of the DSN involved in Viking support. The SITs have been carefully fitted into the overall Ground Data System test schedule for Viking and include CTA 21 and the Spaceflight Tracking and Data Network Merritt Island Station (STDN MILA) as well as all the Deep Space Stations (DSSs).

C. Responsibilities

Overall responsibility for conduct of VMCCCS/DSN system integration testing is assigned to the VMCCC Data System Project Engineer (DSPE), who acts as the Test Conductor. The DSN Network Operations Project Engineer (NOPE) will act as coordinator for the DSN during the SITs. In turn, the NOPE is supported by the Network Control System (NCS) and the Network Analysis Group.

II. CTA 21 System Integration Tests

The first of the scheduled SITs was carried out with CTA 21 over the period April 15 through June 1, 1974. The Viking configuration for CTA 21 used for these tests is given in Figs. 1 and 2 for telemetry and command. A summary of the tests performed and the results compiled by the Viking NOPE are given below:

The tests were conducted in four phases:

- (1) Test the DSN/VMCCCS interface for Lander telemetry.
- (2) Test the DSN/VMCCCS interface for Orbiter telemetry.
- (3) Test the DSN/VMCCCS interface for Viking Lander/Viking Orbiter (VL/VO) command.

- (4) Test all functional interfaces simultaneously with maximum loading.

1. SIT 1, April 16, 1974: Lander telemetry. The objectives of SIT 1 were to verify the VMCCC/DSN telemetry interface for specified Lander telemetry modes and data rates. The specified data rates were the Lander direct telemetry data at 8- $\frac{1}{2}$ bps and engineering at 250, 500, and 1000 bps for science data. Forty-five science format changes were planned; of these, 37 were accomplished prior to the termination of the test. The prime objectives were met; however, a bit stream anomaly in the science data was noted. This anomaly appeared to be a telemetry and command processor (TCP) software problem.

2. SIT 2, April 19, 1974: Lander telemetry. The objectives of SIT 2 were to verify the VMCCC/DSN telemetry interface for three Lander telemetry data streams. The maximum interface loadings for a Lander spacecraft (S/C) are 8- $\frac{1}{2}$ bps engineering, 1 kbps science, and playback of the Lander data from track-8 of the Orbiter at 16 kbps. With this test, all of the Lander telemetry format verification was completed on the 1-kbps direct science data. The 8- $\frac{1}{2}$ bps engineering data were processed without problems; again, as in SIT 1, a bit stream anomaly was observed within the 1-kbps science data; however, this anomaly did not prevent the data from being processed.

High-rate Orbiter data were processed at 4 kbps. Timing problems between the simulation center (SIMCEN) 360/75 and the GCF interface precluded effective testing at bit rates in excess of 4 kbps.

Although the test included the independent Lander telemetry testing, maximum loading at 16 kbps playback from the VO was not accomplished. This problem was attributed to the simulation/Ground Communications Facility (SIM/GCF) interface, and the Orbiter telemetry testing was deferred and replaced with the command testing phase.

3. SIT 5, April 23, 1974: Lander command. The test objectives of SIT 5 were to verify the VMCCC/DSN command interfaces for Lander commanding in both the automatic and manual modes. The TCP at CTA-21 was configured to verify that commands could be processed in the standard configuration without alarms or aborts and that, in a non standard configuration, all warnings, alarms, and aborts occurred when the applicable conditions were established.

This test was successful, despite an early termination when the 360/75 being used for testing had to be released for real-time flight support. In all cases the command software performed properly. Operating personnel, however, were not fully aware of the idiosyncrasies of the new command software redesign because of lack of adequate training with this software.

4. SIT 6, April 26, 1974: Orbiter command. The objectives of SIT 6 for Orbiter commanding were identical to those of SIT 5 for the Lander. The objectives were met and the test sequence of events (SOE) was completed.

5. SIT 7, May 1, 1974: Dual Lander/Orbiter command. Simultaneous dual spacecraft commanding was the objective of SIT 7; this objective was not met.

Although a standard DSS configuration provides that only a single spacecraft be commanded at any specific time, CTA 21 must have dual command capability to satisfactorily conduct compatibility testing. Because CTA 21's second exciter (Block IV) had not been fully implemented, hardware and software workarounds to use the Block III exciter were attempted. These workarounds failed, and two exciters could not be emulated at CTA 21 for the completion of this test.

The remaining test time was utilized to complete the uncompleted sequence from SIT 5 (Lander command), and dual commanding was simulated by simultaneously conducting "in core" Orbiter commanding in the 360/75.

6. SIT 3, May 4, 1974: Orbiter telemetry. The objectives of SIT 3 were to verify the VMCCC/DSN telemetry interfaces for a single Viking Orbiter. These objectives were successful at all data rates except 16 kbps. The data rates processed were: engineering 8- $\frac{1}{2}$ and 33- $\frac{1}{2}$ bps, and science rates of 1, 2, 4 and 8 kbps in both coded and uncoded modes. The SIM 360/75/GCF timing problem, which had caused a delay of Orbiter telemetry testing, still existed, but the problem was less evident on the 50-kbps wideband data line (WBDL). The Mission Test and Computing Facility (MTCF) could not process the high-rate 8-kbps data for time periods greater than approximately 2 minutes, and CTA 21's simulation conversion assembly (SCA) could not lock on the 16-kbps data generated from SIMCEN. The Block IV receiver successfully processed engineering and science data during this test.

7. SIT 4, May 7, 1974: Orbiter telemetry. The SIT 4 objectives were to verify the VMCCC/DSN telemetry interface for maximum data rates and data streams (3) from one TCP. This loading configuration required both Orbiter data streams (33- $\frac{1}{2}$ bps and 16 kbps) and a Lander science data stream at 1 kbps. This TCP loading objective was met, but the 16-kbps data stream could not be sustained by the Simulation Center for a period of time exceeding 1 to 2 minutes. This simulation constraint, which has been previously mentioned as a SIMCEN 360/75/GCF timing problem, was actually isolated to that interface during this test; only the 50-kbps WBDL was exercised during this test.

8. SIT 7 (Retest), May 10, 1974: Dual commanding. The objectives of this test were to configure CTA 21 so that it emulated two independent DSSs commanding two spacecraft simultaneously. Dual commanding was accomplished. An additional objective achieved during this test was the verification of the Lander telemetry interfaces in parallel with the command interfaces. Lander direct data at 8- $\frac{1}{2}$ and 250 bps were successfully processed.

The Lander science data bit stream anomaly, which had been previously observed in SIT 1 and SIT 2, was isolated during this test to the 360/75 SIMCEN/GCF interface.

9. SIT 9, May 14, 1974: Lander telemetry and command. The objective of SIT 9 was to exercise one fully loaded telemetry and command data (TCD) string with the combination of Lander telemetry and commanding simultaneously. The selected data rates were: 8- $\frac{1}{2}$ bps, 1 kbps and Orbiter track-8 Lander playback at 2, 4, 8, and 16 kbps; of these objectives, only the 8- $\frac{1}{2}$ bps, 1 kbps and command were processed. Difficulties in the DSN and VMCCC prevented other data rates from being processed within the allotted time. The test was considered to be only partially successful.

10. SIT 10, June 1, 1974: Two Orbiters and Lander telemetry. The objectives of SIT 10 were to verify that the VMCCC/DSN interfaces could handle the loading of multiple spacecraft telemetry data streams at maximum bit rates. These objectives were met: the VMCCC Simulation Center generated all of the high-speed telemetry data rates, while CTA 21's SCA generated the wideband data rates.

The Simulation Center high-speed data streams were 8- $\frac{1}{2}$ bps, 33- $\frac{1}{2}$ bps and 1 kbps. CTA 21 produced two 16-kbps wideband data streams by using the SCA in the

stand-alone mode. These data rates were all successfully processed using the high-speed data lines and the 50-kbps wideband data line.

Problems were encountered on the 28.5-kbps WBDL portion of the test, but the problems appear to be a MTCF telemetry processor problem and not related to the SCA/TCD or GCF.

11. SIT 11, June 8, 1974: Two Orbiters and Lander telemetry and command. The test objectives were to verify that multiple spacecraft telemetry and command data streams could be processed simultaneously. These objectives were met. The TCPs were able to process data at maximum loading (one 8- $\frac{1}{2}$ bps and one 1 kbps Lander data stream plus two 33- $\frac{1}{2}$ bps and two 16 kbps Orbiter data streams) while commanding the Lander from one TCP and the Orbiter from the other TCP. The preceding configuration simulated all of the nominal data interfaces,

including monitor data, that are expected during a planetary pass, or CTA 21's compatibility testing.

The second phase of this test was to simulate all of the nominal data interfaces that will be used during a planetary pass (full loading) from an overseas station. This configuration requires that the 28.5-kbps WBDL interfaces be exercised by processing two-Orbiter high-rate data streams simultaneously at 16 and 18 kbps. This configuration was also successful, but data processing at MTCF could not be sustained while using the 28.5-kbps WBDL. This 28.5-kbps WBDL problem appears to be a MTCF problem and not related to the TCD or GCF. All high-rate data streams were generated by CTA 21's SCA; as the SIMCEN/GCF interface problems have not yet been resolved.

The concluding tests in this series will be reported in a subsequent article.

References

1. "Viking 75 Project Orbiter System, Lander System and Viking Mission Control and Computing System to Tracking and Data System Interface Requirements Document, General Requirements," Vol. I, ID-3703111 Viking Project document, Langley Research Center, Hampton, Va.
2. "Viking 75 Project Orbiter System, Lander System and Viking Mission Control and Computing System to Tracking and Data System Interface Requirements Document, Viking Mission Control and Computing Center System to Deep Space Network," Vol. IV, ID-3703111 Viking Project document, Langley Research Center, Hampton, Va.
3. "Viking 75 Project Test and Integration Plan for the Viking Mission Control and Computing Center System, Viking Mission Control and Computing Center System to DSN Integration," Vol. IV, 619-6, May 1, 1974 (a JPL internal document).
4. "Network Operations Plan for Viking 75 Project," 614-21, Nov. 1, 1973 (a JPL internal document).

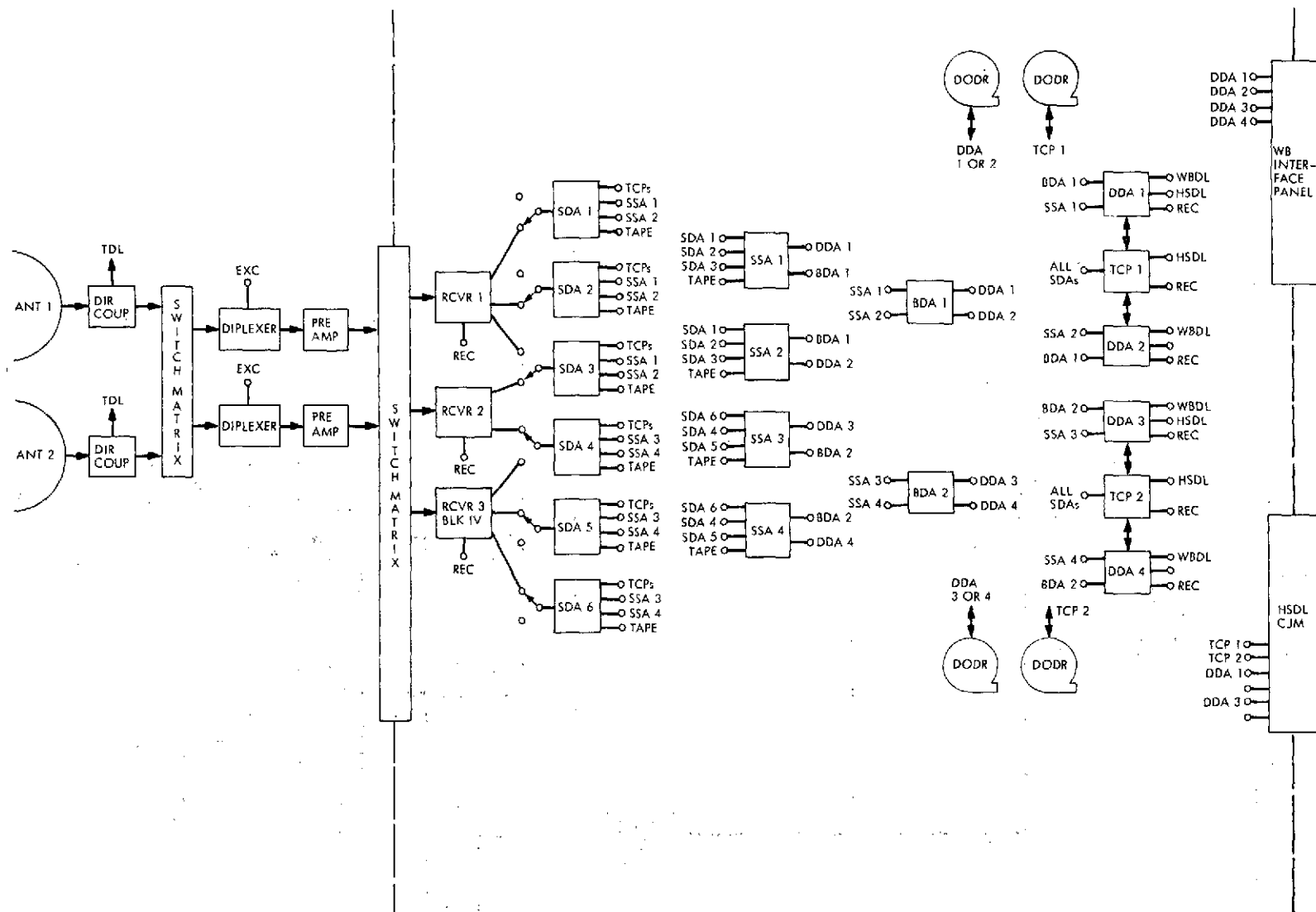


Fig. 1. CTA 21 Viking-75 telemetry configuration

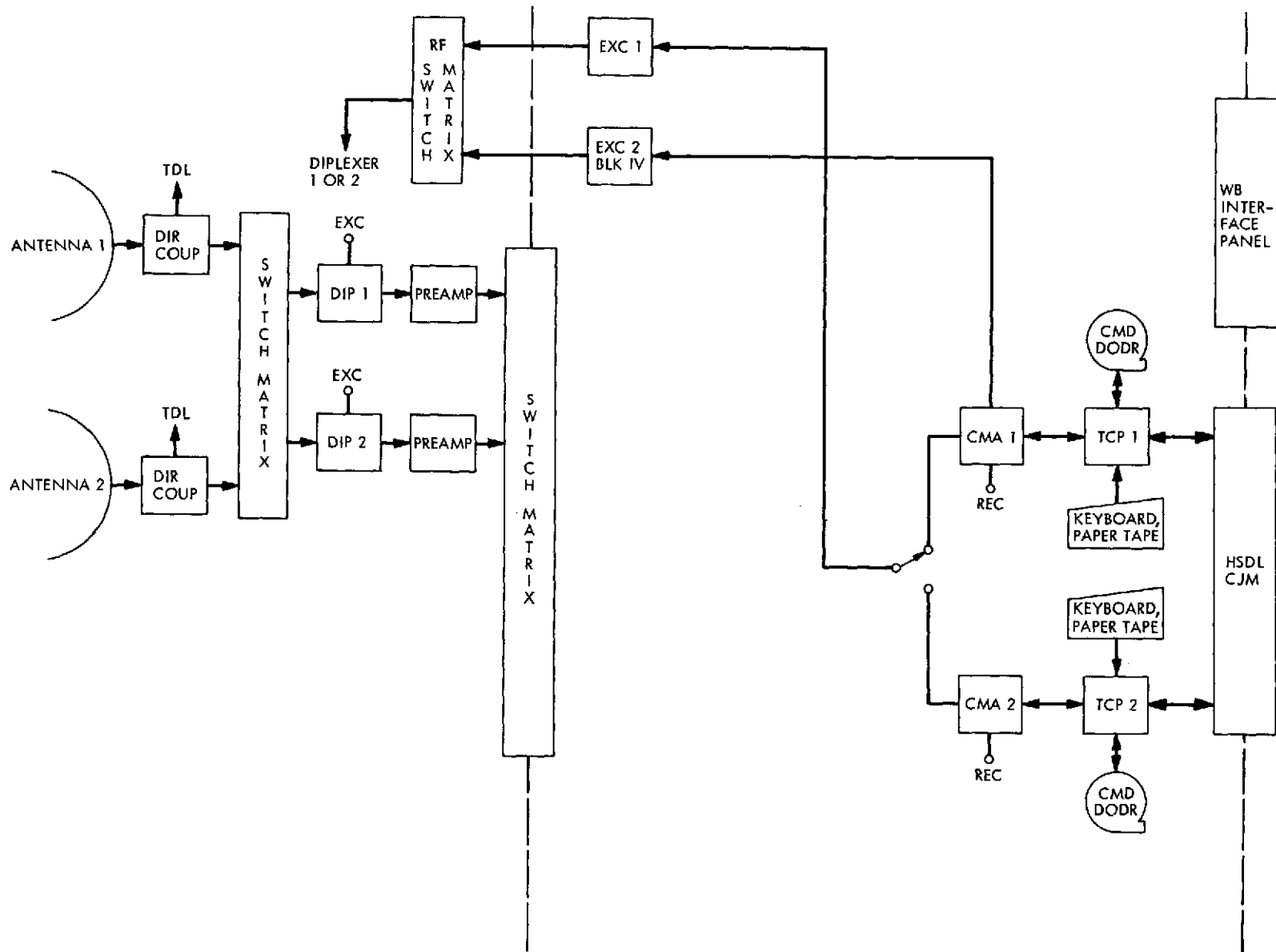


Fig. 2. CTA 21 Viking-75 command configuration

Pioneer 10 and 11 Mission Support

R. B. Miller
Mission Support Office

Pioneers 10 and 11 continue to function normally and return new information on the interplanetary medium beyond the orbit of Mars. This article describes the current state of the Pioneer 10 and 11 missions, including discussions on significant events since Pioneer 10 Jupiter encounter, possible upgrading of communications capabilities for future Pioneer 10 and 11 operations, and the nature of the Pioneer 11 Saturn trajectory.

I. Significant Events Since Pioneer 10 Jupiter Encounter

Both Pioneers 10 and 11 are continuing to function normally and are continuing to return new information on the interplanetary medium beyond the orbit of Mars. Every day that Pioneer 10 is tracked and data returned represents further penetration into new regions of space never before explored by man. This continued study of the propagation of energetic solar events to large distances from the Sun has already produced some scientific surprises. The Pioneer 10 magnetic field, solar wind, plasma, and energetic charged-particle measurements obtained thus far indicate a much higher degree of interplanetary turbulence and a surprisingly smaller gradient in the galactic cosmic rays than had been expected. Already the Pioneer 10 and 11 results require reformulation of present coronal expansion and cosmic ray modulation theory.

In February 1974, both Pioneers 10 and 11 went through a solar conjunction. Simultaneous with the solar

conjunction was the extensive post-Venus closest approach Mariner Venus/Mercury data taking. Since Mariner Venus/Mercury 1973 (MVM73) approached Venus from the dark side, it was during this post-encounter time period when the majority of the good Venus imaging took place. Mariner Venus/Mercury 1973 required 64-meter coverage in this time period in order to achieve the maximum return of imaging data. Pioneers 10 and 11 also required 64-meter coverage in order to safeguard the spacecraft during the solar conjunction. Closest approach of MVM73 to Venus occurred on February 5, 1974; the Pioneer 10 center of solar conjunction occurred on about February 19, 1974; and the Pioneer 11 center of solar conjunction occurred on about February 21, 1974.

There are two important factors affecting Pioneers 10 and 11 during a solar conjunction. The first is the desire to maintain the high-gain antenna pointed as near to the Earth direction as possible in order to maintain the uplink and downlink margin to the spacecraft. When the

Sun, during solar conjunction, gets within a few degrees of the spacecraft-Earth line, the solar sensor on the spacecraft is unable to operate. The solar sensor is utilized to produce a roll pulse which serves as the pointing reference for all of the on-board instruments. It is, therefore, necessary to point the spacecraft slightly off the Earth-spacecraft line in order to avoid loss of roll reference. This requires a successive precessing of the spacecraft during a solar conjunction to step around the Sun position and avoid loss of roll reference while still maintaining good communications with Earth. The second factor during solar conjunction is the fact that the spacecraft design on both Pioneers 10 and 11 has incorporated protection against receiver failure by automatically causing the spacecraft to switch to the redundant receiver in the event that an uplink has not been detected within 36 hours. This requirement necessitates the daily establishment of an uplink to the Pioneer spacecraft right through the solar conjunction period in order to prevent the switching of the radio subsystem. This automatic switching can be inhibited by ground command, so it was decided, since Pioneer 10 had achieved Jupiter encounter, that the risk of inhibiting this function on Pioneer 10 would be acceptable for this solar conjunction. It was held, however, that the risk would be too high for Pioneer 11, so a daily uplink would have to be established. This daily uplink requires, during the height of solar conjunction, a 64-meter antenna in order to break through the solar corona into the spacecraft receiver. On about February 2, 1974, Pioneer 10, with the automatic receiver switching inhibited, was maneuvered off to a position that would cause Earth to come back into the beam of the high-gain antenna after solar conjunction. Communication was then lost during this blind maneuver, as planned, until some time after the solar conjunction. This decision by the Pioneer Project Office greatly relieved the excessive demand on 64-meter coverage in this time period. Pioneer 11-required 64-meter coverage was achieved principally using partial passes shared with MVM73.

Based on the experience with Pioneer 10 at Jupiter encounter, the decision was made by the Pioneer Project Office to re-target Pioneer 11 to enable a gravity-assist at Jupiter encounter to carry the Pioneer 11 spacecraft on to the vicinity of Saturn.

II. The Future of Pioneers 10 and 11

Pioneer 10 will continue to move out from the Sun and eventually escape our solar system. Pioneer 11 will encounter Jupiter on December 3, 1974, where it will swing

around onto a Saturn trajectory with an expected Saturn arrival of September 5, 1979. Plots of the Earth-to-spacecraft range for both Pioneers 10 and 11 are shown in Fig. 1. This figure, designed by A. J. Siegmeth of the Pioneer Project Support Office, also shows the expected communications performance for both spacecraft. The received carrier power on this chart, at which each bit rate thresholds, is pessimistic by about 1 dB. It is anticipated that, with the existing 64-meter antenna configuration with a 12-Hz loop in the receiver, we should be able to continue to receive useful telemetry from Pioneer 10 out to about 19 AU, which corresponds to about a -164.5 -dBmW received carrier power. This range will be reached at about the end of March 1979. Means of extending the range to which we can track Pioneer 10 are being investigated. They include the planned upgrade of the 64-meter network to 68 meters, possible use of the 3-Hz loop in the Block IV receiver, and the ganging of a fourth 64-meter antenna planned for Goldstone, California, with the existing DSS 14 antenna. Allowing for the 1 dB of pessimism, it is seen from the chart that Pioneer 11 at Saturn encounter will have marginal performance at 512 bits per second. The Pioneer Project Office is extremely interested in trying to achieve 1024 bits per second at Saturn encounter. This would be the same bit rate as was achieved at Jupiter encounter. The principal hope for achieving 1024 bits at Saturn encounter is the completion of the fourth 64-meter antenna at Goldstone, which would enable the ganging of two 64-meter antennas with a performance improvement of nearly 3 dB. As can be seen from the chart, the 3 dB should make the 1024-bit rate possible. A 512-bit rate, instead of 1024 bits per second, would mean either loss of color information during the ± 2 days of closest approach to Saturn, or else color imaging with pictures only one-half the height that would be possible at 1024 bits per second. Reference 1 should be consulted for a description of the imaging instrument on board Pioneers 10 and 11.

The imaging photopolarimeter (IPP) instrument takes a full color image over 14 deg of spacecraft roll. As described in the referenced article, a 1024-bit rate is required in order to play back a 14-deg color image. At 512 bits per second, the spacecraft can either play back a 7-deg full color picture or a 14-deg black-and-white image. At closer than approximately ± 2 days to encounter, the uncertainty in spacecraft pointing plus the size of the planet disk exceeds 7 deg. It is hoped that, with two 64-meter antennas ganged in phase, coupled with low-noise listen-only receiving subsystems, full imaging return can be achieved during the September 1979 Saturn encounter.

III. The Pioneer 11 Saturn Trajectory

Figure 2 shows the Pioneer 10 and 11 targeting points at Jupiter encounter. Speaking in terms of the direction that Jupiter moves in its orbit around the Sun, Pioneer 10 was targeted to follow the planet Jupiter in nearly the equatorial plane of the planet. Pioneer 11 has now been targeted to lead the planet Jupiter in a more nearly polar trajectory. The closest approach for Pioneer 10 was at 2.86 Jupiter radii (203,250 kilometers) from the center of the planet. Pioneer 11 will have a closest approach of only 1.6 Jupiter radii (113,000 kilometers) from the center of the planet. That is only 6/10th of a Jupiter radius from the visible surface of the planet. (Note that Fig. 2 does not directly show the radius of closest approach to the planet, but rather where the spacecraft trajectory intersects a plane perpendicular to the hyperbolic approach velocity of the spacecraft.)

There was considerable concern prior to Pioneer 10 Jupiter encounter as to whether the spacecraft could survive the high level of radiation that might be present around the planet Jupiter. It appeared that Pioneer 10 had received about the maximum dosage of radiation possible without sustaining severe damage to the spacecraft. The minor damage that was experienced by Pioneer 10 was mostly of a temporary nature. A natural question to ask is how can Pioneer 11 be sent 1.2 Jupiter radii closer than Pioneer 10 and be expected to survive. There are two principal factors which should make the Pioneer 11 trajectory such that the total dosage of radiation experienced by Pioneer 11 will be the same as Pioneer 10. First, Pioneer 11, because of its closer flight,

will be flying by the planet much faster. A more important factor is that the radiation around the planet Jupiter is latitude-dependent and peaks in a disk about the equator of the planet. Because Pioneer 11 is going to a lower latitude than Pioneer 10, it will actually be crossing the region of peak radiation at a farther distance from the planet.

A potential concern for the DSN in the closer approach to Jupiter of Pioneer 11 is the peak doppler offset and rates that will be experienced. Fortunately, the Saturn trajectory is such that the peak doppler amplitude and rates occur during the Jupiter-Earth occultation. Therefore, the rates that will be experienced during the Pioneer 11 encounter will be equal to or less than those of Pioneer 10.

Figure 3 depicts the Pioneer 11 trajectory from launch to Saturn encounter. Notice that the spacecraft actually gets closer to Earth again after Jupiter encounter on its way to Saturn. This can also be seen in Fig. 1. The spacecraft actually gets closer than 3 AU to Earth on its way to Saturn. Notice also that the spacecraft goes between 1 and 1½ AU; or nearly 15 deg, out of the ecliptic plane in transit to Saturn. Also notice that Saturn is very near solar conjunction at the time of Saturn encounter of Pioneer 11. At the time of closest approach of Pioneer 11 to Saturn, the spacecraft will be only 6 deg from the Earth-Sun line. This means that very little post-Saturn encounter data will be returned. The details of the Saturn flyby have not yet been determined; however, there has been discussion of trying to target Pioneer 11 to thread one of the gaps in the Saturn rings.

Reference

1. Miller, R. B., "Pioneer 10 and 11 Mission Support," in *The Deep Space Network Progress Report*, Technical Report 32-1526, Vol. XVI, pp. 15-21, Jet Propulsion Laboratory, Pasadena, Calif., Aug. 15, 1973.



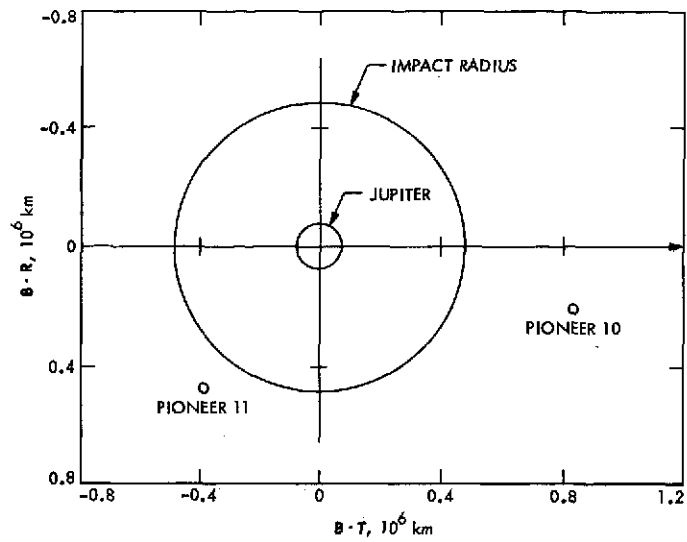


Fig. 2. Pioneer 10 and 11 targeting at Jupiter

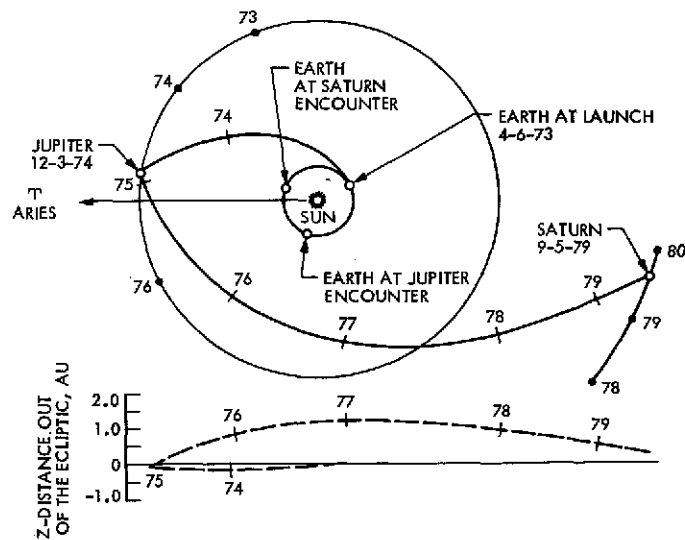


Fig. 3. Pioneer 11 Saturn transfer trajectory

Helios Mission Support

P. S. Goodwin
DSN Systems Engineering

The Helios-A spacecraft is now less than 6 months from launch. DSN activity is shifting from implementation to operational preparations. There have been, however, three significant recent developments which bear discussion: (1) the final selection of the targeted perihelion distance for the Helios-A mission has been established as 0.31 AU; (2) the Helios-A launch trajectory has been changed from a direct-ascent mode to a parking-orbit mode; and (3) the prototype model spacecraft has successfully passed compatibility testing with the DSN. The significance to the Tracking and Data System of each of these developments is discussed.

I. Introduction

With the Helios-A launch now scheduled for the latter part of October 1974, there have been several changes or refinements to the mission plan in addition to what has been previously reported in prior volumes of this report. Of particular interest to the reader will be the following topics: the targeted perihelion distance now being set at 0.31 astronomical units (AU); the use of a parking-orbit launch trajectory; and the results of the compatibility test program between the DSN and the prototype model Helios spacecraft. Each of these is discussed further in the paragraphs that follow.

II. The 0.31-AU Perihelion

Figures 3 and 4 of Ref. 1 depicted typical Helios trajectories for a July 1974 launch, with 0.25- and 0.30-AU

perihelions, respectively. Figure 1 herein depicts a similar fixed Earth-Sun-line plot of the Helios-A trajectory for a September/October 1974 launch and a 0.31-AU perihelion. The principal effect of the combined launch date (September/October vs July 1974) and 0.31-AU perihelion is that the upper loop of Fig. 1 does not achieve a total (geometric) Sun occultation as the spacecraft is viewed from Earth. However, little if any scientific value has been lost by this effect since the Helios-A spacecraft will now have a considerably longer dwell-time in very close proximity to the Sun when expressed in terms of look angle from the Earth. This will permit many weeks of Faraday rotation measurements to determine the influence of the Sun's corona upon the propagation characteristics of the radio signal transmitted from the spacecraft to the DSN. This feature of the new trajectory, plus the fact that the spacecraft is expected to enter into a total occultation starting a little after 270 days from launch,

provides scientific data at least equally important to that which had been previously planned. The change in perihelion and launch date, therefore, is not considered by the Helios Project to have impacted the expected scientific return from the Helios-A Mission.

III. Parking Orbit

Approximately six months prior to the planned Helios-A launch, NASA and the German Ministry for Research and Technology (Der Bundesministerium fuer Forschung und Technologie, BMFT) mutually agreed to alter the planned launch trajectory for Helios-A from a direct-ascent mode to a parking-orbit mode. The motivation for this change was the February 1974 partial success/failure of the Titan-Centaur proof-test flight, denoted TC-1, during which the Centaur stage failed to achieve full ignition. Since this launch vehicle will also be used for the future NASA Viking and Mariner Jupiter-Saturn missions, as well as for the Helios-B mission—all of which will use parking-orbit launch trajectories—there was a strong desire to prove out as early as possible the Centaur restart capabilities, especially after a long-duration coast period in the parking orbit. Further, a parking-orbit trajectory for Helios-A would permit the extension of the launch opportunity to the end of January 1975 as opposed to mid-December for the direct-ascent mode. These and other factors, when considered in total, resulted in the aforementioned decision. Admittedly time was short, but it was still possible to modify both the Centaur stage and the near-Earth phase Tracking and Data System support prior to the scheduled Helios-A launch.

From Fig. 1 it can be seen that the Helios-A spacecraft will depart the vicinity of Earth in the late afternoon hours of the day. Using a direct-ascent launch trajectory mode, such a departure could be achieved with a noon or afternoon launch from Cape Canaveral. However, to achieve the same injection conditions with a parking-orbit launch trajectory it is necessary to advance the launch time into the very early morning hours—i.e., before sunrise. These features are depicted in Fig. 2. Though not drawn accurately to scale, Fig. 2 also shows that the parking-orbit mode launch trajectory will have a lower perigee altitude than the formerly planned direct-ascent mode. There is, therefore, an infinitesimal increase in the aphelion distance at injection of the spacecraft.

From a Tracking and Data System viewpoint, the change to a parking-orbit launch trajectory has its great-

est impact on the plan for the near-Earth phase support (i.e., number of supporting stations) and to a lesser extent on the Deep Space Network (which must now switch its initial acquisition from the Madrid facilities to the Australian facilities).

Figure 3 depicts the Earth-track of the Helios-A parking-orbit launch trajectory for the opening (Case I) and closing (Case II) of the Helios-A launch opportunity. It is obvious from this figure that more near-Earth phase network facilities—land-based stations, tracking ship, and aircraft—will be required to support critical launch-phase events than would have been necessary for a direct-ascent mission (see Ref. 1, Fig. 1) whose spacecraft injection would have occurred just after first rise at the Madrid Deep Space Station. At this writing, the near-Earth phase network support plan is still being revised; however, it does appear that there will be sufficient resources available to provide support during the critical launch-phase mission events.

With respect to the DSN, the first-order impact was the shift of the initial postinjection acquisition station location from the Madrid Deep Space Station to the Canberra, Australia, Deep Space Station. This could be done since the Canberra station (DSS 42) is already equipped with an acquisition-aid antenna system—hence no new implementation was required at that facility.

There are, however, two important aspects to performing an initial acquisition at Australia: first, the initial spacecraft rise at Canberra occurs approximately 1 hour after launch as opposed to 15 to 30 minutes for the direct-ascent acquisition at Madrid; second, the length of time the spacecraft is in view during the first pass over Australia is much shorter than it would have been over the Madrid DSS using a direct-ascent launch trajectory. The Australian view-period is shortest for the early portion of the launch opportunity and gradually lengthens towards the end. The primary tasks for the Canberra DSS will be to perform the initial acquisition and provide for an early checkout of the spacecraft conditions. Once this is accomplished, the Canberra and Madrid DSSs will share the responsibility (depending upon launch date) of individually or jointly supporting the Step I maneuver and subsequent near-Earth science instrument turn-on (see Ref. 1). This level of activity is sufficiently high that there is not enough time remaining during the first Madrid DSS pass to initiate and complete the Step II maneuver, which is to be performed after the spacecraft passes lunar distance from Earth. The latter task is sufficiently time-consuming

that it is reserved for the first Goldstone pass—with a possibility of performing the final trim of the Step II maneuver during the second Goldstone pass. However, the delay in the rise time for Goldstone due to the parking-orbit mode also means that the spacecraft will be farther from Earth at the initiation of the Step II maneuver. The increased space loss due to this increased distance amounts to approximately 4 dB, which is not available in the telecommunications link design margins and must therefore be compensated by the use of the 64-meter antenna instead of 26-meter antennas at Goldstone.

The previous direct-ascent mode Step II maneuver support plan called for the Goldstone 26-meter DSSs to be equipped with a fixed linear polarizer to support the first part of the Step II maneuver with the polarizer in the plane of the ecliptic and then to switch to the polarization being normal to the plane of the ecliptic at a prescribed point during the maneuver. However, the Goldstone 64-meter station (DSS 14) has a continuously variable linear polarizer as opposed to a fixed polarizer. After considerable study, it was mutually decided between the DSN and the Helios Project not to attempt to continuously track the polarization of the incoming signal during the Step II maneuver but rather to emulate the plan previously developed for the 26-meter stations. The main reason for this is that the spacecraft omniantenna radiation pattern had not been measured for linear polarization reception at angles other than 0 and 90 degrees with respect to the spin axis, and further, there was insufficient time or resources to accomplish such measurements prior to launch. While it might be possible to achieve a small increase in performance by continuously tracking this changing polarization, the concurrent unknown risks were considered to be too high in relationship to the potential gains. Further, calculations show that there is sufficient margin to accomplish the Step II maneuver using the Goldstone 64-meter antenna in conjunction with the polarization step-changing techniques developed for the 26-meter stations.

Once the Step II course and fine maneuver adjustments are completed, which should be by the end of the second Goldstone pass, the DSN support of the Helios-A parking-orbit mission closely approximates that which had been previously planned for the direct-ascent mission—i.e., as depicted in Fig. 1. The impact of the change to a parking-orbit mission is therefore confined to the first few days after launch.

IV. DSN/Helios Prototype Model Compatibility Tests

The Helios prototype model spacecraft arrived at the Jet Propulsion Laboratory in late April 1974 for a series of environmental and ground system compatibility tests. Formal compatibility testing with the DSN Compatibility Test Area (CTA 21) occurred between 17 and 31 May 1974. Prior to that time, the spacecraft underwent thermal/vacuum testing in the JPL 25-foot-diameter space simulator chamber. Alerted by the fact that telemetry system incompatibilities had been discovered during compatibility tests in Germany using the Weilheim station and the upgraded engineering model spacecraft, the DSN arranged for some "quick look" telemetry system gross tests while the prototype spacecraft was still in the thermal/vacuum chamber at JPL. These "quick look" telemetry checks disclosed problems in addition to the inverted tail (synchronization word) discovered during the German compatibility tests. The additional telemetry problems were traced to a specification ambiguity regarding the sequence of transmitting the two components of the Helios convolutional code.

Technically speaking, the spacecraft and DSN telemetry systems were incompatible. Since it was obviously too late in the spacecraft manufacturing cycle to introduce modifications to that design, remedies were sought within the DSN. Fortunately, the software sequential decoding scheme employed by the DSN for convolutionally encoded telemetry streams was sufficiently well modularized to allow temporary instructions (i.e., patches) to be inserted into the software. These "patches" were developed and tested using the prototype spacecraft while it was still in the thermal/vacuum chamber. Compatibility testing with the DSN was therefore able to commence on schedule on May 17. The ensuing formal compatibility tests with the DSN disclosed no further incompatibilities, and in fact pointed out that the Helios spacecraft transponder design was very well executed—especially with respect to the stability of the ranging delay through the transponder. The success of the prototype compatibility tests is doubly significant when one considers the fact that the Helios transponder was developed in Germany without benefit of frequent interfacing with the DSN. The discrepancies noted during the April 1972 compatibility tests using the engineering model transponder and the DSN facility at Cape Kennedy (DSS 71) had been corrected by a complete redesign of the spacecraft transponder receiver portion with only a subsequent spot check of the receiver at CTA 21. The Helios Project is certainly to be commended for these efforts.

While the prototype spacecraft/CTA 21 compatibility tests are considered completely successful, the coded telemetry *technical* incompatibility mentioned above requires further DSN effort. The DSN's software sequential decoding package developed for Helios (known as Model B) had been distributed and tested within the Network prior to the discovery of the aforementioned incompatibility. Either this software had to be changed or new software introduced into the Network, tested, and subsequent operator training accomplished prior to the start of Mission Operations System training for the Helios-A launch.

Since a Model C version of the DSN software was nearing completion to support both Helios and Viking, it was decided to make the modifications required for the Helios telemetry in the Model C software package rather than to attempt to upgrade the Model B software in the field. Since the Model C version would also require Network testing and training, the Network test/training recycle

time could be shortened by using the latter of the two approaches. Therefore, it is now planned to support the Helios-A launch and premission training using the Model C telemetry software in the Network.

The net result of the *technical* telemetry incompatibility is a one-month delay in DSN readiness to support the Helios premission training. However, this one-month delay could be absorbed in the schedule without significant overall impact.

V. Conclusions

Despite the unexpected circumstances that led to these near-last-minute changes to the DSN support plans for Helios-A, the DSN has put into effect modifications that will permit the Helios-A mission to be supported without a slip in launch date. This fact, plus the overall success of the compatibility test plan with the prototype spacecraft, leads the DSN to be optimistic about its role in the support of the Helios-A mission.

References

1. Goodwin, P. S., "Helios Mission Support," in *The Deep Space Network Progress Report*, Technical Report 32-1526, Vol. III, pp. 20-28, Jet Propulsion Laboratory, Pasadena, Calif., June 15, 1971.

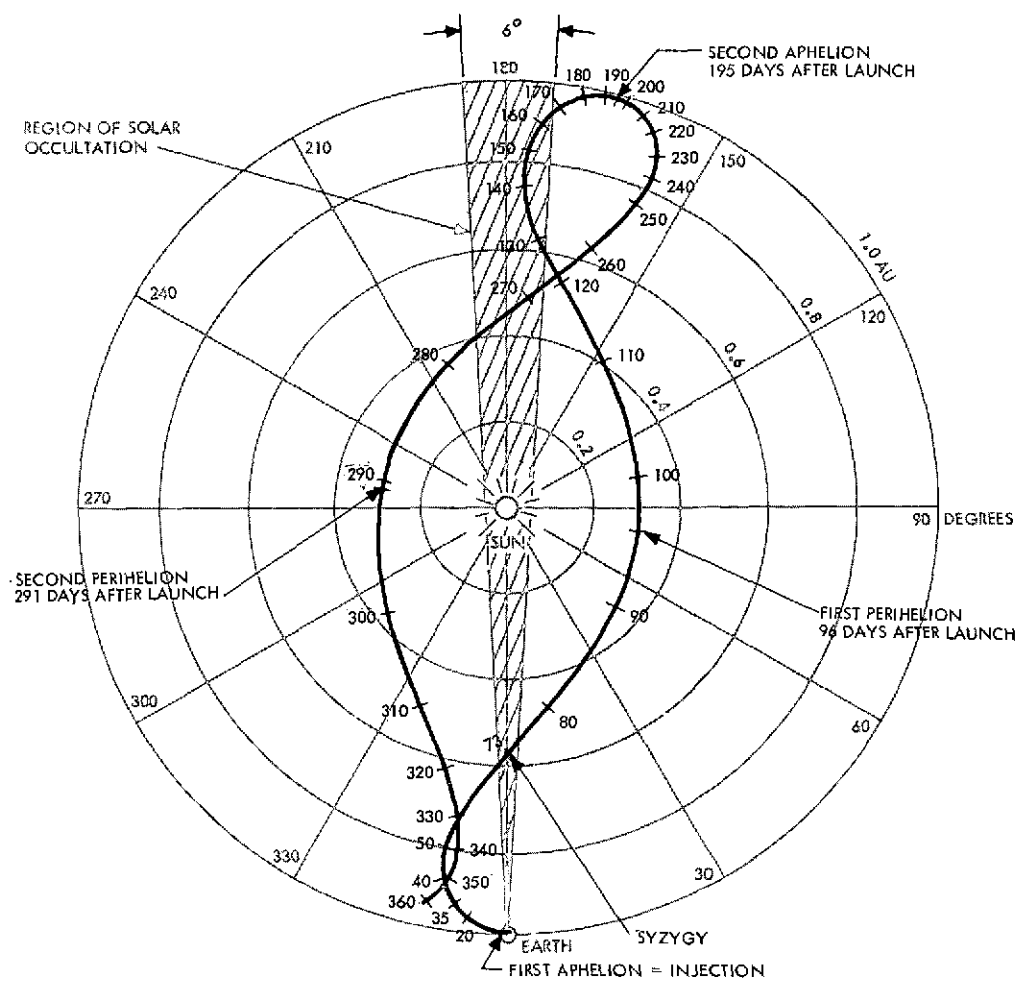


Fig. 1. Fixed Earth-Sun-line plot of Helios-A trajectory, 0.31-AU perihelion, September/October 1974 launch

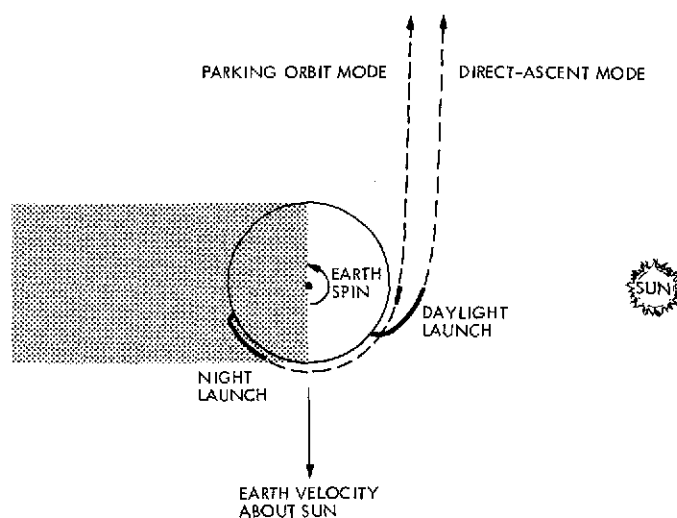


Fig. 2. Parking-orbit mode requires night launch

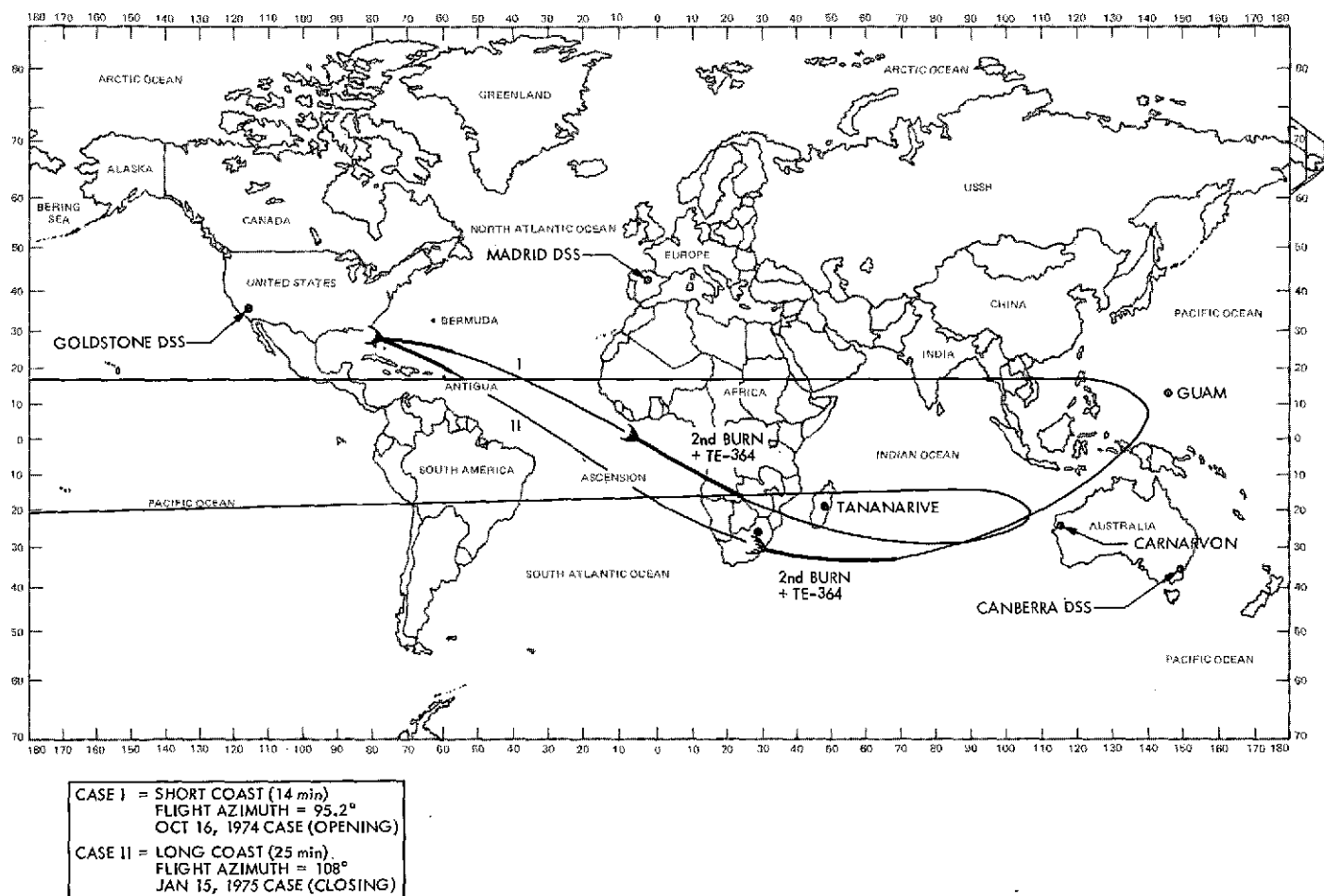


Fig. 3. Typical Helios-A parking orbit trajectories

The Measurement of Dispersive Effects Using the Mariner 10 S- and X-Band Spacecraft to Station Link

G. A. Madrid

Tracking and Orbit Determination Section

The techniques used to measure dispersive effects from radio metric observables taken at S- and X-band frequencies during the Mariner Venus/Mercury 1973 mission are described. A derivation of the phase and group delay effects is presented based on basic electromagnetic propagation principles and the communication link configuration between the spacecraft and DSS 14.

I. Introduction

The experimental use of an S- and X-band communications link between the Mariner 10 spacecraft and the ground receiver at DSS 14 permitted the measurement of dispersive effects due to charged particles in the transmission media. The dual-frequency capability was made possible by the installation of an experimental receiver developed by G. Levy, et al., at DSS 14 and by the inclusion of an X-band transponder on the spacecraft to complement the operational S-band equipment. Figure 1 illustrates the basic communications interface between the spacecraft and the station: a 2100-MHz uplink received at the spacecraft is retransmitted at S-band frequencies after multiplication by a factor of 240/221; the same signal is retransmitted from the spacecraft at X-band frequencies after multiplication by a factor of 880/221 (or a factor of 11/3 of the S-band retransmission frequency). Dual-frequency techniques for measuring the electron content along the station-spacecraft line of sight

were used during the Pioneer 6 and 7 missions and reported by Koehler of the Stanford Electronics Laboratory (Ref. 1). The major difference between the Stanford experiment and the one performed with Mariner 10 is that, in the former, a dual-frequency uplink was used with the results telemetered back to the tracking station, while, in the latter, a dual-frequency downlink was used, providing the capability of detecting both phase velocity and group velocity changes on the doppler and ranging channels, respectively.

The basic principle used in the dual-frequency technique is that electromagnetic propagation in a dispersive medium, by definition, is frequency dependent. In the transmission of a signal at S- and X-bands, however, the frequency separation is such that, upon differencing, the tropospheric dispersive effects remain negligible¹ while

¹The maximum dispersive effects due to troposphere correspond to a phase path change of about 1 cm at the observers' zenith.

the charged-particle effects remain distinguishable and may be computed. The dispersive effects of charged particles on the downlink phase and group velocities can be determined from the basic characteristics of electromagnetic propagation in a dispersive medium (Ref. 2). The change in phase path length induced by charged particles is given by

$$\begin{aligned}\Delta l &= -\frac{b}{w^2} \int_1^s N dl \quad (\text{meters}) \\ &= -\frac{Q}{f^2} I\end{aligned}\quad (1)$$

where

N = local electron content density

I = integrated content along the ray path, i.e., $\int_1^s N dl$

f = frequency of the transmitted signal

w = radian frequency, $2\pi f$

$b = e^2/2\epsilon_0 M$

$Q = b/4\pi^2 \cong 40.3$ in mks units

e = charge on an electron

m = mass of an electron

ϵ_0 = electric permittivity of free space

The group path delay is merely $-\Delta l$, due to the fact that the phase and group effects are equal and opposite. The phase path delay can usually be used only to obtain the charged-particle content relative to the first point of comparison, while group delay provides an absolute measure of the electron content because a point of reference can be found at that first point. By differencing the S- and X-band doppler and range observables from DSS 14, a measure of the dispersive phase and group effects was obtained. The use of these dispersive effects to calibrate the radio metric observables is reported by Winn and Yip in Ref. 3 and in the following article of this volume.² Additionally, a measure of the charged-particle content along the ray path was extracted using the relationship stated in Eq. (1) and the information provided to the Mariner Venus/Mercury 1973 Radio Science Team for their examination. A derivation and description of the algorithms used to process the doppler and range observables for the dispersive effects follows.

²F. B. Winn and K. B. Yip, "DSN-MVM'73 S/X Dual-Frequency Doppler Demonstration."

II. Dispersive Phase Effects

Referring to Fig. 1, the relationship required to measure the dispersive effects in phase velocity may be derived from the received doppler frequencies as follows:

For S-band, let

$$\begin{aligned}S_1 &= K_1 \cdot f_{os} \\ S_2 &= S_1 \left(1 - \frac{\dot{\rho}_1}{c}\right) + \Delta S_{1E} \\ S_3 &= \frac{240}{221} \cdot S_2 \\ S_4 &= S_3 \left(1 - \frac{\dot{\rho}_2}{c}\right) + \Delta S_{2E} \\ &= K_1 \cdot \frac{240}{221} \cdot f_{os} \left(1 - \frac{\dot{\rho}_1}{c}\right) \left(1 - \frac{\dot{\rho}_2}{c}\right) \\ &\quad + \frac{240}{221} \cdot \Delta S_{1E} \left(1 - \frac{\dot{\rho}_2}{c}\right) + \Delta S_{2E} \\ S_5 &= K_1 \cdot \frac{240}{221} \cdot f_{os} - S_4 + f_b\end{aligned}\quad (2)$$

and, for X-band,

$$\begin{aligned}X_3 &= \frac{240}{221} \cdot \frac{11}{3} \cdot S_2 \\ X_4 &= X_3 \left(1 - \frac{\dot{\rho}_2}{c}\right) + \Delta X_{2E} \\ &= K_1 \cdot \frac{240}{221} \cdot \frac{11}{3} \cdot f_{os} \left(1 - \frac{\dot{\rho}_1}{c}\right) \left(1 - \frac{\dot{\rho}_2}{c}\right) \\ &\quad + \frac{240}{221} \cdot \Delta S_{1E} \left(1 - \frac{\dot{\rho}_2}{c}\right) + \Delta X_{2E} \\ X_5 &= K_1 \cdot \frac{240}{221} \cdot \frac{11}{3} \cdot f_{os} - X_4 + f_b\end{aligned}\quad (3)$$

where

S_i = S-band frequencies at points i in link shown in Fig. 1

X_i = X-band frequencies also at points indicated in Fig. 1

ΔS_{1E} = frequency change due to charged particles on uplink,

$\Delta S_{2E}, \Delta X_{2E}$ = frequency change due to charged particles on downlink

f_{os} = station oscillator reference frequency,
 ~ 44 MHz for block IV receiver

f_b = bias frequency, 5 MHz for block IV receiver

ρ_1 = spacecraft topocentric velocity on uplink

ρ_2 = spacecraft topocentric velocity on downlink

c = velocity of electromagnetic propagation in vacuum

K_1 = uplink multiplier: 48 when $f_{os} \cong 44$ MHz;
 96 when $f_{os} \cong 22$ MHz

Then, by subtracting f_b from (2) and (3), factoring 11/3 from (3), and subtracting the results, we find that only the downlink dispersive effects remain, since

$$\frac{(X_s - f_b)}{\frac{11}{3}} - (S_s - f_b) = S_s - \frac{X_s}{\frac{11}{3}} = \Delta S_{2E} - \frac{\Delta X_{2E}}{\frac{11}{3}}$$

However, it is well known that, due to charged particles, $\Delta f \propto 1/f$ (Ref. 2) so that

$$\Delta X_{2E} : \Delta S_{2E} = S : X$$

and, since $X/S = 11/3$, then

$$\Delta X_{2E} = \frac{\Delta S_{2E}}{\frac{11}{3}}$$

Letting $K_X = 11/3$, this means that

$$S_s - \frac{X_s}{K_X} = \Delta S_{2E} - \frac{\Delta S_{2E}}{K_X} = \frac{K_X^2 - 1}{K_X^2} \Delta S_{2E}$$

from which we deduce that

$$\Delta S_{2E} = \left[\frac{K_X^2}{K_X^2 - 1} \right] \left[S_s - \frac{X_s}{K_X} \right]$$

or, equivalently, that

$$\Delta S_{2E} = \left[\frac{K_X^2}{K_X^2 - 1} \right] \left[\frac{X_s - f_b}{K_X} - (S_s - f_b) \right] \quad (4)$$

Thus relating the downlink dispersive effects in frequency to a difference of the two received doppler frequencies.

III. Dispersive Group Effects

The dispersive effects in group velocity may be derived in a simpler manner by noting that the S-band uplink effects are common to both S- and X-band range measurements, and, since the spacecraft multiplication factor applies only to the carrier and not to the range modulation, any difference between the range measurements at the two frequencies is due entirely to dispersive effects on the downlink, i.e.,

$$\Delta R_{SX}(t) = R_S(t) - R_X(t) = \Delta R_{SS} - \Delta R_{EX}$$

where

$R_S(t)$ = S-band range measurement

$R_X(t)$ = X-band range measurement

ΔR_{SS} = group delay due to charged particles at S-band

ΔR_{EX} = group delay due to charged particles at X-band

Since dispersive path delay is inversely proportional to the square of the received frequency (Ref. 2), then

$$\Delta R_{EX} = \frac{\Delta R_{SS}}{K_X^2}$$

and, therefore,

$$\Delta R_{SX} = \Delta R_{SS} \left(1 - \frac{1}{K_X^2} \right) = \Delta R_{SS} \left(\frac{K_X^2 - 1}{K_X^2} \right)$$

Solving for ΔR_{SS} we then obtain

$$\Delta R_{SS} = \left[\frac{K_X^2}{K_X^2 - 1} \right] [R_S(t) - R_X(t)] \quad (5)$$

thus relating the dispersive group effects to a difference of two simultaneous range measurements taken at two distinct frequencies.

IV. Application

The doppler and range observables obtained from DSS 14 are not in the form such that Eqs. (4) and (5) may be applied directly. Doppler is reported as a cumulative cycle count obtained by measuring the received frequency at predetermined intervals. The contents of the counter are reported at specific sample time τ_c . The cumu-

lative S- and X-band doppler counts may be represented as (see Fig. 1)

$$D_s(t_i) = \sum_{i=1}^n \tau_c S_s(t_i)$$

$$D_x(t_i) = \sum_{i=1}^n \tau_c X_s(t_i)$$

and the dispersive phase delay equation equivalent to (4) as

$$\begin{aligned} \Delta\rho_E(t) = & \left[\frac{c}{K_1 K_2 f_{os}} \right] \left[\frac{K_X^2}{K_X^2 - 1} \right] \\ & \times \left[\frac{[D_x(t) - D_x(t_0) - f_b \cdot (t - t_0)]}{K_X} \right. \\ & \left. - [D_s(t) - D_s(t_0) - f_b(t - t_0)] \right] \end{aligned} \quad (6)$$

where

$\Delta\rho_E$ = dispersive effect expressed in terms of meters of phase delay relative to t_0

K_1 = ground transmitter multiplier

K_2 = S-band spacecraft transponder multiplier 240/221

K_X = additional spacecraft multiplier required to obtain the downlink X-band frequency, 11/3

$D_s(t), D_x(t)$ = S- and X-band doppler counts accumulated up to time t

$D_s(t_0), D_x(t_0)$ = initial counter readings at time t_0

Similarly, the range equation (5) must be modified in consideration of the fact that the range reported by the sequential ranging machine contains phase velocity effects as well as the theoretically expected group velocity effects³ (Ref. 4). After adding the appropriate conversion factors

to obtain units of meters, the corresponding equation for range is

$$\Delta\rho_E(t) = \left[\frac{c}{64 \cdot K_1 \cdot f_{os}} \right] \left[\frac{K_X^2}{K_X^2 - 1} \right] \left[\frac{R_s(t) - R_x(t)}{2} \right] \quad (7)$$

where $R_s(t)$ and $R_x(t)$ are the range values, in range units, obtained from the R&D ranging machine, which was used in conjunction with the Block IV receiver. Range values from this machine are defined as follows (Ref. 5):

$$\begin{aligned} R = & \left[T - M \frac{128 \cdot 2^N}{3 f_{os}} + \frac{B_{DSN}}{64 \cdot K_1 \cdot f_{os}} \right. \\ & \left. + B_{s/c} - Z \right] 64 \cdot K_1 \cdot f_{os} \end{aligned}$$

where

T = round-trip light time

M = modulo number

N = number of components

B_{DSN} = ground equipment bias

$B_{s/c}$ = spacecraft bias

Z = zero delay device factor

(The distinction between S and X values corresponds to the carrier frequency which is modulated by the ranging signal.)

Due to anomalous conditions in the experimental receiver hardware, which were corrected as the mission progressed, discontinuities in the doppler data occurred which caused values produced using Eq. (6) to be grossly in error. These problems were ameliorated, however, by merely redefining the interval $(t - t_0)$ to be $(t_i - t_{i-1})$.⁴ In this manner each point computed could be evaluated to determine its validity; invalid points were replaced using an estimate of the information lost. A cumulative effect was then produced by summing the incremental points computed over the tracking pass, viz.,

$$\Delta\rho_E(t) = \sum_{i=1}^n \hat{\Delta\rho}_E(t_i)$$

⁴Based on a suggestion by John Ondrasik, Section 391.

³The range measurements produced by the sequential ranging machine are influenced by both phase and group velocity effects in an additive manner. The transmitted range modulation is affected in group velocity, while the receiver's synthesized signal is affected by the phase velocity errors inherent in the doppler used for the rate-aided control loop. Differenced range measurements must therefore be divided by 2 to obtain actual dispersive effects.

where $\hat{\Delta\rho}_B(t_i)$ is the incremental phase delay defined over the interval $t_i - t_{i-1}$, and n is the number of points in the pass.

V. Verification

The experience reported by Winn and Yip (Ref. 3 and Footnote 2) provides adequate verification of these techniques. Figure 2 illustrates, however, the generally good comparison between electron content obtained from the dual-frequency doppler technique and the Faraday rotation technique described by Mulhall, et al., in Ref. 6. Naturally, the case shown represents the data obtained

on a day when interplanetary plasma effects were negligible.⁵ By verifying the accuracy of the technique on cases of this sort, differences between the two data types on other occasions can be attributed to either interplanetary effects or Faraday mapping errors with a high degree of confidence. The exceptional cases occur when, because of hardware problems, the data become inconclusive.

⁵Faraday rotation measurements, taken using the signal from a linearly polarized antenna on an Earth satellite, only provide information regarding the Earth's ionosphere. The dual-frequency techniques described here provide a measure of the change in total columnar content on the downlink path between the spacecraft and station.

References

1. Koehler, R. L., *Interplanetary Electron Content Measured Between Earth and the Pioneer VI and VII Spacecraft Using Radio Propagation Effects*, Report 67-051, Stanford Electronics Laboratories, Stanford University, May 1967.
2. Laurence, R. S., Little, C. G., and Chivers, H. J. A., "A Survey of Ionospheric Effects Upon Earth-Space Radio Propagation," *Proc. IEEE*, Jan. 1964.
3. Winn, F. B., and Yip, K. W., *S/X Dispersive Doppler Demonstration, Report 1*, IOM 391.3-772, Feb. 1, 1974 (JPL internal document).
4. MacDoran, P. F., and Martin, W. L., "DRVID Charged-Particle Measurement With a Binary-Coded Sequential Acquisition Ranging System," in *The Deep Space Network*, Space Programs Summary 37-62, Vol. II, pp. 34-41, Jet Propulsion Laboratory, Pasadena, Calif., Mar. 31, 1970.
5. Chaney, W. D., *Ranging Equations for MVM-73*, IOM 401-3223, June 23, 1972 (JPL internal document).
6. Mulhall, B. D., Ondrasik, V. J., and Thuleen, K. L., "The Ionosphere," in *Tracking System Analytic Calibration Activities for the Mariner Mars 1969 Mission*, Technical Report 32-1499, pp. 45-68, Jet Propulsion Laboratory, Pasadena, Calif., Nov. 15, 1970.

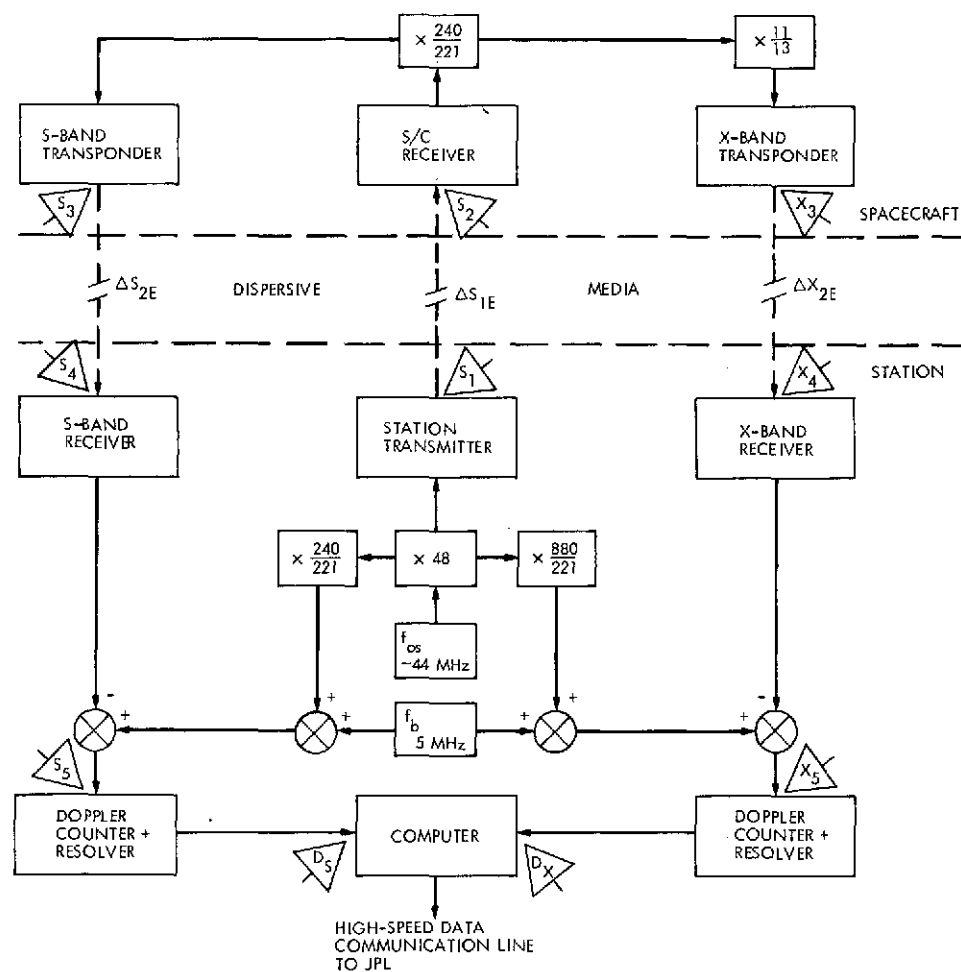


Fig. 1. Conceptual diagram of Mariner 10-DSS 14 dual-frequency doppler configuration

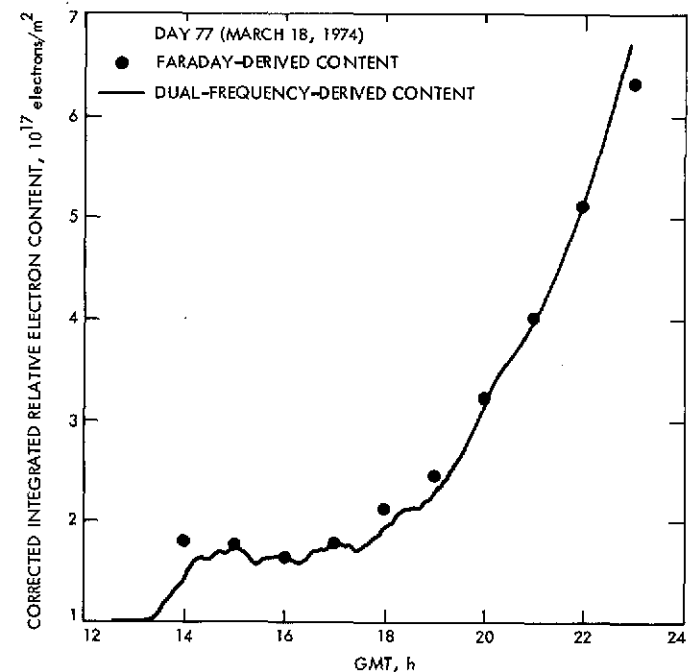


Fig. 2. Comparison of computed dispersive effects and Faraday rotation-derived data on day with apparent negligible plasma activity

DSN-MVM'73 S/X Dual-Frequency Doppler Demonstration

F. B. Winn, K. W. Yip, and S. J. Reinbold
Tracking and Orbit Determination Section

Doppler charged-particle calibrations derived from S/X dual doppler data have been demonstrated successfully. The accuracy of the S/X dual doppler has been verified by comparisons to Faraday polarization data. This verification, limited by the accuracy of "mapped" Faraday data, is to the 10- to 30-cm level. The S/X dual doppler exhibits subcentimeter resolution and, thus, its potential accuracy. The S/X dual doppler calibrations are significant to the Mariner 10-Mercury encounter orbit determination. The error of the estimate of the Mariner 10-Mercury target plane coordinate was reduced by ~ 500 km ($\sim 80\%$ improvement).

I. Introduction

The DSN successfully used the Mariner Venus/Mercury 1973 (MVM'73) mission (Mariner 10) to demonstrate that dual-frequency doppler measurements, when differenced, provide line-of-sight, radio metric doppler calibrations for charged-particle influences. These calibrations assess collectively the influences of the space plasma and Earth's ionosphere. Thus, when the plasma electron content variations are insignificant, the dual-frequency doppler data compare quite well with Faraday polarization data. In these instances, both measure variations in the Earth's ionospheric electron content.

The dual-frequency doppler was used to significantly improve the Mercury target plane position determinations based on the tracking data acquired from the one tracking station with a dual-frequency capability—DSS 14. The Mariner 10 position estimate error was reduced by $\sim 80\%$ (~ 500 km).

II. S/X Dual Doppler Quality (Verification)

A 2200-MHz (S-band) radio wave is transmitted from a DSS to the Mariner 10 spacecraft. The received frequency is then retransmitted at an S-band frequency 240/221 times higher. Simultaneously, the received frequency is also retransmitted at an X-band frequency. This transmitted X-band frequency is equal to the spacecraft received frequency multiplied by 880/221. The S- and X-band transmissions from the spacecraft are then received at DSS 14, which has the only dual-frequency receiver currently existing within the DSN. S/X dual Doppler exploits the inverse frequency squared dependence of the phase velocity change of a radio signal traversing a tenuous plasma. The doppler shifts present in the received S- and X-band tones measure two occurrences: the radial motion of the spacecraft as seen from DSS 14, and the net change in the total number of electrons encountered along the ray path. That portion of the doppler shift resulting from radial motion of the

probe is removed by differencing the doppler shifts, and the balance is due to charged particle effects. In equation form, the procedure to compute the balance is

$$\text{Balance} = K(S - \frac{3}{11}X)/f_{q_s}$$

In other words, the X-band frequency is multiplied down to an equivalent S-band frequency and differenced from the S-band received frequency. This difference in the net frequency change at S-band is then due entirely to electron content variations. The ratio of the S-band frequency change to the S-band frequency can be easily converted to electron content variations or apparent range change of the spacecraft. (A detailed discussion of this physical process and the specific equations used are presented in the preceding article of this volume by G. A. Madrid, "The Measurement of Dispersive Effects Using the Mariner 10 S- and X-band Spacecraft to Station Link.)

To date, only two charged-particle calibrators can achieve submeter level precision: S/X dual doppler and Faraday polarization data (Ref. 1). Other calibrators, differenced range versus integrated doppler (DRVID) (Ref. 2) and dual S/X range, provide charged-particle assessments to the precision of the DSN range data which is typically meters.

It should be noted that the Faraday rotation data are obtained from measurements to geostationary satellites. At the Goldstone DSN complex (site of DSS 12 and DSS 14), three Faraday polarimeters¹ continuously monitor the amount of rotation experienced by the plane polarized transmissions of the Applied Technology Satellites ATS-1 and ATS-5. These observations provide a measure of Earth's ionospheric electron content and its time-rate of change. The Faraday polarization data must be mapped from the DSS-satellite line-of-sight to a planetary spacecraft. This mapping technique is based on a mathematical model (Ref. 1), which is frequently inadequate at low topocentric elevation angles. Typically, the uncertainty of mapped Faraday for lines-of-sight taken above 30 deg elevation is ~ 0.1 m (1σ). For elevation angles below 30 deg, the uncertainty is 0.3 m (1σ).

The situation can be stated thus: If the S/X dual doppler data and the "mapped" Faraday polarization data show the same electron content history, within the precision of the "mapped" Faraday data, no plasma activity of significance is assumed to exist and the S/X dual

doppler data are valid; if the S/X doppler data cannot be favorably compared to the Faraday data, it is possible that the S/X dual doppler is "seeing" solar plasma activity. In short, the S/X dual doppler can be verified only if it compares to the mapped Faraday data on some occasions.

The Faraday polarization data used in these comparisons were sampled every 10 min. The S/X dual doppler, as processed, only provides $\frac{1}{2}$ the high-frequency resolution inherent in the data. A subsequent analysis will address the high-frequency structure of both data types in more detail.

Space plasma activity was usually insignificant during the MVM73 mission (December 15, 1973 to March 29, 1974), thus permitting favorable comparisons of Faraday and S/X doppler data. A detailed analysis of the first three S/X dual doppler passes is available in the Appendix. About 60% of the S/X data passes compare well with the "mapped" Faraday data. For the other 40%, it was known that, some of the time, the differences between the S/X dual doppler and the Faraday data had nothing to do with charged particles. On these occasions, the DSS 14 experimental dual-frequency receiver (especially developed and installed for this demonstration by G. Levy and others) was being tested in a nonstandard operating mode or some component of the R&D ground-based hardware was known to be malfunctioning. When the DSS 14 R&D hardware was in a standard operating mode and functioning, usually the dual doppler and the Faraday data agreed.

Comparisons of the available S/X dual doppler and "mapped" Faraday data through Mercury flyby (March 29, 1974) are shown in Fig. 1. As can be seen, for some passes (ten in number), the dual doppler and Faraday agree over the entire tracking pass, i.e., the two calibrations do not differ by more than 0.1 m in cumulative range error change. Some passes (twelve in number) show similar agreement for the two calibrations when the elevation angle associated with the S/X dual doppler observation is greater than 30 deg. There are still other passes (seven in number) for which the differences between the two calibrations are in excess of 1 m. The passes shown having this character are believed to be exhibiting real space plasma effects. The evidence in support of this conjecture comes in four parts:

- (1) S/X dual doppler data detection of high plasma activity.
- (2) The charged-particle detector aboard the spacecraft recorded high ion levels and fluctuations.

¹One of the polarimeters is deployed and used by the Stanford Radio Science Laboratory under the direction of T. Howard, the MVM73 Radio Science Team Leader.

- (3) S-band radio metric doppler showed structure not related to the normal phenomena encountered.
- (4) Earth's ionosphere, as measured by the Faraday polarization data, was excited. This excitement stems from the solar plasma interaction with the ionosphere. The ionosphere showed activity 2.5 times higher than the normal at times.

There are six additional passes of S/X dual doppler data which do not correlate with the "mapped" Faraday data, and there are other indications that the dual doppler are unreasonable. These passes are still undergoing investigation.

Table 1 tabulates 27 S/X dual doppler-Faraday comparisons. From this tabulation it is apparent that ~40% of the dual doppler sample agrees with the Faraday. Another ~40% of the passes shows agreement for all data acquired above 30-deg elevation. The remaining 20% of the sample exhibits space plasma effects.

Besides the gross structure of the S/X dual doppler, which contains the charged-particle information, the dual doppler shows a high-frequency noise. An examination of the high-frequency data noise of the December 15, 1973 pass reveals the resolution of the dual doppler calibration technique (Fig. 2). Figure 2 plots about a 1-h segment of the S/X doppler data. The plot provides a high-resolution view of these data. The S/X dual doppler was acquired at a rate of one point per minute. A parabola was fit to the data shown. The detrended residuals produced by the fit have a standard deviation of 0.76 cm. Thus, the S/X data of Day 349 have near centimeter resolution. This is the anticipated noise level.

III. MVM'73 Orbit Determination: Short Data Arc Analysis—A Problem

Mariner 10 arrived at Mercury on March 29, 1974. It was launched from Earth 5 mo earlier. The Mariner 10 spacecraft moved along transfer orbits that carried it from Earth to Venus and from Venus to Mercury (Fig. 3). The Earth-Venus, Venus-Mercury ballistic trajectories were altered by corrective maneuvers of the spacecraft rocket and by gas leaks developed on the spacecraft. In all, there were six instances when the spacecraft experienced "large" nongravitational accelerations:

- (1) Earth launch (November 3, 1973).
- (2) Trajectory correction maneuver 1 (TCM1) (November 13, 1973).
- (3) TCM2 (January 21, 1974).

- (4) Gas leak (January 28, 1974).
- (5) Gas leak (February 10, 1974).
- (6) TCM3 (March 16, 1974).

Figure 3 shows their locations along the trajectories.

An examination of the Faraday and S/X dual doppler data shows that plasma activity appears to be insignificant for the time periods following the first five events: Earth launch, TCM1, TCM2, the January 28 gas leak, and the February 10 gas leak. Faraday polarization data were used to remove the ionospheric charged-particle effects from the DSS 12 and DSS 14 tracking data acquired during these periods. The improvements realized in the encounter navigation are detailed in Refs. 4, 5, 6, and 7. DRVID, as well as Faraday, was used for calibration for the post-Earth launch data segment. The DRVID calibrations and their significance to navigation is the subject of Ref. 8.

After each nongravitational acceleration of the probe, it is desirable to estimate the new orbit of the spacecraft and determine how this orbit will carry the probe to the target planet. This was accomplished by S. J. Reinbold, C. S. Christensen, and G. E. Pease of the Navigation Team. Initial estimates of the new trajectory used four days of tracking data. Now it is known that short data arc solutions of this kind are prone to be sensitive to charged-particle influences, i.e., erroneous orbit solutions can result (Ref. 3). This is particularly true of the plasma activity which is unusually high.

Plasma ion levels and fluctuations during the week following TCM3 seriously degraded the Mercury approach navigation. The existence of plasma disturbances was ascertained by three direct measurements: S/X dual doppler measurements from DSS 14, DRVID measurements from DSS 43 and DSS 63, and ion detector measurements² on the spacecraft. There are two additional sources that indicate large plasma activity: the earth's ionosphere became most excited during this time, frequently being over 2.5 times more active than normal; the S-band doppler, the principle data type used to track the spacecraft and to navigate the spacecraft, showed a medium amplitude structure (~10 mHz amplitude) (Fig. 4) of a nonperiodic nature during the week.

The analysis by the Navigation Team on the doppler tracking data, corrupted by such plasma variations, provided Mercury encounter position estimates which were inconsistent. The Mercury encounter position estimates

²C. Yeates, Radio Science Team, private communication.

were scattered over 550 km (5 day arc). To circumvent the plasma degradation, a data editing process was conducted by R. E. Koch (Navigation Team) that eventually deleted ~50% of the doppler tracking data acquired by DSS 14, DSS 43, and DSS 63. Only after this editing did the Mercury encounter solutions become consistent and reasonable. Post-Mercury encounter knowledge reveals that the error was less than 40 km at Mercury.

The distribution of the S/X dual doppler tracking passes over the 9-day data arc is pictured in Figs. 5a and 5b.

IV. Elimination of Charged-Particle Effects by S/X Dual Doppler Calibration

The phase velocity change of doppler induced by charged-particle variations can be interpreted falsely as an apparent range change of the spacecraft. Figure 1 shows what the apparent range change is for specific times as measured by Faraday polarization data and S/X dual doppler. However, it is doppler, not range, that is to be calibrated for electron content variations. Thus, it is the time-rate-of-change of the apparent range that is required.

During the 9 days following trajectory correction maneuver 3 (TCM3), when known plasma activity was occurring, six tracking passes of S/X dual doppler were acquired at DSS 14. The doppler calibrations computed from this dual S/X data are pictured in Fig. 6, along with the corresponding Faraday-based doppler calibrations.

Each plot in this figure corresponds to a tracking pass. Two of the plots, namely that of March 18 and March 24, show the two calibrations in reasonably good agreement. Thus, little plasma activity is present during these two passes. The remaining four passes, however, reveal plasma activity.

Figure 7 shows the doppler residuals that result when the Mariner 10 orbit is adjusted in a least squares process which fits the doppler tracking data (119 doppler data points) and range tracking data (20 range data points). These residuals exhibit biases (March 20, March 23), and slopes (March 16, March 18, and March 24).

Figure 8 shows how the after-the-fit doppler residuals appear when the doppler tracking data are calibrated for charged-particle effects before least squares fitting. The residuals that involved S/X dual-frequency data calibrations (with the one exception of the March 16 pass) do not show biases or slopes. The quality of the Doppler fit

is improved in terms of the sum of the squares of the doppler residuals. The unit standard deviation of the doppler residuals decreased by over 70%. When Faraday polarization data were used as the doppler calibration source, the standard deviation of the doppler residuals decreased by ~50%.

V. Significance of Calibration to MVM'73 Navigation at Mercury Encounter

When the MVM'73 Navigation Team used the tracking data (doppler and range from DSS 14, DSS 43, and DSS 63) that was acquired in the 9 days following TCM3 (March 16, 1974), the estimates of the Mariner 10-Mercury encounter coordinates scattered over 200 km. Valid predictions of the Mariner 10 encounter coordinates were obtained by rejecting much of the plasma-affected doppler data. This "predicted" position is shown in Fig. 9 along with the actual position known to be "true" from Mercury flyby data.

When the DSS 12 and DSS 14 doppler tracking data are used to estimate the encounter coordinates of Mariner 10 with and without Faraday calibrations, it is found that the calibrations reduced the error of the estimates by ~60% (~110-km displacement) (Fig. 9). When DSS 14 data are used to estimate the encounter coordinates with and without S/X dual doppler calibrations, it is found that the calibrations reduce the error of the estimates by ~80% (~500-km displacement) (Fig. 10). These two solutions did not support Mercury approach navigation—they were arrived at after Mercury encounter as a demonstration of navigation capability improvements.

Another estimate of the encounter coordinates was made with a combination of the Faraday and S/X dual doppler calibrations. If S/X dual doppler existed for a pass, it was used. If it was not available, the Faraday calibrations were used. The improvement realized by the joint use of the two calibration types is ~80% (180-km displacement) (Fig. 11).

Charged-particle calibrations used in this data arc reduction, and in other data arc reductions (Refs. 4, 5, 6, and 7) have consistently decreased the error of the encounter position estimates.

VI. Summary

The S/X dual doppler has measured space plasma and the Earth's ionospheric charged-particle variations. These measurements were used in support of MVM'73 mission navigation.

Table. 1. MVM'73: S/X data quality relative to Faraday

Month	Day of month																															
	1	2	3	4	5	6	7	8	9	10	11	12	13	14	15	16	17	18	19	20	21	22	23	24	25	26	27	28	29	30	31	
Nov.																																
Dec.															1																2	
Jan.			1											1	1							2	3	3		2					1	
Feb.					2	2	2		2							1			2			3										
Mar.	1						2			2						3	3	1		3			3/1	1				2	2			
Apr.																																

S/X dual doppler populations:

- Population 1. S/X dual doppler and Faraday rotation data agree (difference < 0.1 m).
- Population 2. S/X dual doppler and Faraday agree at higher elevations (difference < 0.1 m above 30 deg).
S/X dual doppler and Faraday differences < 0.3 m above 10-deg elevation.
- Population 3. Partial agreement or no agreement.

Entries in table indicate quality of S/X dual doppler-Faraday data comparisons.

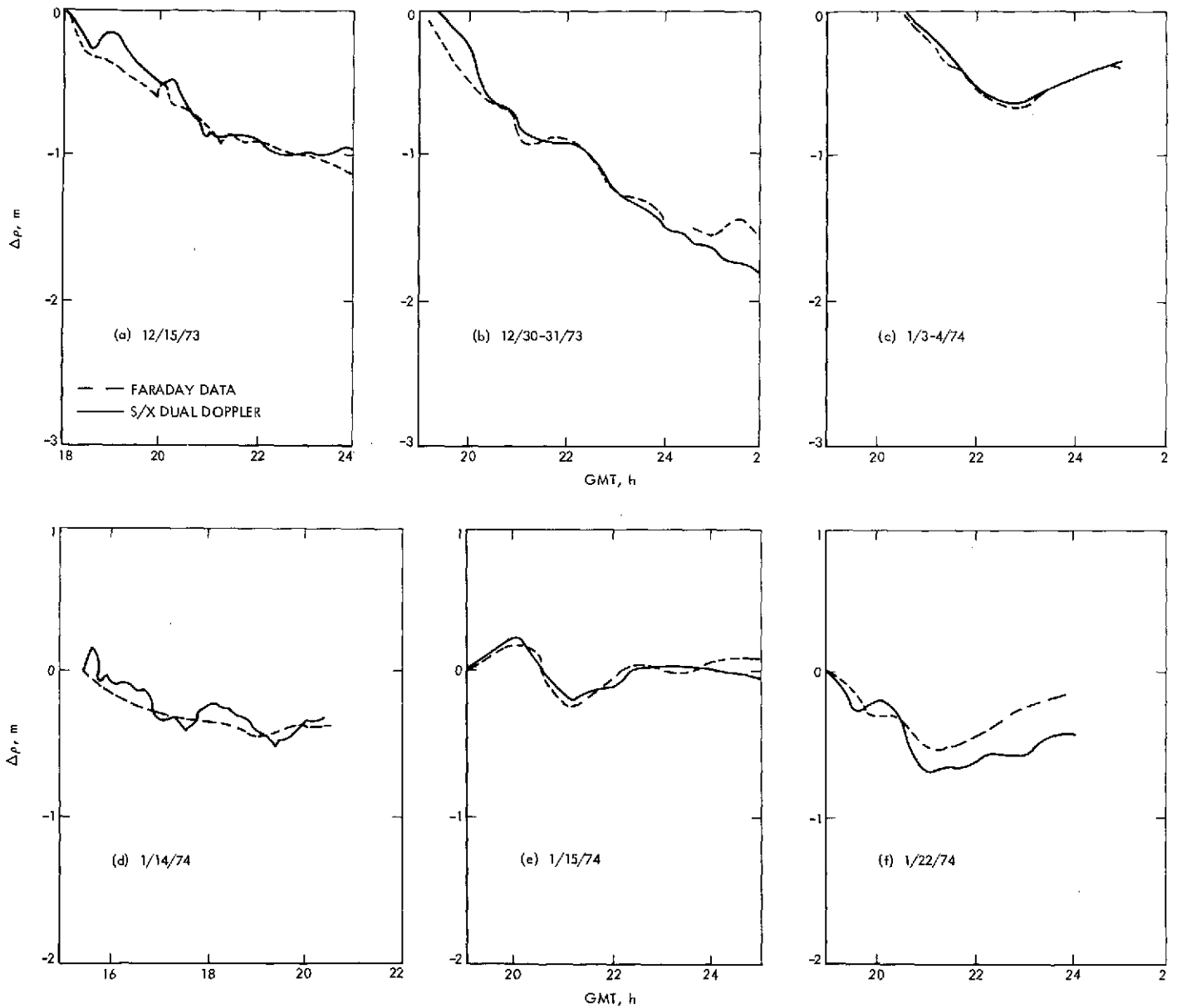


Fig. 1. S/X dual doppler and Faraday polarization data comparisons

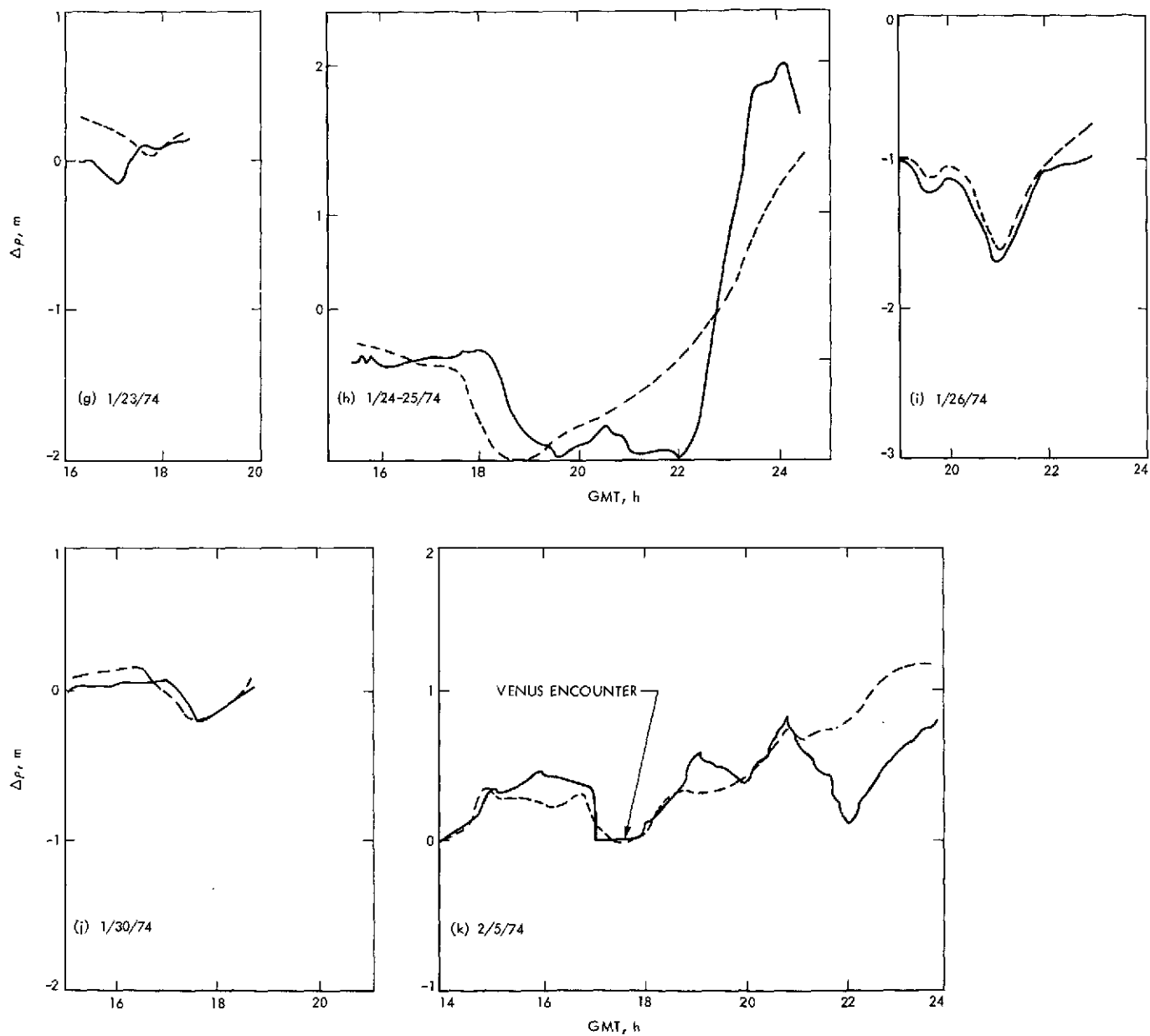


Fig. 1 (contd)

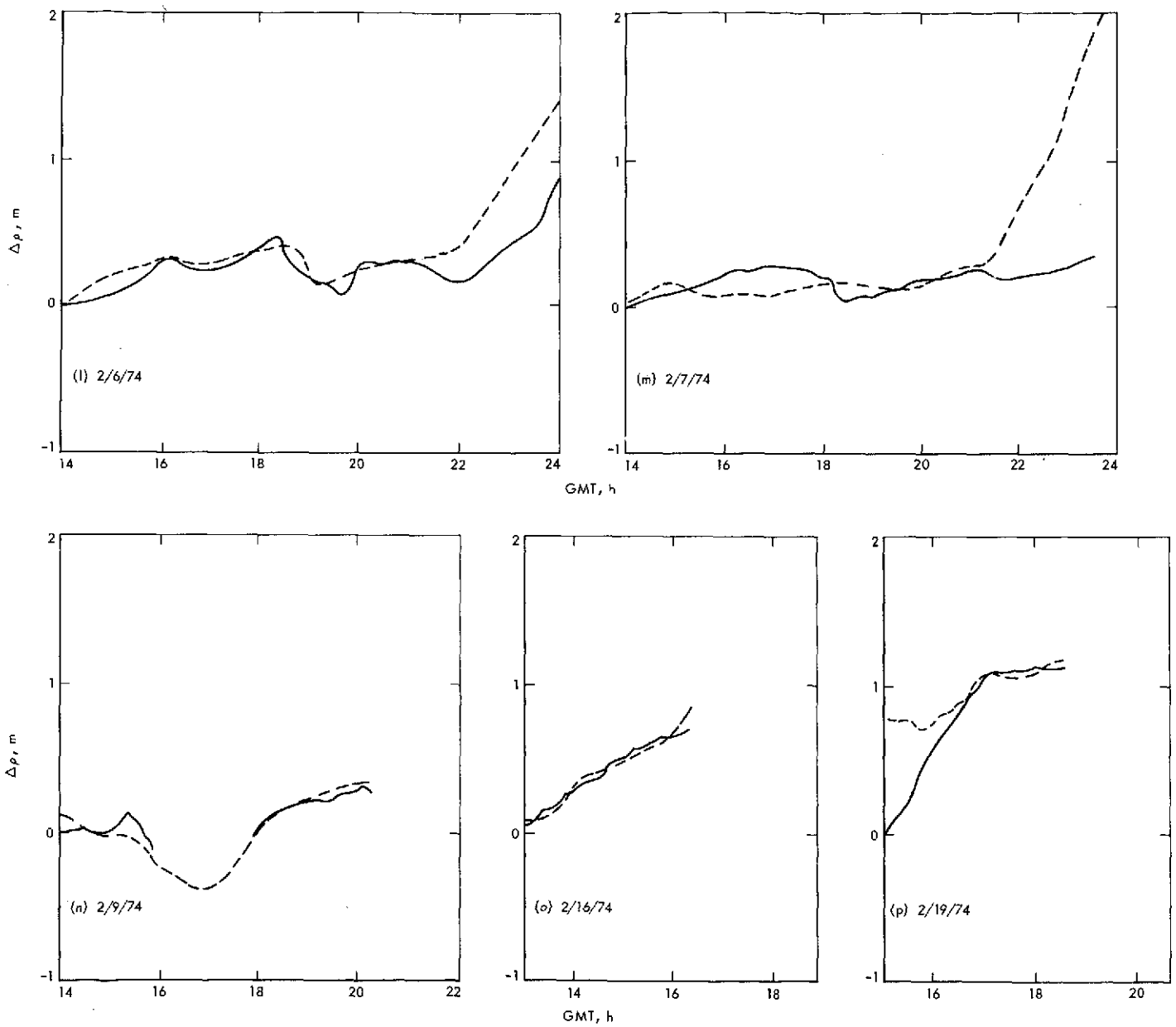


Fig. 1 (contd)

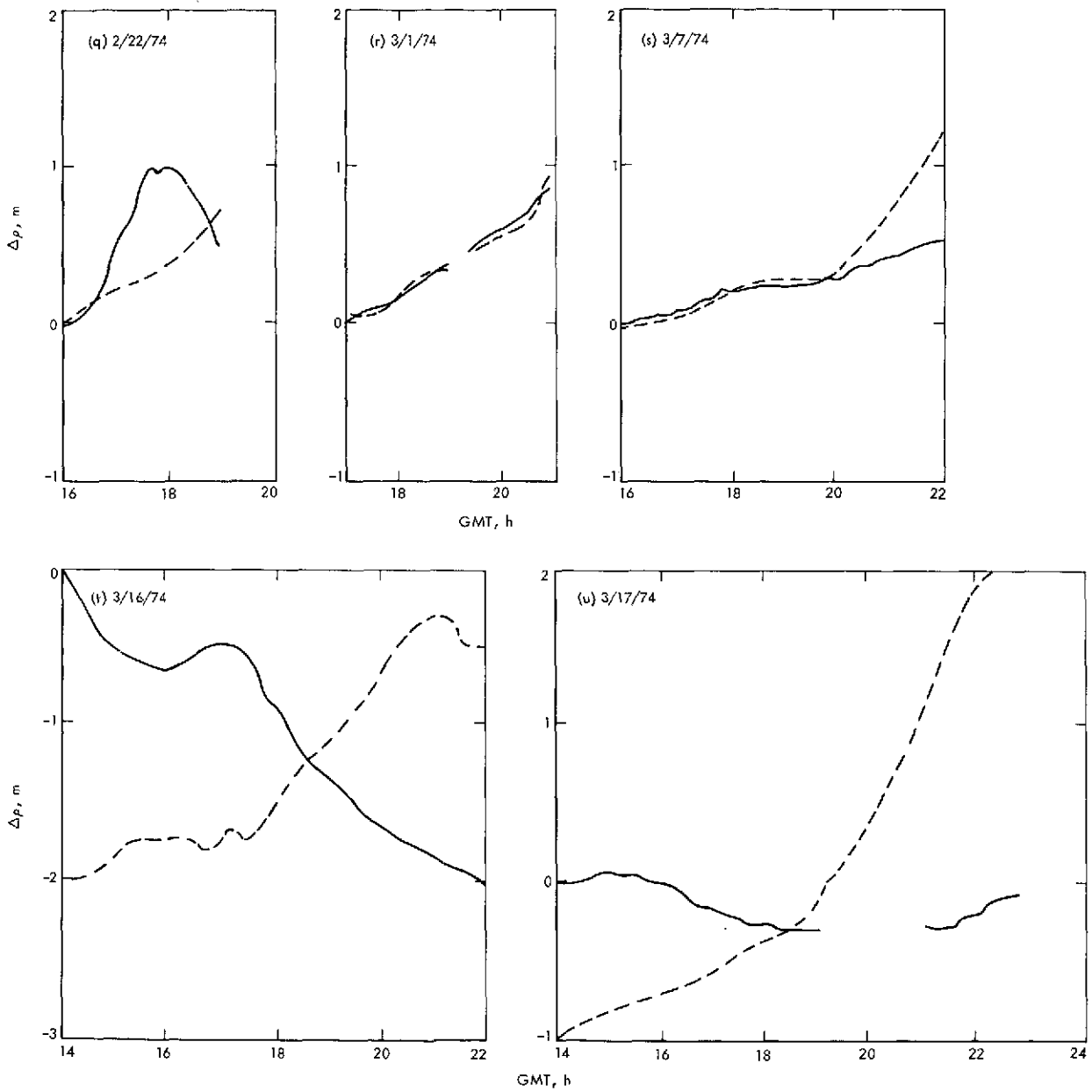


Fig. 1 (contd)

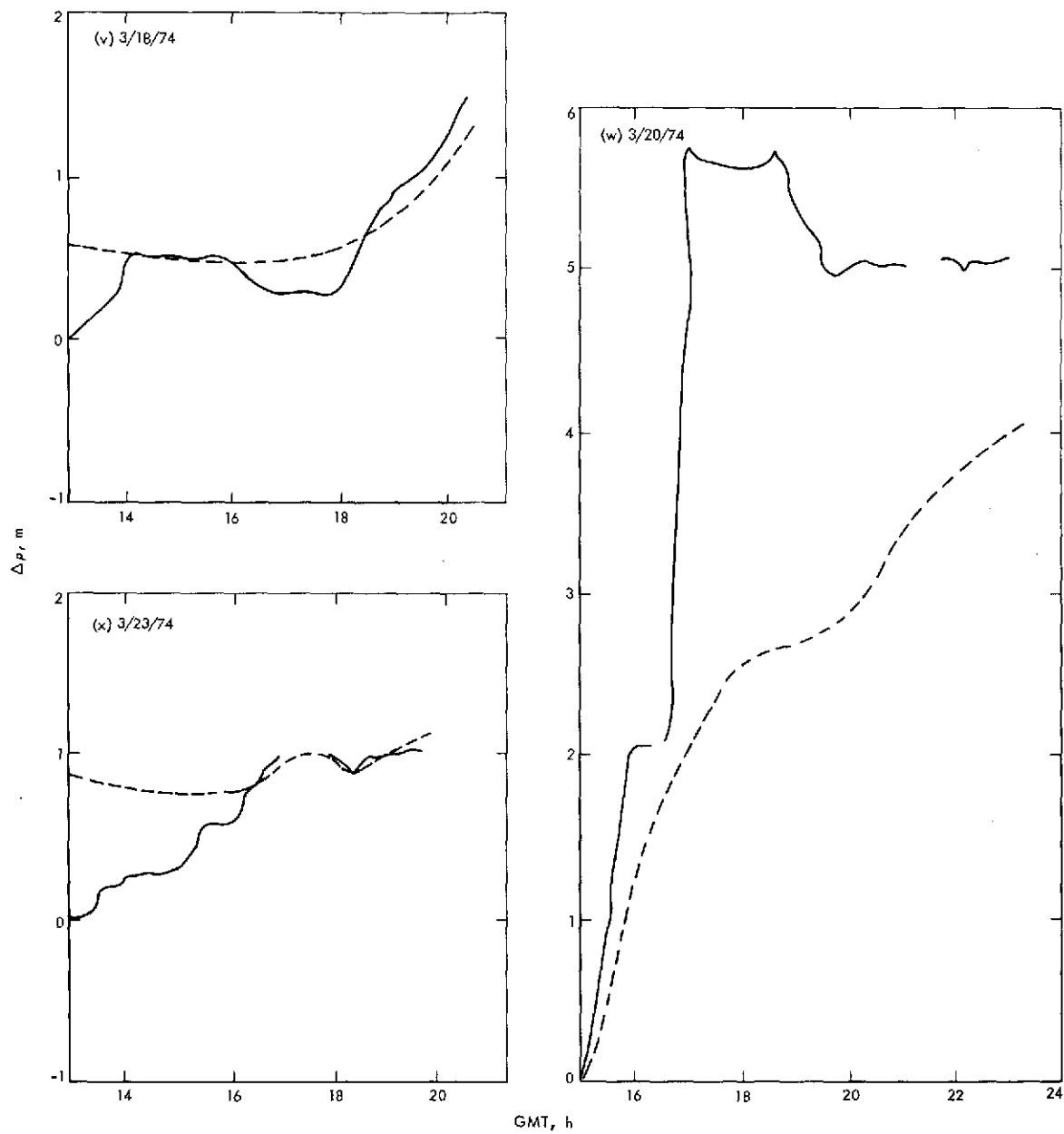


Fig. 1 (contd)

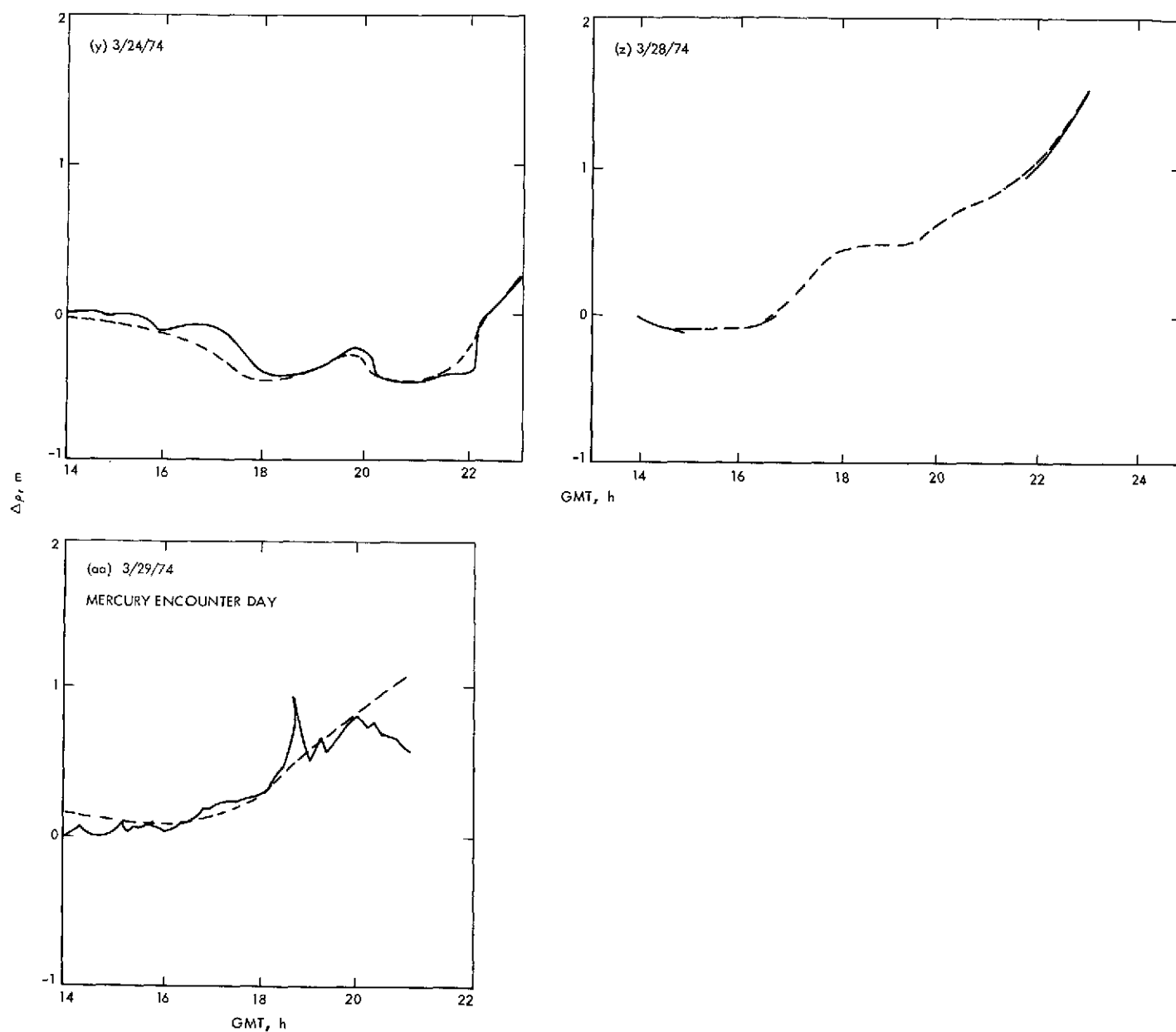


Fig. 1 (contd)

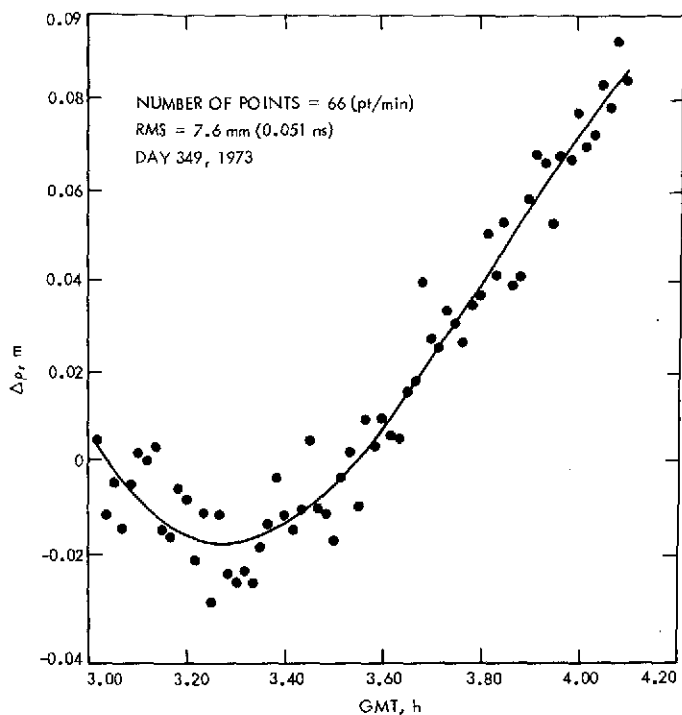
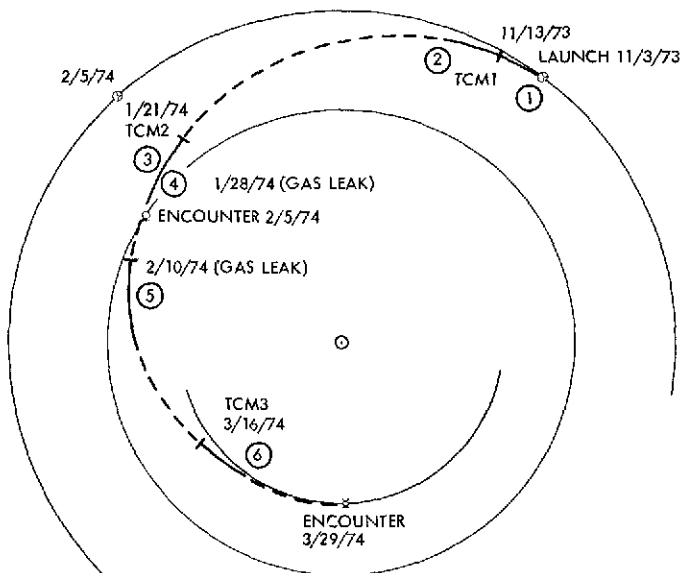


Fig. 2. High-frequency S/X dual doppler noise



TRAJECTORY ARC 1: CALIBRATED FOR CHARGED PARTICLES VIA FARADAY AND DRVID (REFS. 2-6)
 TRAJECTORY ARC 2: CALIBRATED FOR CHARGED PARTICLES VIA FARADAY (REF 3)
 TRAJECTORY ARC 3: CALIBRATED FOR CHARGED PARTICLES VIA FARADAY (REF 4)
 TRAJECTORY ARC 5: CALIBRATED FOR CHARGED PARTICLES VIA FARADAY
 TRAJECTORY ARC 6: CALIBRATED FOR CHARGED PARTICLES VIA FARADAY AND S/X DUAL DOPPLER (REF 5)

Fig. 3. Trajectory segments: short data arcs calibrated and reduced

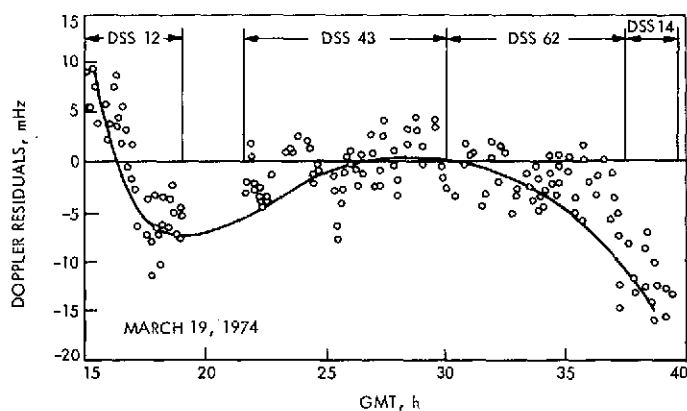


Fig. 4. Space plasma signature present in doppler residuals (count time = 600 s)

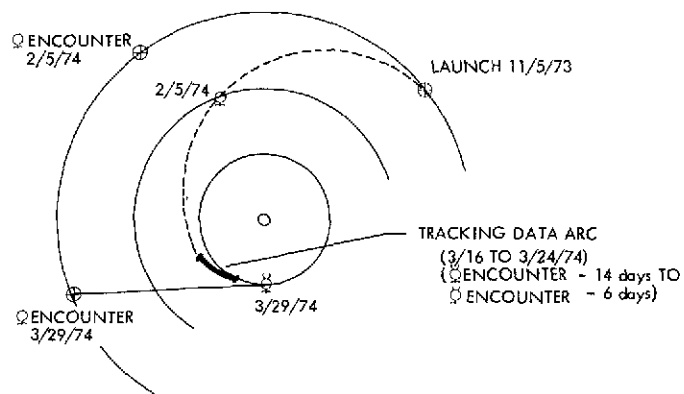


Fig. 5a. Heliocentric plot: MVM'73 transfer trajectory with short data arc shown

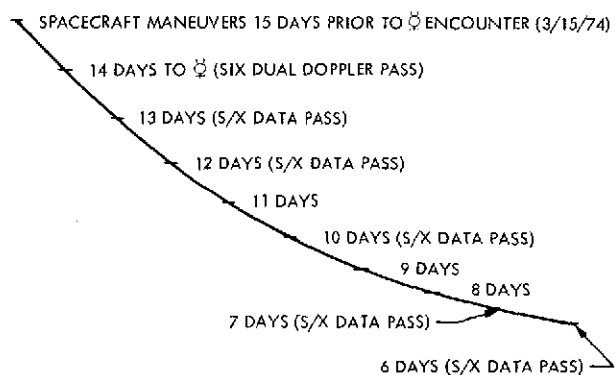


Fig. 5b. S/X dual doppler distribution over tracking data arc

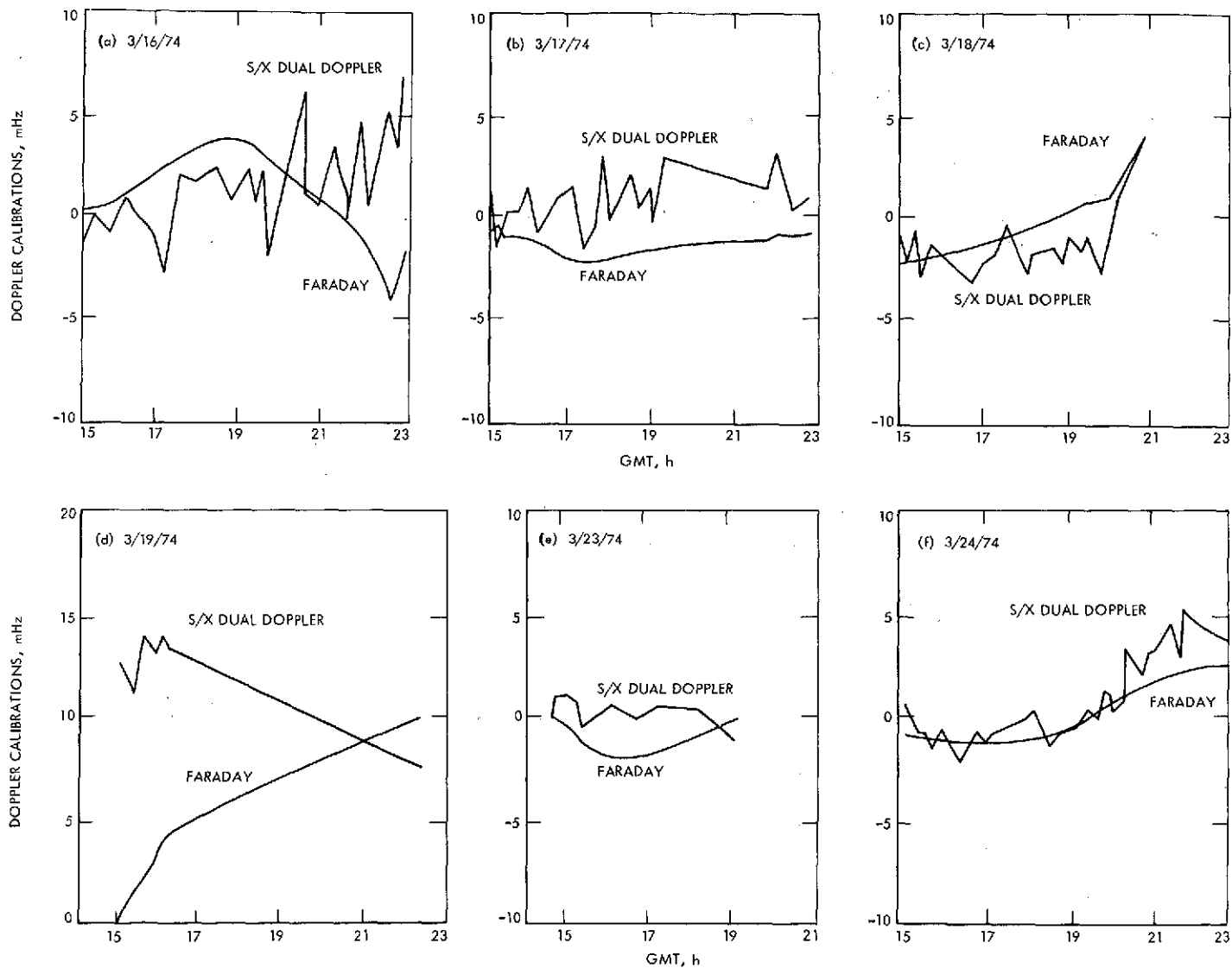


Fig. 6. Doppler calibrations: S/X dual doppler and Faraday polarization

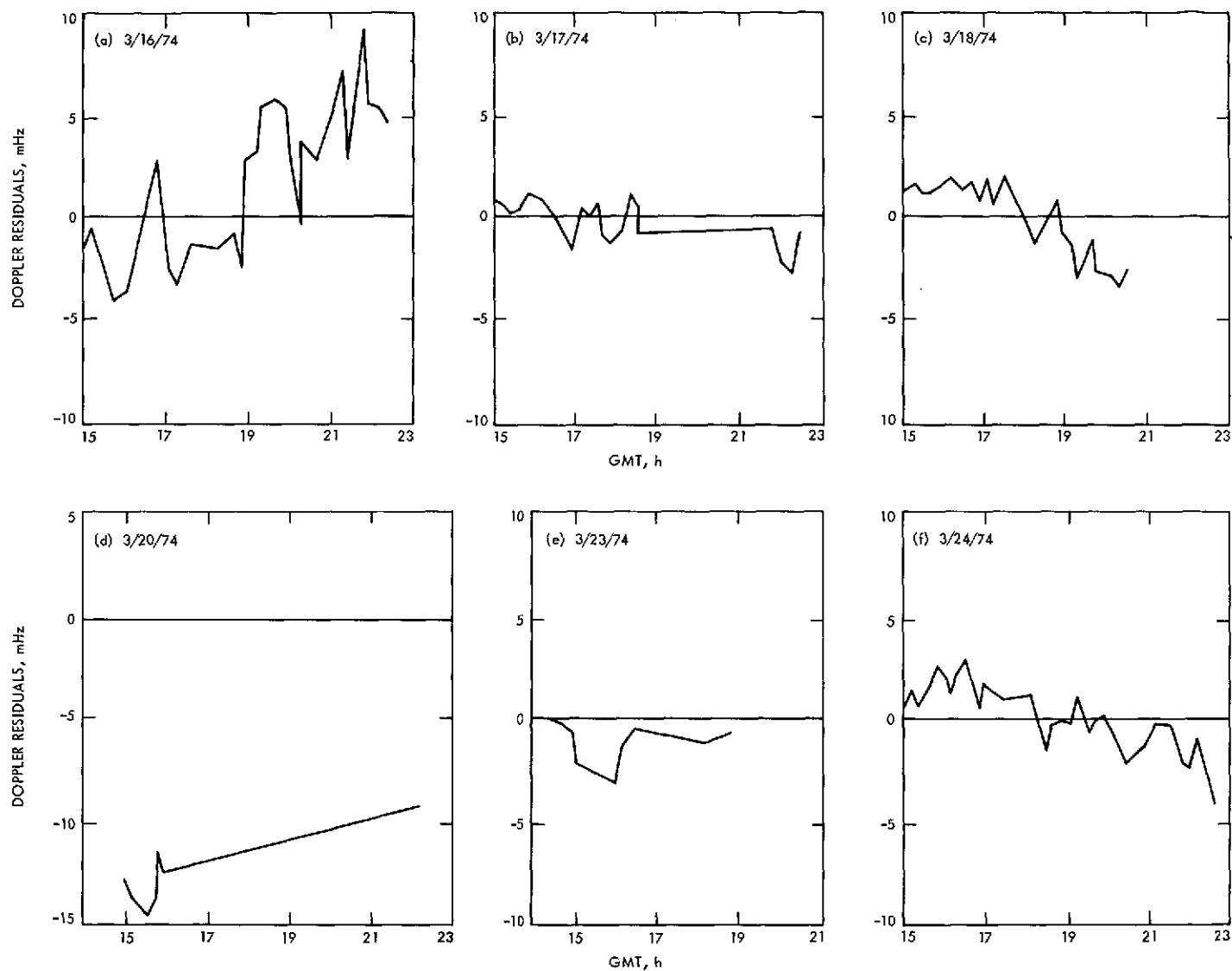


Fig. 7. S-band doppler residuals (600-s count time; no charged-particle calibrations)

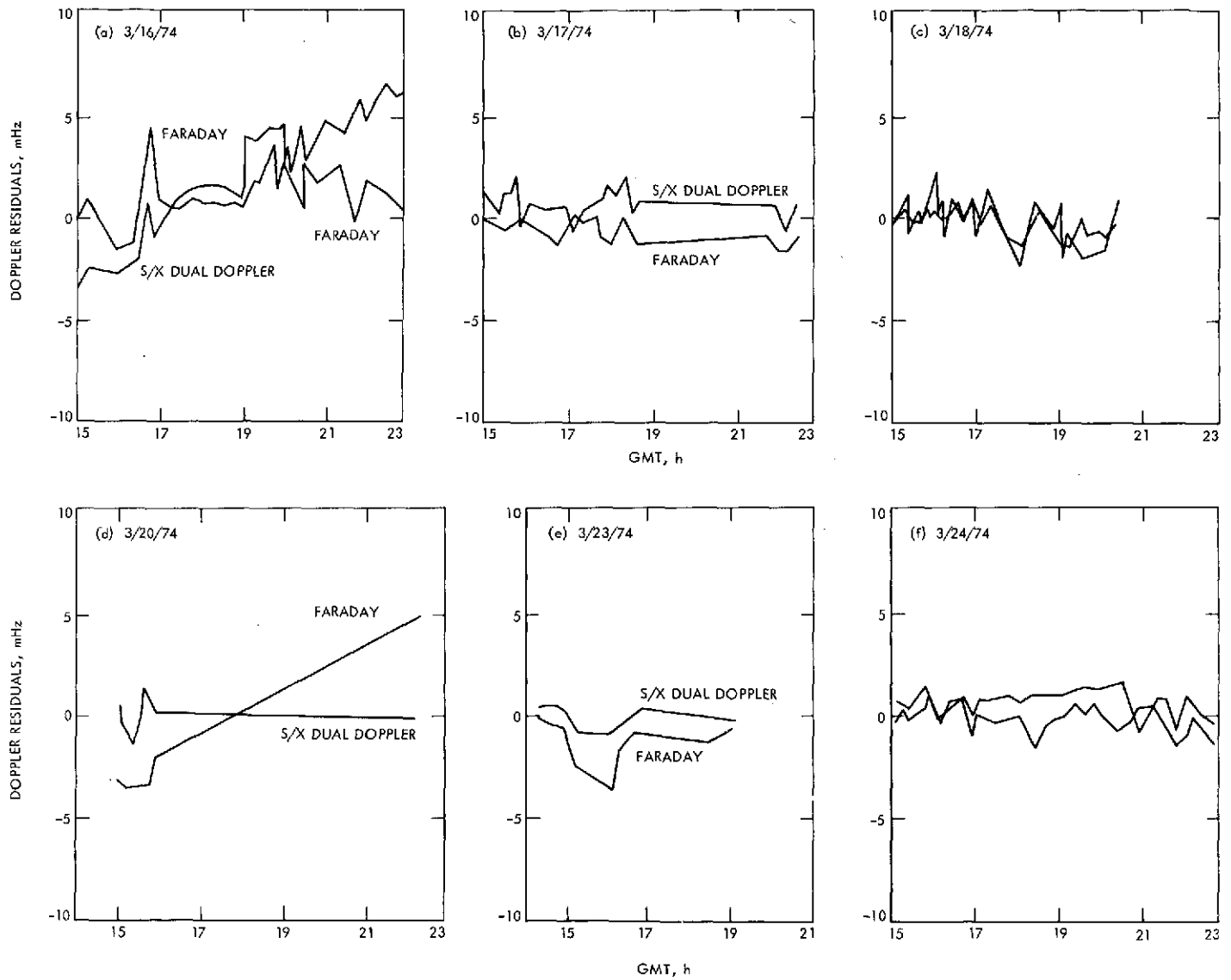


Fig. 8. Doppler residuals: calibrated for charged-particle influences

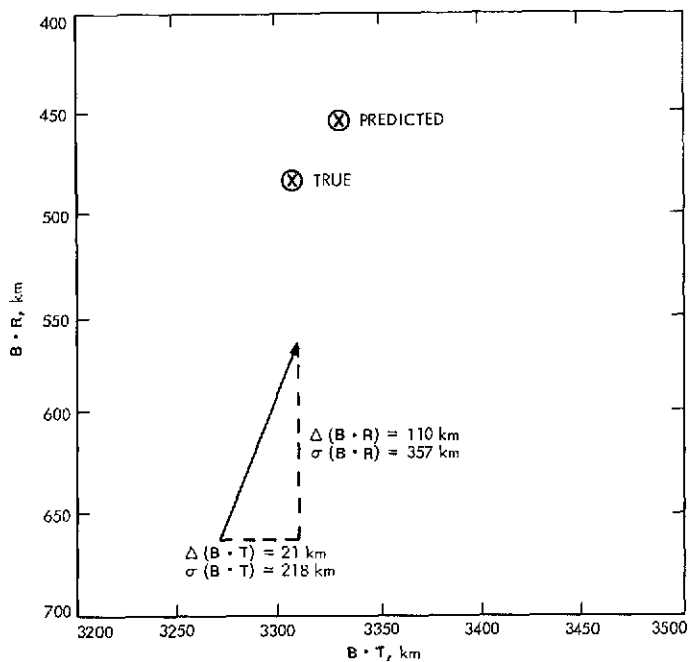


Fig. 9. MVM'73 Mercury encounter plane coordinate estimates: Impact of Faraday calibrations

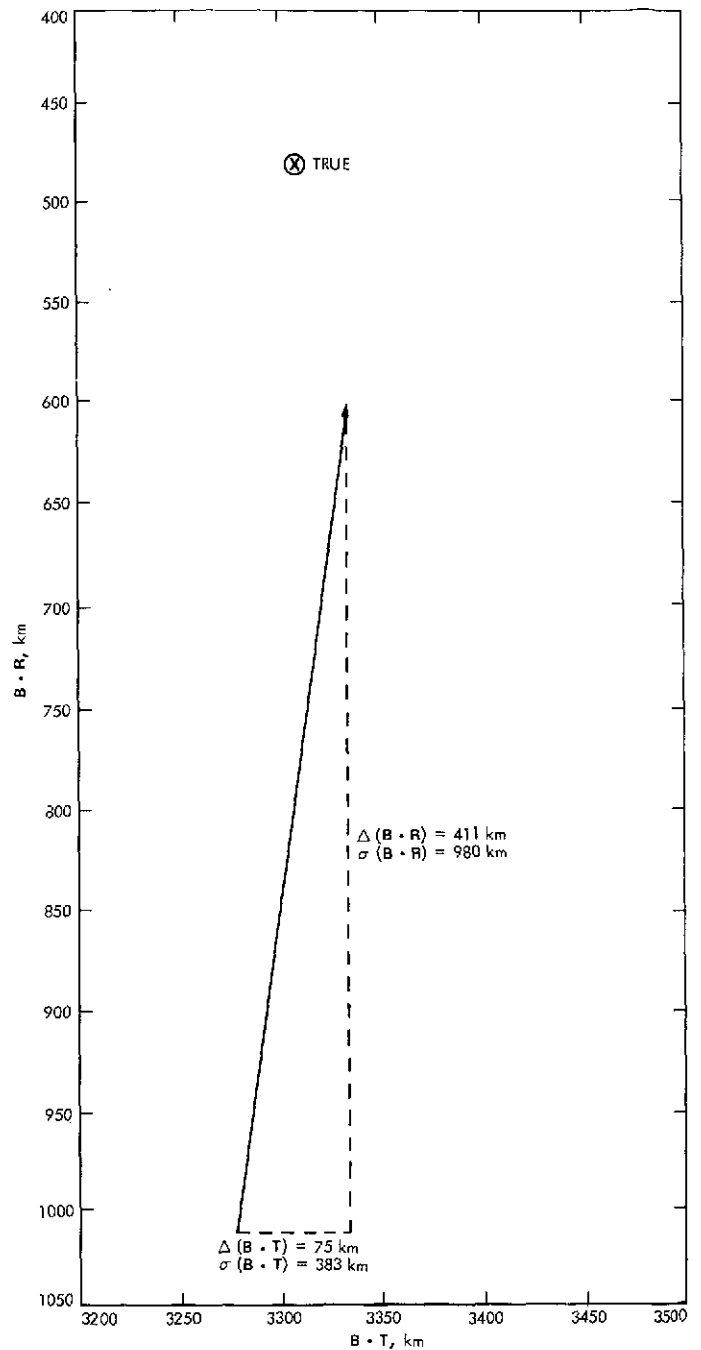


Fig. 10. MVM'73 Mercury encounter plane coordinate estimates: Impact of S/X dual doppler calibrations

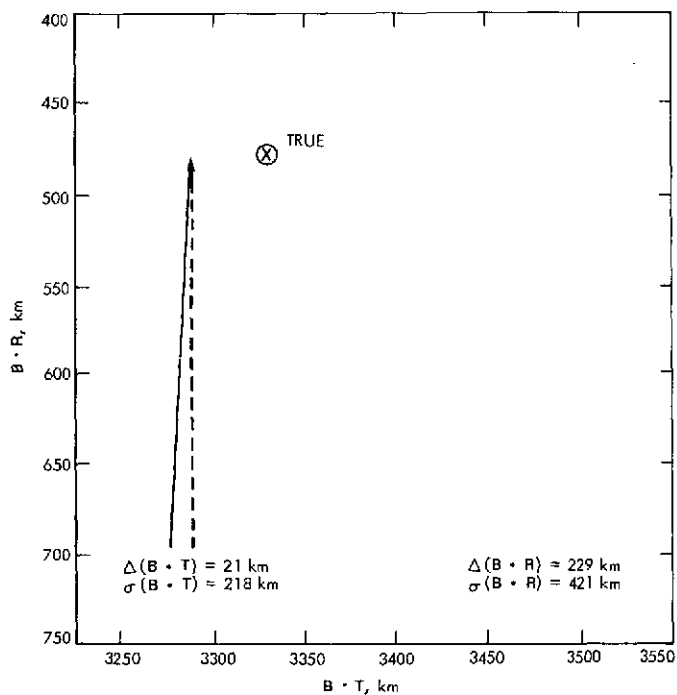


Fig. 11. MVM'73 Mercury encounter plane coordinate estimates: Impact of charged-particle calibrations

Appendix

Verification of S/X Dual Doppler Charged-Particle Calibrations

I. Introduction

S/X dual doppler is demonstrated to provide reasonable charged-particle measurements. This statement is based on the comparisons of three S/X dual doppler and Faraday rotation data passes. Thus, the S/X data quality can only be validated to the accuracy of the Faraday charged-particle computations. The accuracy limitation of the Faraday charged-particle evaluations is discussed.

II. S/X Pass 1: Day 349, 1973

The first S/X data of suitable quality were obtained at DSS 14 on December 15, 1973 (Fig. A-1). The data spans ~ 6 h. They reveal a long-term decrease in the line-of-sight electron content: a 1-m decrease over the 6-h interval. In addition to the long-term signature, there is also a repetitive short-term structure (~ 40 min from one local maximum to the next). These short-term structures have been found to be correlated with the roll limit cycle of the spacecraft by B. W. Dysart and W. Martin. Modifications of the DSS 14 experimental dual-frequency receivers corrected this problem. Subsequent S/X data passes do not show this repetitive structure.

The Faraday rotation data (Fig. A-2) only assess the variation of the electron content of the Earth's ionosphere, while the S/X dual doppler data assess the variation of the electron content of the ionosphere and the space plasma collectively. Since the S/X and Faraday data yield electron contents that do not drift relative to each other by more than 0.2 m, the plasma must not exceed this level during this 6-h period.

Earth's ionosphere is being monitored by means of Faraday rotation measurements to the geostationary satellite ATS-1 from DSS 13. However, this only gives the total electron content along this line of sight. These columns of electron content are then projected to the zenith at the ionospheric reference point (the point where this line of sight pierces the ionosphere at 350 km, longitude = 239.5 deg, latitude = 32.6 deg) before they are time-translated to the MVM'73-DSS 14 line of sight (Fig. A-3). The Z's in the Faraday rotation plots (Fig. A-4) represent the time-translated zenith columns. These are then mapped to the respective elevation angles of the station-spacecraft line of sight in the view period by

means of a ray trace technique based on a Chapman ionospheric model (Ref. 1). These are the R's in the Faraday plots. As will be seen later, this mapping technique is relatively accurate for elevation angles > 30 deg (Ref. 1). As expected, the Chapman model fails when dawn, dusk, and nighttime ionospheric regions are involved, i.e., the model fails when the solar zenith angle, X , exceeds 80 deg ($-80^\circ < X < 80^\circ$) (Ref. 9).

The latitude and longitude variations of the subionospheric reference points of the DSS 14-MVM'73 and the DSS 13-ATS-1 lines of sight (Fig. A-3) are ~ 1 deg apart at 24 h UT. This separation is ~ 100 km in the ionosphere (at reference height of 350 km). If this geometry were the only consideration, the S/X and Faraday data would be matched in range at 24 h UT, by adding a bias to the S/X data. However, there is a second consideration. The DSS 13-ATS-1 data are mapped to the "reference zenith" as previously stated. To be consistent with the total zenith electron contents of other ionospheric observatories, this "mapping in elevation" is accomplished by simply multiplying the acquired data by the cosine of the elevation angle at the subionospheric reference point. The zenith electron content is then mapped to respective elevation angles as mentioned. The error in the first mapping is $\sim 1\%$. The error in the second mapping is $\sim 5\%$ for elevation angles > 30 deg and 20% for angles between 15 and 30 deg. Consequently, the S/X and Faraday data are to be matched in range midway between the time of "closest approach" and "meridian crossing."

A pictorial of the ionospheric and the DSS 14 (December 15, 1973) tracking data acquisition pattern (Fig. A-5) shows the DSS-probe line of sight to pass through the "active region" of the ionosphere for most of the tracking pass. The maximum electron content encountered during this tracking period is encountered just after spacecraft rise and the least electron content encountered at spacecraft set. As a consequence, the ionosphere most influences the doppler data early in the pass, and its influence diminishes as the pass progresses.

The elevation angle is lowest early in the tracking pass (Fig. A-2); thus, at the time when the electron content is largest, the radio signal traverses more ionosphere. As the pass proceeds, the amount of ionosphere traversed decreases.

A comparison of the Faraday rotation and S/X evaluations of the electron content history over the pass reveals the long-term trends to match (Fig. A-2). The maximum disagreement is ~ 0.15 m at 23 h 51 min. This is $\sim 10\%$ of the total correction at that time. The short-term variations of the Faraday and S/X evaluations do not correlate.

Short-term variations of the ionospheric electron content with amplitudes less than tenths of meters are usually localized (10 to 100 km, Ref. 10). Hence, fine structure variations along the DSS 14-MVM73 line of sight can not be obtained by mapping the fine structure variations from the DSS 13-ATS-1 line of sight. The short-term variations (Fig. A-2) of the Faraday and S/X data do not correlate and the maximum difference is < 0.2 m. From the differences pictured in Fig. A-2, it can be deduced that the localized, short-term, ionospheric variations are ~ 0.25 m/h ($\sim 3 \times 10^{16}$ electrons/m²/h). This is quite reasonable.

III. Pass 2: Day 364, 1973

The seven hours of S/X doppler data for Day 364 (December 30, 1973) is similarly compared with the Faraday rotation data and plotted in Fig. A-6. Again, the agreement of the gross trends is good. In this pass, however, the agreement of the S/X and Faraday data at the beginning and the end of the pass is only at the 0.2–0.3-m level. Although the elevation angle of the spacecraft is quite high (~ 40 deg) in the beginning of the pass, the separation of the DSS 14-MVM73 and DSS 13-ATS-1 lines of sight is more than 5 deg (~ 600 km). Moreover, transient electron content irregularities along either line of sight can amount to 0.2–0.3 m. Towards the end of the pass where the elevation angle to the spacecraft dropped to less than 30 deg, the elevation mapping uncertainty

becomes larger. Moreover, calculations show that the solar zenith angle (X) on this day becomes larger than 90 deg at UT $\simeq 25$ h. It is known that the Chapman profile for the ionospheric electron distribution is valid only for $X \lesssim 80$ deg (Ref. 9). Towards dusk, the free electrons in the ionosphere recombine with the positive ions and the electron distribution may not be well defined. A new model for the ionosphere, which treats the daytime, nighttime, dawn, and dusk regions individually, has been theoretically developed (Ref. 1). The implementation of this new model is still not ready, however. Therefore, it is not possible at the present time even to guess what the actual errors will be, using the Chapman model for these dawn and dusk transition zones. In short, the disagreement towards the end of this pass is probably due to a combination of the uncertainties in the elevation angle mapping technique and in the application of the Chapman ionospheric profile.

IV. Pass 3: Day 003, 1974

The S/X-dual doppler data acquired on Day 003 (January 3, 1974) compare even better with the Faraday measurements (Fig. A-7). This stems from two developments: DSS 14 S/X hardware had been modified, and the data were taken only at the higher elevation angles. The maximum difference between the mapped Faraday and the S/X measurements is < 0.05 m.

V. Summary

S/X dispersive doppler from DSS 14 does measure the charged particles along the station-spacecraft line of sight at least to the accuracy of the "mapped" Faraday polarization data (0.1–0.3-m level). This conclusion is based on the analyses of data from three DSS 14 tracking passes.

References

1. Yip, K. W., and Mulhall, B. D., "A System Analysis of Error Sources in the Technique Used for Ionospheric Calibration of Deep Space Probe Radio Metric Data," in *The Deep Space Network Progress Report*, Technical Report 32-1526, Vol. XVII, pp. 48–67, Jet Propulsion Laboratory, Pasadena, Calif., Oct. 15, 1973.
2. MacDoran, P. F., "A First-Principles Derivation of the Differenced Range Versus Integrated Doppler (DRVID) Charged-Particle Calibration Method," in *The Deep Space Network*, Space Programs Summary 37-62, Vol. II, pp. 28–34, Jet Propulsion Laboratory, Pasadena, Calif., Mar. 31, 1970.

References (contd)

3. Winn, F. B., and Trask, D. W., *VK75 Mission B Solar Plasma Sensitivities*, TM 391-437, Apr. 9, 1973 (JPL internal document).
4. Winn, F. B., Yip, K. W., and Dysart, B. W., *Current MVM'73 Charged Particle Calibration Experience (21 November 1973)*, IOM 391.3-763, Dec. 5, 1973 (JPL internal document).
5. Winn, F. B., and Yip, K. W., *Ionospheric Charged Particle Influence on Mercury B-Plane Coordinate Estimates (Report 4—March 16 to March 24, 1974)*, IOM 391.3-787, Apr. 5, 1974 (JPL internal document).
6. Winn, F. B., and Yip, K. W., *Actual Corruption of the MVM'73 B-Plane Coordinate Estimates: Ionospheric Charged Particle Influences on Goldstone DSN Tracking Data (Report 3—January 21 to February 5, 1974)*, IOM 391.3-775, Feb. 22, 1974 (JPL internal document).
7. Winn, F. B., and Yip, K. W., *Actual Corruption of the MVM'73 B-Plane Coordinate Estimates: Ionospheric Charged Particle Influences on Goldstone DSN Tracking Data (Report 2—December 20, 1973)*, IOM 391.3-770, Jan. 29, 1974 (JPL internal document).
8. Winn, F. B., and Yip, K. W., *MVM DRVID and Its Use in the Orbit Determination Process*, IOM 391.3-789, Apr. 1974 (JPL internal document).
9. Rishbeth, H., *Introduction to Ionospheric Physics*, Academic Press, New York, 1969.
10. Titheridge, J. E., "Large Scale Irregularities in the Ionosphere," *J. Geophys. Res.*, Vol. 68, p. 3399, 1963.

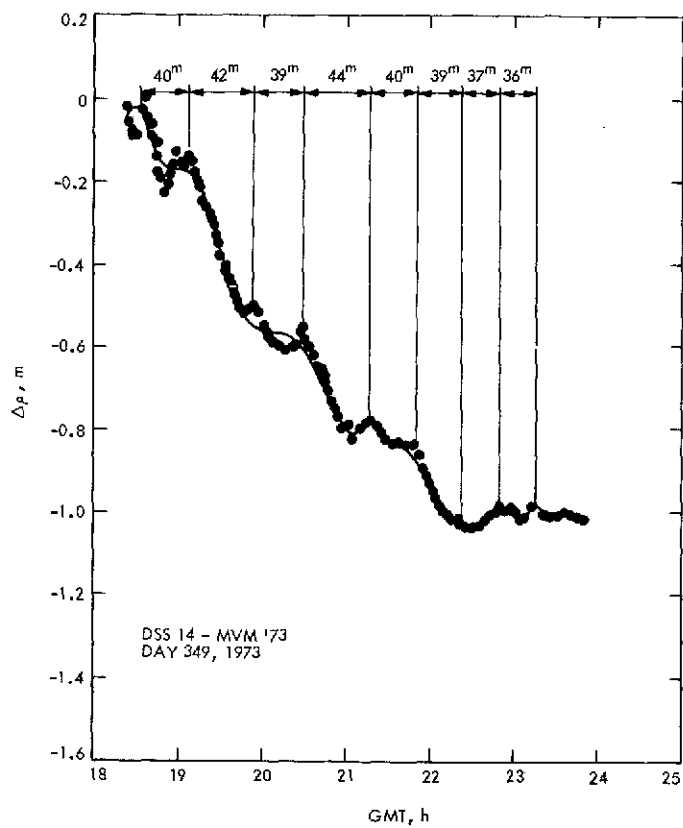


Fig. A-1. S/X dual doppler measurements

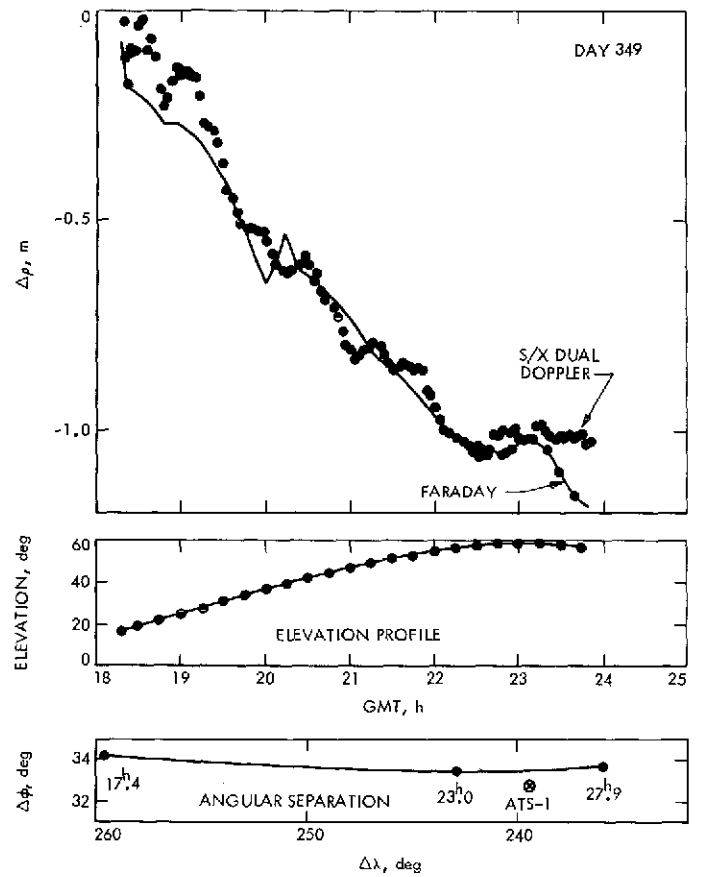


Fig. A-2. S/X dual doppler vs Faraday polarization data

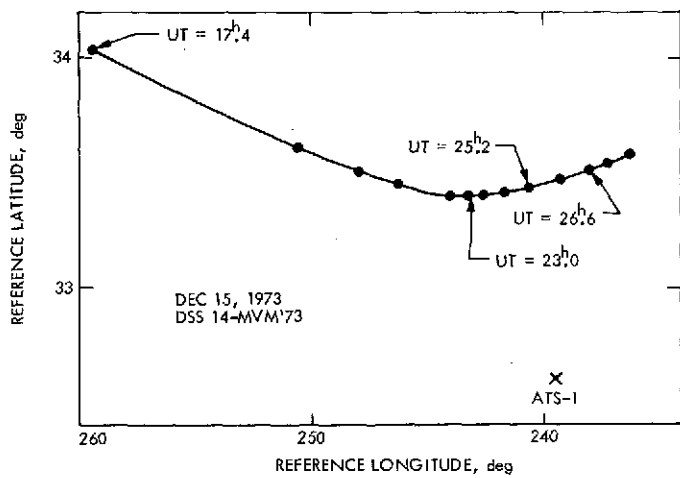


Fig. A-3. Variation of ionospheric reference coordinates

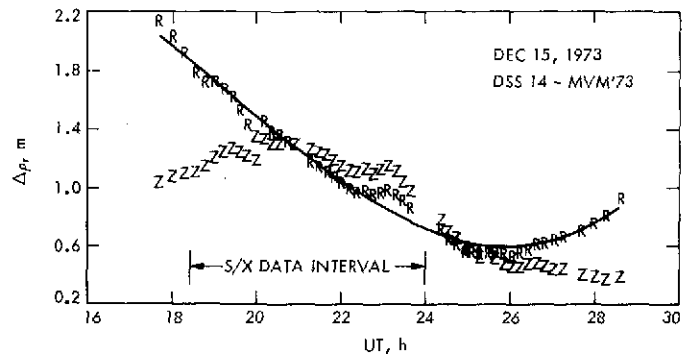


Fig. A-4. Electron content at zenith and along spacecraft line of sight

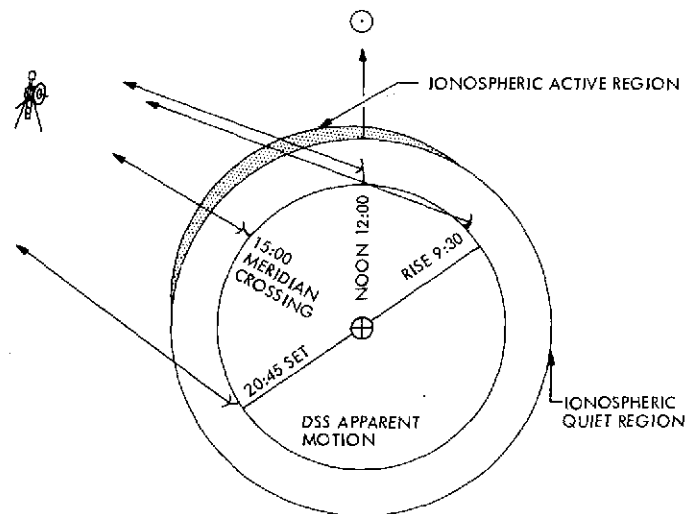


Fig. A-5. Pictorial of the ionosphere involved

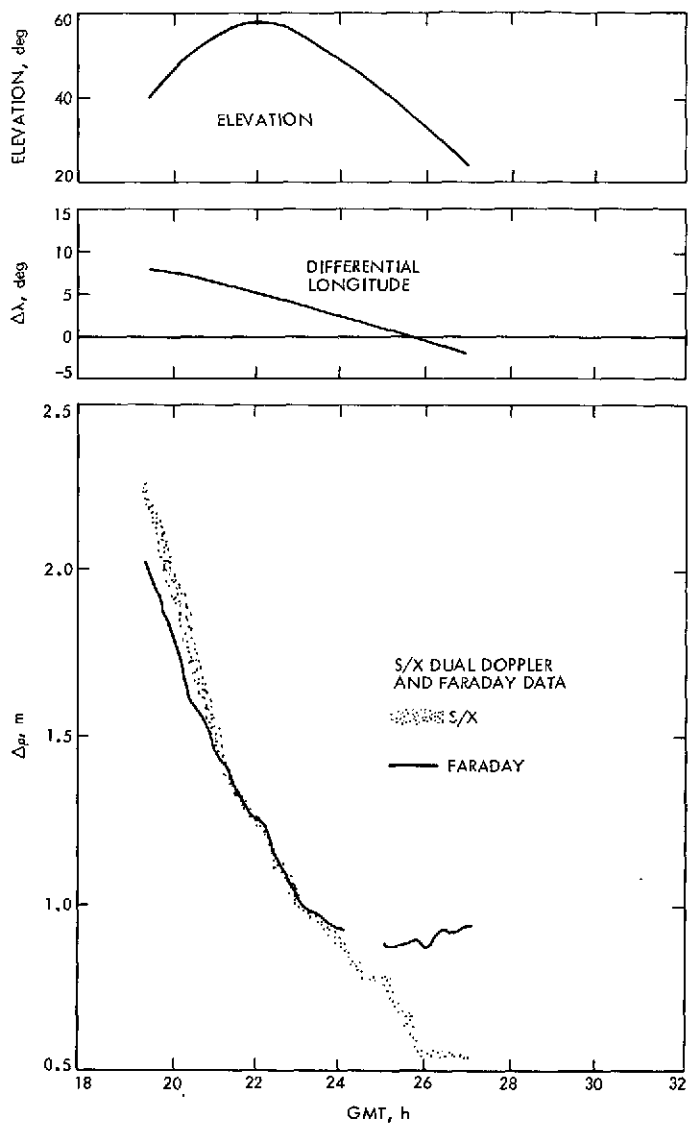


Fig. A-6. S/X pass of Day 364, 1973

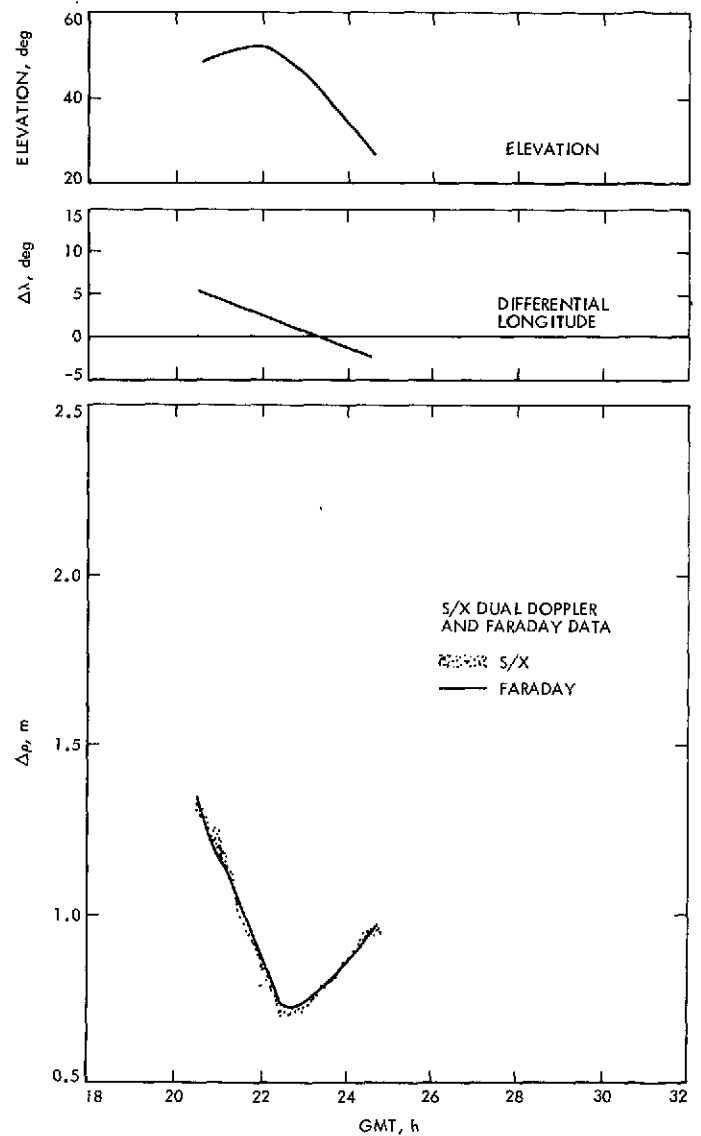


Fig. A-7. S/X pass of Day 003, 1974

Dual-Spacecraft Radio Metric Tracking

R. A. Preston

Tracking and Orbit Determination Section

When two interplanetary spacecraft lie along similar geocentric lines of sight, navigational advantages may be achieved by navigating one spacecraft with respect to the other. Opportunities to employ this technique will become more common: the two Viking spacecraft will be within two degrees of each other for the last seven months of their cruise phase; the two Mariner Jupiter/Saturn 1977 (MJS77) spacecraft will be within three degrees of each other for the last three years of their mission. This article describes the advantages of this technique in both conceptual and mathematical terms and discusses the various data types that might be formulated. The opportunities for testing and utilizing this technique are also outlined.

I. Introduction

Two spacecraft often approach to within a few degrees of each other in the sky. This will be especially true during the coming decade, when both the Viking and MJS77 missions will involve two spacecraft that virtually "fly in formation" to their target planets. Such occurrences offer unusual navigational opportunities, since when the two spacecraft are tracked from neighboring ground sites, many of the error contributions to the range and doppler data will be common to both spacecraft. If the data types for one of the spacecraft are subtracted from the corresponding data types for the other spacecraft, new data types can be formed in which these common error sources tend to cancel out. Specifically, the sensitivity to antenna site location, UT1, polar motion, troposphere, ionosphere,

space plasma, and sometimes instrumental effects can be significantly reduced (Fig. 1). The information retained by the new data types will include the differences in right ascension and declination of the two spacecraft as well as the difference in geocentric range rate (differenced doppler data) or the difference in geocentric range (differenced range data). Under certain conditions, relatively error-free determinations of these quantities should improve trajectory estimates.

In addition, a new navigation data type, differential very long baseline interferometry (Δ VLBI), is now in early stages of experimental development and should provide another and perhaps more accurate means of navigating one spacecraft with respect to another. As

presently conceived, this data type will be formed by alternately pointing a single pair of antennas (long baseline) at two nearby celestial radio sources and performing conventional VLBI observations on each source. If corresponding VLBI data types for the two radio sources are differenced, mutual errors are cancelled, and the resultant data types provide a precise measure of the angular separation of the two sources.

II. Applications of Dual-Spacecraft Tracking

It has been previously noted (Ref. 1) that dual-spacecraft tracking offers potential scientific benefits when two spacecraft are extremely close to another planet. If one planetary orbiter is tracked relative to another orbiter, the gravitational field of the planet can be more accurately determined; if a planetary atmospheric probe is tracked relative to another probe, orbiter, or flyby, the atmospheric dynamics of the planet can be more easily deciphered. In these particular applications, the two spacecraft would probably have such a small angular separation that it would be possible to simultaneously track both spacecraft from a single antenna or antenna pair (long baseline), providing even better cancellation of platform parameter and transmission media effects. Some cancellation of instrumental errors would also occur, as much of the ground instrumentation would be used in common by the two spacecraft signals.

Applications of dual-spacecraft tracking also arise when one or both of the spacecraft are in the cruise phase of their flights. Such a technique would afford some relief from the problems incurred in short arc trajectory estimation, since the limiting error sources are generally platform parameter and transmission media effects. If the orbit of one of the two spacecraft is well known from a long arc solution, then dual-spacecraft tracking will provide better short arc solutions for the second spacecraft's orbit than could be obtained by conventional means. Short arc solutions are especially important to spacecraft navigation after a disruptive influence to the orbit of a spacecraft, such as a maneuver, an encounter, or a sudden gas leak.

When a mission involves two spacecraft which encounter the same planet within a short time span, the first spacecraft to arrive may be used to guide the second to a much more accurate encounter if the planet's ephemeris is not well known. That is, normal doppler tracking can tie the first spacecraft to the planet very precisely during that spacecraft's encounter. Then dual-spacecraft tracking can tie the two spacecraft together, and hence

tie the second spacecraft to the planet well before its encounter. This technique can become even more powerful when the first spacecraft to arrive is a planetary orbiter, providing a constant "homing" beacon for navigating the second spacecraft.

Dual-spacecraft tracking also offers a partial solution to the problem of estimating small spacecraft declinations. At times of low spacecraft declination, determinations of declination with conventional data types are plagued not only by a lack of sensitivity to declination but also by increased sensitivity to the effects of spin radius errors and atmospheric/ionospheric modeling errors (Ref. 2). With dual-spacecraft data types the insensitivity to declination still remains, but the corrupting effects of spin radius errors and transmission media mis-modeling are greatly reduced.

Because of the inherent accuracy of the dual-spacecraft data types, the required number of tracking passes for some spacecraft might be reduced, thus easing the strain on the DSN antenna schedule. For example, in the case of lengthy dual-spacecraft missions, navigation needs might be adequately satisfied during sizable portions of the missions by tracking only one of the spacecraft by conventional means while tracking the other exclusively by dual-spacecraft techniques. In order to provide estimates of the two spacecraft orbits that are of comparable accuracy, the second spacecraft would not need to be tracked as often.

One other efficient characteristic of dual-spacecraft data types should also be noted. Since transmission media effects tend to cancel, low elevation angle dual-spacecraft observations are much more useful than low elevation observations of a single spacecraft.

When dual-spacecraft tracking is performed, the conventional data types need not always be differenced to accrue some navigational advantage. If only one of two nearby spacecraft possesses a means of calibrating the effects of charged particles along the line of sight to that spacecraft (S/X or DRVID), the calibration could also be used to correct the radio metric data from the other spacecraft. During the Viking and MJS'77 missions, both interplanetary spacecraft associated with each mission will possess S/X capability, but there will be only a single S/X ground receiver for each 120-deg longitude sector. Since each pair of spacecraft will be closely spaced for most of their mission, continuous S/X charged particle calibration for both spacecraft would not be possible unless this technique is applied.

Finally, aside from the possible navigational benefits of dual-spacecraft tracking, we should also note that during planetary encounters, tracking the encountering spacecraft relative to another well-located spacecraft might prove useful to celestial mechanics and occultation experimenters. Since much of the celestial mechanics and occultation information is contained only in short intervals of data, the experiments are very sensitive to any noise contributions to the data. Hence, a data type that is relatively free of transmission media effects may improve the results.

III. Mathematical Description of Dual-Spacecraft Data Types

The information content of dual-spacecraft radio metric data types is easily displayed using a simplified mathematical approach. The range from a tracking station to one spacecraft can be approximately given by (Ref. 3):

$$\rho_1(t) = r_1(t) - z_s \sin \delta_1(t) - r_s \cos \delta_1(t) \\ \times \cos [\omega t + \phi + \lambda - \alpha_1(t)]$$

where

- ρ_1 = range from tracking station to spacecraft (subscript "1" denotes first spacecraft; all distances are in light seconds).
- r_1 = geocentric range of spacecraft
- δ_1 = declination of spacecraft
- α_1 = right ascension of spacecraft
- r_s = distance of tracking station from Earth's spin axis
- z_s = distance of tracking station from Earth's equator
- λ = longitude of tracking station
- ω = Earth's rotation rate
- ϕ = a phase angle which depends on choice of epoch
- t = time past epoch

The range to a second spacecraft (subscript "2") may be similarly written as

$$\rho_2(t) = r_2(t) - z_s \sin \delta_2(t) - r_s \cos \delta_2(t) \\ \times \cos [\omega t + \phi + \lambda - \alpha_2(t)]$$

where for mathematical simplicity the tracking station associated with the second spacecraft has been assumed to be collocated with the tracking station associated with the first spacecraft. If these two expressions are differ-

enced, we create a new data type: dual-spacecraft range. Using the following substitutions:

$$\Delta\alpha = \alpha_2 - \alpha_1 \\ \Delta\delta = \delta_2 - \delta_1 \\ \Delta r = r_2 - r_1$$

and neglecting second-order terms in $\Delta\delta$ and $\Delta\alpha$, the dual-spacecraft range data type may be represented as

$$\rho_2 - \rho_1 = \Delta r + \Delta\delta [-z_s \cos \delta_1 + r_s \sin \delta_1 \\ \times \cos (\omega t + \phi + \lambda - \alpha_1)] \\ - \Delta\alpha r_s \cos \delta_1 \sin (\omega t + \phi + \lambda - \alpha_1)$$

where for notational convenience, the explicit dependence on time of the spacecraft position parameters has been omitted.¹

In an analogous manner, we can derive an expression for the dual-spacecraft doppler data type. The approximate range rate from the common tracking station to each spacecraft may be written as:

$$\dot{\rho}_1 = \dot{r}_1 + \omega r_s \cos \delta_1 \sin (\omega t + \phi + \lambda - \alpha_1) \\ \dot{\rho}_2 = \dot{r}_2 + \omega r_s \cos \delta_2 \sin (\omega t + \phi + \lambda - \alpha_2)$$

The dual-spacecraft doppler data type may be represented as²

$$\dot{\rho}_2 - \dot{\rho}_1 = \Delta\dot{r} - \omega r_s [\Delta\delta \sin \delta_1 \sin (\omega t + \phi + \lambda - \alpha_1) \\ + \Delta\alpha \cos \delta_1 \cos (\omega t + \phi + \lambda - \alpha_1)]$$

Using these formulas, we can draw some approximate conclusions about what information might be extracted from a single pass of dual-spacecraft data. With either of the dual-spacecraft data types, if the position of spacecraft 1 and the equatorial projection of the geocentric vector to the tracking station are assumed known, the differential right ascension and declination of the two spacecraft may be determined from the amplitudes of diurnal sinusoidal and cosinusoidal variations in the data.

¹The same result may be obtained by direct differentiation of the expression for spacecraft range.

²In the above expressions for the differenced data types, the diurnal term involving $\Delta\delta$ becomes small at low declinations, and second-order terms in $\Delta\alpha$ and $\Delta\delta$ need to be included to show the correct influence of $\Delta\delta$ on the data. Namely, the quantity $(\Delta\delta^2 + \Delta\alpha^2) (\cos \delta_1)/2$ should be added to the term $\Delta\delta \sin \delta_1$. There are also additional small terms involving $\Delta\dot{\alpha}$, $\Delta\dot{\delta}$, and $\Delta\dot{r}$ that might be included in the simplified expressions for these data types, but these terms can be neglected in most cases.

Additionally, if the polar component of the observing site position is known, the differential geocentric range between the two spacecraft may be determined from the bias portion of dual-spacecraft range data; similarly, the differential geocentric range rate of the two spacecraft may be determined from the bias portion of the dual-spacecraft doppler data.

The sensitivity of these differenced data types with respect to certain parameters is greatly reduced compared to the original data types; indeed, this property of the dual-spacecraft data types is responsible for much of their navigational value. This might lead one to believe that the information content of these differenced data types might be relatively poor. However, it is a fortunate property of the dual-spacecraft data types that their sensitivity to differential range, range rate, declination, or right ascension is essentially identical to the sensitivity of the original data types to the corresponding absolute spacecraft position parameter (i.e., the partial derivatives are nearly identical).

One of the advantages of dual-spacecraft tracking is that the data types are relatively free of corruption due to troposphere, ionosphere and space plasma, although the explicit cancellation of these effects has not been shown in the simplified derivations above. The experience gained by the JPL VLBI experimenters indicates that this cancellation should be significant up to angular separations as large as 10 deg (Ref. 4). Because the dual-spacecraft data lack sensitivity to atmospheric and ionospheric modeling errors, data acquired at very low elevation angles may be as useful as data acquired at high elevation angles. An example of the cancellation of low elevation transmission media effects for two closely spaced ray paths is shown in Fig. 2. Here, two- and three-way doppler data from Pioneer 10 are being received at two nearby ground stations, DSS 11 and DSS 14. Notice the systematic rise in both sets of doppler residuals at low elevation angles due to a lack of transmission media modeling. When these two data types are differenced (QVLBI), the resulting residuals no longer display this systematic rise. The two ray paths in this case were separated by about 5 km as they passed through the atmosphere and ionosphere. With dual-spacecraft data types, it should be noted that there is no cancellation at all of the space plasma in the geocentric range gap between the two spacecraft and that the cancellation of the uplink transmission media effects will be separated in time by the difference in the round trip light times to the two spacecraft. These error sources may be a problem if the two spacecraft are not at similar geocentric ranges.

Another advantage of dual-spacecraft data types is that the errors in site position coordinates, polar motion, and UT1 also cancel to a high degree. For example, the simplified expression for a single pass of normal doppler data shows that the declination of the spacecraft is principally determined from the amplitude, $\omega r_s \cos \delta_1$, of the diurnal sinusoidal signature in the data. If we solve for only the spacecraft angular position, an error in the assumed spin radius ϵ_{r_s} would produce a compensating error in the determination of declination equal to:

$$\epsilon_\delta = \frac{\cos \delta}{\sin \delta} \left(\frac{\epsilon_{r_s}}{r_s} \right)$$

For a spacecraft with a declination of 20 deg, an error in spin radius of 1 meter would cause an error of 0.1 sec of arc in the determination of declination. Since the error in declination is proportional to $\cot \delta$, these errors will be significantly greater for spacecraft with smaller declinations. The right ascension of the spacecraft is determined from the phase angle, $\omega t + \phi + \lambda - \alpha$, of the same sinusoidal signature. An error in station longitude is directly compensated by an equal error in the determination of spacecraft right ascension. A longitude error equivalent to 1 meter at the Deep Space Stations would cause an error of about 0.04 sec of arc in the determination of right ascension. With a full pass of dual-spacecraft doppler data, the differential declination of the two spacecraft is determined from the amplitude, $\Delta \delta \omega r_s \sin \delta_1$, of the diurnal sinusoidal signature in the data. If we solve for only the angular separation of the spacecraft, a percentage error in the assumed value of r_s will in most cases cause a similar percentage error in the determination of $\Delta \delta$. If the two spacecraft are separated by 5 deg, an error in spin radius of 1 meter will cause an error of only about 0.003 sec of arc in the determination of differential declination. Moreover, this error is nearly independent of the declination of the spacecraft.³ The differential right ascension of the two spacecraft is determined from the amplitude, $\Delta \alpha \omega r_s \cos \delta_1$, of the diurnal cosinusoidal signature in the data. Here again, a percentage error in r_s will cause a similar percentage error in the determination of $\Delta \alpha$. That is, an error in spin radius of 1 meter will also cause an error of about 0.003 sec of arc in the determination of differential right ascension. It could also be shown that station longitude errors generally have little effect on the determination of $\Delta \delta$ or $\Delta \alpha$.

³Second-order terms in $\Delta \alpha$ and $\Delta \delta$ need to be considered at low declination. In this case, estimates of $\Delta \delta$ can be corrupted by spin radius errors and other error sources if δ_1 and $\Delta \delta$ are nearly equal in magnitude but opposite in sign.

Last, we should mention that dual-spacecraft data types are subject to two of the same problems that plague conventional radio metric data types: unmodeled accelerations and zero declination singularities (Ref. 2). Not surprisingly, these problems may be alleviated by methods similar to those used with the more conventional data types.

Unmodeled accelerations corrupt the conventional tracking data types principally through the geocentric range and range rate contributions to the data types. If the same spacecraft is simultaneously tracked from two widely separated tracking stations⁴, differencing of the corresponding data types from the two stations provides new data types (QVLBI range and doppler) that are free of geocentric range and range rate terms and hence relatively uncorrupted by unmodeled accelerations. With dual-spacecraft data types, the effects of unmodeled accelerations enter the data types mainly through the terms involving differential geocentric range and range rate. These terms may be eliminated in an analogous manner to the case of a single spacecraft. That is, if the same two spacecraft are simultaneously tracked by two separate pairs of tracking stations, the dual-spacecraft data types gathered by these antenna pairs may be differenced to cancel the geocentric terms and hence cancel most of the effects of unmodeled accelerations. This dual-spacecraft tracking technique will be referred to as differential QVLBI (Δ QVLBI).

With conventional navigation data types, low declination observations adversely affect determinations of declination for two reasons: (1) the effects of certain systematic error sources are greatly magnified, especially where diurnal error signatures are exhibited as is the case with spin radius errors and atmospheric/ionospheric mis-modeling; and (2) the data types become very insensitive to declination. With dual-spacecraft tracking, we have already noted that errors incurred in the estimation of differential declination due to errors in tracking station coordinates remain at rather low levels in most situations. In addition, atmospheric and ionospheric effects are greatly reduced. However, the dual-spacecraft data types do become very insensitive to differential declination at low declinations, so only part of the low declination problem is avoided. With conventional data types, the problem of determining declination at low declinations can be

greatly alleviated by the use of "simultaneous" ranging (QVLBI range). With dual-spacecraft data types, "simultaneous" differential ranging (Δ QVLBI range) offers an answer to the low declination problem. This is an obvious consequence of the fact that the declination of each of the two spacecraft would be well determined if the raw ranging data were used to independently create a QVLBI range data type for each spacecraft.

IV. Differential Very Long Baseline Interferometry

Differential very long baseline interferometry (Δ VLBI) (Ref. 5) offers an additional and possibly more accurate means of navigating one spacecraft relative to another. Usually Δ VLBI refers to "simultaneously" performing conventional VLBI observations (Refs. 6-8) on a spacecraft and a nearby extragalactic radio source (ERS) and then differencing the corresponding VLBI data types to permit cancellation of common error sources.⁵ The resultant data types have high sensitivity to the angular separation of the two radio sources. Such a technique could also be applied to the case where both radio sources are onboard spacecraft.

The present plan of implementing Δ VLBI involves only a single widely separated pair of antennas that move back and forth in unison between two radio sources with a cycle time of a few minutes. Since the VLBI observations of the two sources will be made at slightly different times, some interpolation will be necessary before the differenced data types can be formulated. With present spacecraft, the most useful VLBI data type is "fringe phase."⁶ This data type may be thought of as being analogous to (but not identical to) counted cycles of QVLBI doppler. For the case of a monochromatic source, the fringe phase data type is formed by continually measuring the phase difference of the signals being received at the two antennas and counting the total number of cycles of differenced phase incurred since the initial observation time. Because each source is not being continually observed, it is necessary to extrapolate the differenced (fringe) phase through the nonobserving periods without "slipping" any full cycles.

⁵Thus Δ VLBI allows the spacecraft to be accurately navigated with respect to the precision "inertial" reference frame formed by the ERSs.

⁶Fringe rate is not as sensitive to the angular separation of the two radio sources. To obtain accurate VLBI delay measurements, special wide-bandwidth transmitters would have to be installed on the spacecraft.

⁴Either by simultaneous two-way and three-way tracking, alternate two-way tracking, simultaneous interference tracking, or simultaneous one-way tracking.

A simplified mathematical description of the principal information content of the differenced fringe phase data type $\Delta\phi_f$ is given by

$$\Delta\phi_f(t) \approx \mathbf{B}(t) \cdot [\mathbf{e}_2(t) - \mathbf{e}_1(t)] - \mathbf{B}(t_0) \cdot [\mathbf{e}_2(t_0) - \mathbf{e}_1(t_0)] \quad (\text{cycles})$$

where

\mathbf{B} = the baseline vector in wavelengths

$\mathbf{e}_{1,2}$ = unit vectors that point toward sources "1" and "2"

t_0 = the initial observation time

or

$$\Delta\phi_f \approx -[r_b \sin \delta_1 \cos \theta] \Delta\delta - [r_b \cos \delta_1 \sin \theta] \Delta\alpha - C$$

where

r_b = the equatorial component of the baseline

θ = the hour angle of source "1" with respect to the meridian intersected by the baseline

C = a nearly constant term which is not very valuable for determining $\Delta\delta$ and $\Delta\alpha$

Differential right ascension and declination can be determined from the amplitudes of the diurnal sin and cosine functions. Note that only the equatorial component of the baseline influences these amplitudes and that the sensitivity to differential declination is small at low declinations.

To demonstrate the inherent accuracy of the differenced fringe phase data type for dual-spacecraft tracking, a computer error analysis was performed.⁷ The test case considered involved the Pioneer 10/11 spacecraft pair during the month of April (1974) when the spacecraft were only about 2 deg apart in the sky. The simulation is made even more realistic by the fact that a maneuver was executed on the Pioneer 11 spacecraft at this time, and owing to the slow movement of this spacecraft across the sky, only short arc solutions were available for re-establishing the spacecraft's trajectory after the maneuver. It was estimated that one or two months would be necessary to satisfactorily redetermine the Pioneer 11 trajectory with conventional radio metric data types. This problem could probably have been greatly alleviated if the Pioneer 11 spacecraft had been tracked relative to the well-known trajectory of the Pioneer 10 spacecraft.

⁷By J. L. Fanselow

Figures 3a and 3b show the results of this error analysis in which Δ VLBI observations on a number of different baselines have been considered. This analysis was performed with a standard least squares batch filter. It was assumed that one measurement of fringe phase was made for each spacecraft every 6 minutes and that the rms error of these phase measurements was 0.1 cycle at S-band. The resulting uncertainties in differential right ascension range from 10^{-4} to 10^{-3} arcseconds after only two hours of successful observation. Even though the two spacecraft were at low declination (≈ -5 deg), the uncertainties in differential declination are surprisingly small, ranging from 5×10^{-3} to 10^{-2} arcseconds after two hours of observation. For comparison, 10^{-3} arcseconds is equivalent to about 4 km at the distance of Pioneer 11 (≈ 5 AU). Although more complete error analyses are necessary to ascertain Δ VLBI's ability to contribute to the solution of these types of navigation problems, this simple analysis certainly reveals a high potential.

It has been noted that a direct analog of differenced fringe phase might be formulated by utilizing an inherently simpler observational method. With conventional Δ VLBI, the received signals are recorded on magnetic tape and corresponding tapes are later crosscorrelated on a digital computer to determine fringe phase. However, if each time the two antennas were pointed at a particular spacecraft a phase-locked loop at each station was attached to the spacecraft carrier signal, the relative (or fringe) phase of the two received signals could be determined directly. A differenced fringe phase data type might then be constructed in a manner virtually identical to that of conventional Δ VLBI. Unfortunately, the phase-locked loop concept of Δ VLBI has three potential problems, all of which might prevent successful phase extrapolation through nonobserving periods: (1) insufficient accuracy in the relative phase measurements, (2) failure of the phase-locked loop to quickly capture the spacecraft signal, and (3) phase-locked loop transients following acquisition of the signal.

Last, we might compare Δ VLBI with the dual-spacecraft data types obtained by more conventional tracking techniques. To provide a direct mathematical comparison, consider the "conventional" dual-spacecraft data type which can be formed by continuously counting doppler cycles for each of two spacecraft at a pair of nearby antennas and then differencing the cycle counts ("differenced doppler phase"). A simplified mathematical expression for this data type may be constructed from the equation for dual-spacecraft range by subtracting the

value of dual spacecraft range at the initial observation time, or

$$\Delta\phi_a = [\Delta r(t) - \Delta r(t_0)] + \Delta\delta [r_s \sin \delta_1 \cos(\omega t + \phi + \lambda - \alpha_1)] - \Delta\alpha [r_s \cos \delta_1 \sin(\omega t + \phi + \lambda - \alpha_1)] - C \text{ (cycles)}$$

where

Δr and r_s are now expressed in wavelengths

$C =$ a nearly constant term which is not very valuable for determining $\Delta\delta$ and $\Delta\alpha$

Note that the form of this expression is very similar to that for differenced fringe phase. As with that data type, differential right ascension and declination must be determined from the amplitudes of the diurnal sin and cosine functions. The main difference in this case is that the spin radius has taken the place of the equatorial baseline component. Since the spin radii of the Deep Space Stations are of approximately the same magnitude as the available equatorial baseline components, the two data types should have nearly equal sensitivity to differential right ascension and declination. It should also be pointed out that conventional dual-spacecraft tracking passes will generally be significantly longer than those for Δ VLBI.

We might then ask, what are the advantages of Δ VLBI over more conventional dual-spacecraft tracking techniques? One advantage is that instrumental phase instabilities are far less important. Δ VLBI is corrupted by instrumental phase errors that build up over a fraction of the switching cycle (a few minutes), while instrumental phase errors that are accumulated during the length of a pass (several hours) can affect conventional dual-spacecraft tracking. Another advantage of Δ VLBI is that only near-Earth down-link transmission media effects are significant, and the cancellation of these effects is separated by only a few minutes. With conventional dual-spacecraft data types, the cancellation of the near-Earth down-link transmission media effects is nearly simultaneous, but the cancellation of the near-Earth up-link effects is separated by a differential round-trip light time. Additionally, the distant space plasma effects may not cancel very well, and there will be no cancellation of the space plasma effects in the geocentric range gap between the two spacecraft. Finally, conventional dual-spacecraft data types are sensitive to the effects of unmodeled accelerations, while Δ VLBI data types are not. We should note that if Δ QVLBI dual-spacecraft tracking is performed, the information content of the resulting data types would be nearly identical to that of the corresponding Δ VLBI data types, and the main corruptions of unmodeled accel-

erations and transmission media effects would vanish. However, the problem of instrumental phase stability would prohibit Δ QVLBI dual-spacecraft tracking from being competitive in accuracy with Δ VLBI. The instrumental stability problem could be greatly alleviated by either (1) installing hydrogen maser frequency standards at the participating antennas, or (2) providing common frequency standards at the closely spaced antenna pairs.⁸ Table 1 summarizes the significant error sources that affect all conventional and dual-spacecraft radio metric data types.

V. Opportunities for Dual-Spacecraft Tracking

Since interplanetary spacecraft do not wander far from the plane of the ecliptic, close angular approaches of the geocentric lines-of-sight to two such spacecraft are quite common, although often transitory. In missions that involve two spacecraft, these spacecraft will generally be desirable subjects for dual-spacecraft tracking for a significant fraction of their missions.

The current dual-spacecraft project is the Pioneer 10/11 mission to Jupiter. Even though their Jovian encounters are about a year apart, the two spacecraft are close together in the sky for an extended period. The trajectories of Pioneer 10/11 across the sky are shown in Fig. 4. The angular separation of the spacecraft as a function of time is shown in Fig. 5. From this figure we see that the two spacecraft remain within 10 deg of each other for a period of 9 months. At the time of the Pioneer 10 encounter the separation was about 7 deg; at Pioneer 11 encounter, the separation will be 17 deg. Hence, at these encounters, dual-spacecraft tracking between Pioneer 10 and 11 might be considered as a means of reducing the corrupting influence of transmission media effects on occultation and celestial mechanics experiments. Also noted in Fig. 4 is the fact that the MVM73 spacecraft closely approached the Pioneer 10/11 pair for a short period of time, with the angular separation of Pioneer 11 and MVM73 falling below a degree at one point and remaining at less than 10 deg for about half a month. Surprisingly, MVM73 encountered Mercury during this brief time period.

Figure 6 shows the approximate angular separation of the Viking A and B spacecraft as a function of time. The angular separation of the two spacecraft will be less than 10 deg from a month after the launch of the second space-

⁸A common frequency standard now exists at DSS 42/43, and one will soon be available at DSS 61/63.

craft until the end of the mission. During the 7 months preceding the second encounter, the separation will be less than 2 deg. After the first spacecraft has arrived at Mars, it might provide an excellent "homing" beacon for the second spacecraft.

Figure 7 shows a likely history of the angular separation of the two MJS'77 spacecraft as a function of time. Within a month after the launch of the second spacecraft, the separation has dropped to 10 deg. For the next 4 months it continues to drop to about 2.5 deg. For the remaining 3.3 years of the mission, the separation remains less than 2.5 deg, being about 1.5 deg at the time of the Jupiter encounters and 0.5 deg at the time of the first Saturn encounter (no data for second encounter).

NASA's budget for FY75 proposes a dual Pioneer spacecraft mission to Venus in 1978. One spacecraft will send four entry probes into the Venus atmosphere; the other will be an orbiter. For this mission, dual-spacecraft tracking might be especially useful in determining probe trajectories, which will be used in studies of the Venus atmosphere. In addition, the majority of potential interplanetary missions which might also be funded during the coming decade would probably involve dual spacecraft. For example, Mariner/Jupiter/Uranus (1979), Jupiter Orbiter (1981), Venus Orbiting Imaging Radar (1983), Encke (1984), and Saturn Orbiter (1985).

VI. Demonstration of Dual-Spacecraft Tracking

Although continued analyses and computer simulations should be undertaken to investigate the potential worth of dual spacecraft tracking to interplanetary navigation, the usefulness of these data types will not be proven until demonstrations are performed with actual spacecraft data. A possible source of data for a dual-spacecraft tracking demonstration is previously recorded tracking data. The Pioneer 10/11 spacecraft pair provides the best opportunity for performing such a demonstration. These spacecraft were within 5 deg of each other from December 1973 through June 1974, and within 10 deg through mid-August 1974 (see Fig. 4). Another interesting possibility is the Mariner 6/7 spacecraft pair. Here we might attempt to track Mariner 7 into its Mars encounter by means of dual-spacecraft tracking during the encounter phase of Mariner 6.

The navigational utility of dual-spacecraft tracking might be demonstrated by the following method: Use conventional tracking data to perform accurate long arc solutions for the trajectories of the two relevant spacecraft. Then, using data from only a short segment of that long arc, make two independent estimates of one of the spacecraft trajectories. One of these estimates would utilize only conventional radio metric data; the other would utilize only dual spacecraft radio metric data. The results could then be compared with the corresponding long arc solution. Such a procedure could be repeated a number of times using different pairs of DSN antennas, spacecraft angular separations, and dual spacecraft data types.

VII. Summary

When two spacecraft appear close together in the sky, navigational advantages may be accrued by navigating one spacecraft with respect to the other. If the spacecraft are tracked from nearly colocated antennas, many of the error contributions to the conventional radio metric data types will be common to both spacecraft. Thus, by differencing corresponding data types for the two spacecraft, mutual error sources tend to cancel. The resultant "dual-spacecraft data types" will contain accurate information concerning the relative position of the two spacecraft. "Simultaneous" very long baseline interferometry observations of the two spacecraft could provide even more accurate dual-spacecraft data types. The principal benefits of dual-spacecraft tracking are:

- (1) The cancellation of platform parameter and transmission media modeling errors in short arc estimation problems.
- (2) Accurate encounter guidance for the trailing spacecraft in dual spacecraft encounter missions.
- (3) A partial solution of the low declination problem.
- (4) Easing of the strain on the DSN antenna schedule.

Since both the Viking and MJS spacecraft pairs will appear close together in the sky for most of their missions, dual-spacecraft data types might play a useful role in the navigation of these spacecraft. Hence, further investigation of the navigational utility of these data types seems warranted.

References

1. Shapiro, I. I., private communication.
2. Ondrasik, V. J., and Rourke, K. H., "Applications of Quasi-VLBI Tracking Data Types to the Zero Declination and Process Noise Problems," AAS/AIAA Conference, Ft. Lauderdale, Florida, August 17-19, 1971.
3. Hamilton, T. W., and Melbourne, W. G., "Information Content of a Single Pass of Doppler Data from a Distant Spacecraft," in *The Deep Space Network*, Space Programs Summary 37-39, Vol. III, pp. 18-23, Jet Propulsion Laboratory, Pasadena, Calif., May 31, 1966.
4. Fanselow, J. L., private communication.
5. Slade, M. A., et al., "The Mariner 9-Quasar Experiment: Part I," in *The Deep Space Network Progress Report*, Technical Report 32-1526, Vol. XIX, pp. 31-35, Jet Propulsion Laboratory, Pasadena, Calif., Feb. 15, 1974.
6. Thomas, J. B., "An Analysis of Long Baseline Radio Interferometry," in *The Deep Space Network Progress Report*, Technical Report 32-1526, Vol. VII, pp. 37-50, Jet Propulsion Laboratory, Pasadena, Calif., Feb. 15, 1972.
7. Thomas, J. B., "An Analysis of Long Baseline Radio Interferometry, Part II," in *The Deep Space Network Progress Report*, Technical Report 32-1526, Vol. VIII, pp. 29-38, Jet Propulsion Laboratory, Pasadena, Calif., Apr. 15, 1972.
8. Thomas, J. B., "An Analysis of Long Baseline Radio Interferometry, Part III," in *The Deep Space Network Progress Report*, Technical Report 32-1526, Vol. XVI, pp. 47-59, Jet Propulsion Laboratory, Pasadena, Calif., Aug. 15, 1973.

Table 1. Summary of significant error sources in conventional and dual-spacecraft radio metric data types (X = significant)

Significant error sources	Single-spacecraft data types		Dual-spacecraft data types		
	One station	Two-station (QVLBI)	Two-station	Four-station (Δ QVLBI)	Δ VLBI
Troposphere	X	X	^a		
Ionosphere	X	X	^a		
Space plasma	X		^{a, b}		
Antenna site positions or baseline vector	X	X			
UT1	X	X			
Polar motion	X	X			
Instrumental phase drifts	X	X	X ^{d, e}	X ^{c, d}	
Unmodeled Accelerations	X		X		
Zero declination singularity	X	X ^f	X	X ^f	X ^f
Planetary ephemerides	X	X	X ^g	X ^g	X ^g

^aCan be significant if two spacecraft are not at similar geocentric ranges.

^bDistant space plasma may be significant.

^cEffect is not significant if common frequency standards exist at nearby antenna pairs.

^dEffect can be reduced if hydrogen maser frequency standards are utilized at each antenna.

^eFootnote c applies if spacecraft are at similar geocentric ranges.

^fEffect is not significant for QVLBI range, Δ QVLBI range, and Δ VLBI delay data types.

^gEffect can be reduced for trailing spacecraft in dual-spacecraft missions.

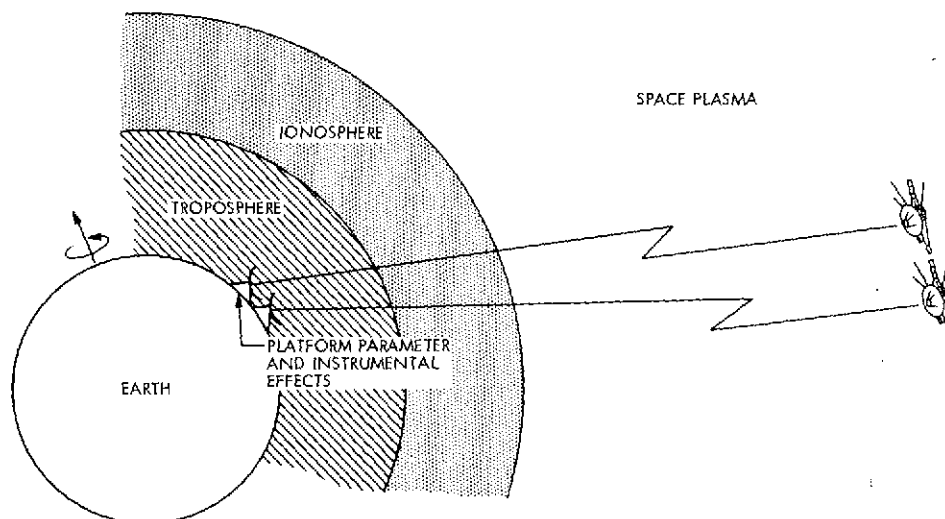


Fig. 1. Dual-spacecraft radio metric tracking: common error sources tend to cancel

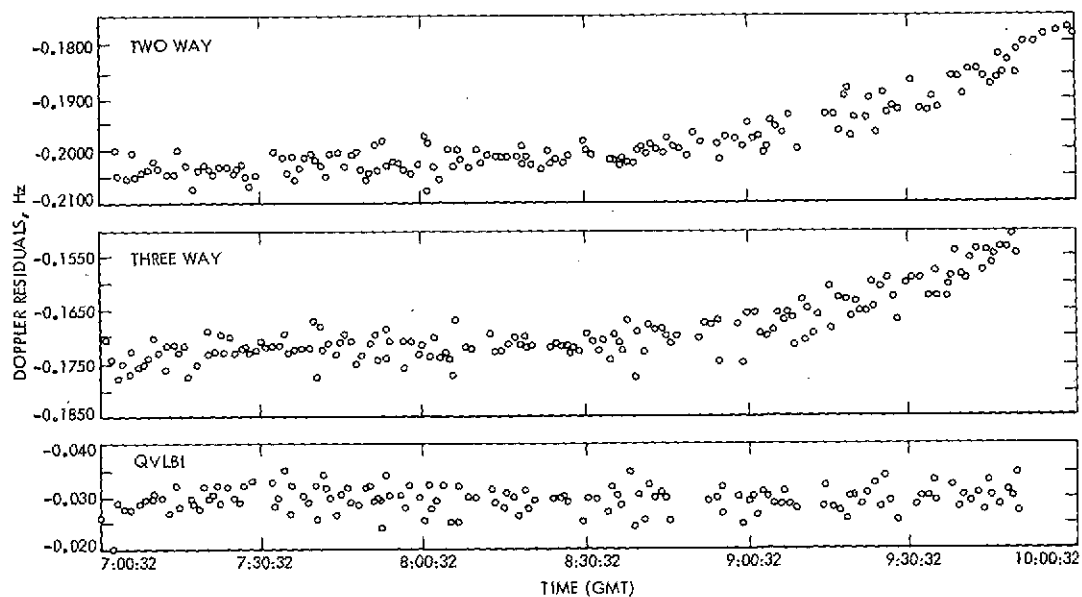


Fig. 2. Cancellation of transmission media effects at low elevation angles (short baseline QVLBI data)

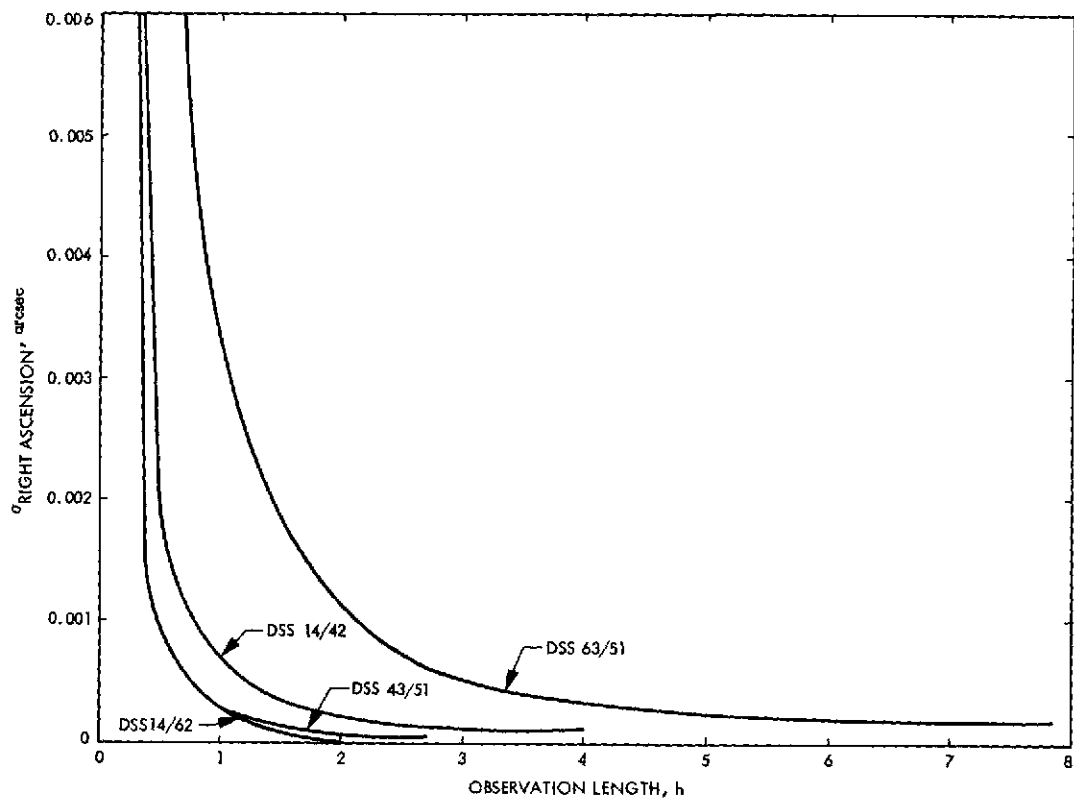


Fig. 3a. Uncertainty in right ascension of Pioneer 11 relative to Pioneer 10 vs VLBI observation length

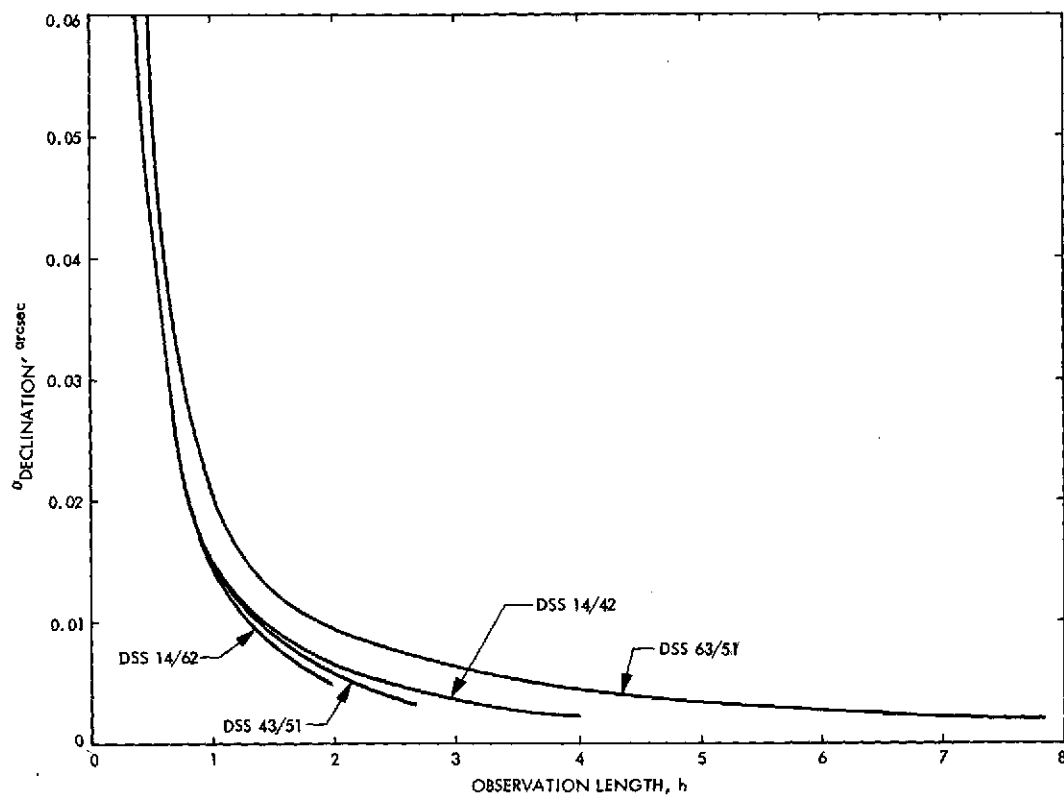


Fig. 3b. Uncertainty in declination of Pioneer 11 relative to Pioneer 10 vs VLBI observation length

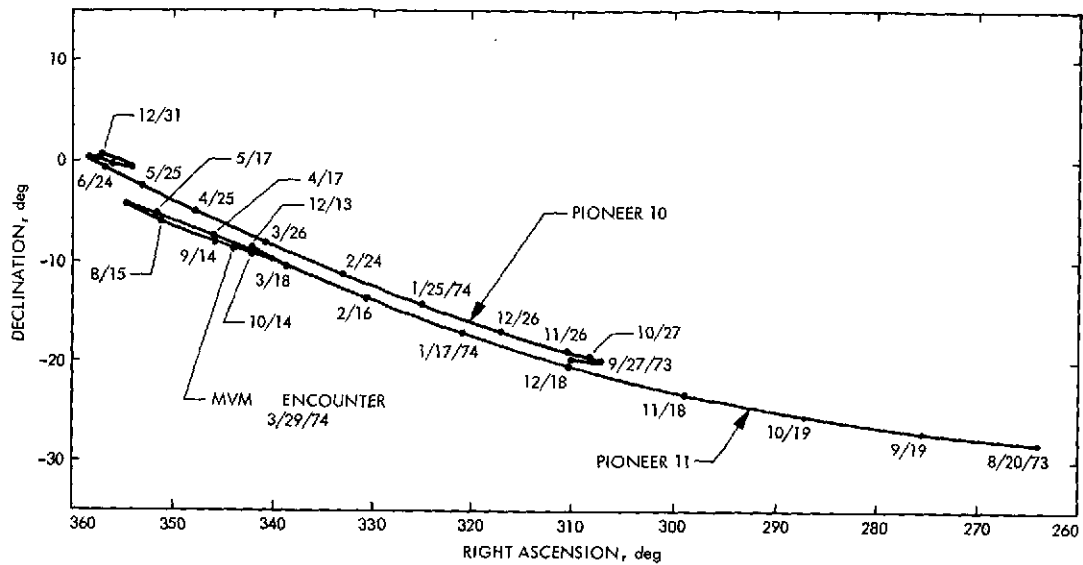


Fig. 4. Angular positions of Pioneer 10 and 11 spacecraft

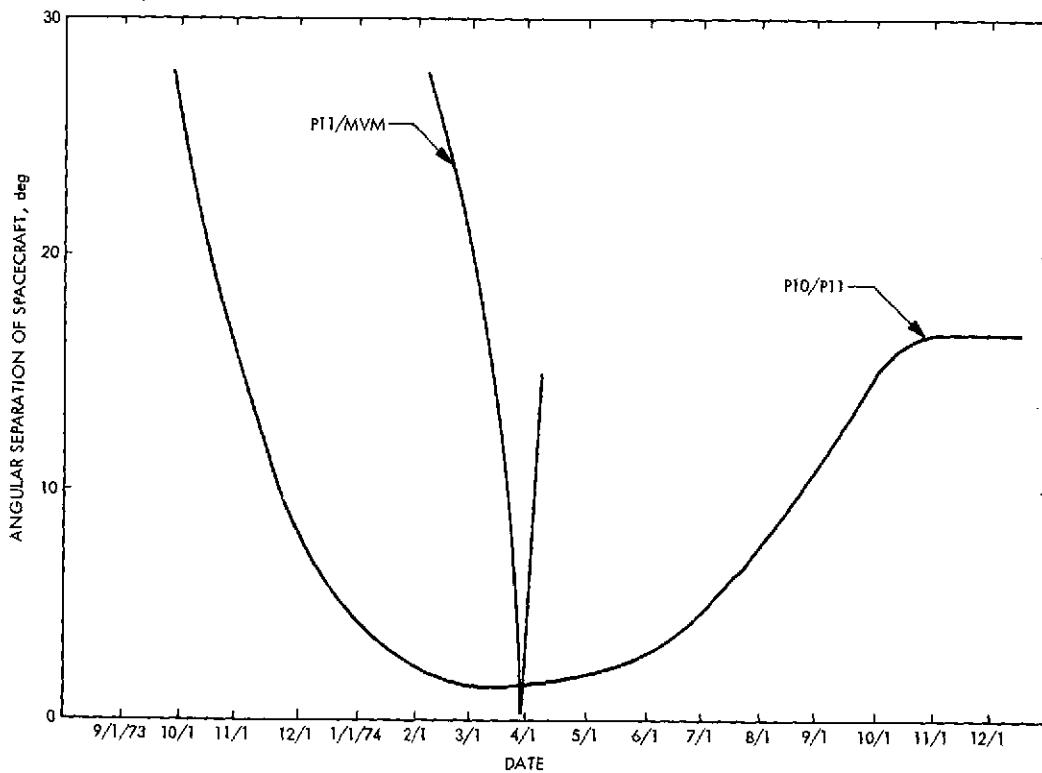


Fig. 5. Angular separations of Pioneer 10, Pioneer 11, and MVM'73 spacecraft

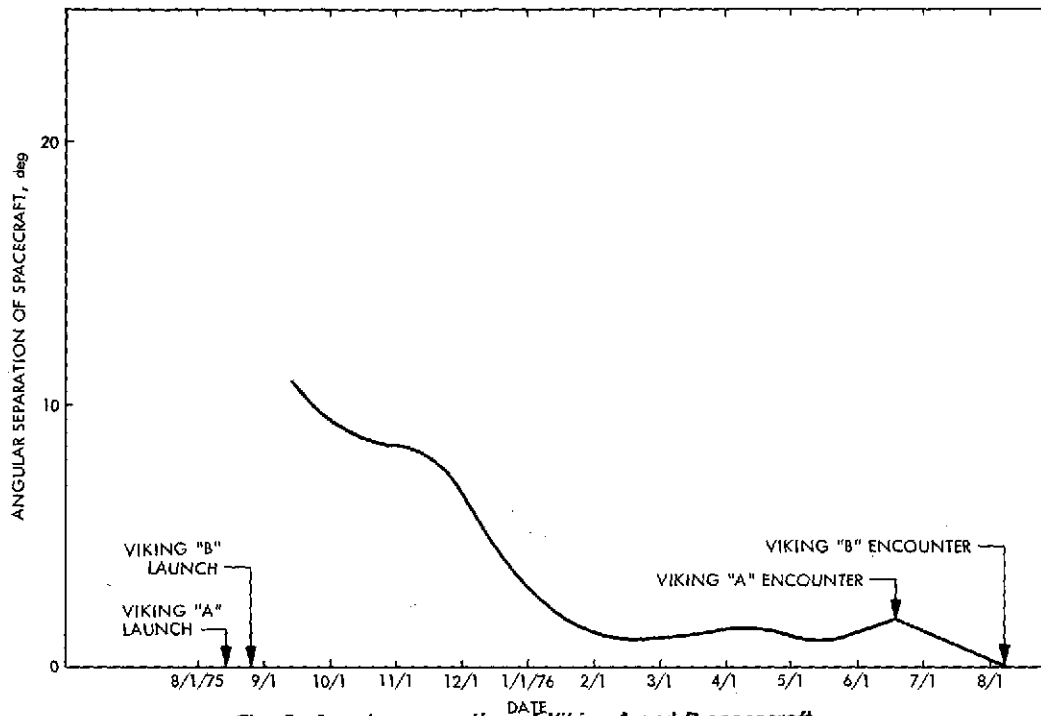


Fig. 6. Angular separation of Viking A and B spacecraft

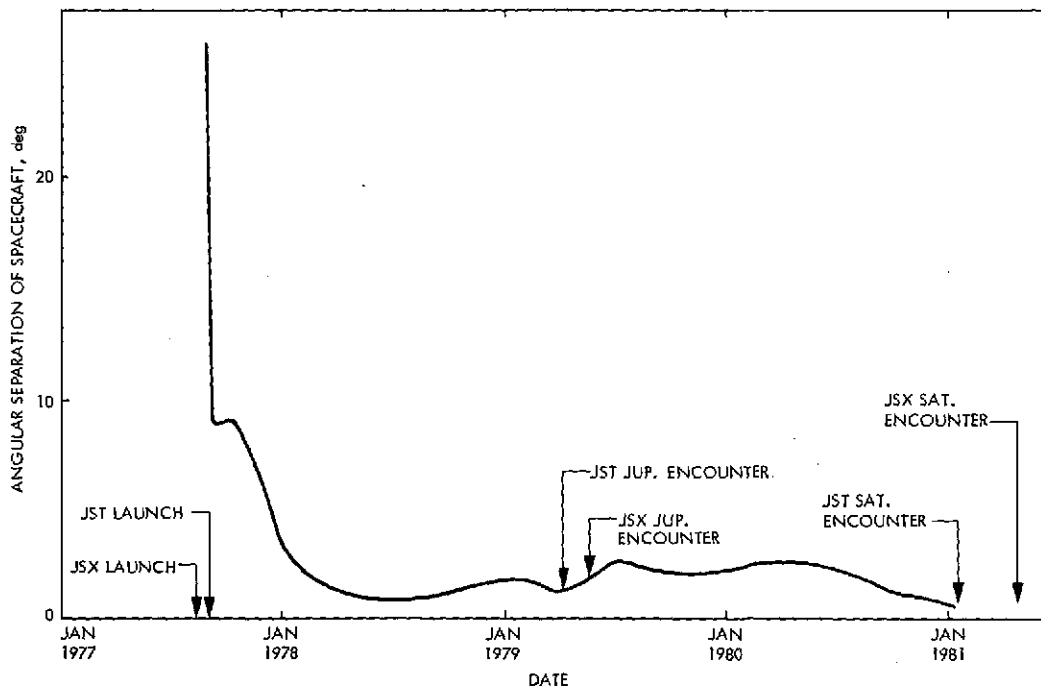


Fig. 7. Angular separation of JST and JSX spacecraft

An Evaluation of QVLBI OD Analysis of Pioneer 10 Encounter Data in the Presence of Unmodeled Satellite Accelerations

B. D. O'Reilly and C.C. Chao
Tracking and Orbit Determination Section

Quasi-very-long-baseline interferometry (QVLBI) has been used to predict Pioneer 10 flyby B-plane coordinates from simultaneous two- and three-way doppler data in the presence of unmodeled accelerations ($\leq \sim 10^{-8}$ km/s²) due to the four massive satellites of Jupiter. It is concluded from this study that the QVLBI technique for processing simultaneous two- and three-way doppler data is capable of predicting the encounter to within ~ 2000 km in the presence of unmodeled accelerations as large as 10^{-8} km/s². Calculations using two-way doppler data alone for the same nominal trajectory and a priori parameter statistics yielded systematic B-plane errors of the order of 100,000 km, with consequently meaningless formal uncertainties.

1. Introduction and Summary

Quasi-very-long-baseline interferometry (QVLBI) has been used to predict Pioneer 10 flyby B-plane coordinates from simultaneous two- and three-way doppler tracking data in the presence of unmodeled accelerations ($\leq \sim 10^{-8}$ km/s²) due to the four massive satellites of Jupiter. (Fig. 1 illustrates the B-plane coordinate system.) The work presented here was carried out in two stages:

A. Preliminary Simulation Study

A preliminary simulation study was performed during October 1973 to determine the sensitivity of the QVLBI

orbit determination process to the unmodeled Galilean satellite accelerations and to determine a suitable tracking pattern for acquiring simultaneous two- and three-way doppler data. Using pessimistic a priori parameter covariance values (in particular 100% mass uncertainties for the four massive satellites of Jupiter), it was found in the simulation study that QVLBI data analysis yielded a final (postencounter) value of ~ 2000 km for the semi-major axis of the B-plane error ellipse (SMAA). Using the same a priori parameter covariance and nominal trajectory, analysis of conventional two-way doppler data predicted a final value of ~ 7500 km for SMAA. In addition, the QVLBI determination of SMAA was found to be an always decreasing function of the length of the data arc,

whereas SMAA predicted from two-way doppler data exhibits a peak value of $\sim 53,000$ km at one day before encounter. The corresponding QVLBI value at one day before encounter is $\sim 12,000$ km (see Fig. 2).

B. B-Plane Accuracy Analyses

B-plane accuracy analyses were performed using both two-way doppler and QVLBI tracking data from the Pioneer 10 spacecraft during the encounter phase of its trajectory. The parameters modeled in the encounter study are listed in Table 1. The epoch and initial state vector and the a priori parameter statistics used in the encounter study appear in Tables 2, 3, and 4. The best B-plane target coordinate values inferred from each data type were obtained by estimating the spacecraft state vector at epoch and the mass, ephemeris parameters, and oblateness of Jupiter. The quality of the final results was ascertained by comparing them to the best estimates of $\mathbf{B} \cdot \mathbf{R}$ and $\mathbf{B} \cdot \mathbf{T}$ obtained by the JPL Pioneer Navigation Team processing almost continuous two-way doppler data with the dynamics of the Galilean satellites accounted for explicitly. (The reference values of $\mathbf{B} \cdot \mathbf{R}$ and $\mathbf{B} \cdot \mathbf{T}$ obtained in this manner are given in Table 5.) The QVLBI estimates of both $\mathbf{B} \cdot \mathbf{T}$ and $\mathbf{B} \cdot \mathbf{R}$ exhibit maximum deviations of ~ 4000 km from the reference values, with their final values deviating by ~ 1500 km (see Figs. 3 and 4). The corresponding final statistical uncertainties were $\sigma_{\mathbf{B} \cdot \mathbf{R}} = 133$ km and $\sigma_{\mathbf{B} \cdot \mathbf{T}} = 188$ km (see Fig. 5). By contrast, the two-way doppler estimates of $\mathbf{B} \cdot \mathbf{T}$ and $\mathbf{B} \cdot \mathbf{R}$ show maximum deviations of $\sim 35,000$ and $85,000$ km from their reference values with final values $\sim 27,000$ and ~ 2000 km (see Figs. 3 and 4). Their deviations from the reference values plotted as functions of the length of the data arc exhibit large amplitude variations which render any interpretation of their formal statistics meaningless.

It is concluded from this study that the QVLBI technique for processing simultaneous two- and three-way doppler data is capable of predicting the encounter coordinates of a spacecraft on a planetary flyby trajectory to within ~ 2000 km in the presence of unmodeled accelerations as large as 10^{-10} km/s².

Since the simultaneous tracking data for this study came almost exclusively from one pair of stations, DSS 14 and DSS 43, and it spans a somewhat limited time period (see the tracking schedule in Table 6), it would appear that 2000 km represents a conservative upper limit to the attainable accuracy for the estimation of targeting coordinates for flyby missions comparable to Pioneer 10. It should be noted especially that there was an irretrievable loss of critically important simultaneous data for several

hours surrounding encounter because of improper synchronization between a pair of tracking stations. With better tracking coverage, it is likely that the accuracy limit could be lowered significantly.

II. Background

Previous articles by V. J. Ondrasik and K. H. Rourke have shown that using differenced two-way/three-way doppler and range data rather than two-way data of these types may significantly improve the accuracy with which the trajectory of a spacecraft can be determined in the presence of process noise (see Refs. 1 and 2). Process noise describes the effect of unmodeled spacecraft acceleration on the processing of tracking data. In many cases it has been observed that unmodeled accelerations change the estimates of the spacecraft velocity and position by tolerably small amounts. However, they tend to degrade the statistical confidence in the trajectory estimate severely so that, for example, position uncertainties of many thousand kilometers may result.

Nearly identical process noise signatures appear in the down-link signals received simultaneously by both the transmitting station and a second station separated from the transmitter by a long baseline. Hence, differencing the data taken simultaneously from a pair of such stations tends to cancel the very similar process noise signatures in the simultaneous tracking signals received by them, thus producing a new data type which is, to high order, free of process noise effects. In a similar manner the effects of charged particles in space plasma can be reduced by using QVLBI.

In the present study of the Pioneer 10 spacecraft orbit determination accuracy during its encounter phase, we consider a somewhat surprising candidate for treatment using the QVLBI data type, namely the unmodeled spacecraft accelerations due to the gravity fields of the four massive satellites of Jupiter (Io, Callisto, Ganymede, and Europa). In the data analysis carried out by the Pioneer Navigation Team, the accelerations were modeled. In the present study they were purposely left unmodeled in order to gauge the ability of QVLBI data analysis to remove the errors in the estimates of the spacecraft orbit parameters due to the presence of their signatures in the two- and three-way tracking data before differencing.

It should be noted here that unmodeled accelerations up to the order of 10^{-8} km/s² are considered in this study.

Other studies are in progress to ascertain the ability of QVLBI to remove unmodeled gas leak and solar pressure signatures due to accelerations of the order of 10^{-11} km/s² acting on the Mariner 10 Venus/Mercury spacecraft (Ref. 3).

III. Scheme for Data Analysis

The QVLBI massive satellite analysis of the Pioneer 10 spacecraft's encounter has been carried out in two stages:

- (1) In advance of the onset of the encounter phase (which has been set at E-30 days), accuracy analysis studies were carried out to determine what errors would result from ignoring the effects of the Jovian satellites' gravity fields. The errors were expressed in terms of the axes of the Jovian B-plane error ellipse as a function of time from encounter (data arc length) using both conventional two-way doppler data and differenced simultaneous two-way/three-way doppler (QVLBI) data.
- (2) Using the results of the simulation study for guidance, a tracking schedule for taking simultaneous two- and three-way data was set up. The resulting two-way and QVLBI data were then processed using first the SATODP orbit determination program (Ref. 4) and then the ATHENA filter program to calculate the spacecraft state and B-plane covariance matrices.

A. Simulation Analysis

The simulation study used continuous two-way data from Stations 14, 51, and 61 with simultaneous three-way data between Stations 61 and 51. Attention was focused on solutions for the state at epoch (E-30 days) in the two-way doppler cases and for the state vector plus frequency bias between Stations 51 and 61 for the QVLBI cases. For two-way doppler simulation the standard deviation of the data noise was assumed to be 0.015 Hz (1 mm/s for range rate). To avoid complete loss of geocentric range rate information due to data differencing, the simulated two-way data, with noise standard deviation set to a very large value of 3.75 Hz, was included along with the QVLBI data (for the reasons given in Ref. 5). In all cases, the simulated data spanned the interval from E - 30 to E + 7 days. The list of error sources (consider parameters) and their sizes (a priori uncertainties), used to evaluate the accuracy of the solution for the state vector at epoch, appear in Tables 7, 8, and 9. The epoch and initial state vector for these calculations are given in Table 10.

Each of the values of the B-plane error ellipse semi-major axis plotted in Fig. 1 was obtained by an appropriate time/coordinate mapping and subsequent diagonalization of the state vector covariance matrix obtained for the indicated time of encounter.

B. Encounter Analysis

A tracking schedule for both two-way and simultaneous two- and three-way doppler data was arranged as dictated by the results of the simulation study and the availability of antenna time. (A summary of data types and corresponding time spans actually used appears in Table 6.) The dominant influence of station location uncertainties on the quality of the simulated B-plane solutions prior to E - 3 days dictated the use of geocentrically sensitive two-way doppler data from E - 30 to E - 10 days. The shift from dominance of station location uncertainties to satellite mass uncertainties after E - 3 days inferred from the simulation study pointed to the use of QVLBI data from that time forward.

To improve the accuracy of orbit determination calculations performed with QVLBI data, care was taken to treat the frequency bias between DSS 14 and DSS 43 as a solve-for parameter and the frequency biases between DSS 43 and DSS 63 and between DSS 63 and DSS 14 as consider parameters (error sources). This was done in light of the fact that it was learned that the relative bias between station frequency standards appears to be the major error source in the QVLBI data type (Ref. 6). The frequency system for this demonstration using the new rubidium standards has a long-term instability of about $\Delta f/f = 3 \times 10^{-12}$ (Ref. 7). It should be noted that the unmodeled accelerations due to Jupiter's inner satellites are as large as 10^{-8} km/s². Such acceleration is equivalent to a long-term noise of $\Delta f/f \approx 3 \times 10^{-8}$. Thus the biases characteristic of the current frequency system are several orders of magnitude below the level which would mask the signature of the satellite accelerations.

The following rationale was used to determine the ratio of the standard deviations of the noise distributions belonging to two-way doppler and QVLBI data. From the short baseline QVLBI study of Chao, Wong, and Lubeley using Pioneer 10 and Pioneer 11 tracking data taken during the spring of 1973 (Ref. 5), it was inferred that a reasonable value for the ratio of two-way-doppler-to-QVLBI noise standard deviations is

$$\sigma_{2\text{-way}}/\sigma_{\text{QVLBI}} \approx 3$$

Thus, the two-way doppler and QVLBI noise sigmas used to analyze the data discussed here were

$$\sigma_{2\text{-way}} = 0.045 \text{ Hz (3 mm/s)}$$

and

$$\sigma_{\text{QVLBI}} = 0.015 \text{ Hz (1 mm/s)}$$

The relatively smaller noise level of the QVLBI data is attributed to cancellation of process and transmission medium noise.

The sequence of calculation processes to which the encounter data were subjected is described below. The numerical results of the calculations and the conclusions drawn therefrom have been presented above in the study summary.

IV. Computational Tools and Data Processing

Below we give a brief account of the computational tools and data processing procedures which were used to obtain the results presented above. A list of computer codes used, their functions, and their authors appears in Table 11.

A. Sequence of Computations for the Encounter Simulation Study

- (1) A modified version of the REVA link of the ATHENA filter program called MACK was used to generate simulated range-rate REGRES and PATH-VARY files for a continuous tracking pattern using Deep Space Stations 51, 61, and 14, spanning the period from $E - 30$ to $E + 10$ days. MACK accounts for the accelerations due to the four massive satellites of Jupiter. The output REGRES file from this calculation describes very nearly the information contained in conventional two-way doppler data for the same spacecraft tracking history.
- (2) The code DERIVE was used to augment the two-way range-rate REGRES and VARY files with effective simultaneous differenced two-way/three-way REGRES and VARY files. In particular, partial derivatives of the differenced range rate observable with respect to an assumed constant frequency bias between DSS 51 and DSS 61 were calculated and used in the formation of the additional files.

- (3) The TOSCA link of the ATHENA filter was used in batch mode to combine the a priori statistics of the parameter sets described in Tables 8 and 9 with the statistical information contained in the simulated REGRES files for both conventional two-way and differenced data types to obtain both "consider" and "estimate" covariance matrices for the heliocentric EME (Earth mean equator) 1950 Cartesian state vector at epoch for a selection of print times ranging from $E - 10$ to $E + 7$ days. "Print time" refers to the time of the last data point included in the data batch under consideration.
- (4) The SCANB link of the ATHENA program was used to map the estimate and consider covariance matrices of the state vector at epoch to the B-plane at encounter. An important ancillary result of the consider covariance mapping is the calculation of the perturbation matrix, which provides a direct measure of the relative importance of the confidence degrading influence of the a priori uncertainties of the consider (unmodeled) parameters on the covariance of the B-plane parameters.

B. Sequence of Computations for Analysis of Pioneer 10 Encounter Data

- (1) With the aid of the orbit data editor (ODE), IBM 360 tracking data tapes obtained from the Mission Operations Analysis Tracking Team (MOATRK) were decoded (converted for processing by the UNIVAC 1108), and two- and three-way doppler data, taken at 60- and 10-s sample rates (mostly at the former rate), were extracted to form a preliminary orbit data file.
- (2) These data were examined to locate blunder points by direct visual inspection.
- (3) The ODE was then exercised to purge the data file of blunder points, and the remaining data points were compressed to ≤ 11 -min count-times. Care was taken to align simultaneous sequences of two- and three-way data points to produce simultaneous two- and three-way compression intervals whenever station overlaps were available for three-way reception.
- (4) The edited and compressed data files obtained from individual tracking tapes were then merged into a single data file using ODE.
- (5) The merged data file was then processed through the links ODINA, PATH, VARY, ODINB, REGRESS,

and ACCUME of the double-precision-orbit-determination processor SATODP/Version D¹ to produce:

- (a) A PATH-VARY file containing the partial derivatives of the state vector with respect to the trajectory parameters listed in Table 1 (excluding frequency biases between stations).
- (b) A file of partial derivatives of the two- and three-way observables with respect to the trajectory parameters.
- (c) A file containing the square-root information matrix which results from combining the square root of the inverse a priori parameter covariance with the matrix of weighted data partials. It also contains appropriately weighted and transformed data residuals. (The initial state vector and epoch appearing in Table 2 were used to generate the nominal trajectory and its associated variational partial derivatives. They represent a converged orbit obtained from the Pioneer 10 operations orbit determination team. The data noise variances described in the preceding section and the a priori parameter covariances given in Tables 3 and 4 were used to prepare the output ACCUME file.)

¹SATODP/version D does not account for Jovian satellite accelerations.

- (6) The ACCUME and PATH-VARY files were next input into the DIFFER code, where they were used to form properly weighted differenced doppler ACCUME and data residual files. The a priori interstation frequency bias estimates, their variances, and the difference data partials with respect to the biases were incorporated into the ACCUME file at this point.
- (7) The output two-way and differenced doppler ACCUME files generated by SATODP and DIFFER were next processed separately in batch mode by the TOSCA link of the ATHENA filter to obtain a set of estimates of the initial state vector and other parameters, the subsets of which belong to a selection of data arc lengths (labeled by the time of the last data point from encounter). The corresponding "estimate" and "consider" covariances of the various parameter estimates are also computed along with a file of partial derivatives of the state vector with respect to its own components at epoch to be used subsequently to perform time-coordinate mappings.
- (8) Finally, the SCANB link of ATHENA was used to map the initial state vector estimates and their covariances to the B-plane at encounter for a selection of print times ranging from $E - 5$ to $E + 2.6$ days. Corresponding perturbation matrices were produced to show the influence of the a priori consider covariance on the B-plane statistics.

References

1. Ondrasik, V. J., and Rourke, K. H., "Applications of Quasi-VLBI Tracking Data to the Zero Declination and Process Noise Problems," AAS No. 71-399, Astrodynamics Specialists Conference, Ft. Lauderdale, Fla., Aug. 1971.
2. Ondrasik, V. J., and Rourke, K. H., "Application of New Radio Tracking Data Types to Critical Spacecraft Navigation Problems," Quarterly Technical Review, Vol. I, No. 4, Jet Propulsion Laboratory, Pasadena, Calif., Jan. 1972.
3. Chao, C. C., "Report of QVLBI Doppler Demonstration Conducted with Mariner 10," EM 391-584, Jet Propulsion Laboratory, Pasadena, Calif., July 1974 (an internal document).
4. Moyer, T. D., *Mathematical Formulation of the Double-Precision Orbit Determination Program*, Technical Report 32-1527, Jet Propulsion Laboratory, Pasadena, Calif., July 15, 1971.

References (contd)

5. Nishimura, T., and Nead, M., "ATHENA Filter Sequential Orbit Determination Program with General Evaluation Capability," 900-605 (a JPL internal document), Mar. 8, 1973.
6. Mulhall, B. D., Chao, C. C., Johnson, D. E., and Zielenbach, J. W., "Report of the Two-Station Doppler (VLBI) Demonstration Conducted with Mariner 9," in *The Deep Space Network Progress Report 42-20*, pp. 27-40, Jet Propulsion Laboratory, Pasadena, Calif., Apr. 15, 1974.
7. Chao, C. C., Wong, S. K., and Lubeley, A., "Short Baseline QVLBI Demonstrations-Part I," in *The Deep Space Network Progress Report*, Technical Report 32-1526, Vol. XVIII, pp. 47-56, Jet Propulsion Laboratory, Pasadena, Calif., Feb. 15, 1973.

Table 1. Parameters included in Pioneer 10 encounter data analysis

Parameter description	Number of parameters	2-way doppler/ Case 1		QVLBI/Case 1		2-way doppler/ Case 2		QVLBI/Case 2	
		Estimate	Consider	Estimate	Consider	Estimate	Consider	Estimate	Consider
EME 1950 Cartesian state vector at epoch	6	✓		✓		✓		✓	
Mass of Jupiter	1	✓		✓		✓		✓	
Frequency bias of DSS 43 relative to DSS 14	1	—	—	✓		—		✓	
Jupiter Set III ephemeris parameters	6		✓		✓	✓		✓	
Jupiter oblateness	1		✓		✓	✓		✓	
Gas leak accelerations	3		✓		✓		✓		✓
DSS 14, 43, 63 off-axis distances and longitudes	6		✓		✓		✓		✓
Frequency biases of DSS 14, 63 relative to DSS 63, 43	2		✓		✓		✓		✓
Earth-Moon barycenter Set III ephemeris parameters	6		✓		✓		✓		✓
DSS 12 off-axis distance and longitude	2		✓		✓		✓		✓

Table 2. Epoch and Jupiter-centered EME 1950 state vector for encounter analysis

Epoch = OCT. 5, 1973, 01 ^h 00 ^m 00 ^s .0000
X = $-0.647705629868 \times 10^7$ km
Y = $0.459338906494 \times 10^8$ km
Z = $0.171826623342 \times 10^8$ km
DX = $0.105757364142 \times 10^1$ km/s
DY = $-0.821591385146 \times 10^1$ km/s
DZ = $-0.311665562776 \times 10^1$ km/s

Table 3. A priori parameter uncertainties for encounter analysis

Parameter	Estimate σ	Consider σ
Position	10^4 km	
Velocity	1 km/s	
GM5	6×10^3 km ³ /s ²	
Off-Axis station location		3 m
Station longitude		5×10^{-5} deg
J205	1.5×10^{-4}	1×10^{-5}
Gas leak acceleration		1×10^{-11} km/s ²
GMM		5×10^{-2} km ³ /s ²
Frequency bias	23 mHz	10 mHz

Table 4. Combined Set III Jupiter/Earth-Moon barycenter covariance for QVLBI data analysis

The combined (12×12) Jupiter/Earth-Moon barycenter (EMB) covariance matrix can be expressed in the partitioned form

$$\Gamma_{\text{comb}} = \begin{pmatrix} \Gamma_{\text{Jup}} & \Gamma_{\text{Jup:EMB}} \\ \Gamma_{\text{Jup:EMB}}^T & \Gamma_{\text{EMB}} \end{pmatrix}$$

The a priori values of the elements of the 6×6 submatrices Γ_{Jup} , Γ_{EMB} , and $\Gamma_{\text{Jup:EMB}}$ are tabulated below.

Γ_{Jup}						
	DMW5	DP5	DQ5	EDW5	DA5	DE5
DMW5	0.497×10^{-12}	0.112×10^{-14}	-0.231×10^{-14}	-0.300×10^{-13}	-0.172×10^{-13}	-0.600×10^{-14}
DP5	0.112×10^{-14}	0.284×10^{-12}	0.153×10^{-13}	-0.345×10^{-15}	-0.555×10^{-16}	0.234×10^{-15}
DQ5	-0.231×10^{-14}	0.153×10^{-13}	0.273×10^{-12}	-0.230×10^{-15}	0.290×10^{-16}	-0.304×10^{-15}
EDW5	-0.300×10^{-13}	-0.345×10^{-15}	-0.230×10^{-15}	0.710×10^{-13}	0.186×10^{-14}	0.499×10^{-14}
DA5	-0.172×10^{-13}	-0.555×10^{-16}	0.290×10^{-16}	0.186×10^{-14}	0.820×10^{-15}	0.414×10^{-15}
DE5	-0.600×10^{-14}	0.234×10^{-15}	-0.304×10^{-15}	0.499×10^{-14}	0.414×10^{-15}	0.683×10^{-18}
Γ_{EMB}						
	DMWB	DPB	DQB	EDWB	DAB	DEB
DMWB	0.134×10^{-18}	-0.153×10^{-15}	0.767×10^{-16}	0.189×10^{-15}	-0.243×10^{-16}	-0.382×10^{-17}
DPB	-0.153×10^{-15}	0.124×10^{-13}	-0.978×10^{-16}	-0.711×10^{-18}	0.327×10^{-18}	0.814×10^{-18}
DQB	0.767×10^{-16}	-0.978×10^{-16}	0.135×10^{-19}	0.222×10^{-17}	-0.132×10^{-19}	-0.525×10^{-18}
EDWB	0.189×10^{-15}	-0.711×10^{-18}	0.222×10^{-17}	0.326×10^{-17}	-0.288×10^{-18}	-0.904×10^{-19}
DAB	-0.243×10^{-16}	0.327×10^{-18}	-0.132×10^{-18}	-0.288×10^{-18}	0.830×10^{-19}	0.147×10^{-19}
DEB	-0.382×10^{-17}	0.814×10^{-18}	-0.525×10^{-18}	-0.904×10^{-19}	-0.904×10^{-19}	0.135×10^{-18}
$\Gamma_{\text{Jup:EMB}}$						
	DMWB	DPB	DQB	EDWB	DAB	DEB
DMW5	0.338×10^{-14}	-0.640×10^{-16}	-0.343×10^{-17}	0.476×10^{-16}	-0.618×10^{-17}	-0.973×10^{-18}
DP5	-0.638×10^{-16}	0.286×10^{-15}	-0.363×10^{-14}	-0.126×10^{-17}	0.556×10^{-19}	0.158×10^{-18}
DQ5	-0.382×10^{-16}	0.340×10^{-14}	0.118×10^{-15}	-0.133×10^{-18}	0.810×10^{-19}	0.216×10^{-18}
EDW5	0.159×10^{-16}	-0.118×10^{-17}	0.128×10^{-17}	0.298×10^{-18}	0.280×10^{-19}	0.420×10^{-19}
DA5	-0.701×10^{-18}	0.189×10^{-17}	-0.970×10^{-18}	-0.810×10^{-18}	0.253×10^{-18}	0.453×10^{-19}
DE5	-0.809×10^{-17}	0.347×10^{-17}	-0.981×10^{-19}	-0.241×10^{-18}	0.224×10^{-19}	0.189×10^{-19}

**Table 5. Current best estimates of encounter parameters
(from S. K. Wong/JPL Pioneer Operations)**

$$B \cdot R = 208887 \pm 54 \text{ km}$$

$$B \cdot T = 836151 \pm 14 \text{ km}$$

Table 6. Tracking data summary for Pioneer 10 encounter phase

Station ID	Data type	Time of first point	Time of last point	Total number of points
DSS 12	Two-way doppler	10/5/73, 02:42:32	11/16/73, 00:57:32	129
DSS 43	Two-way doppler	10/6/73, 08:52:32	12/6/73, 11:28:32	1305
DSS 14	Two-way doppler	10/12/73, 02:57:32	12/6/73, 03:09:32	443
DSS 14	Three-way doppler	11/22/73, 20:08:32	12/6/73, 03:32:32	89
DSS 43	Three-way doppler	11/23/73, 01:09:32	12/6/73, 03:09:32	159
DSS 63	Three-way doppler	11/23/73, 12:44:02	12/3/73, 12:13:32	13
DSS 63	Two-way doppler	11/26/73, 14:23:32	12/6/73, 16:13:32	329

Table 7. Parameters modeled in Pioneer 10 encounter simulation

Parameter description	Number of parameters	Range rate data	
		Estimate	Consider
EME 1950 Cartesian state vector at epoch	6	✓	
Mass of Jupiter	1		✓
Modified Jupiter Set III ephemeris parameters	6		✓
DSS 51, 61, 14 off-axis distances and longitudes	6		✓
Jupiter oblateness	1		✓
Mass of Galilean satellites	4		✓
Axial coordinates of DSS 51, 61, 14	3		✓

Table 8. A priori parameter uncertainties for simulation

Parameter	A priori σ	Comments
Position	10^5 km	
Velocity	1 km/s	
GM 5	2×10^3 km ³ /s ²	
Off-axis station location	5 meters	
Axial station location	10 meters	
Station longitude	10^{-4} deg	
J205	1.469×10^{-4}	1% nominal
GM Io	4.827×10^3 km ³ /s ²	100% nominal
GM Europa	3.140×10^3 km ³ /s ²	100% nominal
GM Ganymede	1.039×10^4 km ³ /s ²	100% nominal
GM Callisto	6.449×10^3 km ³ /s ²	100% nominal
Frequency bias	100 mHz	$\sim 3 \times \text{MM}'71$ estimate

Table 9. Modified Set III Jupiter ephemeris covariance at encounter for simulation

	DA	DE	DMW	DP	DQ	EDW
DA	2.893×10^{-13}	1.963×10^{-13}	9.996×10^{-14}	2.433×10^{-16}	-8.969×10^{-16}	-1.867×10^{-13}
DE	1.963×10^{-13}	1.946×10^{-13}	7.288×10^{-14}	8.254×10^{-16}	-1.751×10^{-15}	-1.233×10^{-13}
DMW	9.996×10^{-14}	7.288×10^{-14}	5.189×10^{-13}	2.391×10^{-15}	-4.858×10^{-15}	-1.041×10^{-13}
DP	2.433×10^{-16}	8.254×10^{-16}	2.391×10^{-15}	2.703×10^{-13}	-1.267×10^{-14}	-1.070×10^{-16}
DQ	-8.969×10^{-16}	-1.751×10^{-15}	-4.858×10^{-15}	-1.267×10^{-14}	2.952×10^{-13}	-3.723×10^{-16}
EDW	-1.867×10^{-13}	-1.233×10^{-13}	-1.041×10^{-13}	-1.070×10^{-16}	-3.723×10^{-16}	1.869×10^{-13}

Table 10. Epoch and initial heliocentric EME 1950 state vector for simulation

Epoch = Nov. 3, 1973 03 ^h 00 ^m 00 ^s .0000	
X =	$0.533909756719 \times 10^9$ km
Y =	$-0.460598183846 \times 10^9$ km
Z =	$-0.212212398617 \times 10^9$ km
DX =	$0.101088969303 \times 10^2$ km/s
DY =	0.754694585646 km/s
DZ =	0.525514523035 km/s

Table 11. Computer codes

Code name	Reference	Comments
ATHENA	Nishimura, T., and Nead, M., 900-605, "ATHENA Filter Sequential Orbit Determination Program with General Evaluation Capability," Mar. 8, 1973	System consists of three links: (1) REVA—An orbit data simulator (2) TOSCA—A statistical filter. Accepts both simulated regress files from REVA and type 66 regress files from SATODP (3) SCAN—Routine for coordinate-time mapping
Modifications to ATHENA	Hildebrand, C. E. (unpublished)	MACK—A modified version of the REVA simulator which accounts specifically for the accelerations due to the massive Jovian satellites
DERIVE	Rourke, K. and Finley S., IOM 391.7-59 (a JPL internal document), Sep. 29, 1972	Code combines ATHENA-simulated two- and three-way regress files to produce simulated differenced (QVLBI) regress files. Accounts for frequency biases between pairs of stations. It is specifically adapted to accept regress files in the format produced by the ATHENA simulation link
ODE	Bramble, P. L., Jr., 610-188, "Mariner Mars 1971 Orbit Data Editor User's Guide" (a JPL internal document) Bramble, P. L., Jr., IOM 914.34/120 (a JPL internal document), Mar. 4, 1973	Performs following tasks: (1) Decodes IBM 360 tracking data tapes to produce raw tracking data files (2) Merges raw tracking data files (3) Edits data; removes user-selected data from file to produce file with only those data actually to be used (4) On request compresses doppler data to user-specified count-times (5) Merges edited/compressed data files
SATODP/Version D	Moyer, T. D., JPL TR 32-1527, Mathematical Formulation of the Double-Precision Orbit Determination Program, July 15, 1971	Implements an (almost) exhaustively detailed model of spacecraft motion in the solar system and uses it in conjunction with the method of differential corrections to set up and solve nonlinear regression analyses of many kinds of measured observables which depend on large numbers of parameters. Its modular (link) structure makes it possible to perform selected combinations of the basic computational tasks which together constitute a complete orbit determination calculation
DIFFER	Johnson, D. E., TM 391-333 (an internal document), June 9, 1972	Combines two- and three-way data files in SATODP (type 66) regress file format to produce QVLBI (differenced) data files in the same format. It incorporates a priori values, variances, and data partials with respect to frequency biases into the QVLBI file

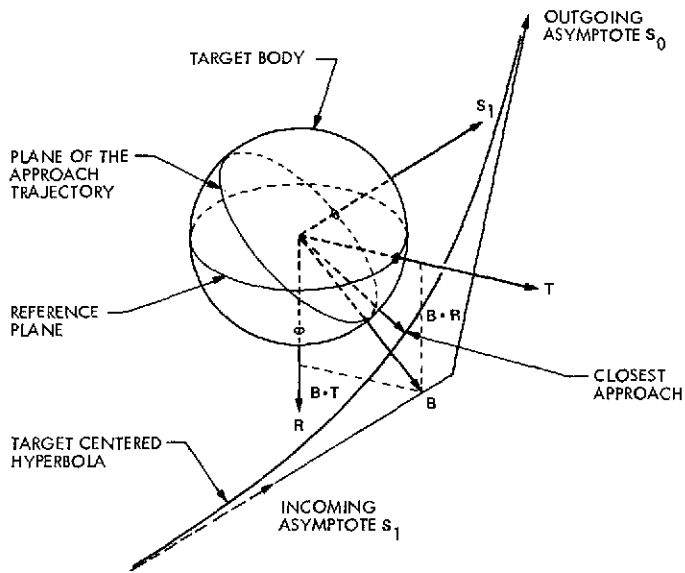


Fig. 1. Target parameters

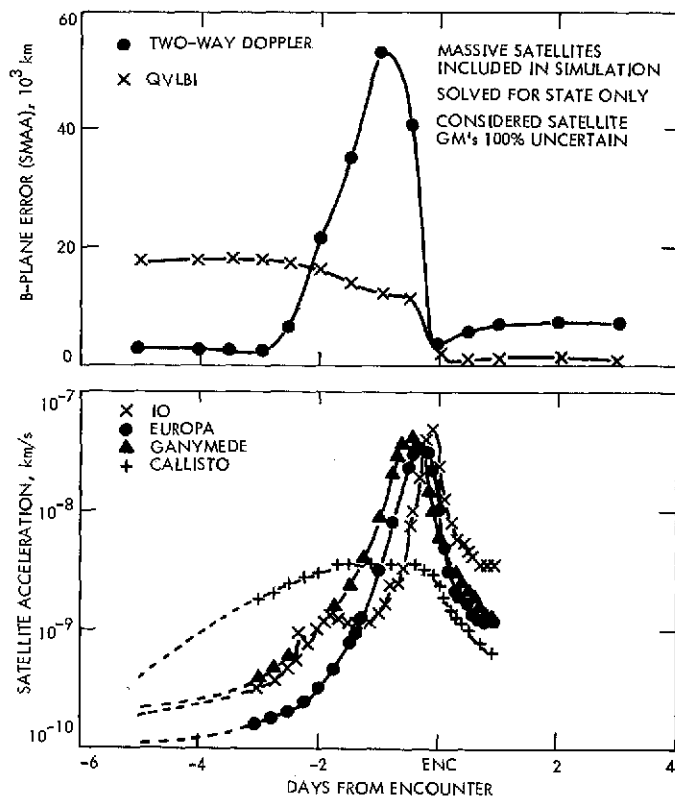


Fig. 2. Simulation study of B-plane errors

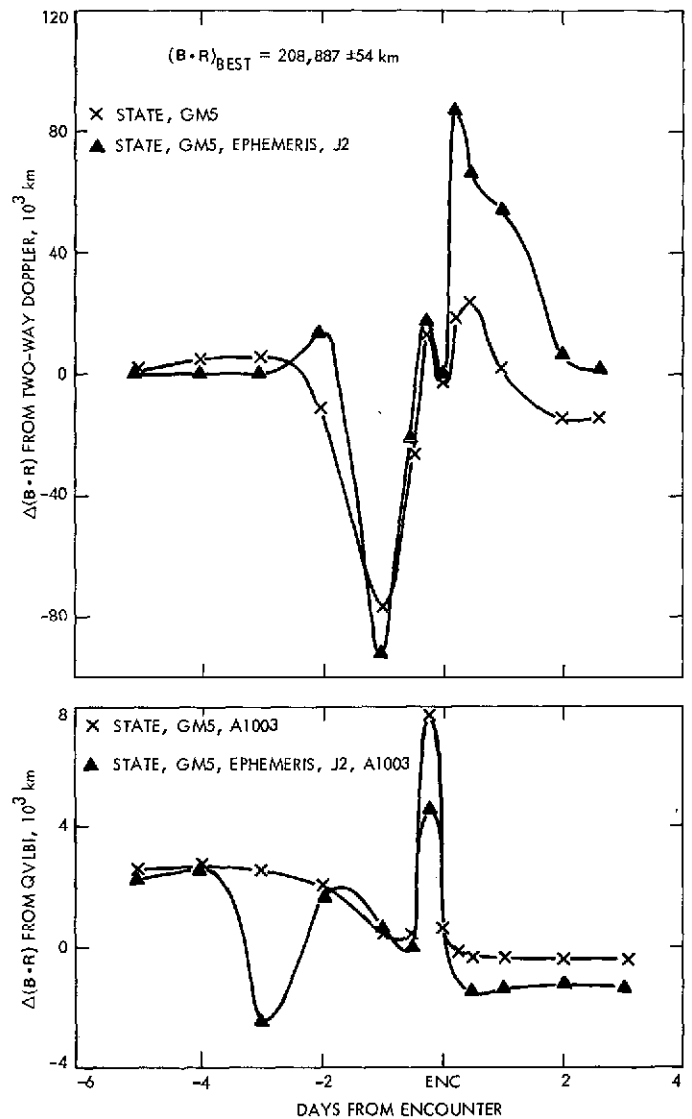


Fig. 3. $\Delta(B \cdot R) = B \cdot R - (B \cdot R)_{\text{best}}$ vs time from encounter

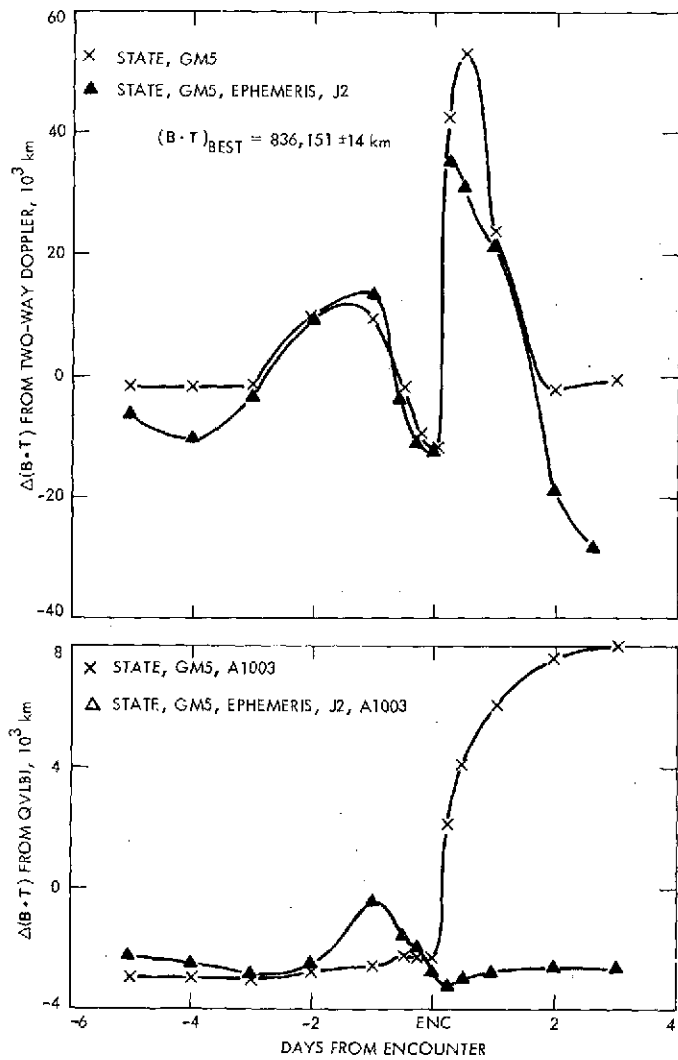


Fig. 4. $\Delta(B \cdot T) = B \cdot T - (B \cdot T)_{\text{best}}$ vs time from encounter

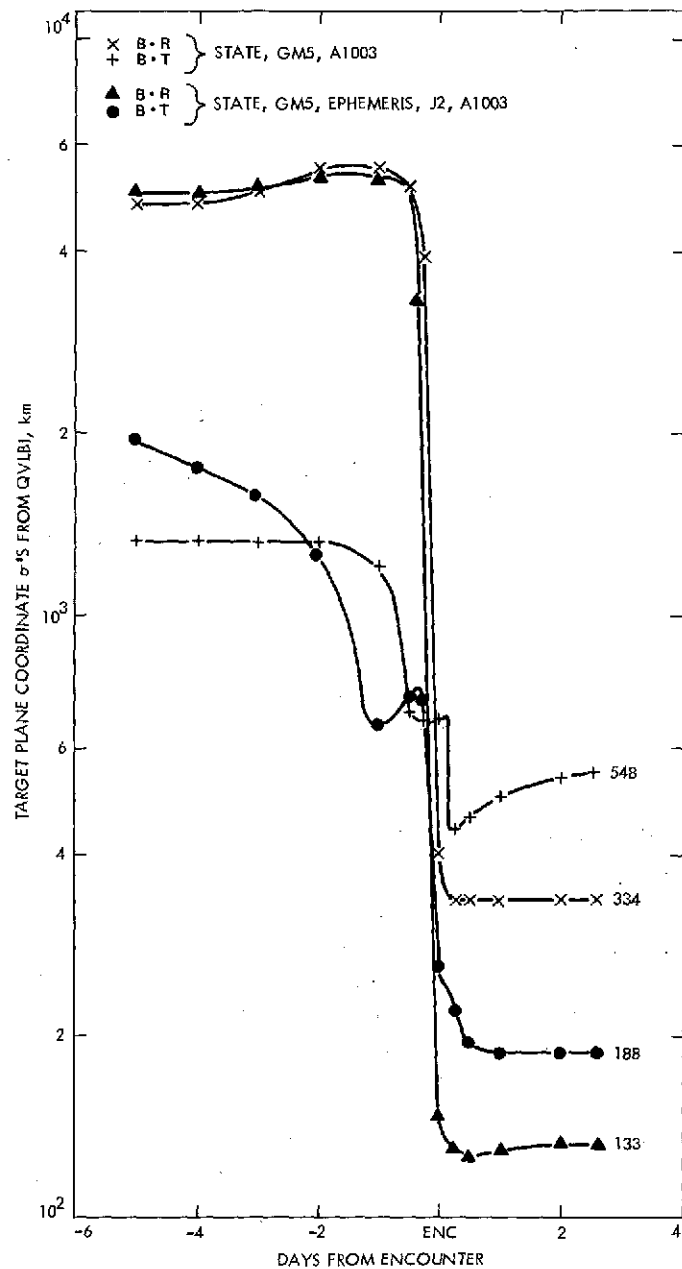


Fig. 5. Uncertainties in $B \cdot R$ and $B \cdot T$ vs time from encounter

The Ultimate Limits of Binary Coding for a Wideband Gaussian Channel

S. A. Butman and R. J. McEliece
Communications Systems Research Section

This article presents, in graphical form, the theoretical relationship between bit signal-to-noise ratio, bit error probability, and bandwidth expansion factor for binary coded telemetry on a wideband Gaussian channel.

I. Introduction

In this article we calculate the theoretical limits of the performance of binary coding on a wideband Gaussian channel, such as the deep-space downlink on the National Aeronautics and Space Administration's (NASA's) planetary probes. Our results show the inescapable tradeoffs which must be made between signal power, data rate, bit error probability, and bandwidth occupancy.

Our motive, primarily, is to provide a convenient reference for system designers and coders. For example, it is known (Ref. 1) that a rate $\frac{1}{2}$ (rate R of a binary-coded system is the number of information symbols per transmitted encoded symbol), constraint length 7 convolutional code, which is decoded with the Viterbi algorithm, requires a bit signal-to-noise ratio (E_b/N_0) of 2.6 dB in order to achieve a bit error probability (P_E) of 0.005. Figure 1 shows that it is theoretically possible to achieve the same P_E at the same rate with binary coding at a value of E_b/N_0 of only -0.1 dB. The minimum conceivable E_b/N_0 required to achieve $P_E = 0.005$ with no

restriction on bandwidth expansion is seen to be about -1.8 dB. (Although current *Mariner* bit rates of the order 10^5 bits per second make binary codes of rates much less than $\frac{1}{2}$ impractical, probes to the very distant outer planets will have much smaller bit rates and will allow the use of codes with larger bandwidth expansion, i.e., larger symbol-to-bit ratios. Thus it is important to know the theoretical limits of binary codes for arbitrary small values of R .)

The above example illustrates the usefulness of our results. They provide yardsticks against which the performance of an actual system can be measured.

II. Calculations

Let us consider a communications channel which accepts one of two real numbers, $\pm\alpha$, and adds to the transmitted number a normally distributed random variable z which has mean 0 and variance 1. This channel is an accurate model of a wideband Gaussian channel in which binary

modulation is used and for which the output is sampled at the Nyquist rate, i.e., at a rate of $2W$, where W is the bandwidth of the signal. If a code of rate R is being used, the value of α turns out to be $(2RE_b/N_0)^{1/2}$. The formula for the capacity of the above two-input Gaussian channel is (Ref. 2)

$$C_2(\alpha) = \alpha^2 - \frac{1}{\sqrt{2\pi}} \int_{-\infty}^{\infty} e^{-y^2/2} \log \cosh(\alpha^2 + \alpha y) dy \quad (\text{nats/symbol}) \quad (1)$$

Hence, according to well-known results of information theory, a bit error probability of p is achievable as long as

$$R(1 - H(p)) \leq C(\alpha), \quad \alpha = (2RE_b/N_0)^{1/2} \quad (2)$$

where $H(p) = -p \log p - (1-p) \log (1-p)$ is the natural entropy function. Formula (2), with equality substituted for the inequality, gives the relationship between

the rate R and the error probability P_E , which we have plotted in Fig. 1.

We have restricted our attention to binary input schemes in this note because of their widespread, almost universal, use in practical systems. However, it is interesting to compare binary codes to codes which are allowed to use an arbitrary number of input levels. Here the formula corresponding to (2) is

$$R(1 - H_2(p)) \leq \frac{1}{2} \log_2(1 + \alpha^2) \quad (3)$$

where $H_2(p) = H(p)/\log 2$ is the binary entropy function. Rather than give another figure like Fig. 1 for nonbinary codes, we present Fig. 2, which compares the minimum possible value of (E_b/N_0) required to achieve $P_E = 0$ for binary and nonbinary codes as a function of the rate R . Notice that the gain possible by going to nonbinary codes is negligible until R reaches a value of 0.5 or more.

References

1. Baumert, L. D., and McEliece, R. J., "A Golay-Viterbi Concatenated Coding Scheme for MJS77," in *The Deep Space Network Progress Report*, Technical Report 32-1526, Vol. XVIII, pp. 76-84, Jet Propulsion Laboratory, Pasadena, Calif., Dec. 15, 1973.
2. McEliece, R. J., "An Introduction to Information and Coding Theory," Caltech Lecture Notes, 1974.

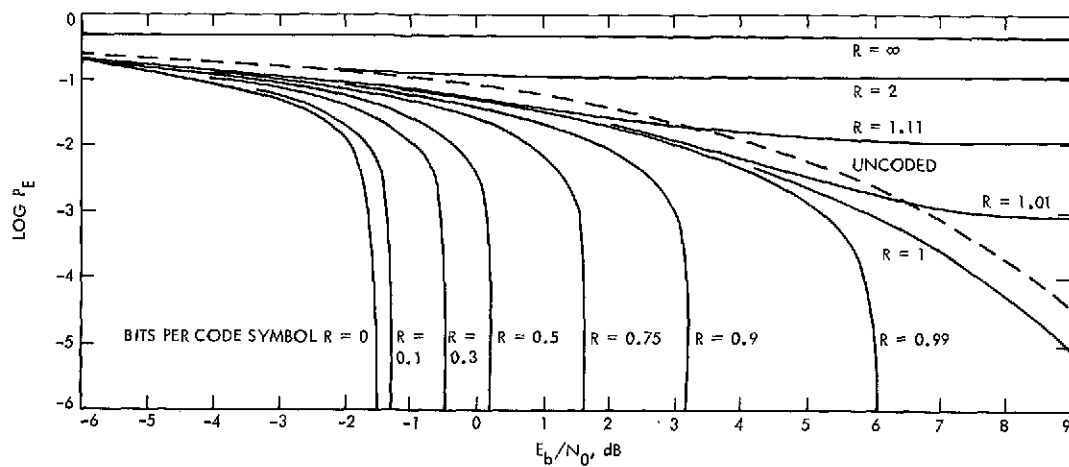


Fig. 1. Binary coding limits

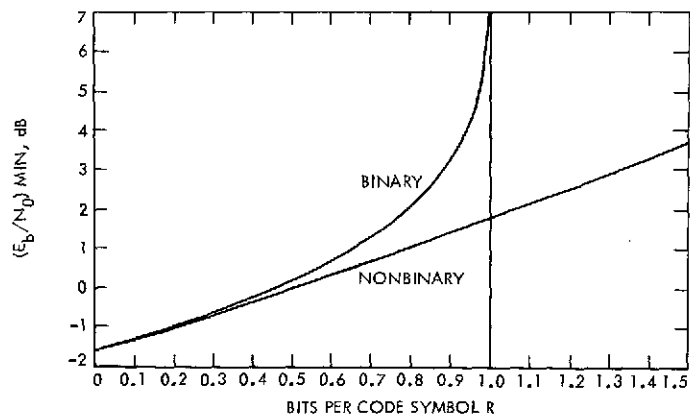


Fig. 2. Comparison of binary and nonbinary coding limits

S/X Experiment: DSS 14 Pre- and Post-Track Ranging Calibrations for Mariner 10 Tracking Passes and Associated Problems

T. Y. Otoshi

Communications Elements Research Section

Ground system ranging calibration data for DSS 14 are presented for 1974 Day 12 through Day 150. Associated ranging problems are discussed and recommendations for calibration improvements are presented.

I. Introduction

Ranging calibrations on the ground system at DSS 14 are currently being performed with the Zero Delay Device (ZDD) in the cable configuration that was described in Ref. 1. The ranging calibrations are normally done during pre- and post-calibration periods of Mariner 10 tracking passes at the signal levels and frequencies applicable to the particular tracking pass. These ZDD pre- and post-calibration data are used along with the ground station Z-correction (Ref. 2) and spacecraft radio system bias correction to enable determination of the true range to the spacecraft (Ref. 3).

For purposes of observing the long-term performance of the ZDD, pre- and post-track calibration data have been systematically tabulated at DSS 14 as functions of ambient temperature, signal levels, and other range-dependent parameters. This article presents some of these data in plotted form for convenient reference purposes.

II. Calibration Data

Systematic tabulation of ranging calibration data for the S/X system at DSS 14 was begun after 1974 Day 12 when the new ZDD cable configuration was installed (see Ref. 1). Figures 1 through 10 show plots of the S/X ground system ranging calibrations for Mariner 10 tracking passes from 1974 Day 12 through Day 150.

From Day 47 through Day 85, unexpected Block 4 doppler instability problems made accurate ranging values very difficult to obtain. In this period many system configuration and component changes were implemented by a "Tiger Team" that was formed to investigate and correct the source of the Block 4 receiver doppler instabilities. The doppler instability problem was solved on Day 85, after which the DSS 14 ranging configuration was left virtually unchanged.

From the plotted results, it can be seen that during periods when the range configuration was left unaltered

and the same transmitter used, the peak-to-peak range variations were typically within 10 ns for S-band and X-band. It is of interest to observe that the jitter in the data noticeably decreased around the time of Mariner 10 Venus and Mercury encounters, which were Days 36 and 88, respectively.

It can be seen that a significant change of range occurs whenever different transmitters (klystron amplifiers) are used. The ground system S- or X-band group delay is anywhere from 5 ns to 18 ns longer when the 100-kW transmitter is used rather than the 20-kW transmitter. Based on data on the configuration after Day 82, it was found that, when Receiver 3 is used for S-band instead of Receiver 4, the S-band group delay through the DSS 14 ground system is about 28 ns longer. When Receiver 4 is used for X-band instead of Receiver 3, the X-band range delay through the DSS 14 ground system is about 19 ns shorter.

The ground station range delay using the Block 4 system has recently been found to be strongly dependent on received signal level. Variations of delay with signal level have been reported in the following article of this volume (T. Y. Otoshi and P. D. Batelaan, "S/X Experiment: DSS 14 S/X Ground System Ranging Tests). This signal level change is a long-term effect, however, and does not explain the short-term peak-to-peak variations. Some of the short-term variation is correlated with ambient temperature changes. The dependence on temperature, however, is not conclusive because this effect appears to be nonlinear and only a limited amount of reliable data has been available.

III. Discussion of Ranging Problems and Recommendations

It has been found that many variables or factors can affect the ranging calibration values on a day-to-day basis. Therefore, it is important that the ZDD ranging calibration data be applied only for the particular tracking pass for which calibrations were done. Use of some average value for the station delay can result in significant error.

In summary, some of the known major factors that can change ranging calibrations or introduce errors are:

- (1) Interchanging transmitters (20-kW or 100-kW klystron).
- (2) Interchanging receivers (Receiver 3 or 4 for S or X).

- (3) Interchanging exciters (Block 3 or Block 4). The Block 4 exciter is not currently used during pre- and post-calibrations or tracking passes.
- (4) Maser gain and tuning.
- (5) Ambient temperature.
- (6) Replacement of components or cables in the signal path.
- (7) Received signal level.
- (7) Antenna sag and subreflector defocusing. (This effect cannot be evaluated at DSS 14 with present cable configuration.)
- (9) Incorrect range modulation setting. (This effect has not been completely investigated.)
- (10) Improper calibration configuration (if there is more than one signal path).
- (11) Incorrect voltage-controlled oscillator (VCO) frequency typed into ranging machine by operator.
- (12) Reporting acquisition range instead of updated range.

Note that since many of the above factors cannot be controlled or always be known, it is important that pre- and post-calibration data be used for the same day's tracking pass only. The station configuration should not be altered during the tracking pass after calibrations have been performed. Operator errors described by factors (9) through (11) can be minimized only by operator care and long-term familiarity and training of DSS operators on the new S/X system and Mu-2 ranging machine. Data improvement would result from operator verification of correlation voltages. Data with bad correlation voltages should not be reported. Calibrations not within 10 ns or 0.010 μ s of previous calibrations indicate a need for recalibration.

It should be possible to eliminate inaccuracies due to factors (11) and (12) by using the Engineering Cal Program¹ (DOI-5399-SP) during the pre- and post-calibration periods. This program contains most of the features of the Monitor Program (DOI-5046-OP), with the addition that doppler phase and ranging calibration processing is done in real time at the station. This calibration program is applicable to the Block 3/PRA and Block 4/Mu-2 configurations. Data from this program can be sent

¹This program was written by Harvey Marks of Informatics Inc., Canoga Park, California.

to the Mission Control and Computing Center (MCCC) via the high-speed data line. The program is currently in the DSN program library and is now at all stations in the DSN including CTA 21.

It is recommended that for long-term study of ranging and doppler stability data, S/X tests be done at all stations of the DSN with the Engineering Cal Program (DOI-5399-SP).

Acknowledgments

Ray Allis and Ed Cole of the Philco-Ford Corporation performed most of the systematic calibrations and tabulations of data presented in this article. The ranging data were obtained from the teletyped output of the Mu-2 ranging machine which was developed by Warren Martin and programmed by Art Zygielbaum of Section 331.

References

1. Otoshi, T. Y., and Stelzried, C. T., "S/X Experiment: A New Configuration for Ground Range Calibrations With the Zero Delay Device," in *The Deep Space Network Progress Report 42-20*, pp. 57-63, Jet Propulsion Laboratory, Pasadena, Calif., Apr. 15, 1974.
2. Batelaan, P. D., "S/X-Band Experiment: Zero Delay Device Z Correction," in *The Deep Space Network Progress Report 42-20*, pp. 78-83, Jet Propulsion Laboratory, Pasadena, Calif., Apr. 15, 1974.
3. *TRK-2-8 Module of DSN System Requirements Detailed Interface Design Document 820-13, Rev. A*, July 1, 1973 (JPL internal document).

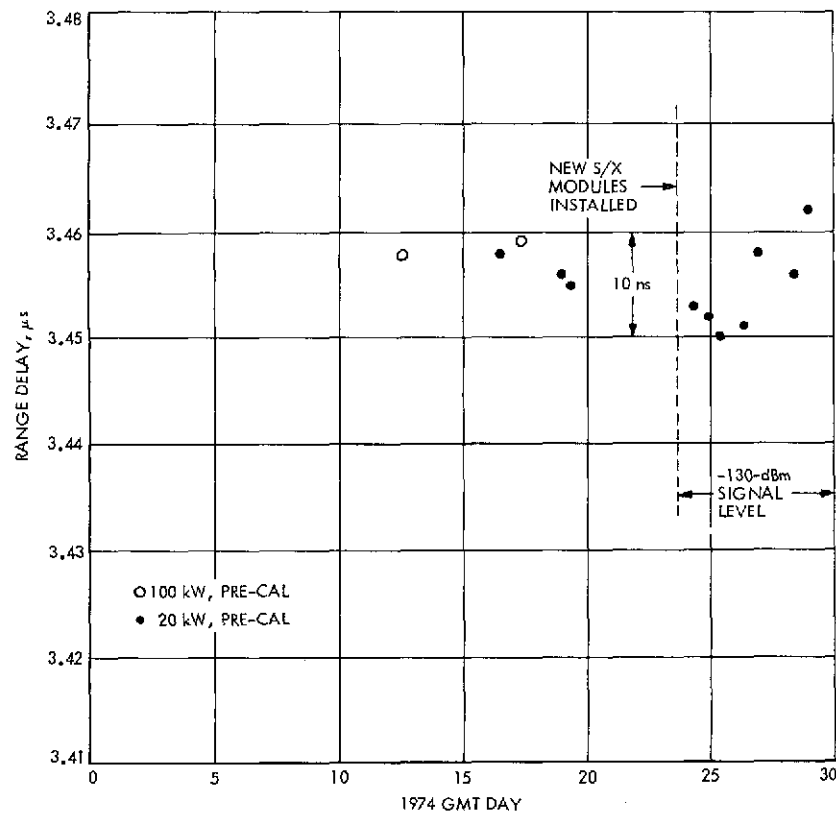


Fig. 1. S-band zero delay range, 1974 Day 1-30 (Jan 1-30)

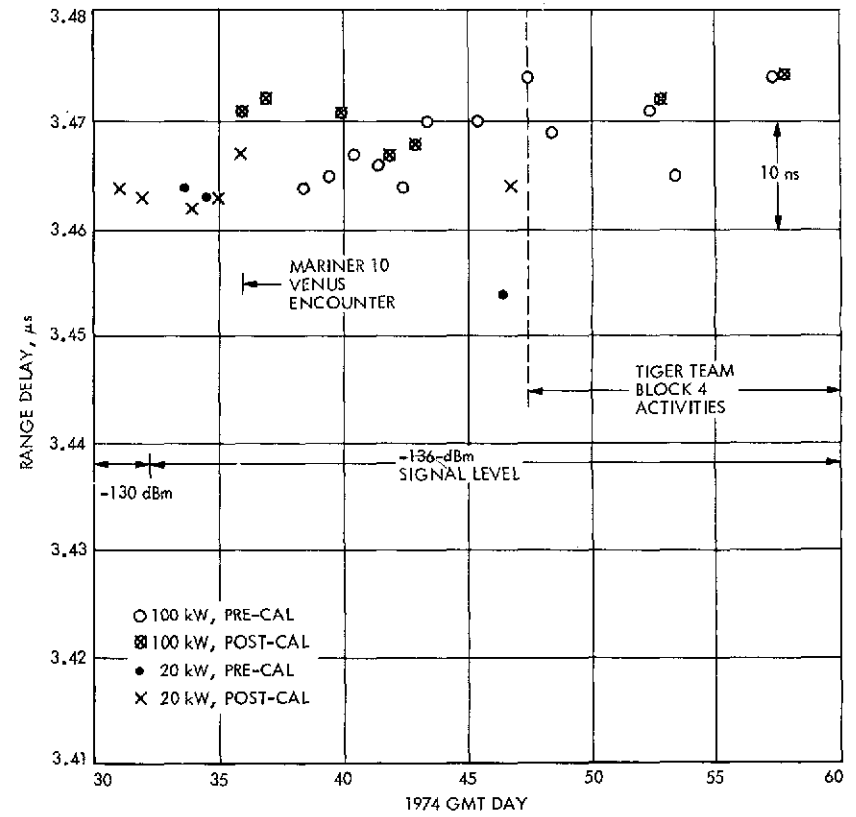


Fig. 2. S-band zero delay range, 1974 Day 30-60 (Jan 30-Mar 1)

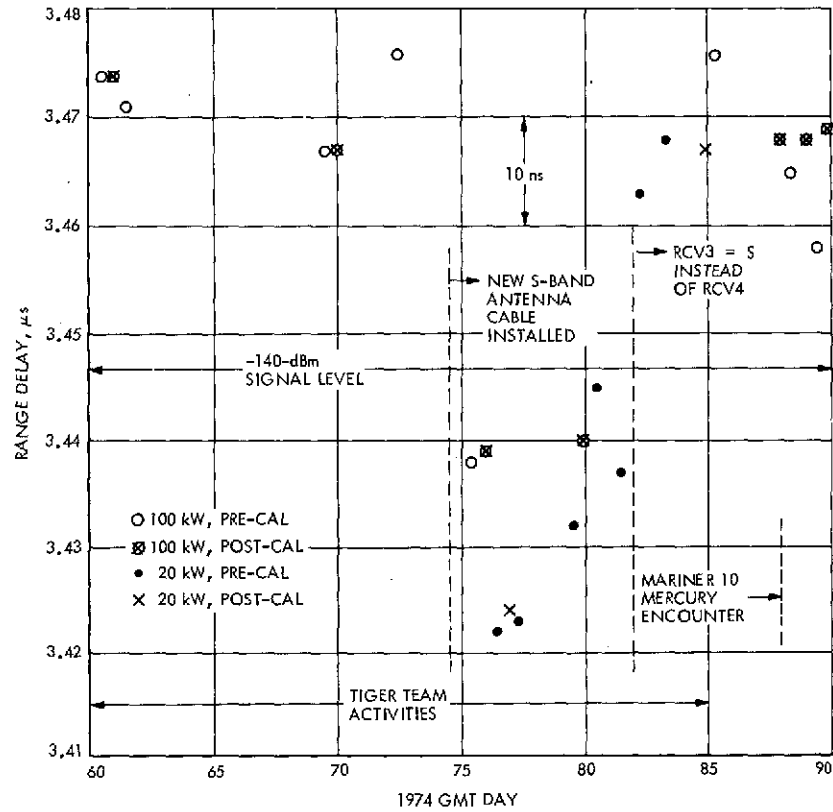


Fig. 3. S-band zero delay range, 1974 Day 60-90
(Mar 1-Mar 31)

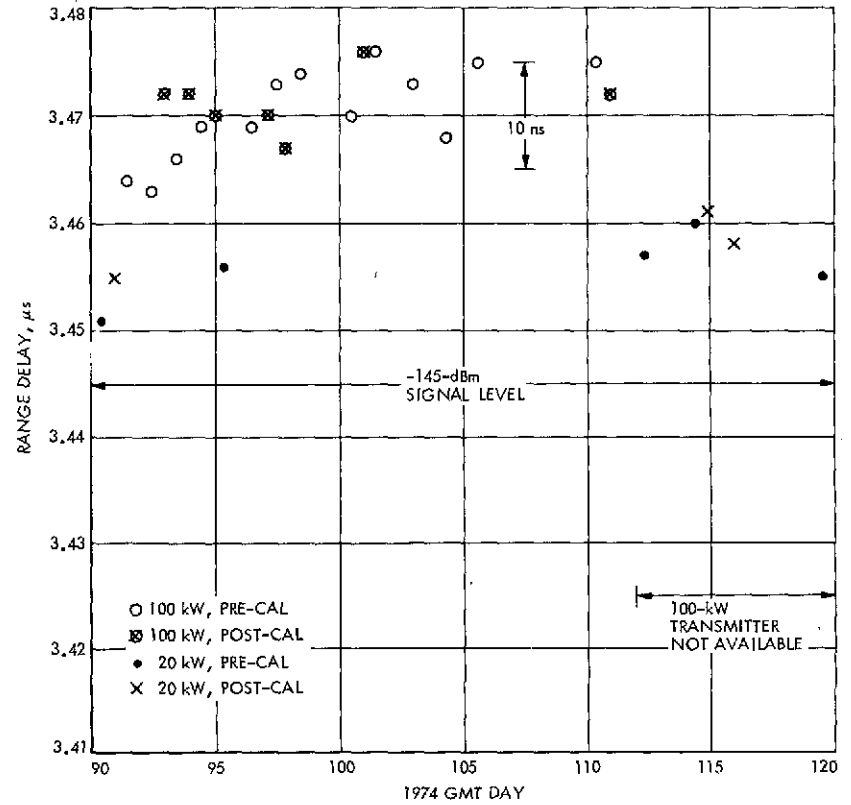


Fig. 4. S-band zero delay range, 1974 Day 90-120
(Mar 31-Apr 30)

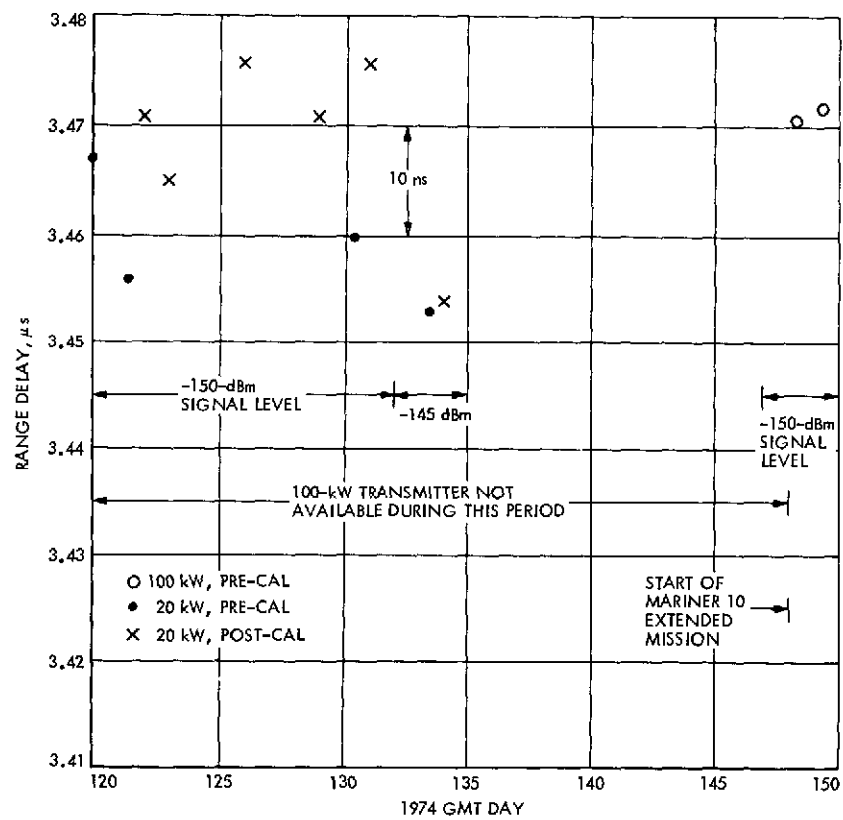


Fig. 5. S-band zero delay range, 1974 Day 120-150
(Apr 30-May 30)

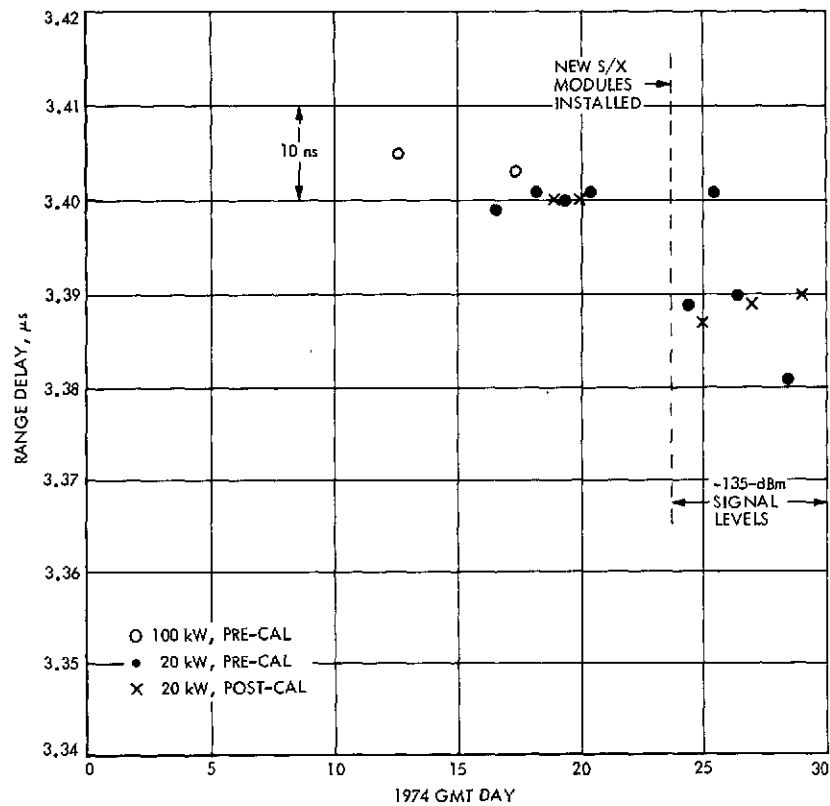


Fig. 6. X-band zero delay range, 1974 Day 1-30 (Jan 1-30)

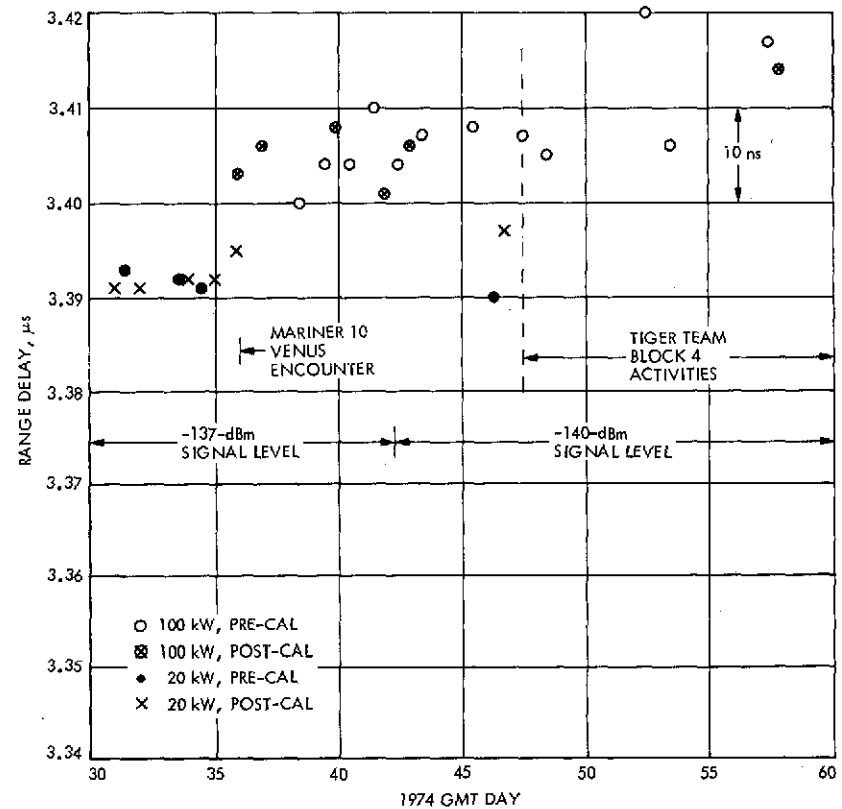


Fig. 7. X-band zero delay range, 1974 Day 30-60 (Jan 30-Mar 1)

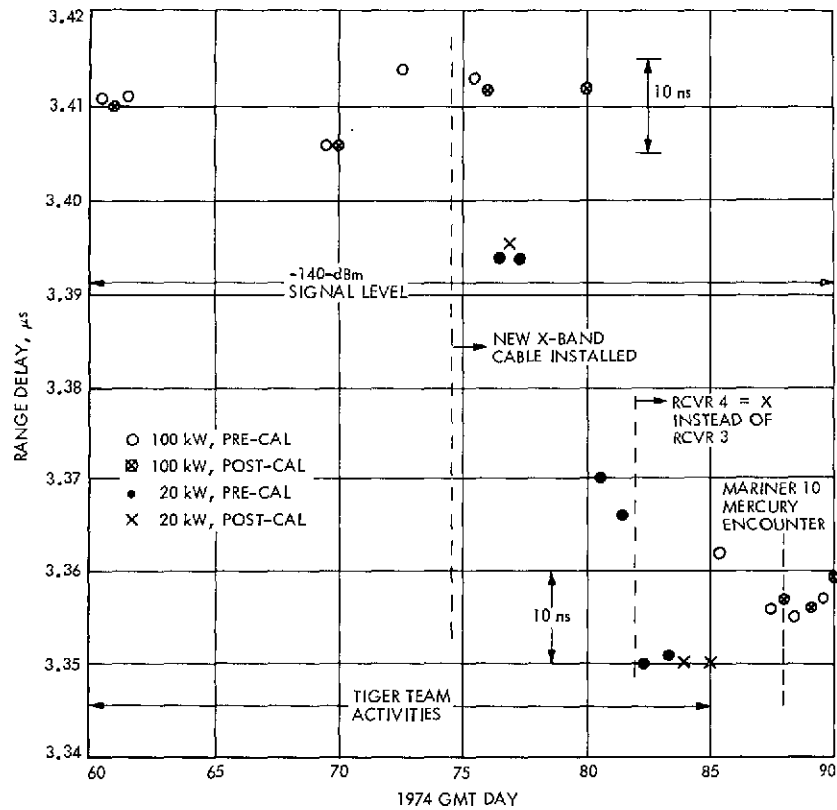


Fig. 8. X-band zero delay range, 1974 Day 60-90
(Mar 1-Mar 31)

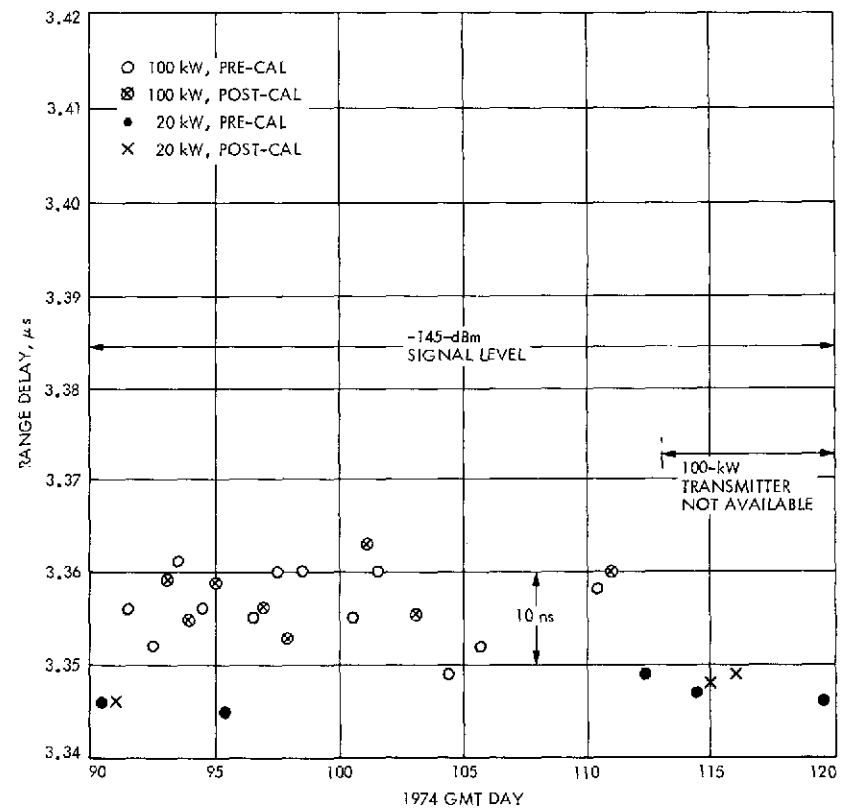


Fig. 9. X-band zero delay range, 1974 Day 90-120
(Mar 31-Apr 30)

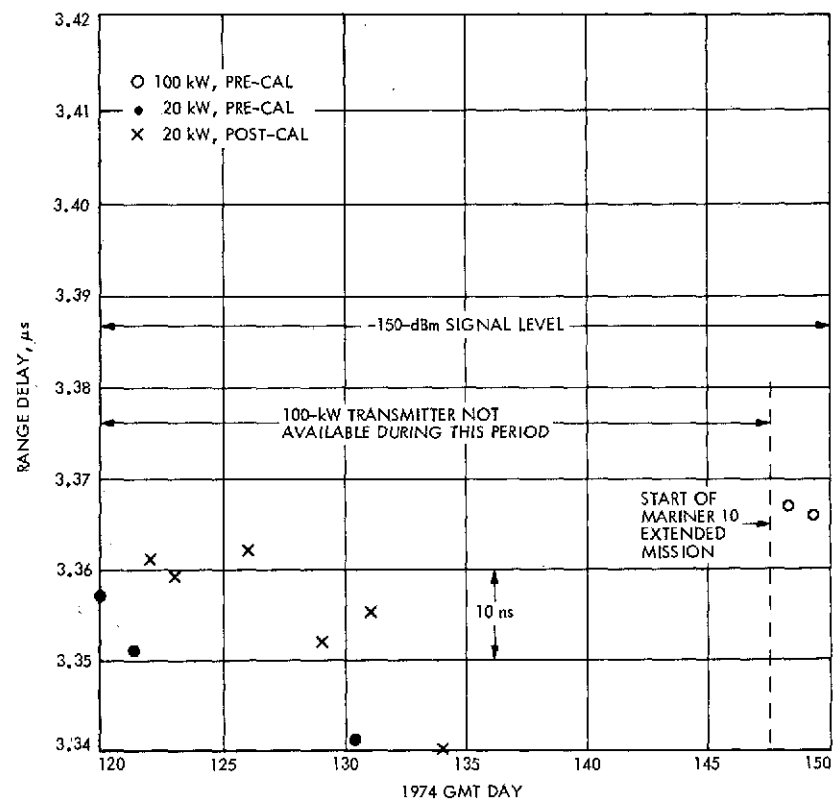


Fig. 10. X-band zero delay range, 1974 Day 120-150
(Apr 30-May 30)

S/X Experiment: DSS 14 S/X Ground System Ranging Tests

T. Y. Otoshi and P. D. Batelaan
Communications Elements Research Section

This article presents special ranging test data obtained on the S/X ground system at DSS 14. The test data consist of ground system range as functions of (1) uplink 100-kW transmitter power, (2) downlink S- and X-band signal levels, and (3) antenna elevation and azimuth angles via the cable path and via the airpath.

I. Introduction

On 1974 Day 12, a new configuration was installed at DSS 14 for ground system ranging calibrations. As described in Ref. 1, this new configuration differs from the conventional one in that the zero delay device (ZDD) uplink and downlink signals are transmitted through calibrated cables instead of through the airpath. Some limited amount of range calibration data on this new configuration was previously reported in Ref. 1.

Due to unexpected doppler stability problems with the Block 4 receiver system during the period 1974 Day 47 through 85, it was difficult to perform useful ranging tests on the S/X system until after the Mariner 10 Mercury encounter on 1974 Day 88.

This article presents results of some recent ranging tests made on the S/X ground system at DSS 14 as functions of various ground station parameters. Pre- and post-

track calibration data for the Mariner 10 tracking passes and discussion of S/X calibration problems are discussed in the preceding article of this volume (T. Y. Otoshi, "S/X Experiment: DSS 14 Pre- and Post-Track Ranging Calibration for Mariner 10 Tracking Passes and Associated Problems).

II. Test Configuration

A block diagram of the present ZDD configuration for the S/X ground system calibrations at DSS 14 may be seen in Fig. 1. As was described in Ref. 1, the ZDD is a ground station antenna-mounted transponder that samples the uplink 2113 MHz from the transmitter and generates coherent downlink S- and X-band test signals of 2295 MHz and 8415 MHz. Transmission of these test signals to the respective masers is possible either through a cable path or a microwave airpath by means of an internal coaxial switch in the ZDD assembly.

As may be seen in Fig. 1, the present ground system configuration being calibrated at DSS 14 consists of the Block 3 exciter, the 100- or 20-kW transmitters, the S/X masers, Block 4 receivers, and the Mu-2 ranging machine. Test data were reduced in real time at DSS 14 by means of the Engineering Calibration Program (DOI-5399-SP), which was specially developed for the S/X Experiment.¹ A sample output from the program may be seen in Fig. 2. This program has many of the features of the Monitor Program (DOI-5046-OP), and can be used to test range and cumulative doppler phase at any DSN station having the Block 3/Planetary Ranging Assembly (PRA) ranging or Block 4/Mu-2 ranging systems. The program is currently in the DSN Program Library and copies of tapes and documentation have been sent to all stations in the DSN including CTA 21.

III. Test Results

Special tests were performed to investigate range as functions of (1) uplink 100-kW transmitter power, (2) downlink S/X signal levels, and (3) antenna elevation and azimuth angles.

Data from special tests obtained with the Engineering Cal Program are presented in graphical form in Figs. 3 through 14. Figures 3 and 4 show plots of round-trip range delay as functions of uplink power from the 100-kW transmitter. It can be seen that the variation of delay is less than 2 ns for either the S- or X-band system when the transmitter power is varied from 75 kW to 100 kW.

Figures 5 through 8 show round-trip range delays as a function of received signal level as defined at the input to the Mod 3 S-band maser and X-band maser. Range is found to be significantly dependent upon signal level when Receiver 4 of the Block 4 system is used for either S- or X-band and less dependent when Receiver 3 is operated for either S- or X-band. In the signal level range of -135 dBm to -145 dBm, the range change is approximately 0.3 ns/dB for Receiver 3 and 0.8 ns/dB for Receiver 4. Tests with the signals injected behind the respective S- and X-band masers showed the same type response and therefore ruled the masers out as possible causes of range change with signal level. Further tests on the Mu-2 ranging machine as well as manual gain control

(MGC) tests on the Block 4 receivers resulted in the isolation of the Block 4 automatic gain control (AGC) loop as being the source of the range changes.

Special tests were also made to study the effects of antenna elevation and azimuth movement on range. The results of these tests for the cable path configuration may be seen in Figs. 9 through 12. The variations of 6 ns as functions of elevation angles in the S-band cable path are larger than reported previously (see Ref. 1). The variations could be due to changes somewhere in the 100-kW Klystron Amplifier Assembly. This fact can be verified in the future by performing a similar test with both the Block 4 translator and the ZDD and comparing the results. This test should give a valid indication since the ZDD samples the uplink signal after the Klystron Amplifier, while the Block 4 translator obtains the uplink signal from the exciter assembly in front of the Klystron Amplifier.

Figures 13 and 14 show the results of range tests with the ZDD in the airpath configuration. The large variation of about 25 ns in the airpath for the X-band is about the same as was reported previously in Ref. 2. The cause of this change in range is still not known. Several tests were made to isolate possible multipath signals in the airpath. One test involved the temporary installation of an RF screen that interconnected the rooftops of the three cones mounted on the Tricone Support Structure. This screen covered the open area between the three cones and blocked potential S- and X-band leakage signals. A small improvement was noticed at S-band and a small (but insufficient) improvement at X-band was also obtained. Another screen placed around the dichroic plate assembly support structure resulted in no further improvement at X-band. Another test showed that the performance of the X-band airpath range could be improved significantly by axial focusing of the subreflector at each elevation angle for optimum antenna gain at X-band. However, optimizing for X-band seriously affected the S-band performance. Although the strange behavior in the airpath is not clearly understood at present, it is felt that airpath tests are still useful for trouble shooting potential problems in the S/X reflex feed system.

IV. Conclusion

Data from special ranging tests on the S/X system at DSS 14 have been presented. These data may be useful for indicating improvement areas needed on the ground

¹This program was written by Harvey Marks of Informatics, Inc., Canoga Park, California.

C - 2

system for future missions such as Viking '75. In addition, these data could be helpful in explaining some of the ranging anomalies seen during the Mariner 10 mission (Refs. 3 and 4). It has been reported that part of the struc-

tured noise in the differenced range versus integrated doppler (DRVID) data seen in the Mariner Venus/Mercury 1973 mission was correlated to ground station received signal level changes (Ref. 5).

References

1. Otoshi, T. Y., and Stelzried, C. T., "S/X Experiment: A New Configuration for Ground System Range Calibrations With the Zero Delay Device," in *The Deep Space Network Progress Report 42-20*, pp. 57-63, Jet Propulsion Laboratory, Pasadena, Calif., Apr. 15, 1974.
2. Stelzried, C. T., Otoshi, T. Y., and Batelaan, P. D., "S/X Band Experiment: Zero Delay Device Antenna Location," in *The Deep Space Network Progress Report 42-20*, pp. 64-68, Jet Propulsion Laboratory, Pasadena, Calif., Apr. 15, 1974.
3. Spradlin, G., *Simultaneous Two-Way/Three-Way DRVID Tests*, IOM 421G-74-197, May 17, 1974 (JPL internal document).
4. Chancy, W. D., *Range Calibration Discrepancies During MVM-73*, IOM NSE-74-105, May 8, 1974 (JPL internal document).
5. Bourke, K. H., *Viewgraphs from DRVID Investigation Initial Phase Report*, IOM 391-8-180, June 5, 1974 (JPL internal document).

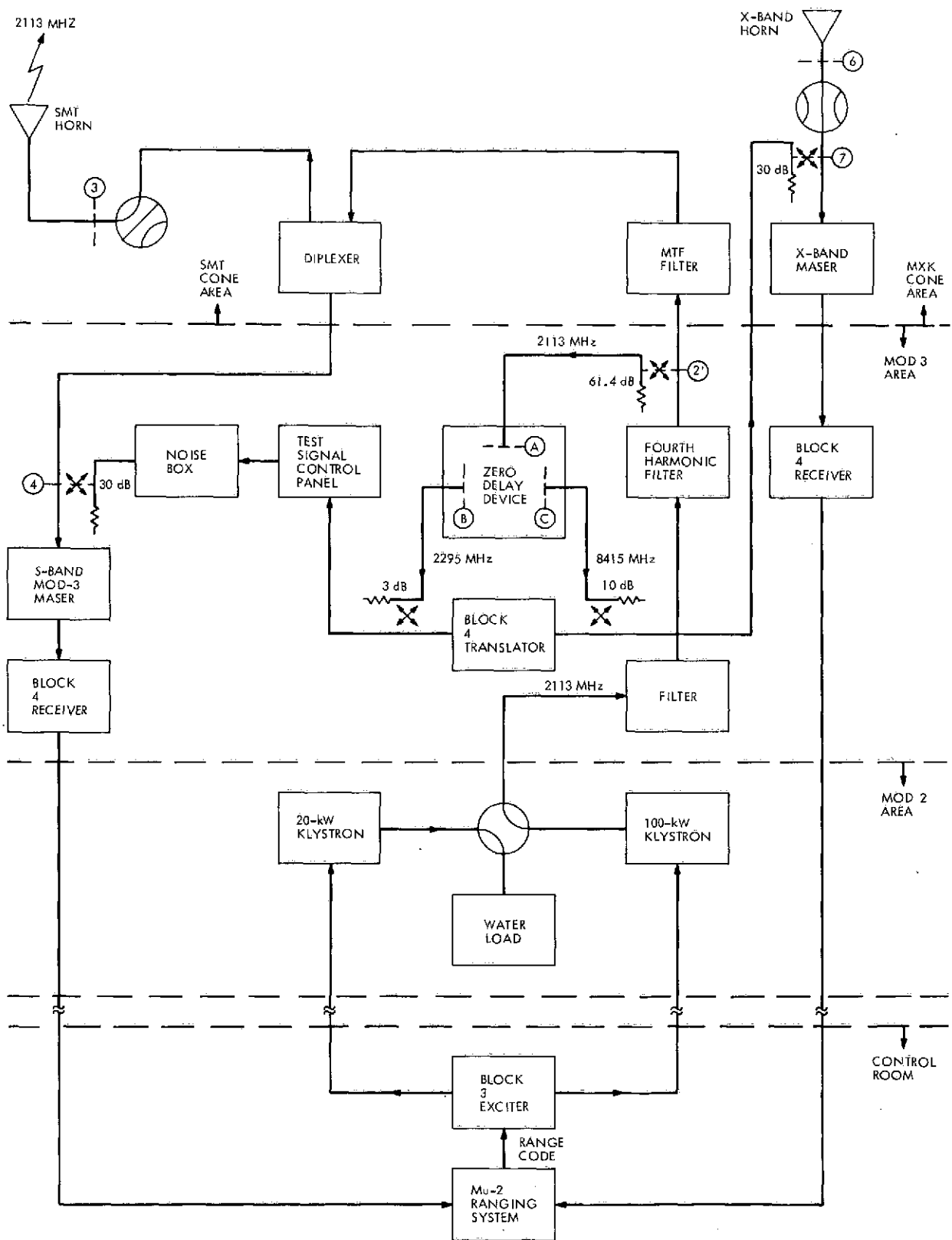


Fig. 1. Block diagram of the new configuration at DSS 14 for ground system range calibrations

ADD CABLE CONFIG											
DAY	ISY	AZ(DEG)	EL(DEG)	SD(USEC)	XD(USEC)	SR(USEC)	XR(USEC)	DR(USEC)	SP(DEG)	XP(DEG)	DP(DEG)
01:24:07	219.998	10.002	-0.0031	.0060	3.4677	3.3656	.1022	.0	18.0	-4.9	
01:24:12	219.998	10.002	-0.0031	.0060	3.4677	3.3656	.1022	18.0	18.0	13.1	
01:24:17	219.998	10.002	-0.0031	.0060	3.4677	3.3656	.1022	18.0	54.0	3.3	
01:24:22	219.998	10.002	-0.0031	.0060	3.4677	3.3656	.1022	.0	18.0	-4.9	
01:24:27	219.998	10.002	-0.0027	.0061	3.4679	3.3655	.1025	.0	18.0	-4.9	
01:24:32	219.998	10.002	-0.0027	.0061	3.4679	3.3655	.1025	18.0	18.0	13.1	
01:24:37	219.998	10.002	-0.0027	.0061	3.4679	3.3655	.1025	.0	18.0	-4.9	
01:24:42	219.998	10.002	-0.0027	.0061	3.4679	3.3655	.1025	18.0	36.0	8.2	
01:24:47	219.998	10.002	-0.0040	.0075	3.4680	3.3655	.1025	18.0	.0	18.0	
01:24:52	219.998	10.002	-0.0040	.0075	3.4680	3.3655	.1025	.0	36.0	-9.8	
01:24:57	219.998	10.002	-0.0040	.0075	3.4680	3.3655	.1025	.0	36.0	-9.8	
01:25:02	219.998	10.002	-0.0040	.0075	3.4680	3.3655	.1025	.0	72.0	-19.6	
01:25:07	219.998	10.002	-0.0032	.0068	3.4681	3.3655	.1026	18.0	54.0	3.3	
01:25:12	219.998	10.002	-0.0032	.0068	3.4681	3.3655	.1026	.0	54.0	-18.7	
01:25:17	219.998	10.002	-0.0032	.0068	3.4681	3.3655	.1026	-18.0	18.0	-22.9	
01:25:22	219.998	10.002	-0.0032	.0068	3.4681	3.3655	.1026	.0	36.0	-9.8	
01:25:27	219.998	10.002	-0.0035	.0058	3.4682	3.3654	.1028	18.0	36.0	8.2	
01:25:32	219.998	10.002	-0.0035	.0058	3.4682	3.3654	.1028	.0	18.0	-4.9	
01:25:37	219.998	10.002	-0.0035	.0058	3.4682	3.3654	.1028	.0	18.0	-4.9	
01:25:42	219.998	10.002	-0.0035	.0058	3.4682	3.3654	.1028	.0	.0	.0	
01:25:47	219.998	10.002	-0.0035	.0065	3.4683	3.3654	.1029	18.0	.0	18.0	
01:25:52	219.998	10.002	-0.0035	.0065	3.4683	3.3654	.1029	.0	36.0	-9.8	
01:25:57	219.998	10.002	-0.0035	.0065	3.4683	3.3654	.1029	.0	36.0	-9.8	
01:26:02	219.998	10.002	-0.0035	.0065	3.4683	3.3654	.1029	18.0	18.0	13.1	
01:26:07	219.998	10.002	-0.0042	.0060	3.4683	3.3653	.1030	-18.0	18.0	-22.9	
01:26:12	219.998	10.002	-0.0042	.0060	3.4683	3.3653	.1030	.0	18.0	-4.9	
01:26:17	219.998	10.002	-0.0042	.0060	3.4683	3.3653	.1030	18.0	18.0	13.1	
01:26:22	219.998	10.002	-0.0042	.0060	3.4683	3.3653	.1030	18.0	18.0	13.1	
01:26:27	219.998	10.002	-0.0052	.0062	3.4682	3.3653	.1029	.0	36.0	-9.8	
01:26:32	219.998	10.002	-0.0052	.0062	3.4682	3.3653	.1029	.0	18.0	-4.9	
01:26:37	219.998	10.002	-0.0052	.0062	3.4682	3.3653	.1029	.0	36.0	-9.8	
01:26:42	219.998	10.002	-0.0052	.0062	3.4682	3.3653	.1029	.0	18.0	-4.9	
01:26:47	219.998	10.002	-0.0036	.0064	3.4683	3.3653	.1030	.0	18.0	-4.9	
01:26:52	219.998	10.002	-0.0036	.0064	3.4683	3.3653	.1030	.0	36.0	-9.8	
01:26:57	219.998	10.002	-0.0036	.0064	3.4683	3.3653	.1030	.0	18.0	-4.9	
01:27:02	219.998	10.002	-0.0036	.0064	3.4683	3.3653	.1030	18.0	36.0	8.2	
01:27:07	219.998	10.002	-0.0035	.0060	3.4684	3.3652	.1032	.0	36.0	-9.8	

Fig. 2. Sample printout page from Engineering Cal Program (DOI-5399-SP) showing S/X DRVIDs, S/X updated ranges, and S/X doppler phases (DSS 14 test data on 1974 Day 157)

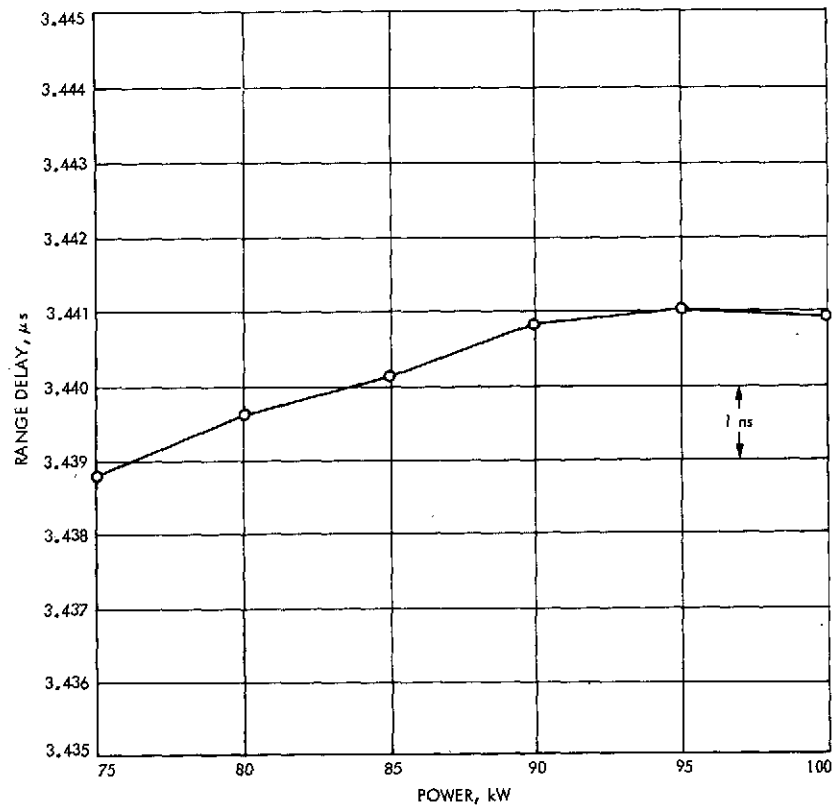


Fig. 3. 100-kW transmitter power vs ZDD S-band range on 1974 Day 75

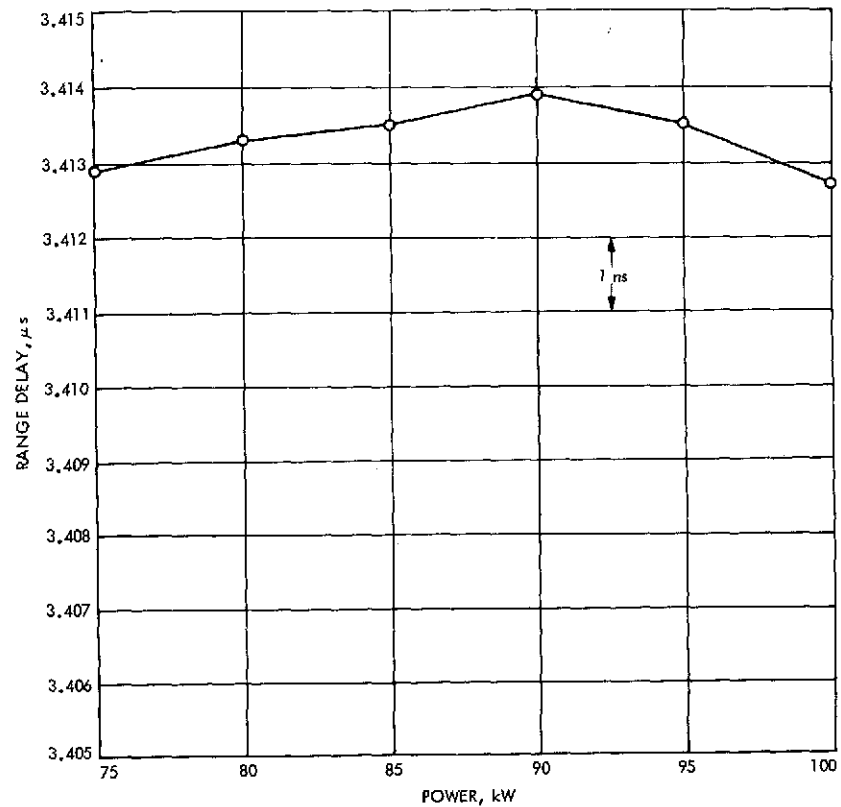


Fig. 4. 100-kW transmitter power vs ZDD X-band range on 1974 Day 75

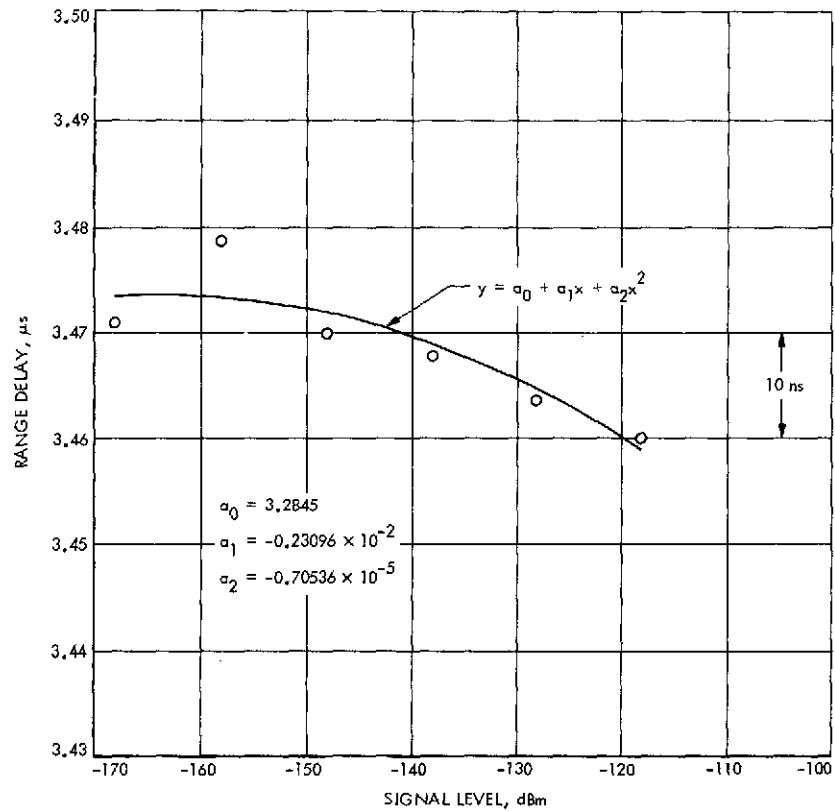


Fig. 5. Signal level vs S-range, 100 kW, ZDD test 1
with RCV3 = S, 1974 Day 110

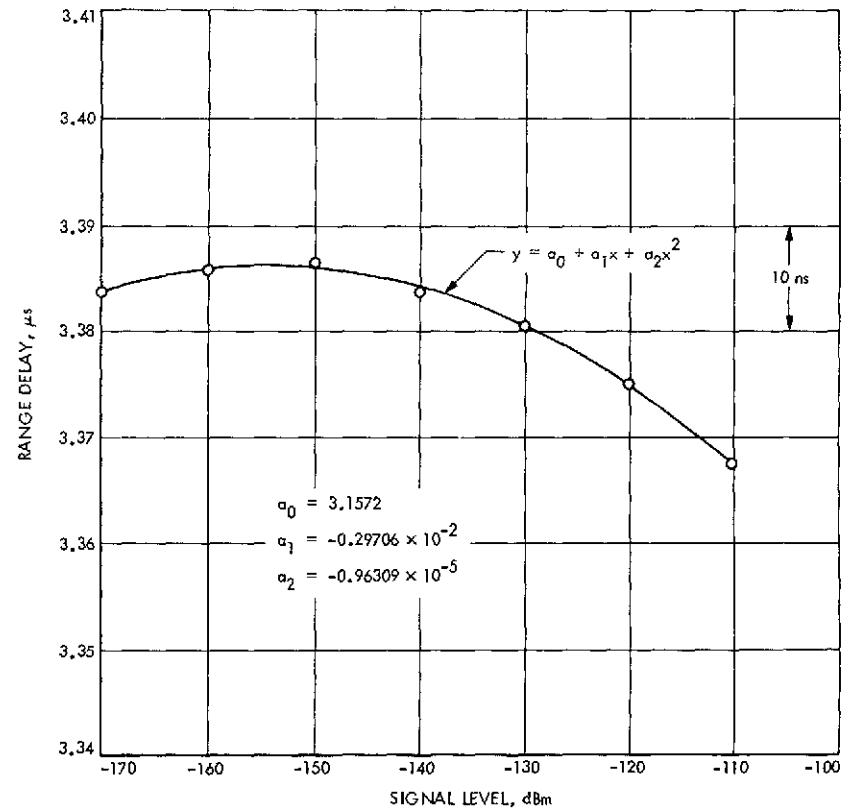


Fig. 6. Signal level vs X-range, 100 kW, ZDD test 2
with RCV3 = X, 1974 Day 110

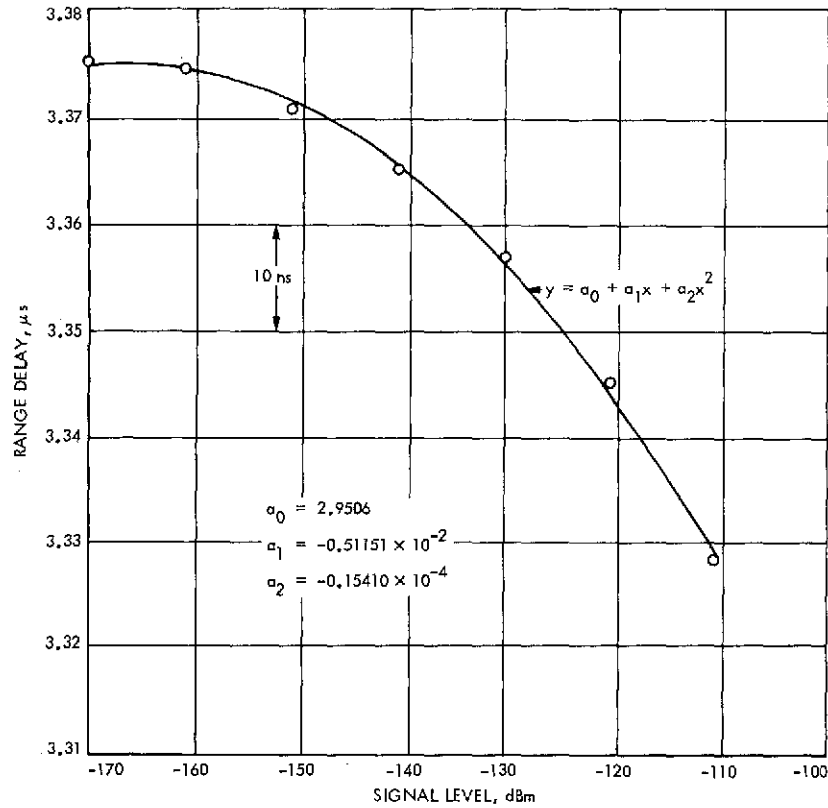


Fig. 7. Signal level vs X-range, 100 kW, ZDD test 1
with RCV4 = X, 1974 Day 110

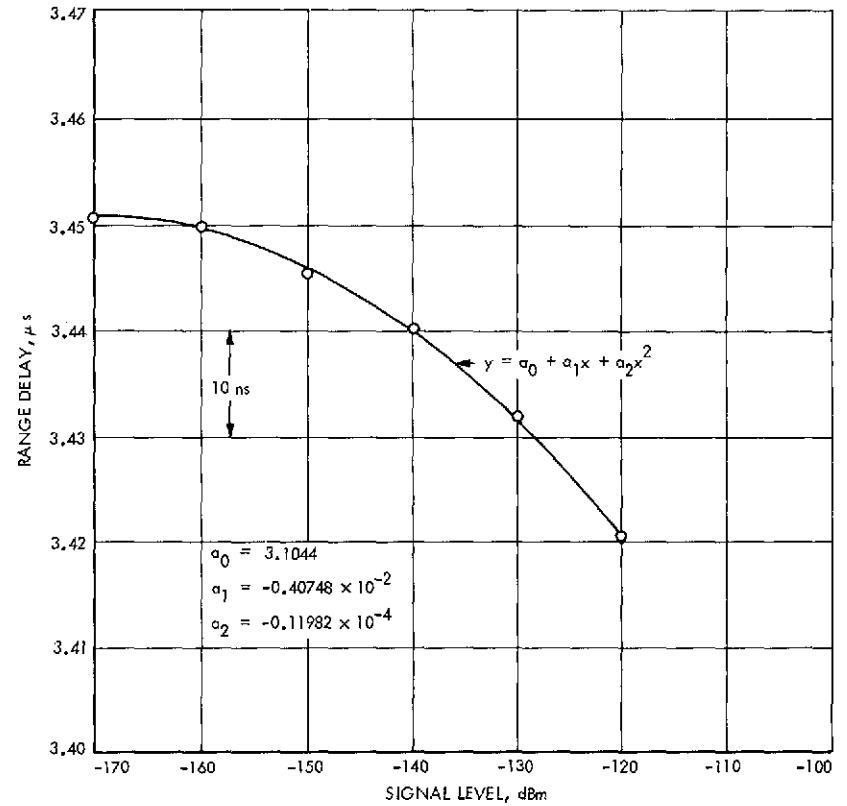


Fig. 8. Signal level vs S-range, 100 kW, ZDD test 2
with RCV4 = S, 1974 Day 110

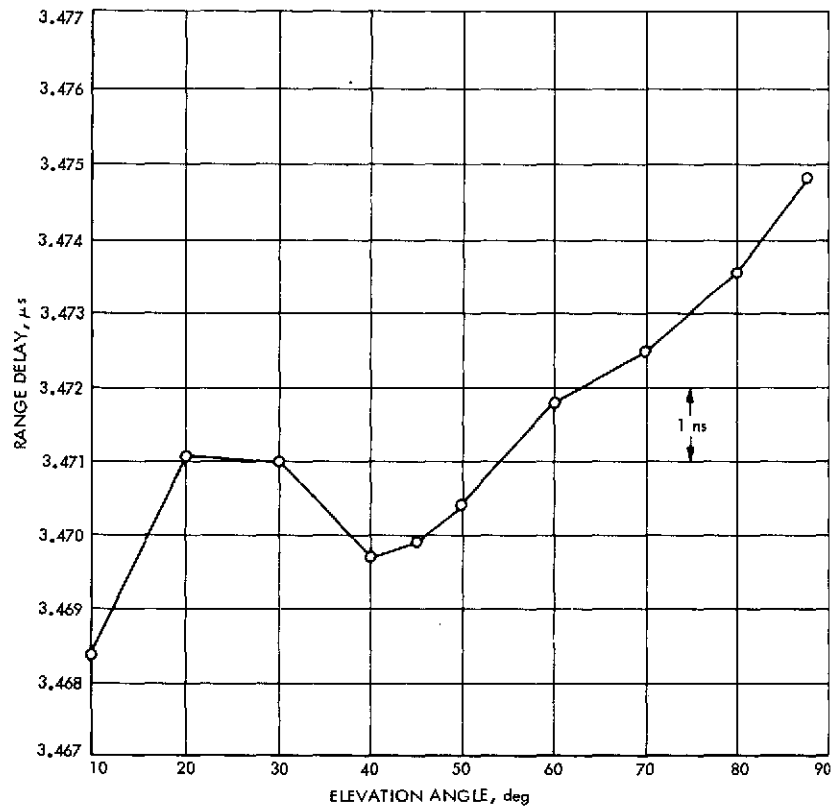


Fig. 9. S-range vs elevation angle via ZDD cable configuration,
AZ = 220 deg, 100 kW, RCV3 = S, 1974 Day 157

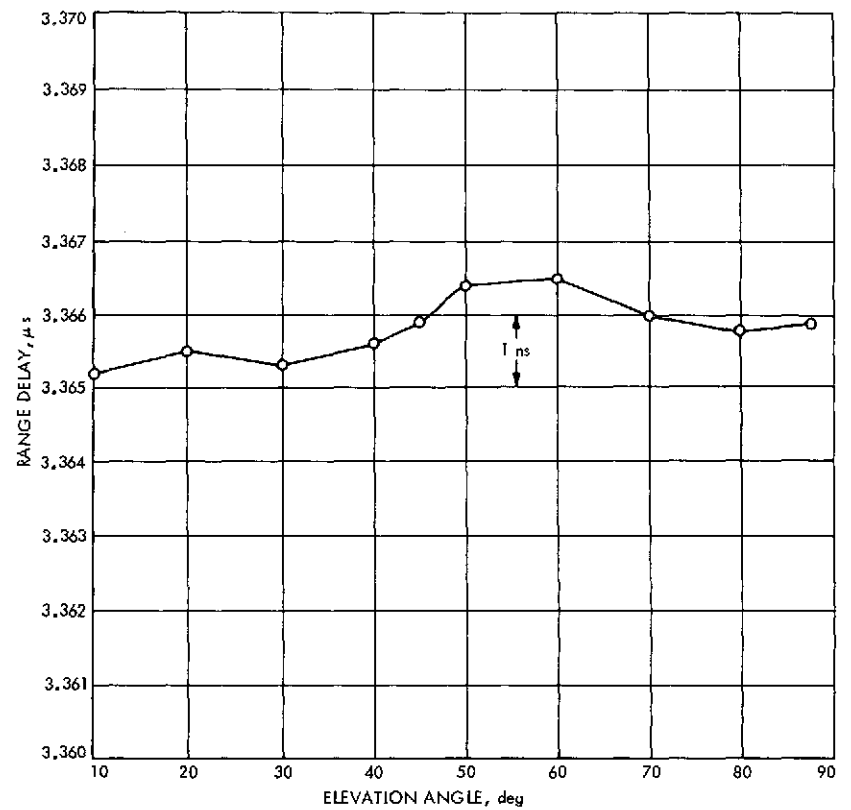


Fig. 10. X-range vs elevation angle via ZDD cable configuration,
AZ = 220 deg, 100 kW, RCV4 = X, 1974 Day 157

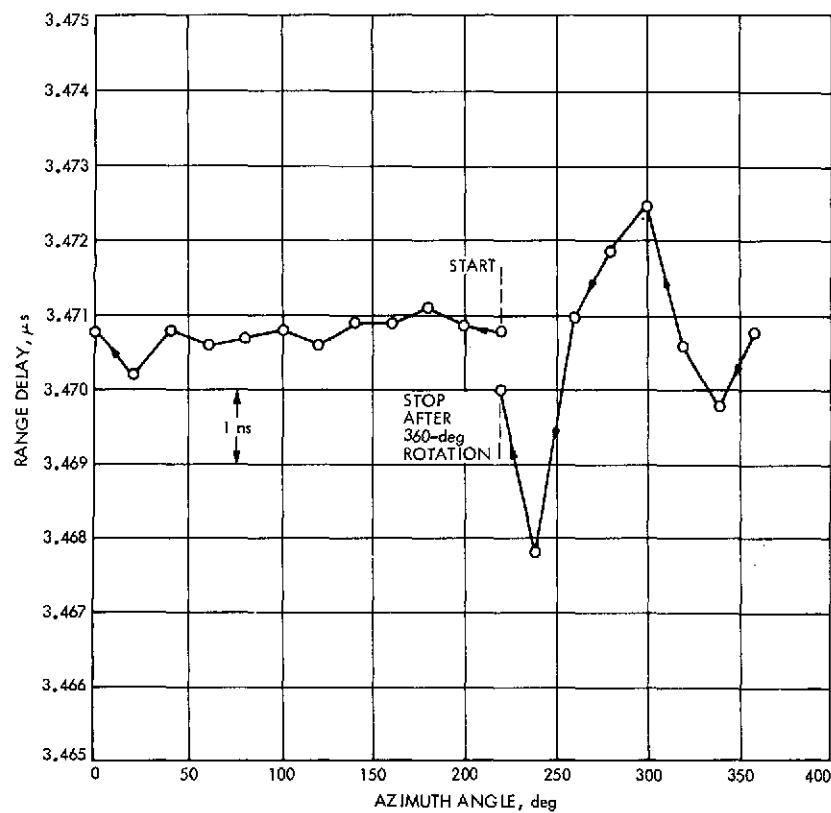


Fig. 11. S-range vs azimuth angle via ZDD cable configuration,
EL = 45 deg, 100 kW, RCV3 = S, 1974 Day 157

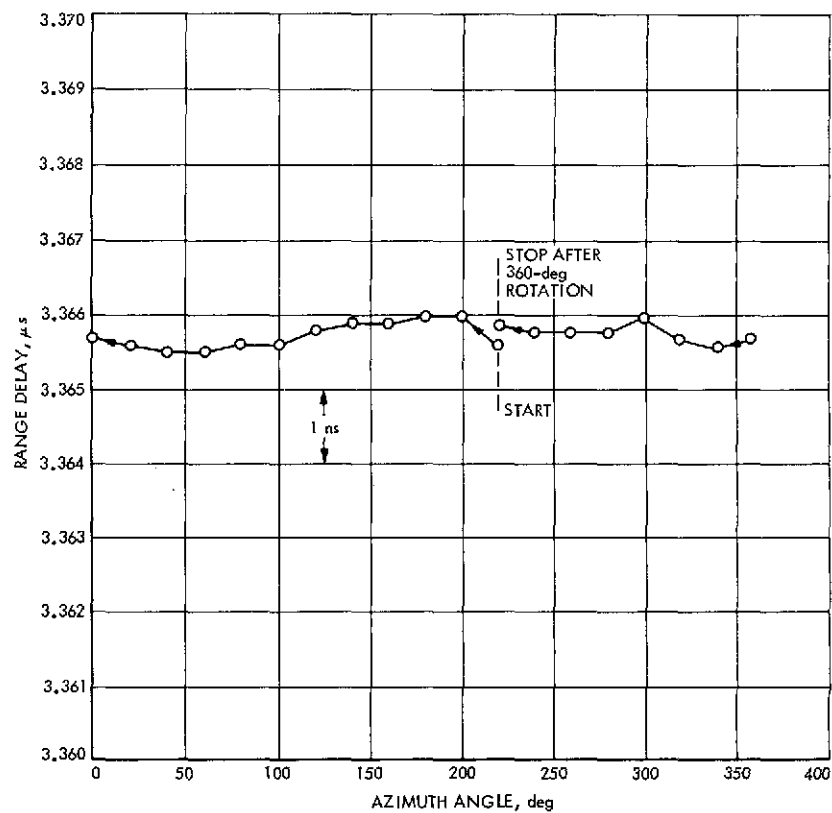


Fig. 12. X-range vs azimuth angle via ZDD cable configuration,
EL = 45 deg, 100 kW, RCV4 = X, 1974 Day 157

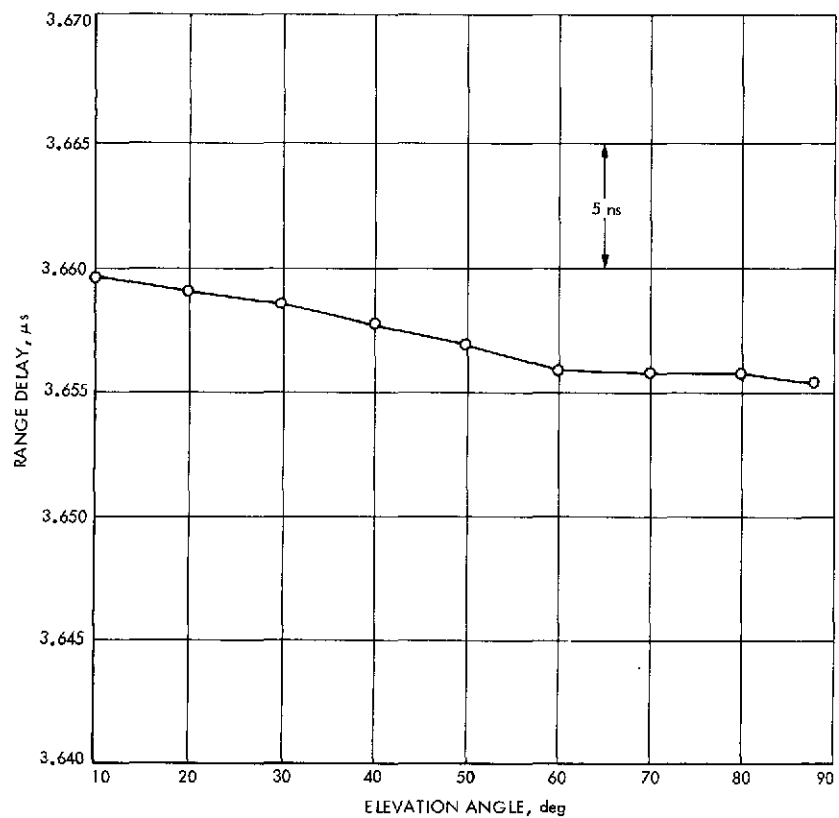


Fig. 13. S-range vs elevation angle via ZDD airpath, 1974 Day 114

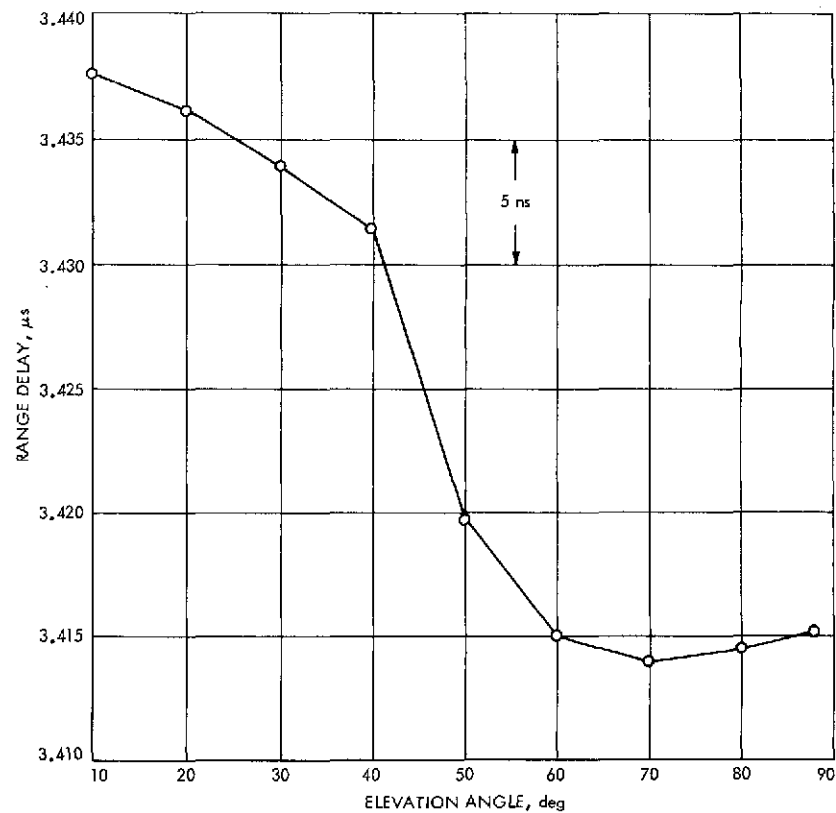


Fig. 14. X-range vs elevation angle via ZDD airpath (X-maser by-passed), 1974 Day 114

A Dual Hybrid Mode Feedhorn for DSN Antenna Performance Enhancement

R. F. Thomas and D. A. Bathker
Communications Elements Research Section

A new microwave horn suitable for use in selected DSN antenna feed applications is described. The new horn uses two hybrid modes propagating within corrugated conical waveguide. Expected aperture efficiency improvement, when feeding DSN reflector antennas, as well as bandwidth information is provided. It is concluded that the new horn provides 0.36 dB gain improvement when feeding a symmetrical Cassegrain antenna; it is estimated that 0.29 dB improvement is available when feeding an asymmetric system such as the DSN 64-m antenna tricone configuration. Bandwidth considerations suggest application at X-band (8.4 to 8.5 GHz) is straightforward; the S-band uplink and downlink bands cannot both be covered at this time.

I. Introduction

A new microwave horn suitable for use in selected DSN antenna feed applications is described. The new horn uses two hybrid modes propagating within corrugated conical waveguide. Expected aperture efficiency improvement, when feeding DSN reflector antennas is given as well as bandwidth information. It is concluded that the new horn provides 0.36 dB gain improvement when feeding a symmetrical Cassegrain antenna; it is estimated 0.29 dB improvement is available when feeding an asymmetric system such as the DSN 64-m antenna tricone configuration. Bandwidth considerations suggest application at X-band (8.4 to 8.5 GHz) is straightforward; the S-band uplink and downlink bands cannot both be covered at this time.

II. Previous Work

Prior to 1970, most Deep Space Network (DSN) S-band ground antenna feeds were based on use of two waveguide modes propagating within smooth conical waveguide. Potter (Ref. 1) first described use of the TE_{11} and TM_{11} modes superimposed to obtain superior radiation characteristics in several respects. The higher order TM mode generating required in such a horn is necessarily accomplished at or near the horn throat; due to the length of high gain horns, proper phase synchronism at the horn aperture between the waveguide modes is achieved over a restricted bandwidth (5 to 10%). In the DSN, this previously meant that enhanced horn performance was taken at the downlink (listen) band, while the

uplink (transmit) band had performance equal to or less than single-waveguide-mode horns (Ref. 2).

Work to realize further horn performance (pattern shaping) was only partially successful at that time. Three- and four-mode smooth conical waveguide horns were devised by Ludwig (Ref. 3). The difficulties of controlling mode amplitudes and phases for specific use on DSN antennas were great. It was concluded that only marginal performance was practically available, beyond the two-mode horns.

By 1970, principles described by Minnett and Rumsey (Refs. 4, 5) were applied to feeds for the DSN with excellent results (Ref. 6). This type of horn is based on one hybrid (TE and TM component) mode conducted along a corrugated conical waveguide. The lowest order hybrid mode, HE_{11} , used within such a waveguide maintains itself nearly distortion free over a very broad bandwidth, since no phase asynchronism problems arise. In the DSN S-band operations context, it was then possible to provide superior performance over both uplink and downlink frequency bands as well as at the experimental high-power radar frequency. With the advent of very high power (100 to 400 kW, CW) uplink transmitters in the early 1970s, the new wideband horn development was timely in maintaining adequate RF safety performance of the large reflector antennas, through superior feed side-lobe, spillover and aperture illumination characteristics (Ref. 7). The wideband horn was further applied at X- and K-bands for moderate bandwidth radio science applications on the Tricone system of the Goldstone 64-m antenna. Finally, to some degree, such high performance horns allow successful operation of beam waveguide devices such as the Reflex-Dichroic S/X-band Feed (Ref. 8).

In a manner analogous to adding individual TE- and TM-modes within a smooth surface conical waveguide, it is possible to add hybrid modes within a corrugated waveguide (Refs. 9, 10). By so doing, it should be possible to approximate the four-mode horn performance sought after by Ludwig (Ref. 3) using only two hybrid modes. Presumably the problems of maintaining phase synchronism between the modes should be comparable with the two-mode smooth waveguide horn developed by Potter, with comparable bandwidth. Bandwidth should be comparable, since again the higher order mode generator (HE_{12}) is located near the horn throat. Nevertheless, some applications do not demand wide bandwidth but would benefit from superior aperture illumination. Thus, development of such a horn was begun at JPL. Potter (Ref. 11), during the course of the experimental work, using

Clarricoats' spherical wave technique and his cylindrical hybrid mode equations (Ref. 10), developed a new computer program to calculate radiation patterns of horns employing either smooth or corrugated walls. Although outstanding agreement has been found for smooth dual mode and corrugated single hybrid mode horn patterns (experimental compared to computed), in general the dual hybrid mode horns exhibit less agreement, probably due to additional higher order modes propagating with small amplitude. Nevertheless, the new computer program was a very useful guide in development, and further analytical/experimental comparisons should be made in the future.

III. Elements of the Dual Hybrid Mode Horn

Figure 1 shows the throat region of the new horn. The TE_{11} input waveguide was constrained to remain the same as previous JPL X-band horns. A center frequency of approximately 8.45 GHz was adopted for development work. The abrupt step, in addition to exciting the HE_{12} mode also plays a major role in controlling the amplitude ratio between the two hybrid modes. The step ratio is finally sized to cut off higher order modes at the upper end of the useable frequency range. The $6^\circ 15' 15''$ half flare angle is the same as existing JPL feedhorns. While somewhat conservative, this moderate flare angle is gradual enough to prevent field distortion at the aperture, for horns with less than 30 dB of gain. Beginning at the interface of Sections 1 and 2 (Fig. 1), the corrugated flare section continues for 109.35 cm (43.050 in.) to an aperture of 31.91 cm (12.563 in.). This aperture size is approximately optimum for the 14.784 deg half-aperture angle of the 64-m antenna with tricone feed subreflector. Corrugations are selected to be $\lambda_0/4$ deep at the center frequency with 5 cycles per freespace wavelength. Although most of the elements of the dual hybrid mode horn influence the impedance bandwidth to a minor degree, the horn is very well matched near the design center frequency, without use of additional elements (Fig. 2). Figure 2 includes all elements shown in Fig. 1. By experiment, the phase center of the new horn is found to be 20 cm (7.88 in.) inside the aperture.

IV. Performance of the Dual Hybrid Mode Horn

The approach adopted in this reporting is to compare the previously existing horn (single hybrid mode), (Ref. 6), with the new horn, at 8.45 GHz. Bandwidth performance will also be given, using 8.45-GHz dual hybrid mode horn performance as a baseline. Performance for a subreflector

edge angle of 14.784 deg will be given (64-m antenna tricone asymmetric subreflectors). The gain maximum subreflector angle will be noted for possible application to higher noise level systems. Finally, subreflector scattered patterns, at 8.45 GHz only, will be given for the single and dual hybrid mode horns. These patterns will show the improved aperture illumination obtained when using the new horn.

Figure 3 shows E- and H-plane amplitude patterns of the single hybrid and dual hybrid mode feedhorns at the selected center frequency. The efficiencies of these horns, based on horn patterns alone, are given in Table 1. In Table 1, data for the single hybrid mode horn are computed (see Fig. 3 of Ref. 11) rather than measured, while data for the dual hybrid mode horn are measured. This results in a slightly conservative estimate of the improvement. In Table 1, it is seen the dual hybrid mode horn pattern exhibits slightly ($<1\%$) improved spillover efficiency and substantial (5%) improvement in illumination efficiency. Table 2 shows the frequency behavior of the new horn. It is seen that the total efficiency peaks at 8400 MHz; at 8600 MHz the performance is approximately the same as a single hybrid mode horn (Table 1). Figure 4 shows measured E- and H-plane amplitude patterns of the dual hybrid mode horn at the frequency extremes of 8300 and 8600 MHz. For operation over the X-band range 8.40 to 8.50 GHz, the new horn is considered totally adequate.

Figure 5 shows E- and H-plane amplitude patterns of the single and dual hybrid mode horn scattered from a 64-m class antenna subreflector. In this case, to save costs associated with scattering computations from large asymmetric reflectors, we have adopted a symmetric equivalent to the existing 64-m Tricone subreflector (Ref. 12). The scattered patterns show essentially the same forward (polar angle = 165 deg) and rear (polar angle $\simeq 65$ deg) spillovers; the more uniform amplitude illumination produced by the dual hybrid mode horn is clear.

Table 3 gives the results of efficiency calculations on the two patterns seen in Fig. 5. For the accepted symmetric subreflector case, a performance increase of 0.36 dB is available. It is interesting to note in Table 3, the improved illumination efficiency and the improved central blocking efficiency; the latter is caused by reduced fields in the center portion of the main reflector (Fig. 5). It is estimated, based on Table 1 of Ref. 11, that a loss of 0.07 dB will be incurred if this feed is used in the 64-m tricone asymmetric system, due to energy converted to $m \neq 1$ modes. The net available improvement is therefore +0.29 dB. One uncertainty in estimating the performance improvement of various methods of obtaining more uniform amplitude illumination remains, that of quadripod blocking. With present illumination functions (relatively weaker near the paraboloid periphery) the wider quadripod shadow in that region is of minor consequence. With more uniform illumination, there may be a detrimental side effect. The magnitude of that possible effect is not known.

V. Summary

A new horn suitable for feeding conventional DSN Cassegrain ground antennas employing parabolic and hyperbolic reflectors has been developed. The new horn offers performance improvements of 0.36 dB in gain for symmetric antennas and an estimated 0.29 dB in gain for the case of the 64-m asymmetric tricone system. Forward and rear spillovers are essentially unchanged from present practice, therefore no noise temperature improvement is realized in the described design. Bandwidth of the new horn is such that it cannot be applied at both DSN S-band uplink (2100 MHz) and downlink (2300 MHz) frequencies simultaneously; it is recommended the new horn be considered for X-band only, in the DSN context. For special S-band low-noise level listen-only applications without transmitter use, the new horn could be applied. The resulting aperture size and overall length will fit a standard feedcone.

References

1. Potter, P. D., "A New Horn Antenna With Suppressed Sidelobes and Equal Beamwidths," *Microwave Journal*, June 1963.
2. Ludwig, A. C., "Antennas for Space Communication," in *Supporting Research and Advanced Development*, Space Programs Summary 37-33, Vol. IV, pp. 249-255, Jet Propulsion Laboratory, Pasadena, Calif., June 30, 1965.

References (contd)

3. Ludwig, A. C., "Antennas for Space Communication," in *Supporting Research and Advanced Development*, Space Programs Summary 37-33, Vol. IV, pp. 261-266, June 30, 1965.
4. Minnett, H. C., and Thomas, B., and Mac, A., "A Method of Synthesizing Radiation Patterns With Axial Symmetry," *IEEE Trans. Antennas and Propagation*, pp. 654-656, September 1966.
5. Rumsey, V. H., "Horn Antennas With Uniform Power Patterns Around Their Axes," *IEEE Trans. Antennas and Propagation*, pp. 656-658, September 1966.
6. Brunstein, S. A., "A New Wideband Feedhorn With Equal E- and H-Plane Beamwidths and Suppressed Sidelobes," in *The Deep Space Network*, Space Programs Summary 37-58, Vol. II, pp. 61-64, Jet Propulsion Laboratory, Pasadena, Calif., July 31, 1969.
7. Bathker, D. A., *Predicted and Measured Power Density Description of a Large Ground Microwave System*, Technical Memorandum 33-433, Jet Propulsion Laboratory, Pasadena, Calif., April 15, 1971.
8. Bathker, D. A., "Dual Frequency Dichroic Feed Performance," presented at AGARD Antennas for Avionics Panel, Munich, Germany, November 26-29, 1973.
9. Thomas, B., and Mac, A., "Theoretical Performance of Prime-Forms Paraboloids Using Cylindrical Hybrid-Mode Feeds," *Proc. IEEE*, Vol. 118, No. 11, November 1971.
10. Clarricoats, P. J. B., and Saha, P. K., "Propagation and Radiation Behavior of Corrugated Feeds, Parts I and II," *Proc. IEEE*, Vol. 118, No. 9, September 1971.
11. Potter, P. D., "A New Computer Program for the Design and Analysis of High Performance Conical Feedhorns," in *The Deep Space Network*, Technical Report 32-1526, Vol. XIII, pp. 92-107, Jet Propulsion Laboratory, Pasadena, Calif., February 15, 1973.
12. Potter, P. D., "Shaped Antenna Designs and Performance for 64-m Class DSN Antennas," in *The Deep Space Network Progress Report 42-20*, pp. 92-111, Jet Propulsion Laboratory, Pasadena, Calif., April 15, 1974.

Table 1. Single hybrid mode and dual hybrid mode horn efficiencies 8450 MHz

Efficiencies at $\theta = 14.784$ deg	Single hybrid-mode horn	Dual hybrid-mode horn
Spillover η_s	0.9483	0.9554
Illumination η_I	0.8443	0.8989
Cross-polarization η_X	0.9999	0.9999
Phase η_P	0.9983	0.9926
TOTAL η_T	0.7993	0.8523
Maximum efficiency η_{MAX}	0.8153 at $\theta = 13.293$ deg	0.8646 at $\theta = 13.784$ deg

Table 2. Dual hybrid mode horn efficiencies as a function of frequency at $\theta = 14.784$ deg

Frequency, MHz	η_s	η_I	η_X	η_P	η_T TOTAL	η_{MAX}
8300	0.9385	0.9437	0.9961	0.9704	0.8496	0.8502 @ $\theta = 14.563$ deg
8400	0.9506	0.9137	0.9998	0.9922	0.8616	0.8685 @ $\theta = 14.000$ deg
8450	0.9554	0.8989	0.9999	0.9926	0.8523	0.8646 @ $\theta = 13.784$ deg
8500	0.9593	0.8849	0.9993	0.9879	0.8380	0.8558 @ $\theta = 13.501$ deg
8600	0.9664	0.8523	0.9969	0.9630	0.7906	0.8245 @ $\theta = 12.937$ deg

Table 3. Subreflector scattered pattern efficiencies, 8450 MHz (tricone symmetric equivalent subreflector)

Efficiencies at 61.104 deg	Single hybrid-mode feed	Dual hybrid-mode feed	Dual hybrid mode improvement, dB
Spillover η_s	0.9447	0.9529	+0.037
Illumination η_I	0.8474	0.9008	+0.266
Cross-polarization η_X	0.9999	0.9999	0
Phase η_P	0.9718	0.9670	-0.021
Blocking η_B	0.9441	0.9616	+0.080
TOTAL η_T	0.7344	0.7981	+3.361

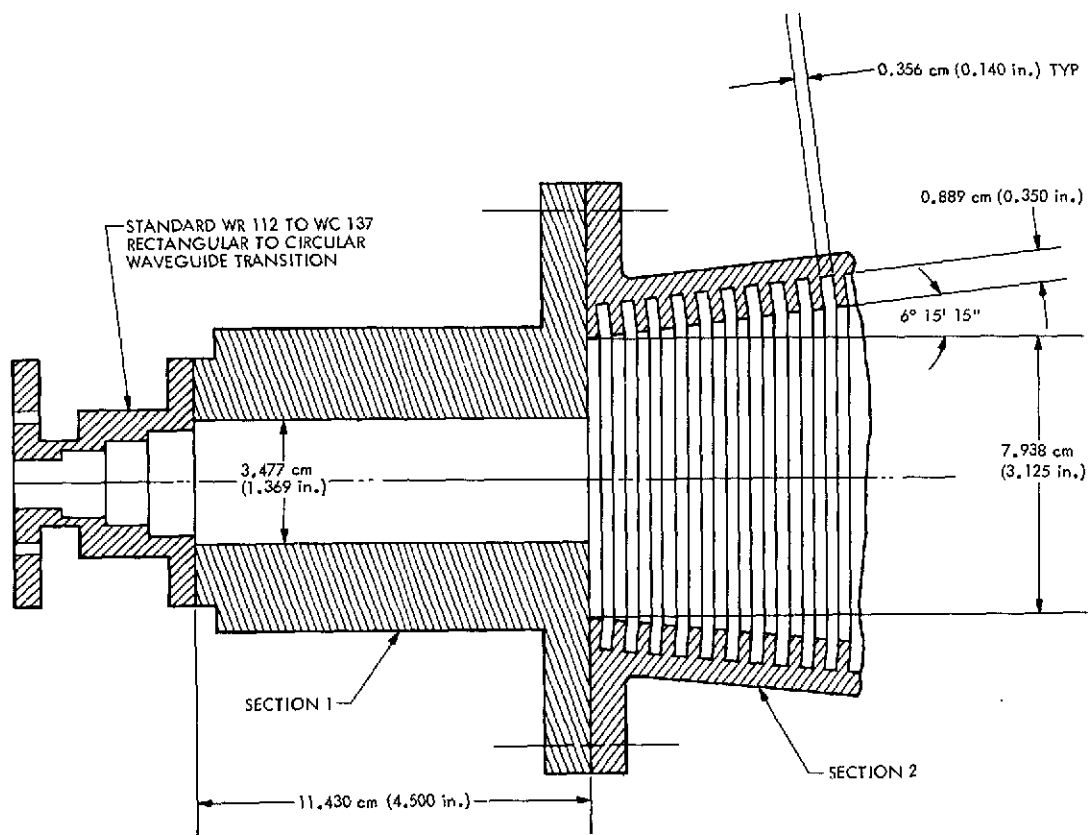


Fig. 1. Throat region of dual hybrid mode horn

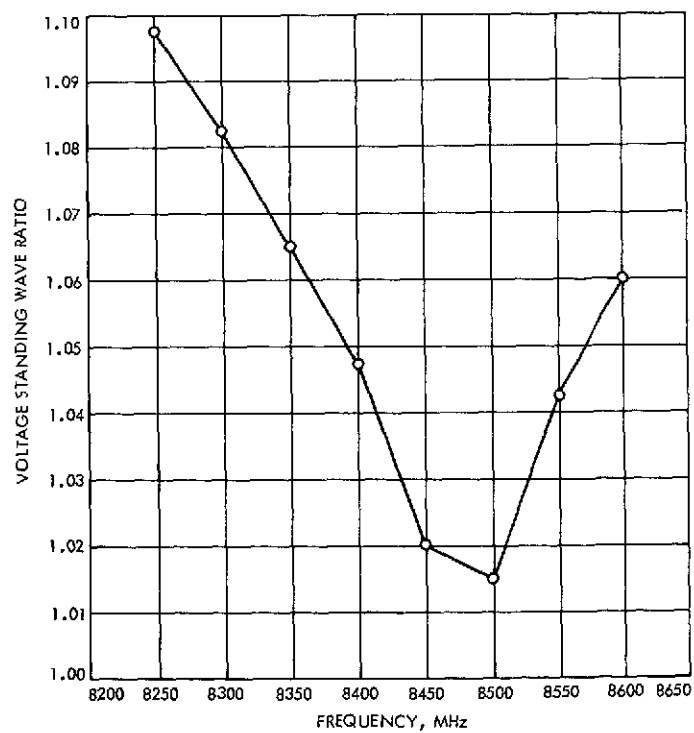


Fig. 2. Impedance bandwidth of dual hybrid mode horn

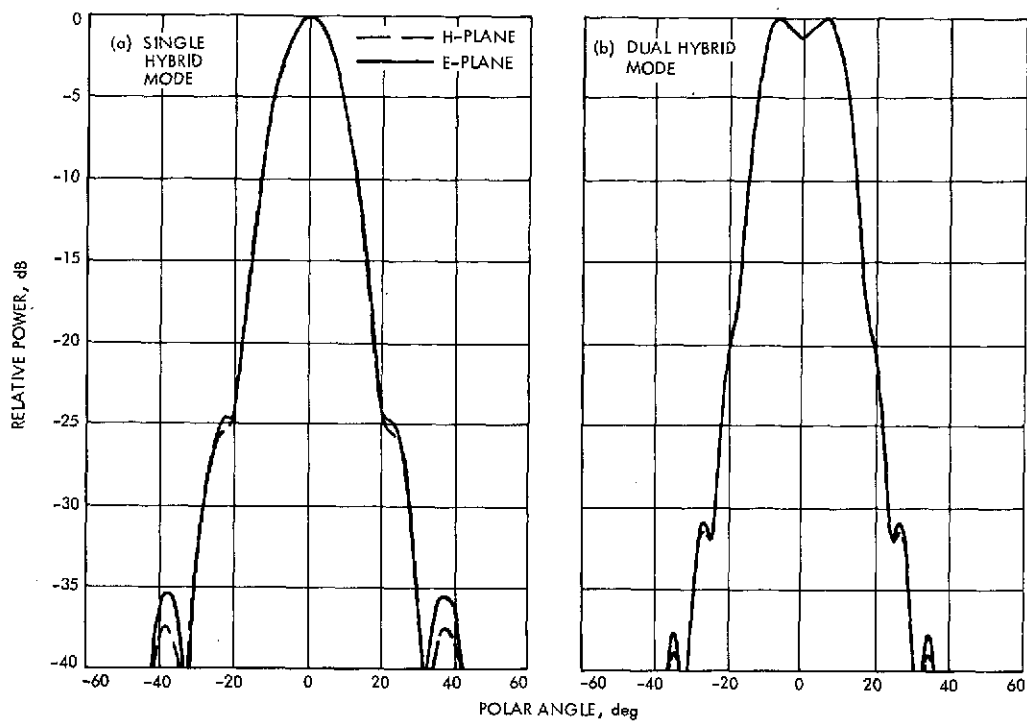


Fig. 3. Feedhorn amplitude patterns, 8.45 GHz

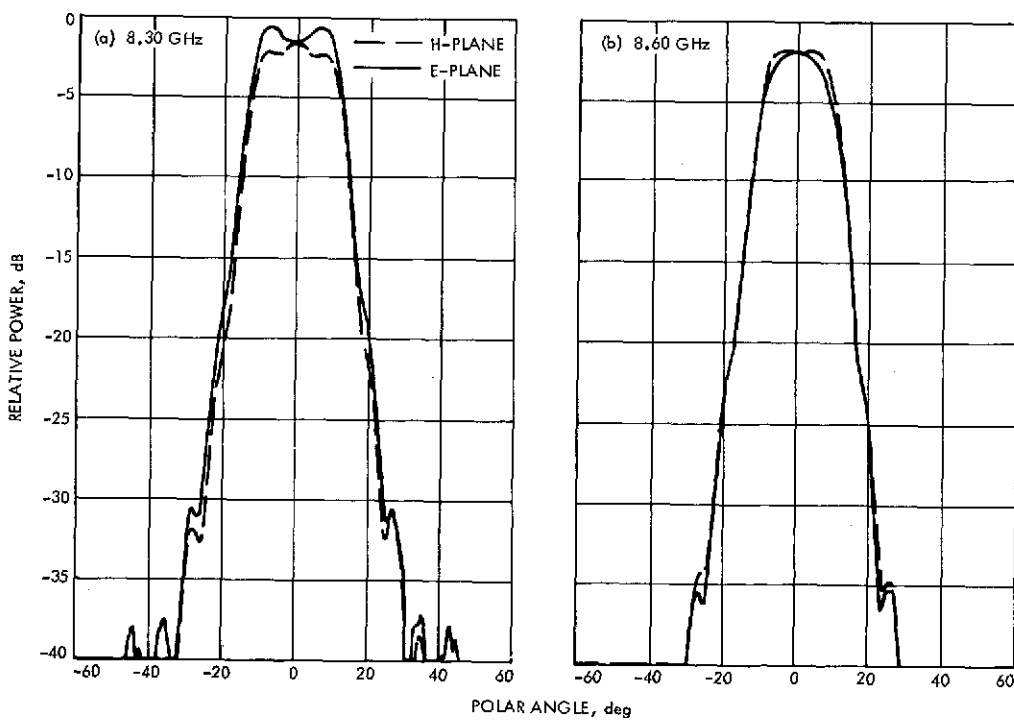


Fig. 4. Dual hybrid mode feedhorn amplitude patterns, 8.30 and 8.60 GHz

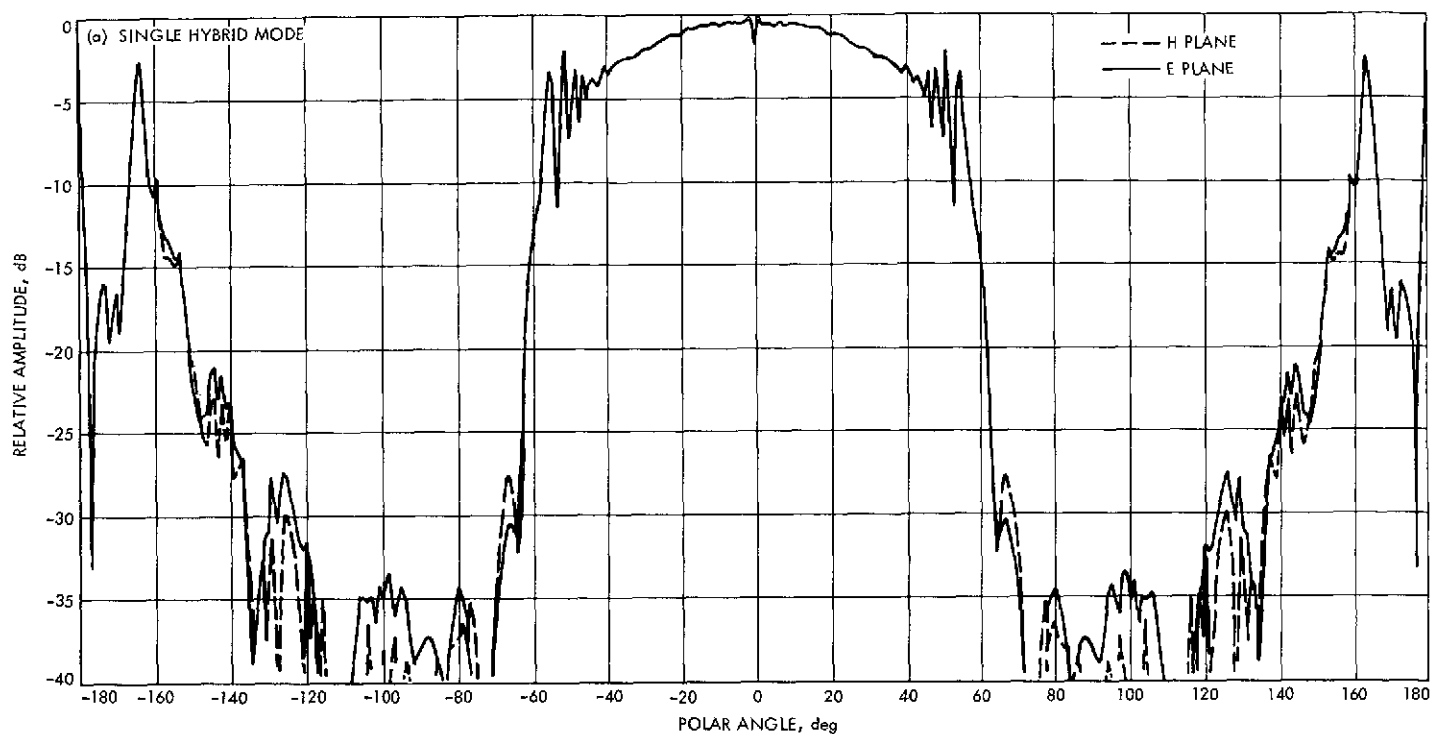


Fig. 5. Symmetric subreflector amplitude patterns, 8.45 GHz

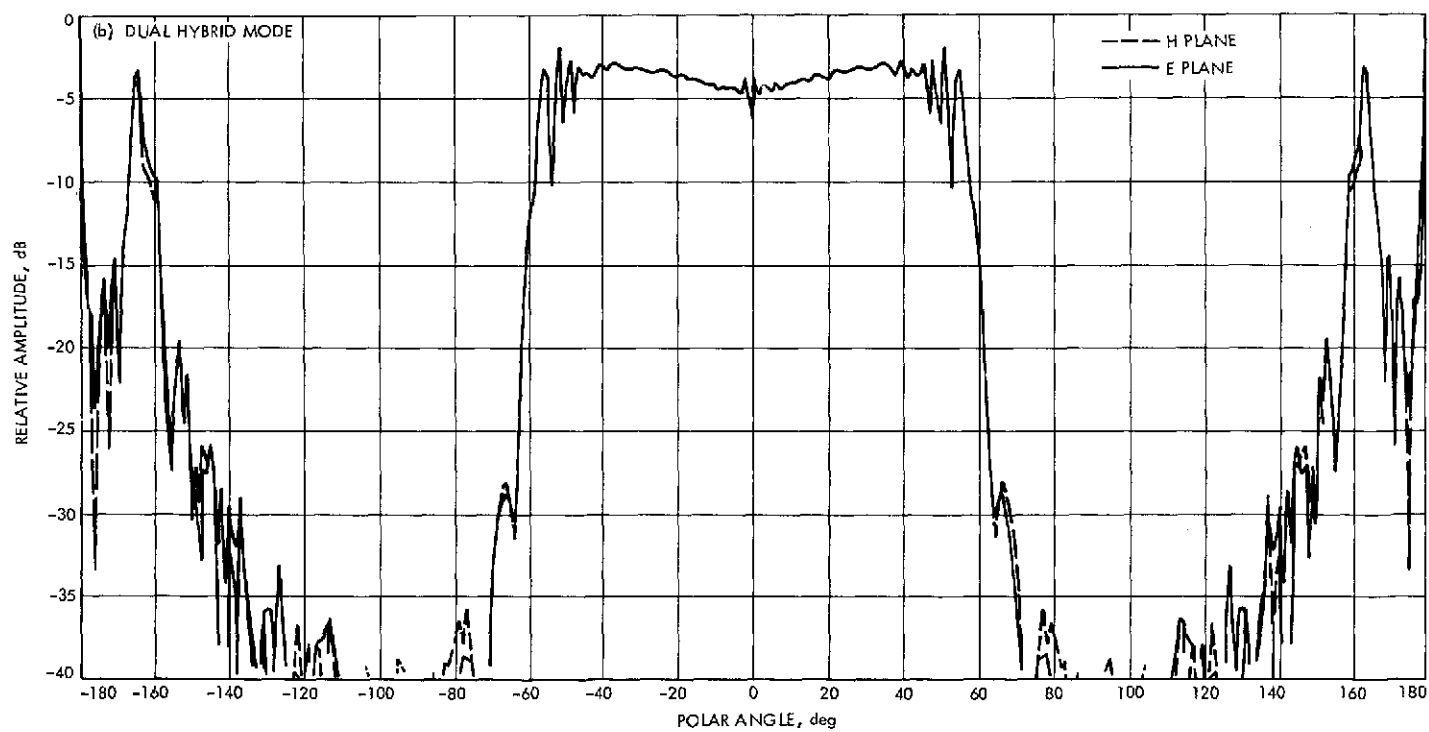


Fig. 5 (contd)

DSN Research and Technology Support

E. B. Jackson

R. F. Systems Development Section

The activities of the Development Support Group in operating and maintaining the Venus Station (DSS 13) and the Microwave Test Facility (MTF) are discussed and progress noted. Major activities include support of testing of the 100-kW transmitters to be installed into the overseas 64-m antennas, testing and modification required for the 400-kW X-band radar system, testing of station automation and pulsar observation, installation of new Faraday rotation polarimeters, and clock synchronization transmissions. Other activities include Pioneer 10 and 11 science support, sky survey, and weak radio source observations.

During the two-month period ending June 15, 1974, the Development Support Group, in its operation of the Venus Station (DSS 13) and the Microwave Test Facility, made progress on various projects as discussed below.

I. In Support of Section 331

A. Station Automation (Pulsars)

As part of the overall DSN Station Automation Project (RTOP 68, "Station Monitor and Control"), a demonstration is planned using the Venus Station to perform a pulsar track under remote control from JPL in Pasadena. To provide the necessary station control, modifications

have been made to the station computers to provide bilateral communications between the two SDS-910's and the "master" computer, the SDS-930. Additionally, the SDS-910 dedicated to pointing the 26-m antenna had a complete PIN-POT chassis added, while the SDS-930, requiring expansion of its interrupt capability, had 8 interrupts added to bring the total available to 16. With successful communication now established between the three station computers and the computer at JPL, 70 hours of automation software and hardware testing was done during this period. Also, 85¼ hours of pulsar observations were performed, during which the pulsars tabulated in Table I were observed at 2388 MHz, left circular polarization (LCP), using the 26-m antenna and the SDS-930 for data taking.

II. In Support of Section 333

A. Weak Source Observation

During the 59¼ hours devoted to routinely observing weak radio sources (Ref. 1), the sources tabulated in Table 2 were observed at 2295 MHz with the 26-m antenna set to receive right circular polarization (RCP).

B. Radio Star Calibration

With the receiver tuned to 2278.5 MHz, and the 26-m antenna adjusted for right circular polarization, flux measurements of radio sources 3C123, 3C218, NGC 4258, Cassiopeia A, and Cygnus A were made during 48½ hours of observing.

C. Sky Survey

With the 26-m antenna fixed at a 180-deg azimuth and progressively positioned between 84.4- and 85.7-deg elevations in 0.1-deg increments, 548½ hours of data were automatically collected during the night and weekend hours when the station was not manned.

D. Faraday Rotation Data Collection

A decision has been made to install ionospheric monitoring equipment at each of the overseas 64-m antenna complexes in support of the Helios and Viking 1975 missions. To provide an opportunity for competitive evaluation, two complete Faraday Rotation Receiving Systems (polarimeters) have been installed at DSS 13, and data are being recorded from each system onto punched paper tape, digital printer, and analog chart recorder. A discussion of this system and evaluation procedures are presented by A. L. Price elsewhere in this volume.

III. In Support of Section 335

A. X-Band Planetary Radar

The DSS 14 Transmitter Control System has been modified by the installation of additional cabinets with which two klystrons can be simultaneously controlled, along with other modifications to the S-band control system. Correct operation of the modified S-band system has been demonstrated and the X-band modification is substantially completed, lacking only some additional wiring. A similar modification to the DSS 13 transmitter control system is 50% completed.

A waveguide switch, which will handle 400 kW in the final system, has satisfactorily completed three continuous hours of testing at 200 kW, and one hour of testing at 300 kW, switching immediately and satisfactorily after each test was completed in the Traveling-Wave Resonator (TWR). Additionally, the feedhorn to be used for this system was tested at 160 kW using the VA-949J klystron.

It is apparent that additional cooling of the waveguide flanges, which carry 400 kW, will be necessary. In order to evaluate various cooling schemes, a device for simulating RF heating of the waveguide, using circulating heated oil, is being assembled at the Microwave Test Facility.

B. DSS 63 100-kW Transmitter Testing

The DSS 43 1.1-MW Transformer/Rectifier was temporarily installed into the test system to verify its capability. A 24-hour heat run at 1 MW dc was satisfactorily completed.

Radio frequency testing of the klystron cabinet has commenced at the 100-kW power level, completion of which will wind up the DSS 63 system testing and packaging, and shipment to Spain will follow. Three additional members of the DSS 63 staff have undergone training at DSS 13 and have returned to Spain.

C. Block IIIC Receiver-Exciter

The planned installation of the Block IIIC Receiver-Exciter at DSS 13 has been delayed because of manpower requirements in other areas. Preliminary groundwork has been completed, however. The Block IIIC system will be installed, intact, with only modifications to update it. The present Mod IV R&D receiver will be reduced in size from three equipment cabinets to one. The 2388-MHz phase-locked loop, as well as the 455-kHz loop and one open-loop channel, will be retained. The present auxiliary receiver cabinet will remain unchanged.

Some cabinet rearrangement will be necessary in the operations building to accommodate the nine additional cabinets in the Block IIIC system.

IV. In Support of Section 422

A. Clock Synchronization Transmissions

Two transmissions to DSS 51, three transmissions to DSS 43, and three transmissions to DSS 63, for a total of

8¼ hours, were made as scheduled by DSN scheduling. The 100-kW X-band transmitter klystron body current is normally monitored with a current sensing probe (transformer) which sees the difference between beam current and collector current. These units output two signals, a fast body fault protection signal, and a slow body metering signal. The slow body portion of both of the X-band transmitters' body current probes have failed while on loan to a development project.

To allow clock synchronization transmissions to continue, the transmitter has been modified slightly. A 1-Ω, 100-W resistance has been placed between the high-voltage positive return path and system ground. Current through this resistance is body current and is used to furnish the slow body signal to the transmitter metering and slow body protection circuits (Fig. 1). The fast body protection is still provided with a body current probe. The second current probe has been returned to the manufacturer for repair.

B. DSN Klystron Testing

The DSN High-Power Transmitter Maintenance Facility at DSS 13 tested a DSN 400-kW klystron (X-3075) S/N H1-101-R1. It did not pass acceptance testing and

was returned to the manufacturer, Varian Associates, for rework as necessary.

V. In Support of Section 825

A. Pioneer 10 and 11 Science Support

Approximately 10 hours per week of routine observing are being provided. Observations of the radiation from Jupiter and radio source calibrators tabulated in Table 3 were made at 2295 MHz with the 26-m antenna adjusted to receive right circular polarization. Observations were made for a total of 80 hours during the two months ending June 15, 1974.

B. Interstellar Molecular Line Search

The 64-m antenna at DSS 14 has been used to search for emission lines from hydrogen and carbon recombination in interstellar space in the vicinity of 2275 MHz. Thirty-four hours of experimental observations were made with the DSS 13 26-m antenna to evaluate usability for this purpose. Searches were made in the direction of Orion A, NGC 2023, LKHA 208, NGC 2068, M431R, 3C286, and 3C295; initial data results indicate the 26-m antenna will be useful for these observations.

Reference

1. Jackson, E. B., "DSN Research and Technology Support," in *The Deep Space Network Progress Report 42-20*, Jet Propulsion Laboratory, Pasadena, Calif., Apr. 15, 1974.

Table 1. Pulsars selected for test observation at DSS 13

0031-07	0823+26	1818-04
0329+54	0833-45	1911-04
0355+54	1133+16	1933+16
0525+21	1237+25	2021+51
0628-28	1604-00	2045-16
0736-40	1642-03	2111+46
		2218+47

Table 2. Weak radio sources observed at DSS 13

3C123	3C286	3C461
3C138	3C309.1	NGC 4218
3C147	3C348	NRAO 530
3C218	3C353	Virgo A

Table 3. Radio source calibrators used for Pioneer science support

3C48	3C147	CTA 21
3C123	3C348	PKS 0237-23
3C138	3C353	

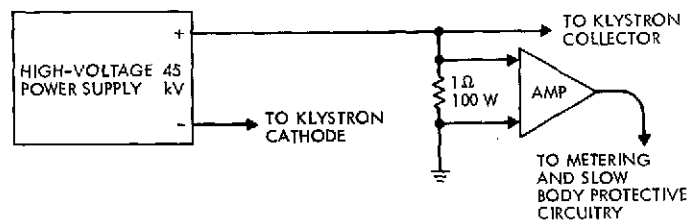


Fig. 1. Simplified slow body current circuit

Forward Error Correction for the Ground Communications Facility?

O. H. Adeyemi and R. J. McEliece
Communications Systems Research Section

Using the recently developed five-state Markov model for the GCF, we have calculated the tradeoffs between block error correction efficiency and block overhead for several forward error correction schemes. The results indicate that this particular kind of error control is not suitable for the GCF.

I. Introduction

It has been determined by both DSN and flight project studies that the errors made in transferring deep space telemetry from the various tracking stations to the Network Operations Control Center (NOCC) are frequently more serious to flight project data systems than the errors caused by the space channel itself. Since at present Ground Communications Facility (GCF) errors must be corrected by later retransmission, any reduction in these errors will result in improved real-time deep space telemetry.

One method of error control which has found wide application in other situations is *block coding*. In a block coding scheme certain parity-checks are added to the source data prior to transmission. If the transmission channel causes some of the data to be received in error, the pattern of parity-check failures can be used to correct the errors, provided the noise is not too severe. There is a large amount of literature dealing with the selection of the appropriate parity checks and error-correction algo-

rithms which can be drawn upon. We now describe one possible application to the GCF.

Let us suppose that a certain fraction α , $0 < \alpha < 1$, of the 1200-bit NASA Communications (NASCOM) data block is available for parity-check information. At present the 33 error-detecting parity checks represent $\alpha = 0.03$. In general α should be kept as small as possible and in any case could never exceed 0.2. In the next section we shall study the tradeoff between α and block error probability for two classes of block codes.

II. Block Coding Study

It is well known that the bit errors in the GCF are not independent but tend to occur in bursts. Thus the block coding techniques we studied were designed to cope with bursts of errors. We first describe the burst error correcting codes. In general, these codes are designed to correct any burst of length $\leq b$ in a block of n bits. (The errors occurring in a block are said to occupy a burst of length b

if the distance between the first and last bits in error is b). For our application, $n = 1200$, and the value of b is determined by the fraction α of the 1200 bits which are parity checks. The smallest possible α for a given value of $\beta = b/1200$ was obtained from Table 11.6 of Ref. 1:

Using Table 1 we simulated the performance of burst error correcting codes for the GCF, using Adeyemi's model (Ref. 2) for generating error events. We obtained the following graphical tradeoff between α , the fraction of the GCF block used for error correction, and γ , the fraction of GCF blocks received in error which could be corrected (see Fig. 1).

The designations "green," "amber," and "red" refer to the classification made by McClure (Ref. 3) of the GCF transmission quality, green being the best state and red the worst. It is seen that when the channel is in its red condition, even 20% redundancy would allow the correction of only 35% of the blocks received in error.

The second type of block coding employed was *symbol* error correcting, whereby the 1200-bit block was divided into n s -bit symbols, where $1200 = ns$. The code employed could then correct a certain number of symbol errors. The best choice of s turned out to be $s = 8$, so $n = 150$. The relation between α , the redundant fraction, and β , the fraction of the 150 symbols which could be corrected, using a Reed-Solomon code, is given in Table 2.

Again using Adeyemi's model we obtained the graph shown in Fig. 2.

It is seen from Figs. 1 and 2 that symbol error correcting codes give performance superior to burst-error correcting codes, but the improvement is not dramatic. We conclude that block error correction in 1200-bit blocks is not appropriate for the GCF. However, it is possible that encoding in blocks (much) longer than 1200 bits could be more attractive. We hope to devote a future article to that subject.

References

1. Lucky, R. W., et al., *Principles of Data Communication*, McGraw-Hill, New York, 1968.
2. Adeyemi, O. H., *Error Control on the GCF: An Information-Theoretic Model for Error Analysis and Coding*, Technical Memorandum 33-699, Jet Propulsion Laboratory, Pasadena, Calif. (in press).
3. McClure, J. P., "4800-bps High Speed Data Error Statistics," Interoffice Memorandum, Jet Propulsion Laboratory, Pasadena, Calif., Jan. 5, 1973 (an internal document).

Table 1. Tradeoff between α and β for burst error correcting codes

α	β
0.01	0.004
0.02	0.008
0.04	0.017
0.07	0.025
0.08	0.035
0.09	0.038
0.12	0.047
0.13	0.048
0.15	0.068
0.19	0.090

Table 2. Tradeoff between α and β for symbol error correcting codes

α	β
0.05	0.027
0.10	0.05
0.15	0.073
0.20	0.10

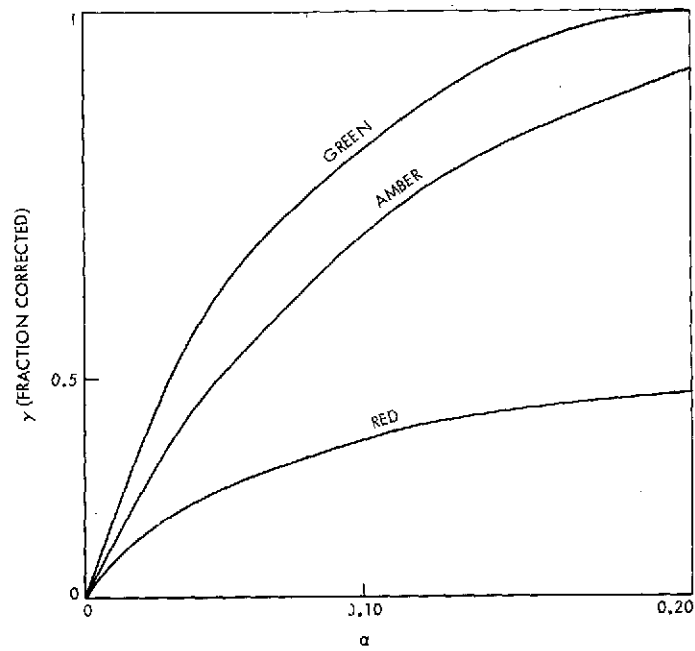


Fig. 1. Relation of α and γ for burst error correcting codes

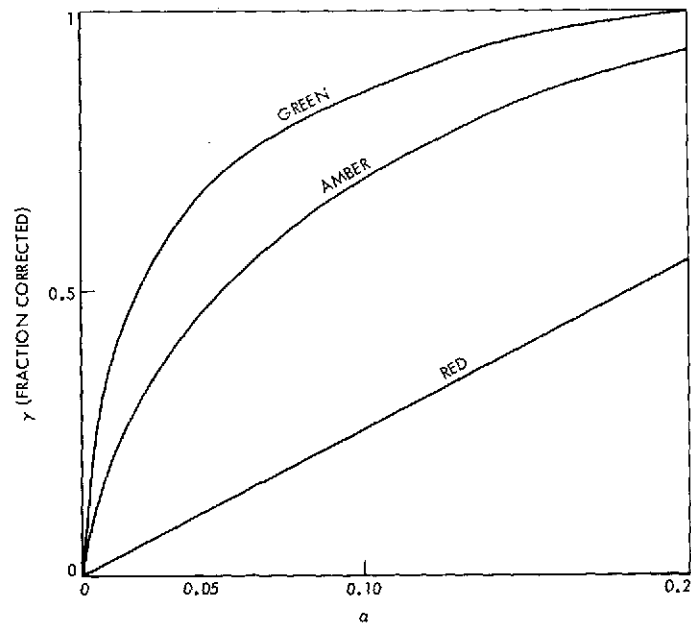


Fig. 2. Relation of α and γ for symbol error correcting codes

Observations on Microprocessors and Computing Efficiency

C. C. Klimasauskas and J. W. Layland
Communications Systems Research Section

This article presents results of a continuation of our previous study of computing efficiency in DSN-related tasks. The two task models considered here are manipulation of man-readable character-string data, and a very simple process variable monitoring operation. Several currently available minicomputers and microprocessors are compared. The principal result is that the microprocessors appear considerably more cost-effective than the more powerful machines for the simple repetitive tasks, but that the opposite is true for more complex operations.

I. An Introduction to the Problem

In the last year, a number of large-scale integrated-circuit (LSI) microprocessors have become available with the promise of more to follow in the near future. At present there is little understanding, or experimental data, to determine which tasks they are best able to perform. This article considers some of the complexities of the general problem of selecting a particular processor/implementation, specifically in the area of processor trade-offs for different tasks. It is a continuation of an earlier study done comparing minicomputer implementations for performing DSN-related computer activities (Ref. 1).

II. Time-Storage Costs

This section considers the cost effectiveness of the implementation of a macroprocessor called STAGE-2 (Ref. 2). STAGE-2 manipulates character-string data supplied from one input/output (I/O) device and emits character-

string data to another device. Its requirements in terms of machine capabilities should be similar to the text manipulation performed by a DSN subsystem controller in conversing with its operator.

STAGE-2 is a language-independent macroprocessor written in a machine-independent language called FLUB. This machine-independence makes it relatively easy to develop alternative implementations on one computer, or many computers, and compare their performance directly. The operation statistics were gathered through a special instrumented version of STAGE-2. Three alternative implementations were studied for the Sigma 5: The first was a straightforward implementation, packing all the information contained in a FLUB word into a single 32-bit Sigma word. The second was an implementation which minimized execution time. In this implementation, FLUB data were stored in 64-bit double words. The third was an interpretive implementation to minimize storage. Our motivation for this implementation comparison may be

found in the work of Savage (Ref. 3), who showed that a bound exists to the minimum time-storage product for any well-defined process. Storage in all implementations included the STAGE-2 instructions and 4000 FLUB memory words. These implementations were compared in two ways: One comparison ignored processor cost, and considered only the resources of storage and execution time. The other included the cost of the processor in the storage requirement. Processor storage equivalent was computed from the following:

Processor storage equivalent kbytes =

$$\frac{\text{Processor cost at initial marketing (\$)}}{\text{\$ for 1 kbyte of processor storage at initial marketing}}$$

The storage-time diagram for the implementations is shown in Fig. 1. The dashed lines represent a constant storage-time product. The single-word implementation appears cheaper than the double-word implementation when the processor cost is ignored. When the processor cost is included, the opposite is true. In both cases, the interpretive implementation is always costlier. This is due to the high time overhead in decoding the FLUB instructions as compared to the savings in storage. However, programs such as high-level language translators may benefit from interpretive implementation, being tasks in which the functions performed are complex, storage large, and the instruction-decoding overhead small. Processor cost is clearly significant here, and is included in all following material.

The two faster implementations fall roughly upon a constant time-storage product line. The interpretive implementation would clearly be a mistake to use. Physical constraints of the task have presented another bound to implementation alternative. We observe that other constraints, such as a requirement to force-fit a task onto predetermined hardware can result in extremely inefficient use of the computing resources.

III. STAGE-2 Processor Comparisons

STAGE-2 was implemented in fact, or hypothetically, on a variety of minicomputers and microprocessors. Processor selection was based on information availability. From manufacturer's published data, instruction counts from the instrumented version of STAGE-2, and knowledge of implementations, the execution time and storage requirements to perform a specific macroprocessing task

were computed for each processor. These data are plotted in Fig. 2. For each processor, the processor storage equivalent was considered part of the storage requirement.

Of historical note, the data on the 8080 were not available when Fig. 2 was first plotted. Without the 8080, it appeared that STAGE-2 was just too complex a job to be implemented on a microprocessor. However, the 8080 is approximately on the same storage-time line as both the PDP-11/20 and Sigma 5. The 8080 implementation is well over 10 times faster than the 8008 (though about 10 times faster in raw processor speed) and requires considerably less program storage. This results from the availability of 16-bit data manipulating instructions on the 8080. These more powerful data manipulating instructions, a faster processor, and more powerful addressing modes compound storage-time savings.

It is worth noting that each of these processors lies within the storage-time products of 1200 kbyte-min and 2400 kbyte-min. This implies that as resources for performing this task, they are essentially equivalent in cost. This may be a phenomenon of implementing a machine-independent task equally poorly on a variety of machines. This warrants future consideration since the trend in computing is away from machine-dependent features and toward, as much as possible, machine-independent algorithms and implementations. For example, Professor Per Brinch Hansen at the California Institute of Technology is working on a transportable multiprogramming operating system written in concurrent PASCAL, soon to be completed on the PDP-11 (Ref. 4).

In these comparisons, it is essential to realize that a salient feature of STAGE-2 is that it does not use indexing nor indirect addressing as such. A task which extensively uses indexing would increase the 8080's and 8008's storage-time product over its competitors, possibly eliminating them from consideration. Also, any task which required 32-bit arithmetic operations would move the XDS 930, PDP-11's, and 8080 out of the competitive region. The same is true of floating point tasks.

This exercise indicates that microprocessors may be competitive with minicomputers for performing simple tasks which utilize direct addressing and some 16-bit data manipulation (for example, emulation of the FLUB machine). At the same time, it is clear that we can find some task which is complex enough to make any specific microprocessor (or minicomputer) uneconomical with respect to a more complex processor.

IV. System Variable Monitoring, Processor Comparison

Within a DSN tracking station, computers are used to monitor an ever increasing number of variables. This enables operators and engineers to identify real and potential failures immediately, to isolate them, and to identify potential bottlenecks in performance. As tracking and flight control complexities increase, variable monitoring is expected to increase in sophistication and scope to meet the new demands. One approach to this problem is to employ a station "master" monitoring computer (MMC) which interfaces to a number of variable monitoring systems (VMSs). Each VMS would be responsible for reporting to the MMC those variables which exceed predetermined limits. This might be done by treating each VMS as a peripheral device of the MMC connected to a channel multiplexer. Through the channel multiplexer, the VMS would periodically test each variable. Figure 3 illustrates the task graphically.

The VMS was hypothetically implemented on a variety of microprocessors and minicomputers. Though better implementations may exist for each processor, an attempt was made for each implementation to maximally utilize speed and processing power. Execution time and storage requirements were computed from manufacturer's specifications. Storage for each processor implementation includes the processor equivalent storage. For purposes of comparison and from practical considerations, a sample interval of 20 ms was assumed. Figure 4 illustrates cost as a function of channel capacity. Whenever the sample interval could not be achieved with a single processor, multiple-processors were employed.

In this job, the 8080 microprocessor and even the 8008/8008-1 are far more cost-effective than any of the minicomputers. At large channel capacities, however, the Modcomp II is competitive with the 8008. The 8080 has about 10 times the capacity of the 8008, because it is a faster processor with more powerful addressing modes and data manipulating instructions. In this task, the high initial cost of the minicomputers is not offset by their faster processors and more powerful instruction repertoires. This small, repetitive task with a data width of 16 bits seems to be an ideal job for microprocessor implementations.

Of possible technological interest is that in the asymptotic limit system cost appears to be a function of date of introduction. Notice that the Sigma 5 and PDP-11/20, the Modcomp II and 8008, the 8008-1, and the 8080 are from increasingly more recent technological eras, and are correspondingly less expensive. This is emphasized by the task which is minimal, fits each processor comfortably, and is tailored to maximally utilize processor power.

The VMS is a task which well fits the capabilities of the microprocessor. The straightforward addressing required, short data word, and low initial cost make it much more attractive than its faster more sophisticated predecessors, the minicomputers.

V. Remarks on Storage Equivalent

Throughout this article, storage has been used as a unit of processor cost. Principally we hoped to minimize the effect of manufacturing processes and technology by assuming that both storage cost and processor cost were directly proportional to technological and manufacturing developments. If this, in fact, were true, the resulting measure of processor storage equivalent should make the comparisons significantly less dependent on the state-of-the-art and more dependent on processor architecture and power. Also, prices for processors and storage are continually changing, and vary enormously between sources. As such, storage equivalent provides a uniform well-defined standard on which to base processor cost.

The principles used in this study can easily be adapted to a direct cost comparison, in which both storage and processor costs are expressed in dollars.

VI. Summary

Though the results of this study are limited in scope and not firmly conclusive, we would like to make three observations. First, processor cost must be included in evaluating processor-implementation performance. Secondly, microprocessors appear competitive in jobs with short data items and simple addressing requirements. Finally, microprocessors appear best-suited for simple repetitive tasks, such as DSN variable monitoring.

References

1. Layland, J. W., and Klimasauskas, C. C., "A Myopic View of Computer-Based System Design," in *The Deep Space Network Progress Report*, Technical Report 32-1526, Vol. XIII, pp. 154-167, Jet Propulsion Laboratory, Pasadena, Calif., Feb. 15, 1973.
2. Waite, W. M., *Implementing Software for Non-Numeric Applications*, Prentice-Hall, Inc., Englewood Cliffs, N. J., 1973.
3. Savage, J. E., "Computational Work and Time on Finite Machines," *J. ACM*, Vol. 19, No. 4, pp. 660-674, Oct. 1972.
4. Hansen, P. B., *DEAMY, A Structured Operating System*, CIT-IS Technical Report 11, California Institute of Technology, Pasadena, Calif., Mar. 1974.

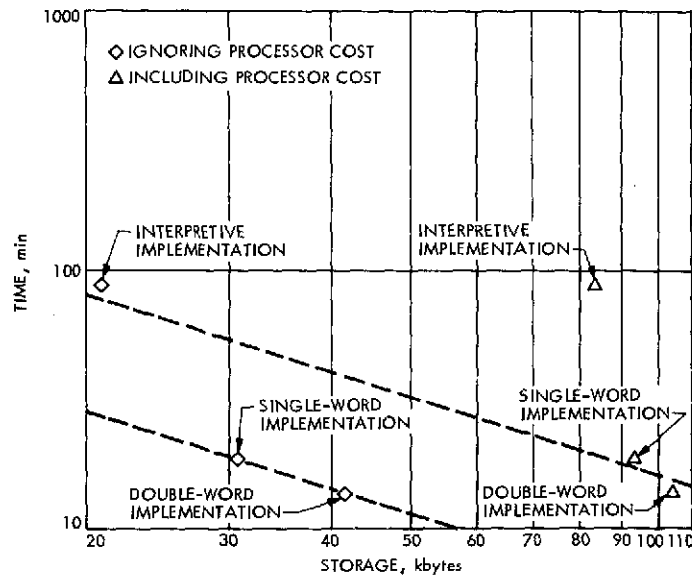


Fig. 1. Storage-time diagram for STAGE-2 implementation on Sigma 5

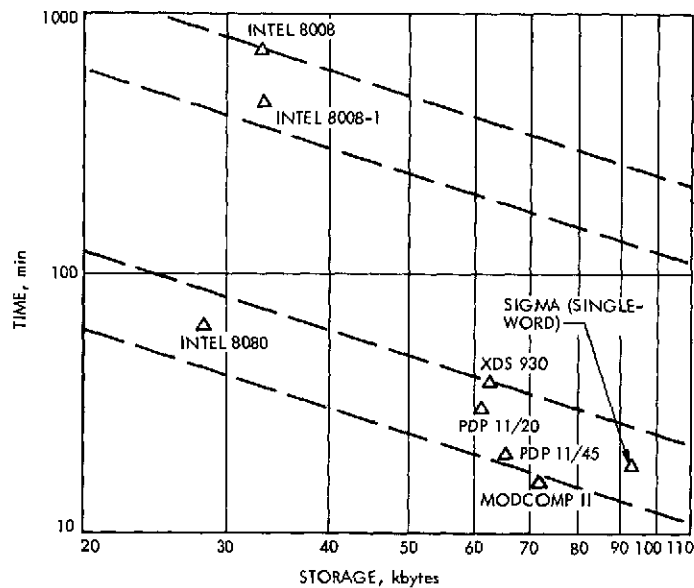
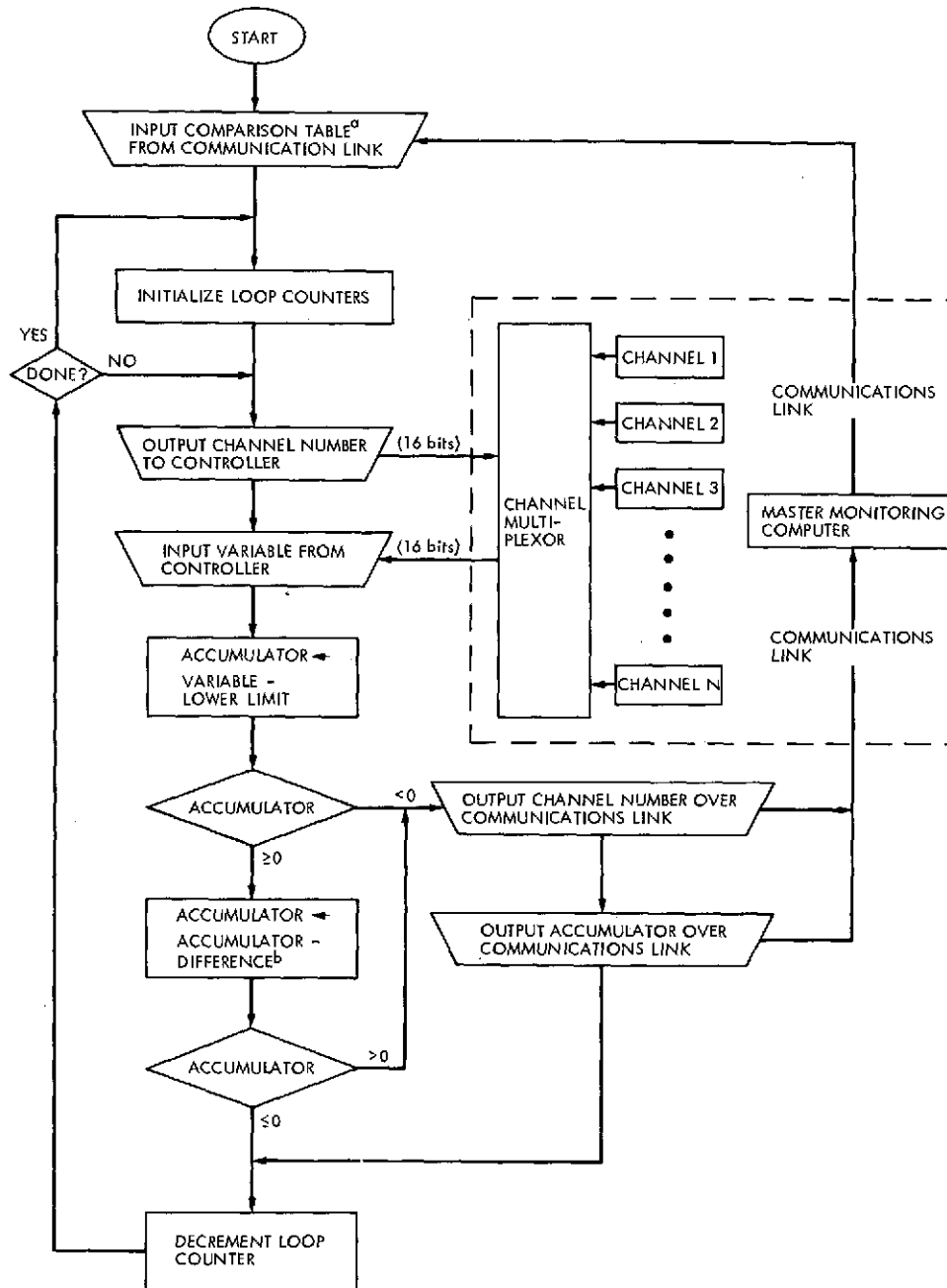


Fig. 2. Storage-time diagram for STAGE-2 on several different processors



^aTABLE IS IN STORAGE-IMAGE FORMAT SPECIFIC TO TARGET PROCESSOR

^bDIFFERENCE IS THE QUANTITY (UPPER LIMIT - LOWER LIMIT), WHERE UPPER AND LOWER LIMIT ARE, RESPECTIVELY, THE MAXIMUM AND MINIMUM ACCEPTABLE VALUES FOR VARIABLE

Fig. 3. Flowchart of the variable monitoring system

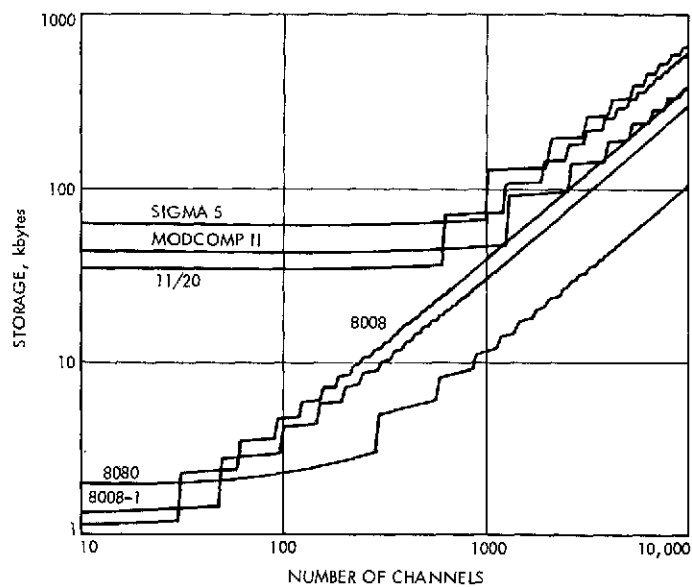


Fig. 4. Variable monitoring system cost as a function of channel capacity and processor

Simulation Study of a GCF Retransmission Scheme

L. R. Welch¹

Communications Systems Research Section

In this article, we study a promising retransmission algorithm for correcting GCF errors, using both actual GCF 4.8 kbps error data and Adeyemi's model. The results indicate that virtually all GCF error bursts can be corrected with a fairly simple scheme.

1. Introduction

In the Ground Communication Facility (GCF), data are transmitted in 1200-bit blocks. While 99% of the blocks are error-free, 1% have errors, and these tend to bunch together in small groups. Since parity bits within the block can be used to detect block errors with a conditional error rate of less than 10^{-6} , the receiver knows which blocks are in error and can request retransmission. In this article, we analyze one possible retransmission algorithm.

Three types of data must be stored. Since the receiver must pass the blocks on in proper sequential order, it is necessary to store blocks correctly received until all prior blocks have also been correctly received. This will be called the receiver buffer. When the transmitter transmits a block, it must retain that block until correct reception has been verified. This will be called the transmit storage. Finally, data entering the transmitter while other blocks are being retransmitted must be stored. This will be called the transmitter buffer. The transmit storage and

transmitter buffer could be part of the same physical device but are treated separately in this simulation.

The operating procedure is as follows. When a data block arrives at the transmitter, it is placed in the buffer. If all error indications have been acted on, the oldest block in the transmitter buffer is transmitted and simultaneously placed in transmit storage. When an error indication is received, the corresponding transmit block is retransmitted and reinserted in transmit storage at the first available block time. The receiver checks the parity bits and sends to the transmitter the information as to whether the block has been received correctly². The receiver stores only those blocks which have been received correctly but for which prior blocks have not yet been received correctly.

¹Consultant, University of Southern California.

²This is done by sending an acknowledgment signal for blocks received without errors, so that a missing acknowledgment means an error has occurred. This technique prevents disaster if the feedback channel is in a noisy condition.

II. Simulation Model

The basic unit of time in the model is the time to transmit one block. For each unit of time, 1200 bits of channel data are examined to determine whether a block error has occurred. The types of data used are discussed later. There are two parameters in the model, NR and LD . The first is an integer describing the input data rate: for every NR transmitted-block time, $NR - 1$ data blocks enter the system at times $t \neq 0 \pmod{NR}$. The choices in this simulation study were $NR = 10$ and 20 . This corresponds to data rates of 0.9 and 0.95 data blocks per channel block. The parameter LD , the loop delay, is the delay from the first transmission to the first opportunity to retransmit after an error has been detected. For the 4.8 -kbps simulation, this was taken as 5 block times, and for the 7.2 -kbps simulation as 10 block times.

Since the transmitter buffer operates on a first-in, first-out principle, the only information needed to indicate its status is the identification number of the oldest and youngest data blocks in the buffer.

The transmit storage operation was described in the Introduction. There are LD block storage locations and LD indicator bits. The block transmitted at time t is also stored at location $t \pmod{LD}$. Some time prior to $t + LD$, the transmitter receives a verification or rejection message and appropriately sets the $t \pmod{LD}$ indicator bit. Since $t + LD \pmod{LD} = t \pmod{LD}$, a retransmitted block is reinserted into the same storage location. When the transmitter buffer is empty and the indicator bit indicates no error, a "blank" must be sent. In this simulation, we assume that blanks received in error are not retransmitted.

The receiver status is more complicated. One could assume that the receiver stores only good blocks, but this leads to some data shuffling or address indexing problems in certain situations. A simple scheme is as follows. If the receiver has correctly received all data blocks with indices less than or equal to k but has not correctly received $k + 1$, and the largest index of a correct block is $k + l$, then each correct block with index n , such that $k < n \leq k + l$, is stored in address $n - k$. With this procedure, when a missed block is corrected before $k + 1$ block, it can be stored in appropriate order. Also, if a block is missed but its index can be determined, it can still be stored in correct position as a hedge against disaster. At any instant of time, the storage allocation is the l in the above description.

III. Channel Data

For the 4.8 -kbps simulations, 29 real data runs obtained by McClure (Ref. 1) were used to provide data patterns. In addition, the Adeyemi model (Ref. 2) was used to generate 124 runs of channel simulations. Half of these used Adeyemi parameters obtained from the worst real data run and the other half used model parameters derived from a combination of the worst three runs. The random data generator generated a run until 5000 errors occurred. The total bit lengths of the runs varied from 6×10^6 to 2.5×10^7 bits.

Since no 7.2 -kbps data were available, only Adeyemi's model was used. The parameters referred to above were modified to increase the expected time in the good state by a factor of $3/2 = (7.2/4.8)$, and to increase the length of garbled transmissions by a similar factor without significantly changing the statistics within the garbled segments. There were 31 runs for each of two parameter sets.

IV. Results

A general conclusion obtained from this study is that the transmitter buffer is much larger than the receiver buffer. This is the case because, when garbled stretches are short, the Receiver Buffer builds up to $LD - 1$ and then quickly recovers, while if garbled stretches are long, the channel becomes busy with retransmissions and data blocks with higher indices build up in the transmitter buffer.

The largest receiver buffer for 4.8 -kbps ($LD = 5$) usage was 11 blocks, and the largest for 7.2 -kbps ($LD = 10$) usage was 18 . This suggests that $2 \times LD$ is the largest size the buffer reaches. A straightforward analysis shows that the transmitter buffer buildup is insensitive to LD but depends strongly on channel statistics.

Neglecting the very bad first real data run, the largest transmitter buffer used was 20 blocks for the 4.8 -kbps channel and a data rate of 0.9 ; the buffer size increases to 25 when the data rate is 0.95 . For the 7.2 -kbps channel, the largest transmitter buffer required was 23 blocks at the 0.9 rate and 30 blocks at the 0.95 rate.

The results are summarized in Tables 1 and 2. The author has available run-by-run buffer size data for the reported simulations and has the program to generate more simulations if desired.

References

1. McClure, J. P., "4800 bps High Speed Data Error Statistics," JPL IOM, January 5, 1973 (JPL internal document).
2. Adeyemi, O., *Error Control in the GCF: An Information-Theoretic Model for Error Analysis and Coding*, JPL Technical Memorandum (in preparation).

**Table 1. Maximum buffer usage for 4.8-kbps channel
(measured in 1200-bit blocks)**

Data type	No. of runs	Info. rate	Largest (and second-largest)	
			Trans. Buffer	Rec. Buffer
Real	29	0.9	162 (14)	12 (9)
Adeyemi (parameters from worst run)	62	0.9	20 (19)	11 (10)
Adeyemi (parameters from worst three runs)	62	0.9	17 (16)	9 (8)
Adeyemi (model of worst run)	31	0.95	25 (22)	10 (9)
Adeyemi (model of worst three runs)	31	0.95	19 (16)	9 (8)

**Table 2. Maximum buffer usage for 7.2-kbps channel
(measured in 1200-bit blocks)**

Data type	No. of runs	Info. rate	Largest (and second-largest)	
			Trans. Buffer	Rec. Buffer
Adeyemi (model of worst run)	31	0.9	21 (19)	18 (18)
Adeyemi (model of worst three runs)	31	0.9	23 (22)	17 (13)
Adeyemi (model of worst run)	31	0.95	30 (25)	17 (17)
Adeyemi (model of worst three runs)	31	0.95	25 (24)	17 (13)

GCF Wideband Switch Subassembly— Application Techniques

E. F. Bird

DSN Data Systems Development Section

Application techniques used in the development of the wideband switch subassembly (WBSS) are discussed. The WBSS is a part of the Ground Communication Facility's (GCF's) wideband subsystem located in the Central Communications Terminal at JPL. It is used to support the Mariner Venus/Mercury 1973 and Viking operations. The WBSS is a complex switching unit that provides for simple control by the operator for effecting the many interconnect configurations of various data sets, coded multiplexers/demultiplexers, and JPL computer systems.

I. Introduction

In FY 1972 the Deep Space Network established functional operations requirements for providing wideband data support to the Mariner Venus/Mercury 1973 and Viking flight projects. The requirements specified complete versatility in providing interchange configurations for wideband data. To meet these requirements the Ground Communications Facility had to devise unique application techniques.

This article discusses the concepts utilized in providing a reliable and easily operated interchanger of wideband data for the Central Communications Terminal (CCT) at JPL. The wideband switch subassembly (WBSS) has been "on-line" since July 1973, and has proven its reliability and ease of operation in service to the Mission

Control and Computing Center, Deep Space Stations, and project locations.

II. Requisite Review

The operational requirements presented in the referenced article describe the complexity of this switching unit. Specifically, it has the capability of arranging 626 interconnecting configurations of data sets (DSs), coded multiplexers (CMDs), and local computer systems, herein referred to as on-site computers (OSCs). The number of signal lines involved per switched interconnection varies from 3 to 6.

The ease with which an operator can program a configuration or interpret those configurations in effect is of

great importance. Factors that could confuse an operator during a critical or busy period must be eliminated.

III. Operator Controls and Indicators

Much attention was given to panel-layout details in order to provide the operator with a positive and readily-recognizable control and display presentation. Since the WBSS is basically a switching matrix, the format of controls and indicators is presented in matrix form to the operator for an associative effect. The control and indicator format is shown in Fig. 1. Briefly, the following are the functions provided. The operator may address any one of the DSs, CMDs, or OSCs by depressing push-buttons ① and ②. The operator may then "enter" or "release" an interconnection (③ and ④, respectively) or "erase" ⑤ an erroneous address selection. This momentary illumination of a light-emitting diode (LED) verifies completion of these three operations (SEQUENCE COMPLETE, ⑥).

Interpretation of the effected interconnections is accomplished by observing the relative positions of illuminated LEDs ⑦ in the display matrices. Pushbuttons 8 and ⑨ aid in the identification of a crosspoint indication by illuminating an entire horizontal row or vertical column of LEDs, respectively.

Data are switch-routed on the basis of the direction they flow with respect to the OSCs, either "inbound" or

"outbound." They are further routed on the basis of the data stream format (e.g., multiplexed, nonmultiplexed, demultiplexed, or regenerated).

IV. Programming Circuits

Behind each of the two control and display panels is a wireplane housing integrated circuits (ICs) that accept the operator's pushbutton inputs and convert these to an ordered sequence of logic commands that control the crossbar switches. See Fig. 2.

These ICs also continuously interrogate the crossbar matrices for contact closures and present the closed-path configuration information via the LED matrices. This monitoring function requires only one level of the crossbar matrix (i.e., a single contact closure is all that is required for active crosspoint identification).

The crossbar switches are mounted on two fully-extending vertical slides located in a separate equipment bay. See Fig. 3.

V. Summary

The objectives of this project have been achieved. The WBSS is reliable, straightforward in its operation, and easy to maintain. The design techniques used in its planning and the construction techniques used in its fabrication have provided these qualities.

References

1. Bird, E. F., "GCF Wideband Switch Subassembly—Requirements and Design Concept," in *The Deep Space Network Progress Report for September and October 1973*, Technical Report 32-1526, Vol. XVIII, pp. 117-119. Jet Propulsion Laboratory, Pasadena, Calif., December 15, 1973.
2. *Wideband Switch Subassembly*, Technical Manual TM 509286. Jet Propulsion Laboratory, Pasadena, Calif., May 30, 1974.

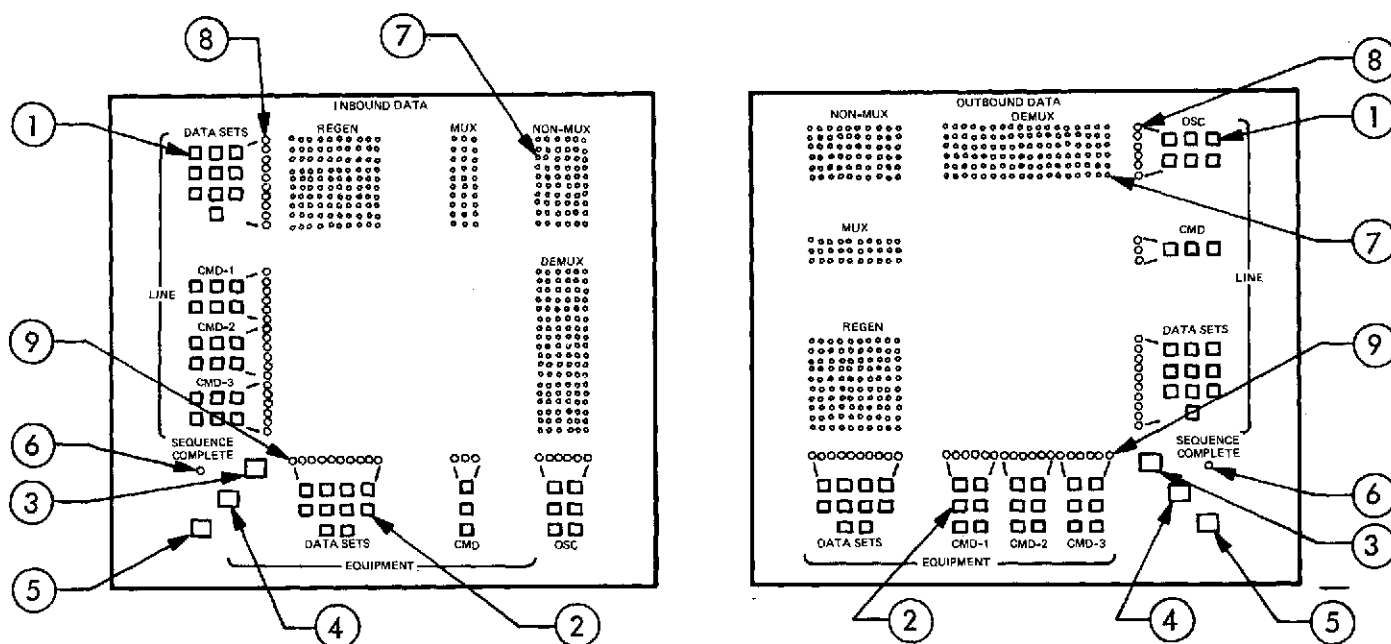


Fig. 1. Control and display units—controls and indicators

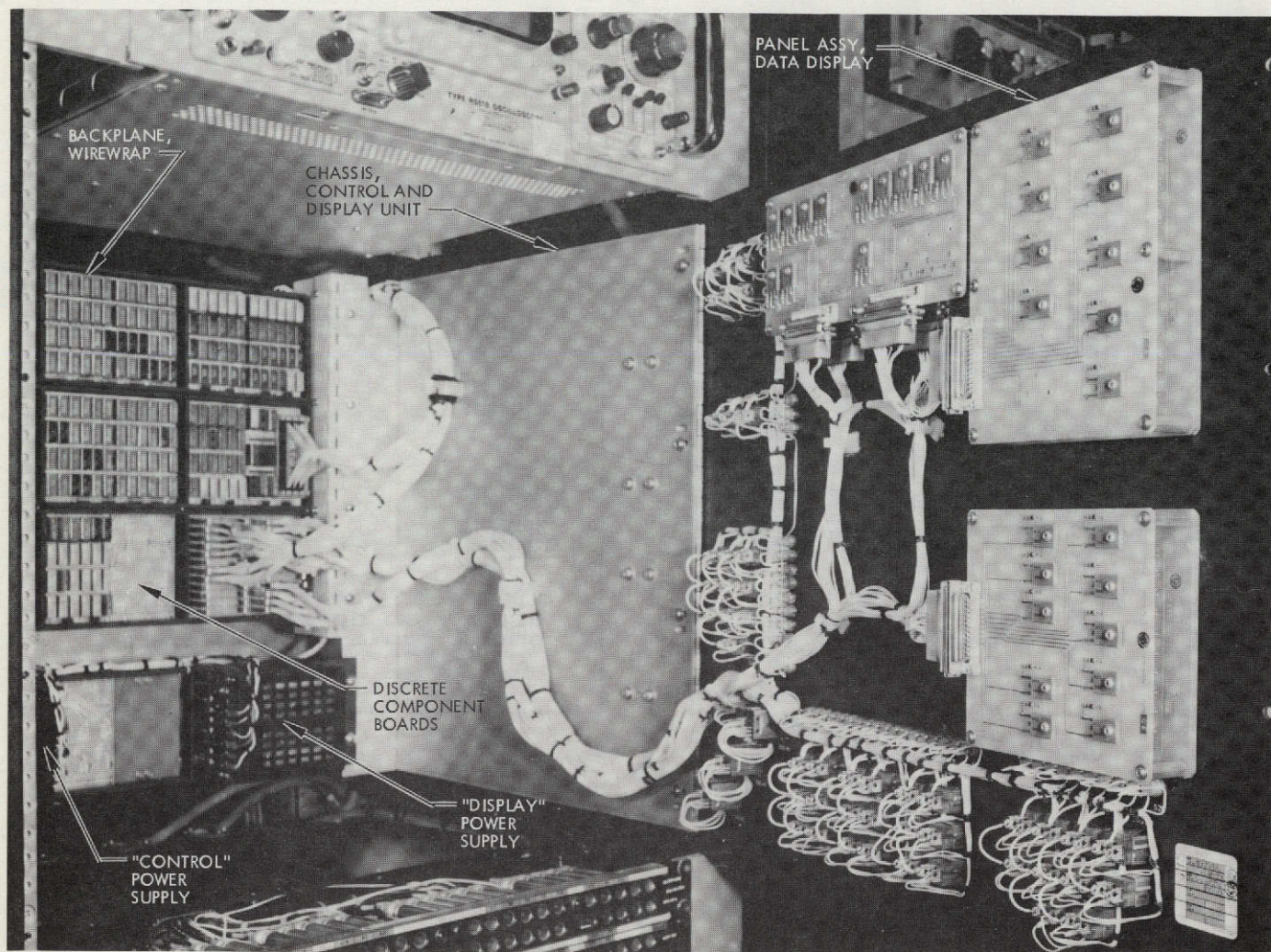


Fig. 2. Outbound control and display unit—parts location

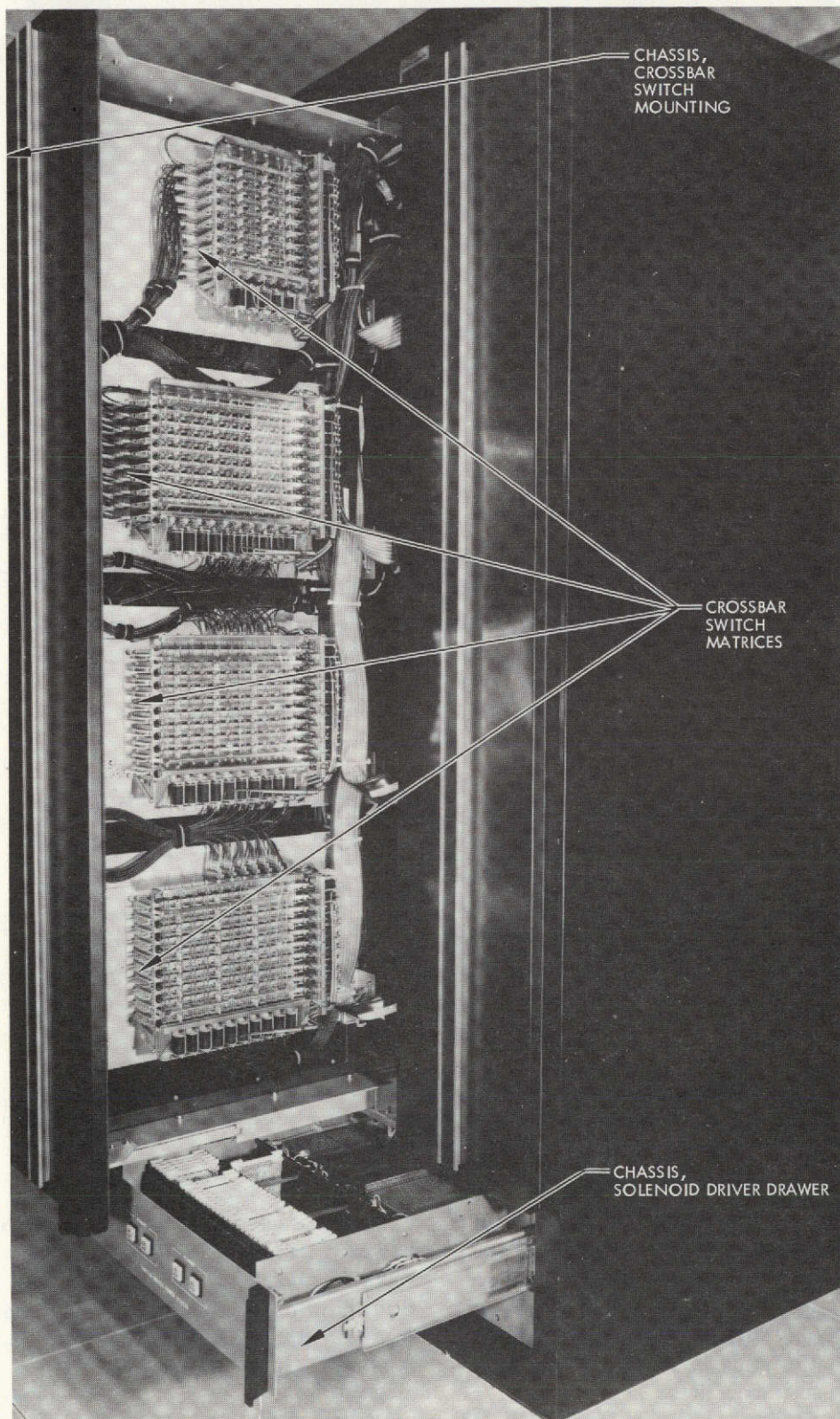


Fig. 3. Crossbar switch cabinet

Control-Restrictive Instructions for Structured Programming (CRISP)

R. C. Tausworthe
DSN Data Systems Development Section

This paper presents a discipline and a set of control-logic statements to extend structured programming to arbitrary existing languages. These statements preempt and replace all control statements in a language, so that all programs written in Control-Restrictive Instructions for Structural Programming (CRISP) are automatically structured. Structures are provided for real-time, as well as nonreal-time programming. The principles set forth do not attempt to specify a standard programming language, but instead, a programming language standard—that is, a way of programming that contributes to stability, maintainability, readability (self-documentation), and understandability of the final product.

I. Introduction

The purpose of a higher-level programming language has historically been to simplify the expression of algorithms or subprogram functions created by an important class of problems. The flexibility and productivity of such languages are gauged by the ease with which, and the degree to which programmers may vary the composition and execution of programs (Ref. 1). The widely diverse classes of problems that exist have, over the years, led to the development of an exceedingly large number of languages, both wide-application (general-purpose) and restricted-application (special-purpose). There is no doubt that standardization is needed, but defining a “standard

language” is probably only feasible within a distinct problem class.

The characteristics sought in a standard language, however, are noble: the language should be capable of solving problems over a wide range of applicability, and contribute to the solution of those problems large measures of stability, maintainability, readability (or self-documentation), understandability, and machine (or installation) independence. Furthermore, it should lend itself as much as possible to program production tools, automatic design methods, easy assessment of correctness, easy or automated verification and testing, and easy or

automated quality assurance measures. To be acceptable, as a *minimum* requirement, a standard computer language must not hinder the programming process. On the contrary, the purpose of a standard is to help.

The principles set forth in this work do not attempt to specify a standard programming language, but instead, do provide a *programming language standard*—that is, a disciplined way of programming to achieve the goals of the preceding paragraph.

Restricted control-logic structures, as proposed by Böhm and Jacopini (Ref. 2) and others (Refs. 3 and 4), and extended by the author (Ref. 5) form the basis of an attractive software design and production methodology known as “structured programming.” Programs written using these restricted control-logic structures, tend to be compatible with and enhance other widely useful techniques, such as top-down methods (Ref. 6), modular programming, and hierarchic design (Ref. 7). Such programs are found to be easier to organize, understand, modify, and manage.

In block-structured programming languages, such as ALGOL and PL/I, structured programs are GOTO-free. Structured programming, however, can be extended to almost any language, and should not be characterized simply by the absence of GOTO's, but rather by the presence of an organized control-logic discipline.

II. The CRISP Concept

Program control-logic is specified in what follows here by way of a set of Control-Restrictive Instructions for Structured Programming, called CRISP, augmenting an arbitrary target language. Programmers construct code using statements from the arbitrary target language, such as FORTRAN, BASIC, or assembly language, except for statements governing the program control-logic (branching, looping, etc.): such control is accomplished by using a CRISP statement instead.

The source-program statements thus consist of a mixture of CRISP and target-language code, which can then be processed into executable instructions for a given computer system. The processor may take the form of a compiler, by which the source statements are translated directly into executable form; but rewriting or modifying an existing compiler to accommodate CRISP can be averted by implementing the translation via a CRISP preprocessor. Neither exists at this writing.

Such a CRISP preprocessor would access the sequential source records, written in CRISP or target-language syntax and replace the control-logic statements by target-language statements that perform the equivalent action.

The CRISP control structures are precisely those needed to write structured programs—even nonreal-time structured programs (Ref. 8). The CRISP concept thus extends the advantages of structured programming to those languages that most fit a particular problem.

CRISP preempts all control statements from the target language and substitutes a set of statements that force programs to be structured; that is, any program written in CRISP is automatically structured without the need for GOTOs. “GOTO-less” structured programming is currently available in some other languages now coming into being, such as BLISS (Ref. 9), IFTRAN (Ref. 10), and SIMPL-X (Ref. 11); a special limited preprocessor for FORTRAN, called SFTRAN (Ref. 12) is also now available.

The strength of CRISP, as opposed to these other structured programming languages lies in the fact that *only* the control statements are preempted. Given an operating CRISP preprocessor for the target language most suitable for the problem at hand, the user may proceed to solve the problem in the language he wants, and is already familiar with. If he is called upon to solve another problem in another familiar language, then he again finds the same set of control-logic statements by which to organize that problem in the other language.

III. Elements of CRISP Statements

A CRISP statement begins with a reserved word identifying the type of structure, or the module within a structure, or the end of a structure. Additionally, CRISP statements may contain strings that belong to the target language, or other CRISP statements. For example, in the CRISP structure of Fig. 1, the substring denoted by *c* is a condition that will be substituted directly into a conditional statement in the target language so as to produce the structure shown in Fig. 1. The strings *s_i* in Fig. 1 are either target statements or other nested CRISP constructions.

The complete superset of CRISP constructions is given in the Appendix, along with flowchart equivalents. (Not all of these will apply to a given target language.) Each program structure will be here referred to as a *CRISP-block* (not to be confused with the definition of a block in

block-structured languages such as ALGOL and PL/I); subdivisions of blocks into constituent parts will be referred to as *modules*. Blocks and modules will be typed by their initiating key-words, as for example, an UNLESS-block, or a THEN-module; in some cases, block names may need further description, such as may be desirable to contrast an IF-THEN-ELSE block from an IF-THEN block, or a FOR-UNTIL block from a FOR-WHILE block.

The CRISP structures can conceptually be iterated and nested to any level desired to produce the intended program. Indentations and annotations for readability (which I shall discuss later), however, will tend to limit the amount of nesting within blocks, because the listing tends to crowd toward the right-hand edge. Rather than contend with this continued crowding, the user naturally finds himself inventing procedures to be linked or called (and programmed later). As a result, CRISP programs, subprograms, and subroutines generally fit on one page each (but link to procedures on other pages).

As Mills (Ref. 4) points out, segmentation of program listings to a predescribed size, such that each segment enters only at the top and exits (normally) at the bottom, is a major asset in coping with program complexity.

CRISP makes allowance for up to three distinct types of procedure calls within a program. The first is of the form

DO *f*

which links to the procedure named *f* in a

PROCEDURE: *f*

```

.
.
.
END

```

block. In some CRISP processors, it is conceivable that the entire procedure *f* could be substituted for the DO *f* statement in the object code. Arguments may sometimes be passed in the calling string *f*.

The second procedure call is

CALL *f*

which creates a subroutine linkage to a named procedure declared in a

SUBROUTINE: *f*

```

.
.
.
RETURN

```

block. Subroutine arguments may be passed in the normal way between CALL and the SUBROUTINE: definition.

The third procedure call is

GOSUB *l*

where *l* is a subroutine label; arguments are not generally passed, except in the form of common variables, tables, and so forth. The labeled subroutine is defined in a block of the form

SUBROUTINE LABEL: *l*

```

.
.
.
RETURN

```

The two different types of subroutine calls are necessary in target languages (Ref. 13) that are capable of calling subroutines both by name and by label. One or the other may be absent in other languages, however.

Functions, when permitted in the target language, are identified by block declarations of the form

FUNCTION:

```

.
.
.
RETURN answer

```

The *answer* string is an optional device that may be required in some target languages to return the function value. Functions are invoked in the usual target-language mode.

The main program is identified as the block

PROGRAM: *name*

```

.
.
.
SYSTEM (or STOP)

```

The directive SYSTEM releases the control of execution to the system; STOP, to the operator. Again, both of

these options may not be available in an arbitrary target language.

IV. A CRISP Preprocessor

Because the CRISP statements are keyword-actuated, it is necessary that target-language noncontrol statements not begin with these keywords. Otherwise, alternate CRISP keywords must be chosen. More detailed restrictions will appear later in this article. The processor functions will only be outlined here.

The CRISP preprocessor functions in a number of modes, and I will describe aspects of each in turn. The main mode is the *translation* mode, which outputs target-code statements. The second and third modes are edit modes: *update* and *annotation*. The update mode is a text-editor that permits insertions, deletions, and alterations of CRISP programs; the annotation mode indents CRISP blocks and supplies them with flowlines and Dewey-decimal reference and cross-reference numbers.

The processor allows comments to appear anywhere in a program, within target-language statements, as well as within CRISP control statements, and are indicated¹ by surrounding the comment string by "<*" and "*>", as, for example, by <* comment *>. The *comment* may then contain any string of characters except "*>". CRISP comments continue automatically on the next line if they are incomplete on the current line.

The strings "<*" and "*>" naturally, must not be permitted constructs in target language statements. If either is, an alternate comment delimiter may be substituted as a convention for implementing CRISP in that target language.

CRISP statements may be continued on several lines by terminating each unfinished line with "&"; target-language statements (also continued using a final "&") are continued only if permitted within the target language syntax.

V. Compile-Time Features of the CRISP Processor

The CRISP processor has a minimal, but useful, compile-time text-macro capability. Target languages having better macro handlers may, therefore, choose not

¹The use of <* . . . *> to enclose comments is apt to be implementation-dependent; similar constructs, such as (* . . . *), or [* . . . *], or /* . . . */ may be advisable in some cases.

to have this particular feature implemented. There are two directives; the first is the *macro definition*,

%template MEANS target string%END

which declares that occurrences of the type *%source string* that match *%template* are to be replaced, both in CRISP control statements, as well as in target statements, by *target string*. An instance of the type *%source string* is an instance of a *macro call*. The *target string* may extend over many lines, defining a procedure and forming a block of text to be transferred; in such cases, each additional line is prefixed by %. The end of a defining macro is signalled by %END.

The macro template may contain formal parameters to be transmitted into the target string; these are signalled by the occurrence of the parameter marker in the template. Whenever a % occurs in an input source line, a scan of the remainder of the line initiates, much the same as in the STAGE2 macro processor (Ref. 14). When a match occurs between the input string calling macro and a macro template, the *target string* corresponding to that template is evaluated with the actual parameters resulting from the template match. The result of this evaluation replaces the matched source string in the output.

Correspondences between actual and formal parameters are set up during template matching. The template is a sequence of fixed strings separated by parameter markers (%), or "holes". When the matching process is complete, each parameter marker corresponds to some substring of the input line and the fixed strings exactly match the other substrings of the line. The *i*th parameter string gets inserted into the target string wherever occurrences of %*i* appear in *target string*.

Macro definitions and calls may be used anywhere in the CRISP source code; in particular, a call can precede the macro definition. Macro definitions may contain macro calls, but not other macro definitions.

The following CRISP program is an example of the use of the macro capability: Somewhere in the program, there is a definition module,

```
%RANDOM ARRAY MEANS A%END
%FILL %(:%) MEANS
%DIM %1(%2:%3)
%FOR DUM=%2 TO %3
%  %1(DUM)=RANDOM
%  NEXT DUM%END
```

The appearance elsewhere in the program of the call

```
%FILL %RANDOM ARRAY(1:50)
```

produces first the intermediate statements

```
DIM %RANDOM ARRAY(1:50)
FOR DUM=1 TO 50
  %RANDOM ARRAY(DUM)=RANDOM
NEXT DUM
```

which are then rescanned for CRISP control statements and possible further translations. In this particular case, there was further macro action, leading to the final CRISP code:

```
DIM A(1:50)
FOR DUM=1 TO 50
  A(DUM)=RANDOM
NEXT DUM
```

Each module can automatically be given a number by the CRISP processor in its annotation mode, and assigned a special module-entry counter to record the number of times that particular module has been executed when the program runs. The execution count for each module through level n can then be printed upon execution of the CRISP directive

```
DISPLAY THRU LEVEL  $n$ 
```

The value n is the level of hierarchical nesting within the program as determined by the decimal count in the Dewey-decimal module identifier, to be described a little later.

This path-execution-count capability is invaluable in program testing, for one may readily identify which paths have been executed and which have not. Moreover, because of the program structure, it is possible to design and provide input data to exercise these paths.

For fully verified programs, the overhead setting up and incrementing of these counters can be removed by prefixing the source program by the CRISP directive

```
CANCEL MODULE COUNT
```

Selected portions of a program may have their module counters enabled and disabled by using the directive

```
ENABLE MODULE COUNT
```

with the CANCEL directive above.

Perhaps the most unique of the compile-time features is what may be termed a "compile-time" edit statement:

```
REQUIRE AT  $m:s$ 
```

This statement causes the statement s to be inserted in the object code immediately before the code for module m , numbered as in the next section. Its purpose is to permit truly top-down development and readability of programs. For example, suppose a DO f appears inside a loop. At the time the DO f statement was written, the programmer envisioned that a certain *definite function* would be performed by an as-yet *undefined algorithm*. However, in programming the PROCEDURE: f at the next level, he may discover that, to program the intended function, an unforeseen variable needs to be declared and given an initial value back at an earlier program level, outside the loop.

But the program development up to this point was not concerned with this value. It has only just become important. Furthermore, the declaration and initialization of a *new* variable does not in any way alter the correctness assessment of the program up to that point (except perhaps in timing, if critical). Hence, it makes sense to associate the statement that initializes a procedure *with* that procedure, rather than back at the previous level. Otherwise, it threatens readability and understanding, both of the previous module ("what is *this* doing here?") as well as that needing it ("where on Earth did I initialize that variable, and what to?")

Every data structure need not be declared using a REQUIRE statement, some are naturally passed on to procedures as data on which they are to operate. Use of the REQUIRE, however, can enhance readability when internal structures need external initializations.

VI. Module Terminations

As I have discussed in another article (Ref. 5), there are times when module exits other than the normal structured exit are needed for program efficiency and clarity. These may take the form of responses to pathological or abnormal events, in which case, they are *abnormal terminations*. Sometimes, however, the event leading to a desired immediate nonnormal (nonstructured) exit is one that is expected. For example, it is a typical practice to

input data until an end-of-file indication signals the program to begin processing in a new mode. I call these non-structured exits from a module *paranormal* terminations (*para* from Greek meaning "beside").

```

IF NO  $t$  DURING  $s$ 
: -> THEN  $s_1$ 
:      :
:       $s_n$ 
:      END
: -> ELSE  $s_m$ 
:      :
:       $s_p$ 
:      ENDBLOCK

```

Here, s refers to a single statement, such as an input statement with t an end-of-file trap, or s may be a CRISP procedure call in which the traps, or t_1, \dots, t_k appear. The t 's can conceivably also refer to logical conditions tested during s . The vertical line of colons and ":->" represent flowlines, supplied by the CRISP processor in its annotation mode.

The CRISP directives that effect extra-normal exits from CRISP procedures are

EXIT t (or EXIT t TO m)

and

ABORT (or ABORT TO m , or ABORT l TO m)

in which t identifies the CASE-label (t may be null for exit to an ELSE-module) and m identifies the CASE- or ELSE- module number. "TO m " is optional on EXIT statements, and also on ABORT if the entire program has only one abnormal-termination procedure.

The CRISP processor restricts a module to having only one normal (structured) exit statement per module. How-

ever, there must have been a CASE- or ELSE-module identified at a previous level of the program to which such transfers are to occur. Two illustrative cases are

```

IF NO  $t_1, \dots, t_k$  DURING  $s$ 
: -> THEN  $s_1$ 
:      :
:       $s_n$ 
:      END
: -> CASE  $t_1:s_m$ 
:      :
:       $s_{m+1}$ 
:      :
:       $s_p$ 
:      END
: -> CASE  $t_k:s_r$ 
:      :
:       $s_r$ 
:      ENDBLOCK

```

ever, the top-down development of program modules having multiple exits may necessitate inserting several nonstructured exit statements into the module, and CRISP, therefore, allows them. However, these can sometimes create difficulty in isolating errors, because the program generally has no convenient way of telling *which* exit of the multiplicity was actuated.

The CRISP programmer should thus take care to use multiple extra-normal exits only whenever the point within the module returned to is insensitive to whichever of the multiple exits to that return point is taken.

VII. CRISP Module Numbering Method

Each CRISP block corresponds to a flowchart structure containing nodes and flowlines, and each CRISP statement either corresponds to a node or a flowline. One natural way of numbering graph nodes is the so called *pre-order traverse* method. A pre-order traverse of the chart enumerates the boxes on the flowchart as follows: starting at the top of a structured flowchart, label boxes and loop-collecting nodes sequentially in order down the chart until a branching node is sensed. Number this node. The general rule to be followed whenever a branching node

is reached is, take the leftmost unnumbered branch. Whenever a decision-collecting node is encountered, return to its corresponding decision node if it has a yet-unnumbered branch, and proceed to number the leftmost unnumbered branch; if all of its decisions have all branches numbered, then continue on.

One way that the hierarchic place a module occupies in a design can be annotated is by a Dewey-decimal cross-reference. For example, suppose that, on a flowchart numbered *m*, a box, numbered *n*, refers to a procedure (not subroutine), to be expanded later in the design process. Then the flowchart for that later expansion could be made Chart No. *m.n*. One reading the flowchart, wishing to trace out *how* the function in box *n* of flowchart *m* is achieved, merely has to locate Chart *m.n* to proceed.

More specifically, suppose a module appears on Chart 1.2.6, and has the number 5. Then one can state that box number 2 on Chart 1 was expanded as Chart 1.2; on that chart, box 6 was expanded as Chart 1.2.6; and module number 5 may appear expanded later as Chart 1.2.6.5.

This process can be altered for subroutines and functions also. The alteration is needed because subroutines, which can be called from many places, would not possess a unique chart number. Therefore, each subroutine will be assigned to its own unique level-1 chart number. One convenient way of distinguishing procedures from subroutines is by the use of an alphanumeric chart number; for example, S6 refers to Subroutine 6, and T4 to Trap routine 4, etc. The choice of an alphanumeric designator can be used to group subroutines with common properties together in documentation. Expansions within subroutine flowcharts follow the normal numbering, as, for example S6.4.2 refers to the box numbered 2 on Chart S6.4.

Comparing flowcharts and their CRISP code structures (see the Appendix) shows that when IF-THEN-ELSE configurations are drawn with *true* to the left of *false*, and when multiple decision branches always are drawn in case-order left to right, then the *code statements corresponding to numbered flowchart boxes always appear in the program in sequential numeric order from the top-down*.

The CRISP system, in its edit mode, can simulate the preorder traverse of flowchart nodes described above, and annotate certain lines of the code with its appropriate number. The format of this annotation for statements

within a procedures block defined by PROGRAM:, PROCEDURE:, SUBROUTINE:, FUNCTION:, or AT, is

.n statement

The *statement* can either be CRISP or target language code. The *.n*, flush with the left margin for easy identification, is the number assigned by the preorder traverse. Module numbers for PROGRAM:, PROCEDURE:, SUBROUTINE:, FUNCTION:, and AT statements are the Dewey-decimal reference numbers assigned earlier in the program; they appear flush at the right-hand margin, as

PROCEDURE: *name* MOD# *d*

Thus a statement *.n* within a procedure with Dewey-decimal number *d* is uniquely identified as the Dewey-decimal *d.n*.

Statements that invoke subroutines (GOSUB, CALL, and AT...) have module numbers of the form *.n/Ai*, which signals that module *n* of the current procedure calls the *i*th subroutine of a class with alphanumeric designation A.

VIII. Indentation and Annotation

Although the syntax does not require it, the program structured hierarchy should be displayed by indenting the lines of code, such as shown in the syntax table in the Appendix. Examples in this article are indented according to the following rule:

If a block contains only one module (such as a FOR-block), then indent statements comprising that module by a prespecified number of spaces (here, two) beyond the block header (the FOR). If a block contains more than one module (such as an IF-THEN-ELSE-block), then indent three spaces past the block header (IF) to the module header (THEN or ELSE), and each line of the module another five spaces beyond the module header. Certain one-module blocks also have a module header within the block, such as the IF-THEN block. These are indented as if they were multiple-module blocks for consistency. The particular numbers of spaces recommended above for indenting were chosen to aid the flowline annotation mode.

Programs indented this way are almost as easy to read as flowcharts, because the block type is identifiable by its

header, which protrudes from the body of the block, and the beginning of each module within the block stands out in the same way. Successive indentations occur for block structures within modules.

The CRISP processor, in its edit mode, supplies the necessary indentation and, in addition, annotates the code with flowlines and module numbers as shown in the following example:

```

PROGRAM: BUBBLE-SORT
:      <* SORT IN-PLACE AND PRINT A SET OF NUMBERS
:      <* INPUT FROM A TERMINAL*>
:
.1  INPUT USING %PROMPTING MESSAGE AND FREE-FORM INPUT: N
:      DIM %ARRAY TO HOLD NUMBERS
:      PRINT 'ENTER NUMBERS TO BE SORTED:'
:      INPUT USING %FREE FORM: %ENTIRE ARRAY
:
.2  FOR N=N BY -1 TO 2 <*DROP OFF TOP ELEMENT EACH CYCLE*>
.3  ↑ FOR I=1 TO N-1 <*BUBBLE LARGEST ELEMENT TO ELEMENT N*>
.4  ↑ ↑ IF %ELEMENTS I AND I+1 OUT OF ORDER
.5  ↑ ↑ :->THEN %EXCHANGE VALUES
:      ↑ ↑ :----->ENDBLOCK
:      ↑ ←←NEXT I
:      ←←NEXT N
.6  PRINT \'SORTED VALUES:\'%ENTIRE ARRAY; <*BACKSLASH GIVES
:      <*CARRIAGE RETURN AND SEMICOLON CONTROLS SPACING WHILE
:      <*ARRAY IS BEING PRINTED*>
:--STOP

```

MOD# 1.

```

<*MACRO DEFINITIONS:*>
%PROMPTING MESSAGE AND FREE-FORM INPUT MEANS
  %'HOW MANY NUMBERS TO BE SORTED? #'%END
%ARRAY TO HOLD NUMBERS MEANS A(N)%END
%FREE FORM MEANS '(#)%END
%ENTIRE ARRAY MEANS A%END
%ELEMENTS I AND I+1 OUT OF ORDER MEANS A(I)>A(I+1)%END
%EXCHANGE VALUES MEANS A(I) == A(I+1)%END

```

The target language in the above example is MBASIC (Ref. 13), which performs exchanges via the operator ==.

It is certainly no more difficult to write structured-program code than it is to draw a flowchart, and both contain approximately the same level of detail. Some may argue, since the code listings have to be produced anyway, that supplying further documentation in the form of flowcharts is a duplication of effort. Moreover, maintaining consistency between human-drafted flowcharts and code listings during an iterative development cycle can be a very time-consuming task.

Furthermore, it can be argued that structured code is more rigorous than a flowchart. For one thing, it is written in a programming language whose syntax and semantics are well defined. For another, the structured code is part of the operating program, no translation being necessary (with its attendant possibility of introducing error).

Nevertheless, structured code, even with annotated flowlines (as in the CRISP example above), tends to be somewhat less graphic than a flowchart, and the rationale and functional specification of subprogram submodules

tends to be a little less understandable in code annotations than it is in the narrative which properly accompanies a flowchart.

Thus, while CRISP goes a long way toward illustrating *what* a program does very graphically as a self-documented product, it may not go quite far enough in communicating all the *whys* necessary for a reader to review and understand the program. I plan to show, in a later article, how

'ABORT'	'ENABLE '
'AT '	'END'
'CALL '	'ENDBLOCK'
'CANCEL '	'EXIT'
'CASE '	'FOR '
'DISPLAY '	'FORK'
'DO '	'FUNCTION:'
'ELSE'	'GOSUB '

As further restrictions, labels and subroutine names may not contain commas or colons, nor may the condition *c* of an IF, WHILE or UNTIL statement begin with the substring 'NO '. Further, the index *i* or value *v* for DO CASE may not contain ' OF '. When the OF form appears, the index *j* may not contain ' THRU '. The index *i* for ON may not contain ' DO ', ' GOSUB ', or ' CALL '.

In FOR-statements, the index *i* may not contain '='; n_1 may not contain ' BY '; and n_2 may not contain ' TO ', ' UNTIL ', or ' WHILE '.

The CRISP processor also requires that all values and labels in ON *i* and DO CASE statements must be defined as CASE labels within the ON *i* or DO CASE block. The ON *i* CALL (or GOSUB) statement (or both) may be absent if the target language does not allow calls by name or calls by label. Similarly, some of the other construc-

CRISP source programs can contribute to automatic flowcharting and automatic narrative documentation.

IX. Other Restrictions

CRISP must limit the use of some of its primitives within the syntax of the target language so that proper statement recognition is possible. The restrictions are as follows: target-language statements may not begin with the strings

'IF '	'REQUIRE '
'JOIN'	'RETURN'
'LOOP:'	'STOP'
'NEXT '	'SUBROUTINE '
'ON '	'SYSTEM'
'PROGRAM:'	'THEN'
'PROCEDURE:'	'UNLESS '
'REPEAT'	'UNTIL '
	'WHILE '

tions may not be implementable (in a useful form) for a particular target language.

If *t* is a trap list in an IF NO *t* DURING *s* statement, the ELSE module must be replaced by CASE modules corresponding to the trap identifiers.

X. Conclusion

This article has described a method and processor that extends the advantages of structured programming to arbitrary target languages. The use of CRISP facilitates and encourages top-down, hierarchical, modular development of structured programs, and contributes a large measure of self-documentation capability within the language constructs, annotations, and macro-expansion features.

References

1. Perlis, Alan J., "The Synthesis of Algorithmic Systems," *JACM*, Vol. 14, No. 1, pp. 1-9, Jan. 1967.
2. Böhm, C., and Jacopini, G., "Flow Diagrams, Turing Machines and Languages With Only Two Formation Rules," *Communications of ACM*, Vol. 9, pp. 366-371, 1966.
3. Dijkstra, E. W., "Structured Programming," *Software Engineering Techniques*, pp. 83-93. Edited by J. N. Burton and B. Randall. NATO Science Committee, 1969.
4. Mills, H. D., *Mathematical Foundations for Structured Programming*, IBM Document FSC72-6012. Federal Systems Division, IBM, Gaithersburg, Md., Feb. 1972.
5. Tausworthe, R. C., "Program Structures for Non-Proper Programs," in *The Deep Space Network Progress Report 42-21, March and April 1974*, pp. 69-81. Jet Propulsion Laboratory, Pasadena, Calif., June 15, 1974.
6. Hamilton, M., Zeldin, S., *Top-Down, Bottom-Up Structured Programming and Program Structuring*, Report E-2728. Charles Stark Draper Laboratory, MIT, Dec. 1972.
7. Dahl, O. J., and Hoare, C. A. R., "Hierarchical Program Structures," in *Structured Programming*. Academic Press, New York, 1972.
8. Brinch Hansen, P., *Operating System Principles*. Prentiss-Hall, Inc., New York, 1973.
9. Wulf, W. A., et al., *BLISS Reference Manual*, revised Oct. 25, 1971. Dept. of Computer Science, Carnegie-Mellon University, Jan. 15, 1970.
10. Miller, E. F., Jr., *A Compendium of Language Extensions to Support Structured Programming*, Report RN-42. General Research Corp., Santa Barbara, Calif., Jan. 1973.
11. Basili, V. R., *SIMPL-X, A Language for Writing Structured Programs*, National Technical Information Service Report AD755-703. U. S. Dept. of Commerce, Springfield, Virginia, Jan. 1973.
12. Flynn, J., *SFTRAN User's Guide*, Computing Memorandum #914-337. Jet Propulsion Laboratory, Pasadena, Calif., July 1973. (Internal document.)
13. *Fundamentals of MBASIC: Volumes I and II*, Jet Propulsion Laboratory, Pasadena, Calif., March and October 1973. (Internal document.)
14. Waite, W., *Implementing Software for Nonnumeric Applications*, Appendix A. Prentice-Hall, Inc., Englewood Cliffs, N. J., 1973.

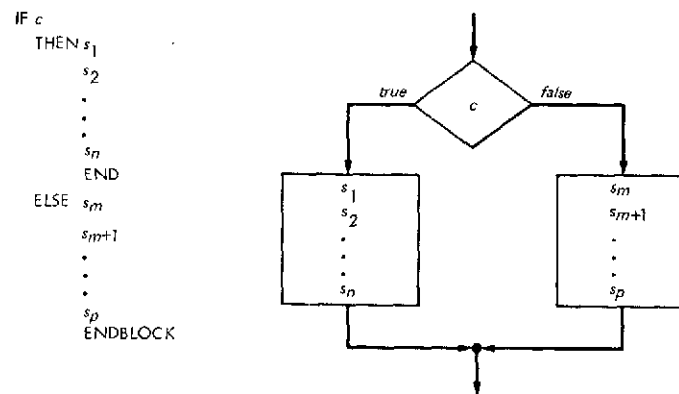


Fig. 1. The CRISP IF-THEN-ELSE structure

Appendix

Formats of CRISP Syntax and Flowchart Structures

This appendix identifies all the CRISP statements and indicates the pertinent context for the blocks and modules within blocks. *Italic elements in the listing below represent strings translated directly into either the target language syntax, or else strings to become CRISP procedure names and the like:*

- c*: condition, value corresponds to TRUE or FALSE convention
- f*: program, procedure, or subroutine name
- i*: index variable names in target language
- j, h, k*: integers

- l*: case or subroutine label
- m*: CRISP module number
- n*: numeric index quantifiers in target language
- s*: statement, either target language or CRISP
- t*: trap, or event quantifier in target language
- v*: variable in target language

The flowchart structures for FOR-NEXT loops are shorthand conventions. The trap-handling conventions in ⑮-⑲ are discussed in Ref. 5. All subscripts in the table below represent integers.

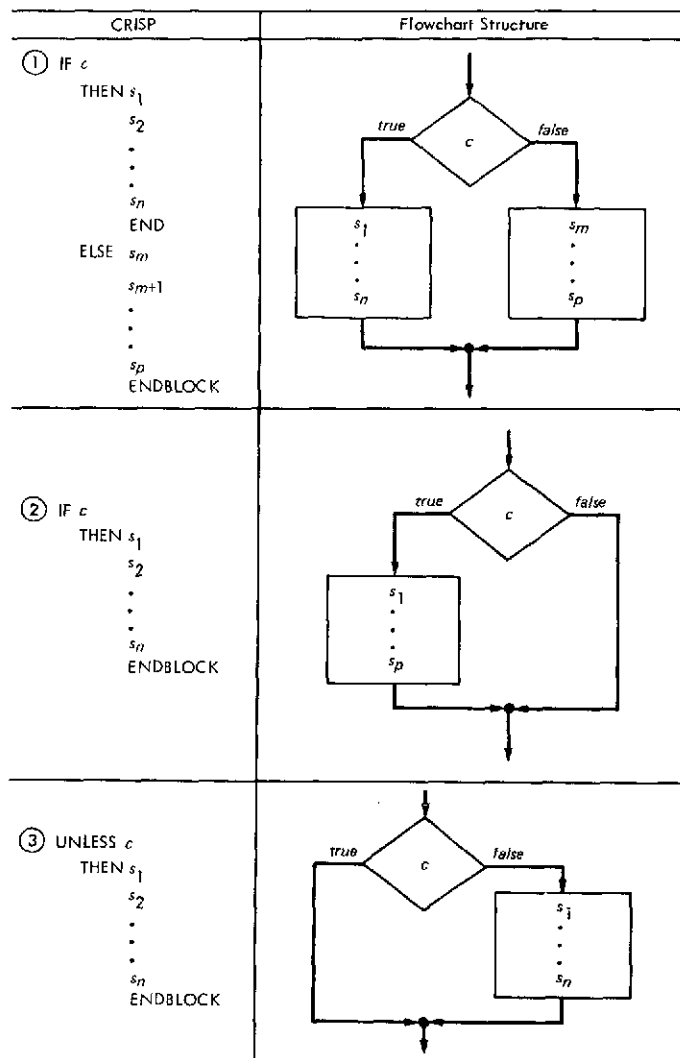


Fig. A-1. CRISP syntax and structure outline

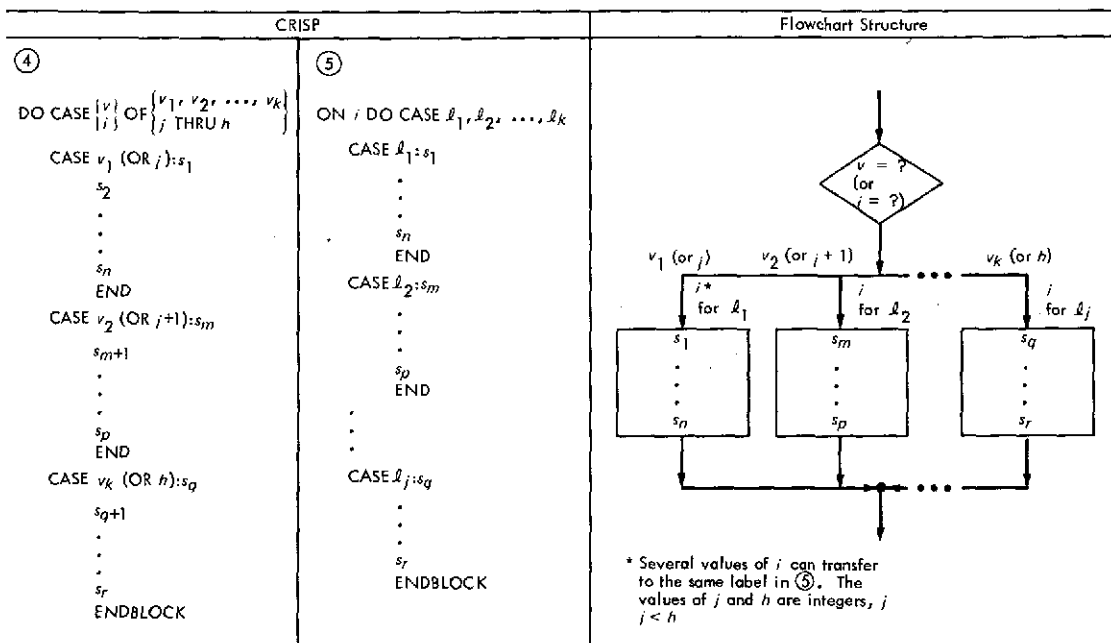


Fig. A-1. (contd)

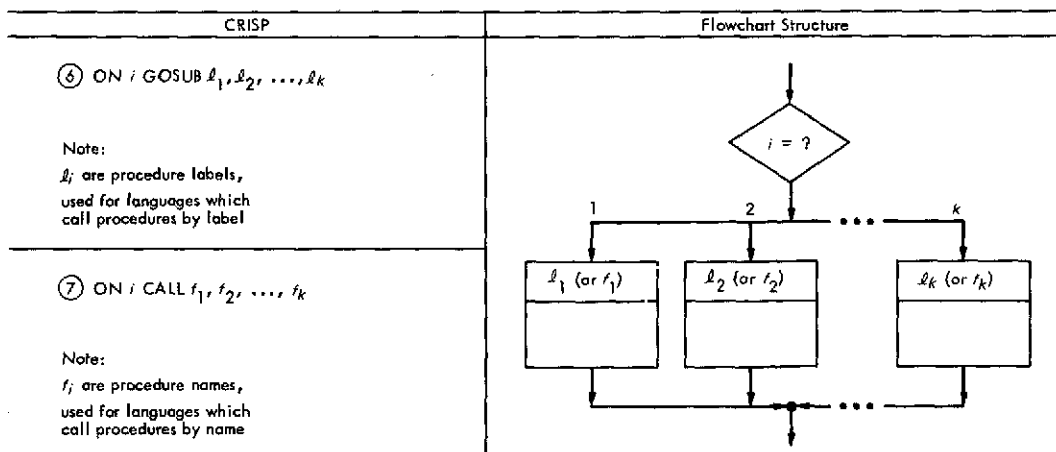
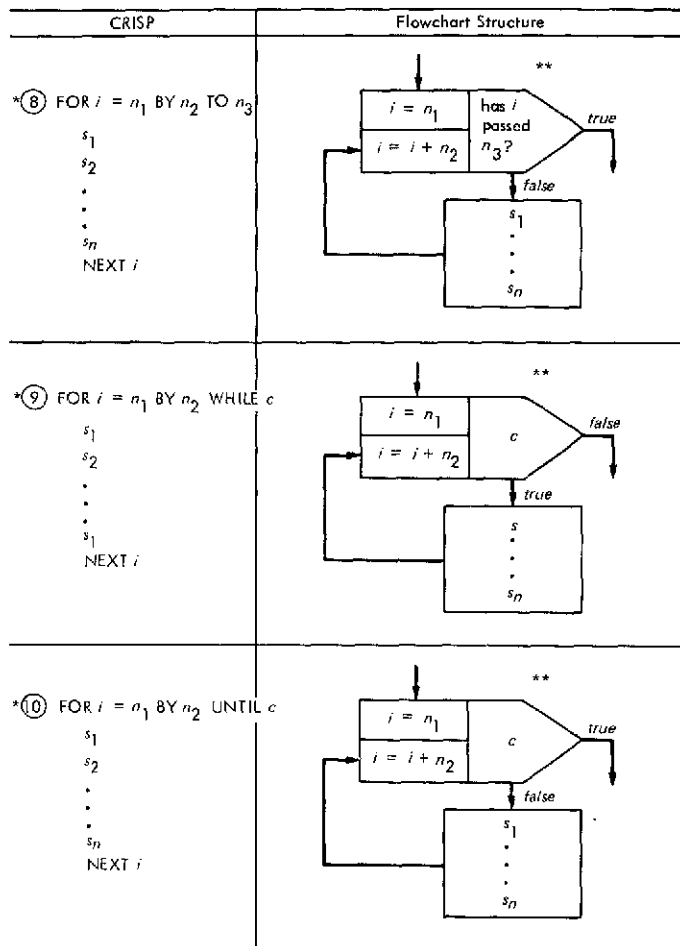


Fig. A-1. (contd)



* BY n_2 is optional on all FOR-blocks; BY 1 is assumed if omitted
 ** This flowchart symbol is a shorthand convention, merging initialization, decision, and update boxes together

Fig. A-1. (contd)

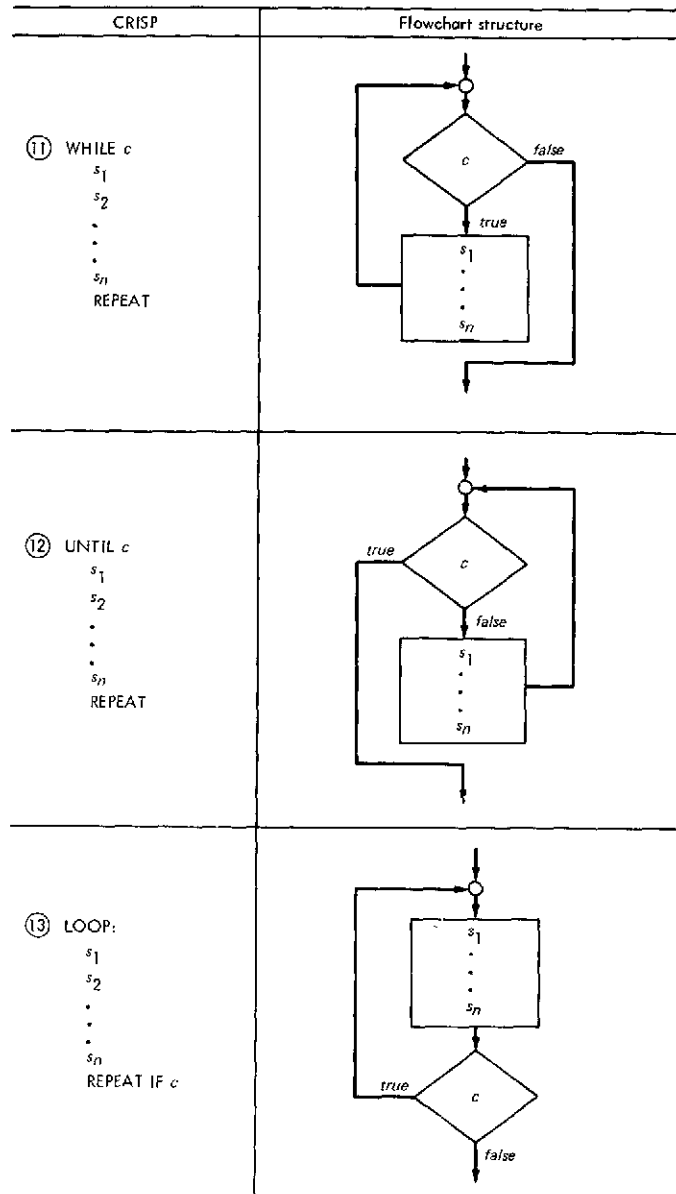
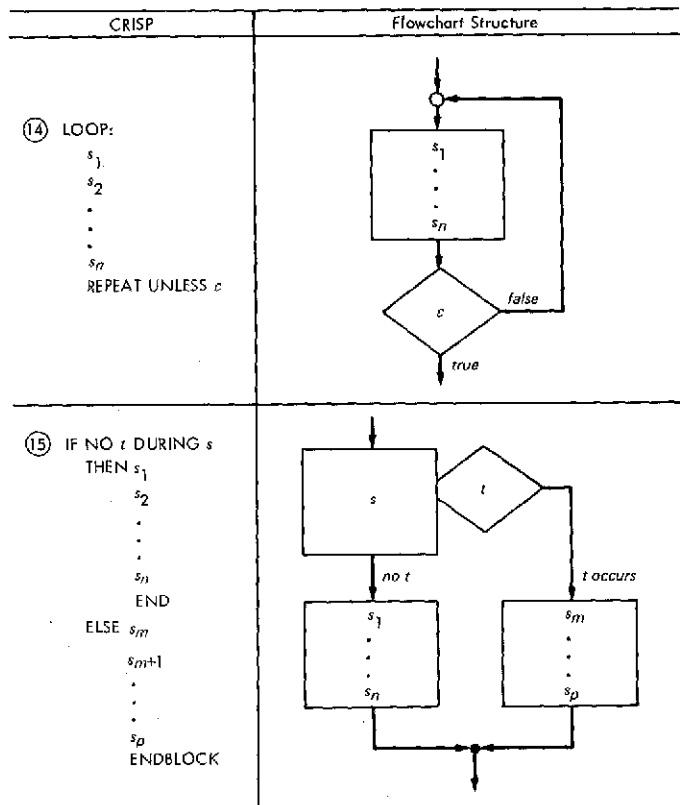


Fig. A-1. (contd)



Note:
Multiple CASEs may replace
ELSE module here if t
during s results in multiple
transfers. (See ⑤)

Fig. A-1. (contd)

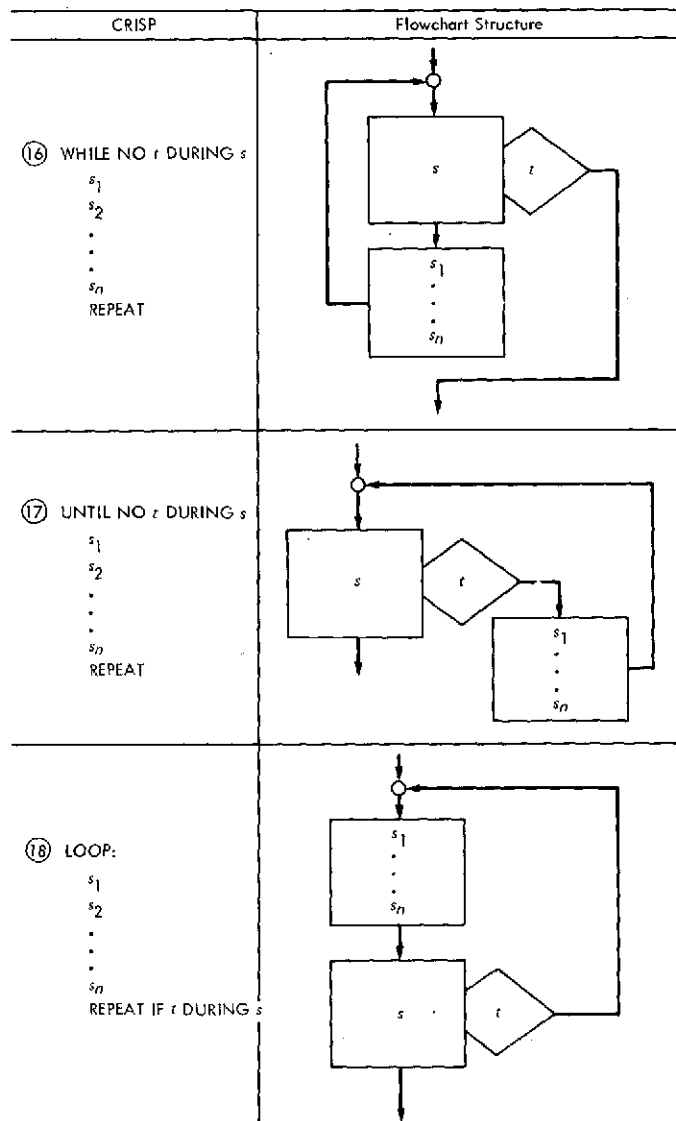


Fig. A-1. (contd)

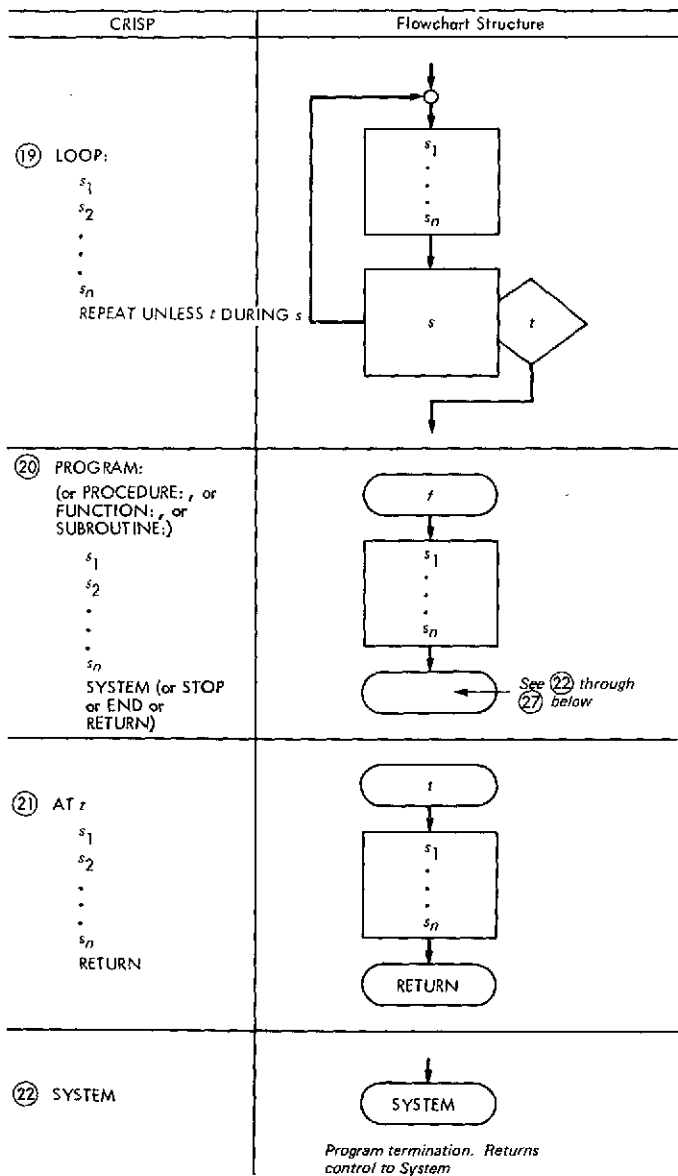


Fig. A-1. (contd)

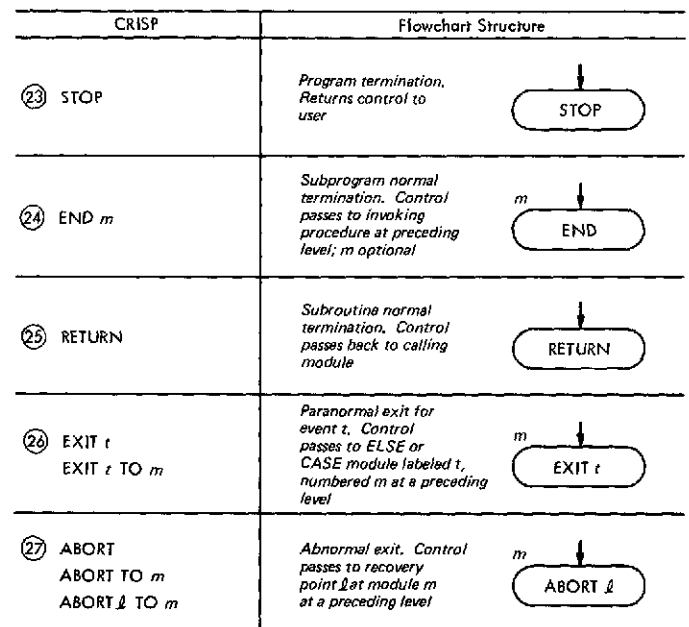


Fig. A-1. (contd)

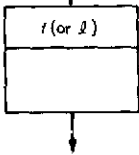
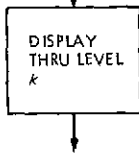
CRISP	Flowchart Structure
②8 DO <i>i</i> ②9 GOSUB <i>l</i> ③0 CALL <i>i</i>	
③1 DISPLAY THRU LEVEL <i>k</i>	
③2 ENABLE MODULE COUNT	CRISP processor directives: enable/disable module-counters
③3 CANCEL MODULE COUNT	
③4 REQUIRE AT <i>m:s</i>	CRISP processor directives: inserts statement <i>s</i> into code at the beginning of module <i>m</i> . Source must be annotated with module numbers
③5 % <i>macro</i>	CRISP processor directive. Creates or invokes a user-defined macro

Fig. A-1. (contd)

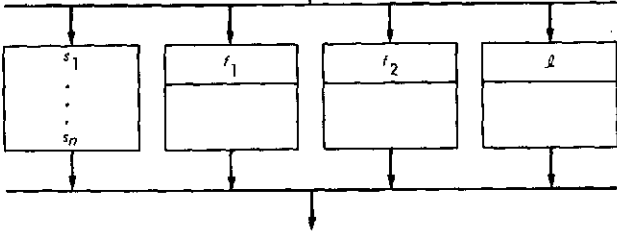
CRISP	Flowchart Structure
③6 FORK PROCEDURE: <i>s</i> ₁ . . . <i>s</i> _{<i>n</i>} END DO <i>i</i> ₁ CALL <i>i</i> ₂ GOSUB <i>i</i> JOIN	

Fig. A-1. (contd)

NCS Minicomputer Systems Status Report

R. G. Petrie

DSN Data Systems Development Section

Implementation of the Network Control System (NCS) requires the use of 17 minicomputer systems. The functional requirements for these systems within the NCS are discussed, and details of the minicomputer block diagrams, mechanical configuration, interface characteristics, and software support are presented.

I. Introduction

Implementation of the Network Control System (NCS) entails the use of 17 minicomputer systems (14 on-line systems and three operational backup systems) to accomplish the necessary processing tasks assigned to the NCS. A competitive procurement was initiated to obtain the required minicomputer systems, and a JPL Source Evaluation Board (SEB) was convened to select the successful proposer. The contractor selected by the SEB is Modular Computer Systems Incorporated (ModComp), Fort Lauderdale, Florida, and on December 21, 1973, JPL Contract No. 953793 was awarded ModComp to provide the required hardware, software, and support services associated with the minicomputer systems. This article presents a synopsis of the equipment and services being supplied by ModComp.

II. Functional Requirements

The NCS implementation requires six unique minicomputer system hardware configurations. Table 1 indicates the NCS subsystem application for each of the six con-

figurations; Table 2 presents a summary of the required interface capacity and certain key characteristics of the Central Processing Unit (CPU) for each of the six minicomputer configurations. Each minicomputer system is a stand-alone, self-contained assembly, in its own equipment cabinets, and does not share electronic assemblies or power supplies with any other minicomputer system.

A. Functional Block Diagrams

Figure 1 is a functional block diagram of the NCS showing the interconnection between the various minicomputer systems and their peripheral equipment and the functional use of all the equipment. Figures 2 and 3 illustrate the detailed block diagrams of the minicomputer systems themselves. Since minicomputer system Configurations 1 through 5 are basically similar, varying only in memory size and number of interfaces, Fig. 2 illustrates a Configuration 3 system as a typical representative of Configurations 1 through 5. The Configuration 6 minicomputer system is sufficiently more complex in its interfaces to warrant the inclusion of the separate block diagram shown in Fig. 3.

B. Mechanical Configuration

The minicomputer systems are housed in standard DSIF equipment cabinets supplied to the vendor by JPL. Figure 4 illustrates a typical physical layout of minicomputer system Configurations 1 through 5. The Configuration 6 minicomputer system (not illustrated) requires three cabinets because of the expanded interface capacity.

Connector panels are installed in the minicomputer system cabinets to provide a common point of interface for all interconnecting cables. The interface connector panel is used for all underfloor cable connections to the minicomputer system. The front connector panel allows easy connection of rollup peripheral devices such as paper tape handling equipment.

C. Interfaces

Standardization of electrical interfaces to the minicomputer systems permits a large degree of freedom in functional assignment of many of the interface ports. The various types of electrical interfaces available are described below:

1. DSN standard interface. Each minicomputer system is equipped with several DSN standard interface ports conforming to the requirements of JPL Specification ES 508534. These ports are used in the NCS to interconnect several minicomputer systems, through the use of the Star Switch Controller, and to connect to magnetic tape units.

2. RS-232 interfaces. Both synchronous and asynchronous serial interfaces conforming to EIA Standard RS-232 are provided for interfacing peripheral equipment such as cathode-ray tube (CRT) terminals, line printers, and card readers. The RS-232 interface type will also accommodate the console I/O device and paper tape reader/punch assemblies.

3. Interrupts. Up to 14 externally generated interrupt signals can be accommodated by the minicomputer systems via 50-ohm coaxial cable connection. Signal levels and timing are such that interrupt signals generated by existing equipment designed to interface to older computers can be handled without modification.

4. Time interface. Provision has been made in the minicomputer systems to input GMT in both binary and

BCD format. Six parallel 16-bit-word digital interfaces are provided for this purpose.

5. Disk interfaces. Since disk drive interfaces are somewhat specialized and contain device-peculiar timing signals, no attempt has been made to standardize them. Therefore, all minicomputer system disk drives are connected through the manufacturer's standard interface.

6. Software. ModComp is providing standard software in both object and source code form for use in the minicomputer systems. The standard software includes:

- (1) Loaders/dumps.
- (2) MAX III operating system.
- (3) MAX II/III support system.
- (4) Diagnostics.
- (5) SAX III.
- (6) MAX II/III extended macro-assembler.
- (7) Extended FORTRAN IV.
- (8) Overlay FORTRAN IV.
- (9) Math library.
- (10) FORTRAN run-time library.
- (11) Process input/output (I/O) and system subroutines.

In addition to the standard software, ModComp is providing special I/O handlers and diagnostic programs to accommodate DSN standard peripheral equipment procured to JPL specification requirements.

III. Installation

As of June 1974, 13 minicomputer systems have been delivered by ModComp. Nine systems are installed in Building 230 for NCS Block II testing and integration; one system is temporarily installed at Foothill-B for use in the ModComp maintenance training courses; one system is temporarily installed in Building 161 for use in NCS software development; and two systems are awaiting installation in the permanent NCS facility in Building 202.

Additional system information and performance history will be provided in future articles.

Table 1. NCS subsystems

Configuration	NCS subsystem title	Quantity required
1	Display (DISP)	2
2	Network Communication Equipment (NCE)	2
3	Test and Training (T&T)	2
4	Command Real-Time Monitor (RTM) (CMD-RTM)	1
4	Monitor RTM (MON-RTM)	2
5	Telemetry RTM (TLM-RTM)	2
5	Tracking RTM (TRK-RTM)	1
6	Central Communications Terminal (CCT)	2
Note: The three spare minicomputer systems are Configuration 3 systems		

Table 2. Minicomputer system configuration summary

Item	Interface	Configuration					
		1	2	3	4	5	6
		Configuration quantities required					
		2	2	2	3	3	2
		NCS application					
		DISP	NCE	T&T	CMD-RTM MON-RTM	TLM-RTM TRK-RTM	CCT
Quantities per configuration							
MOD II/25 CPU		1	1	1	1	1	1
Memory Size		32K	32K	64K	32K	64K	32K
Hardware floating point option				1		1	
Interval timer option		1	1	1	1	1	1
2.5-M-byte cartridge disk	ModComp standard	2	2	2	2	2	2
20-M-byte disk file	ModComp standard						1
Console I/O device port	RS-232C async	1	1	1	1	1	1
Paper tape read/punch port	RS-232C async	1	1	1	1	1	1
DMA port	NCS standard	3	5	3	3	3	32
Magnetic tape unit port	NCS standard	1		1			2
External interrupts	Coax	6	6	6	6	6	6
I/O interrupts	Coax	8	8	8	8	8	8
GMT input	Digital	96 bits	96 bits	96 bits	96 bits	96 bits	96 bits
High-speed printer	RS-232C sync	1					
Low-speed printer	RS-232C async	1		2			
Card reader	RS-232C <i>async</i>	1		1			
CRT operator terminal	RS-232C <i>async</i>	2		2	1	1	

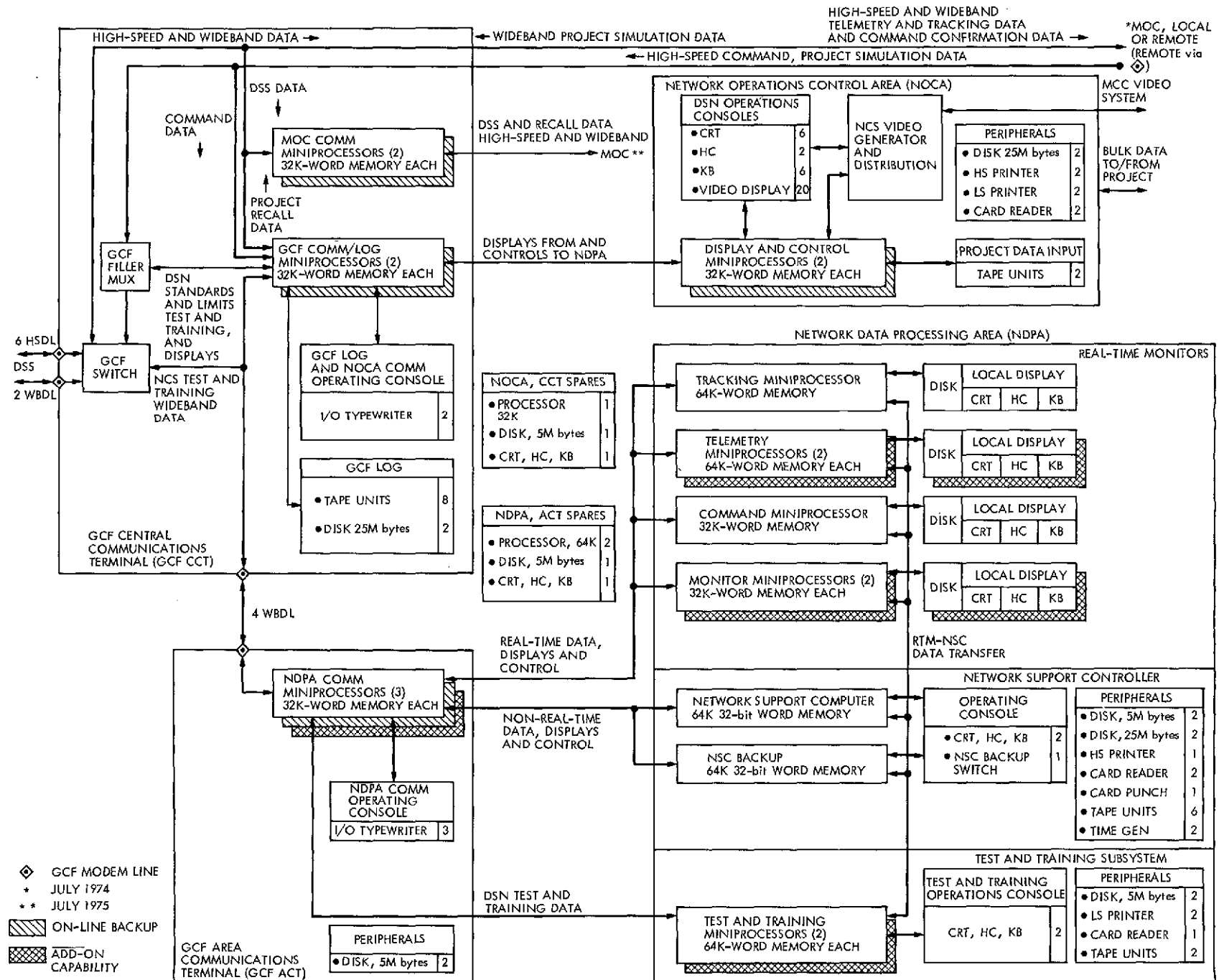


Fig. 1. Network Control System detailed configuration diagram

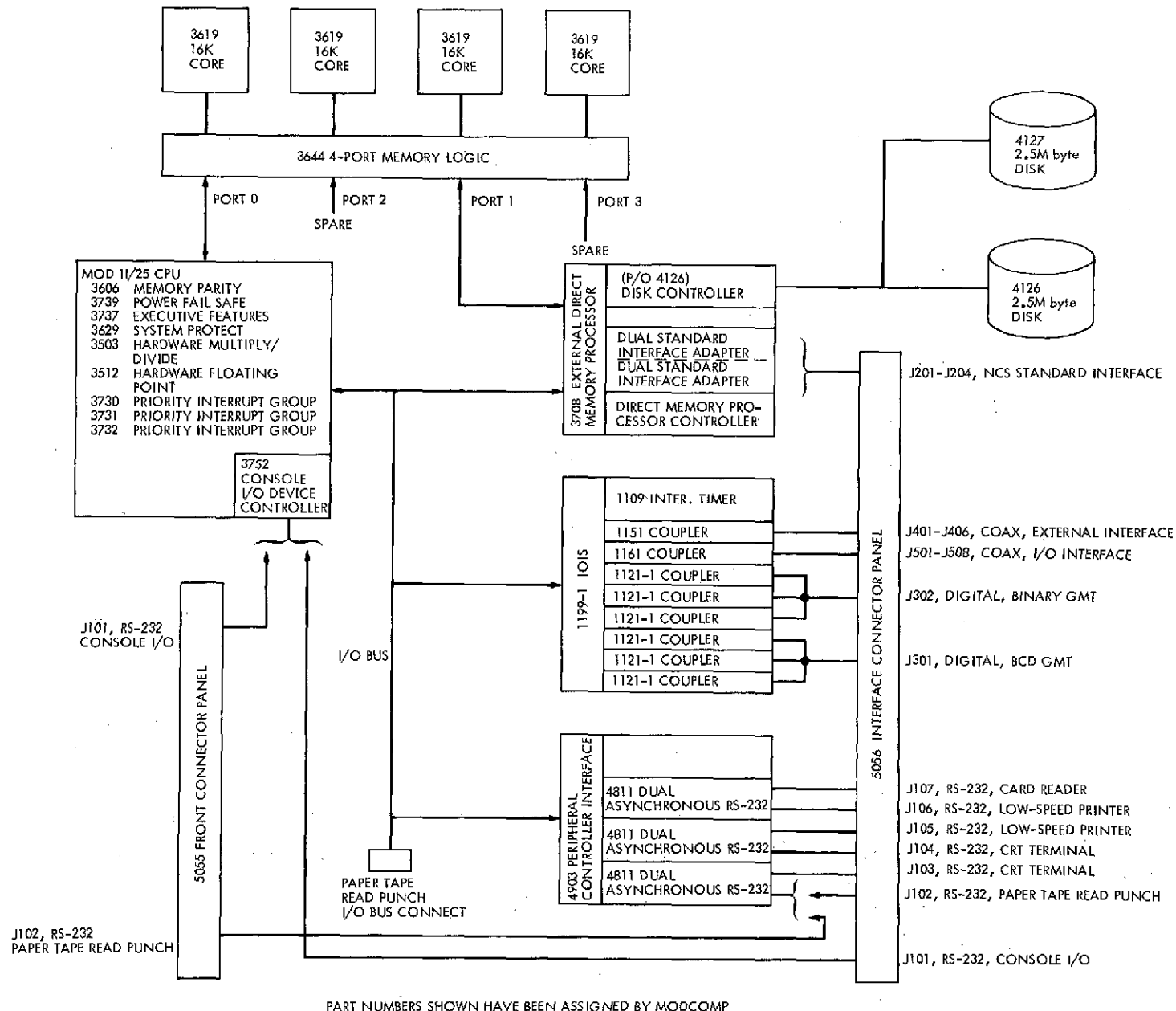


Fig. 2. Minicomputer system Configuration 3 block diagram

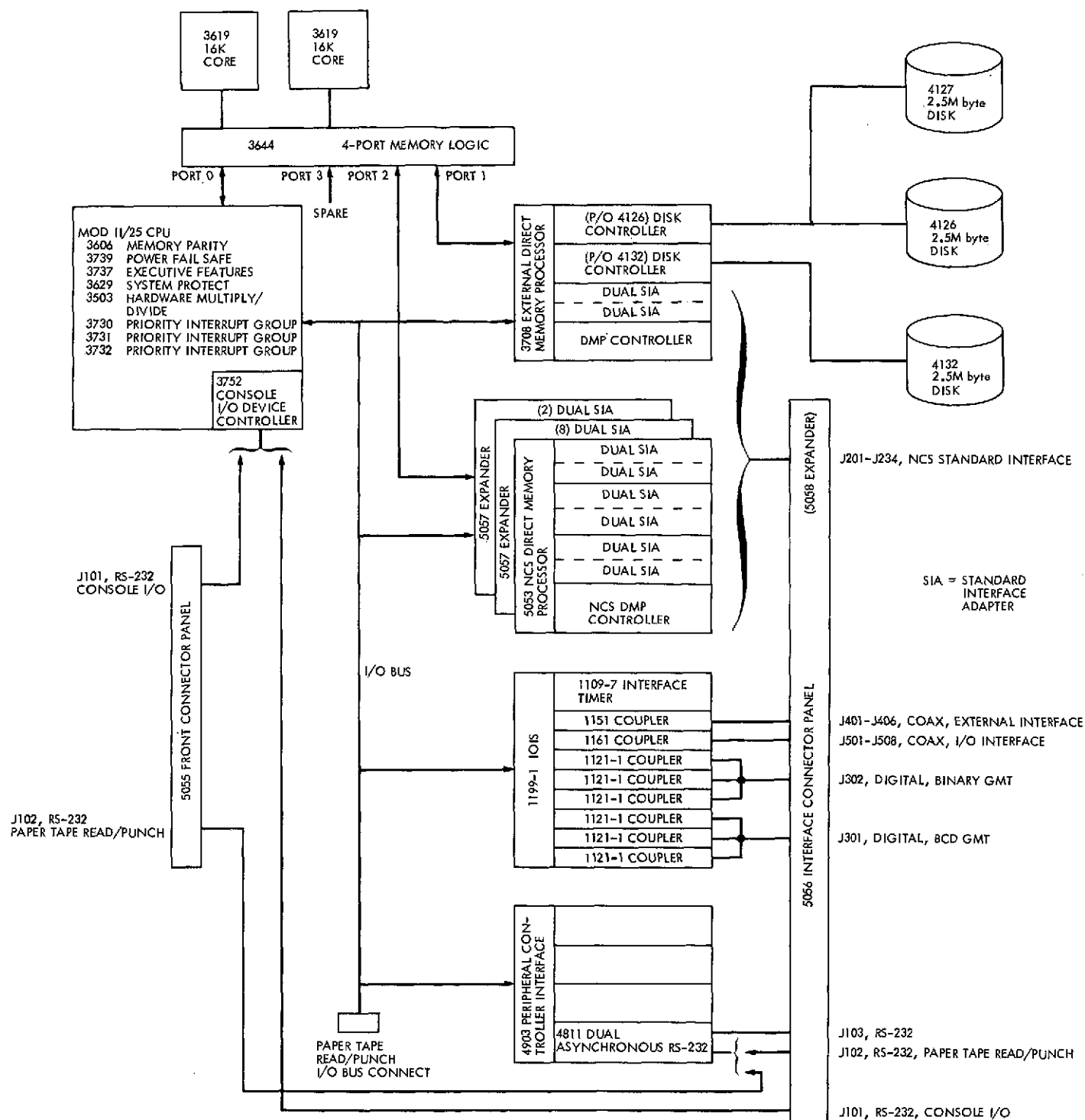
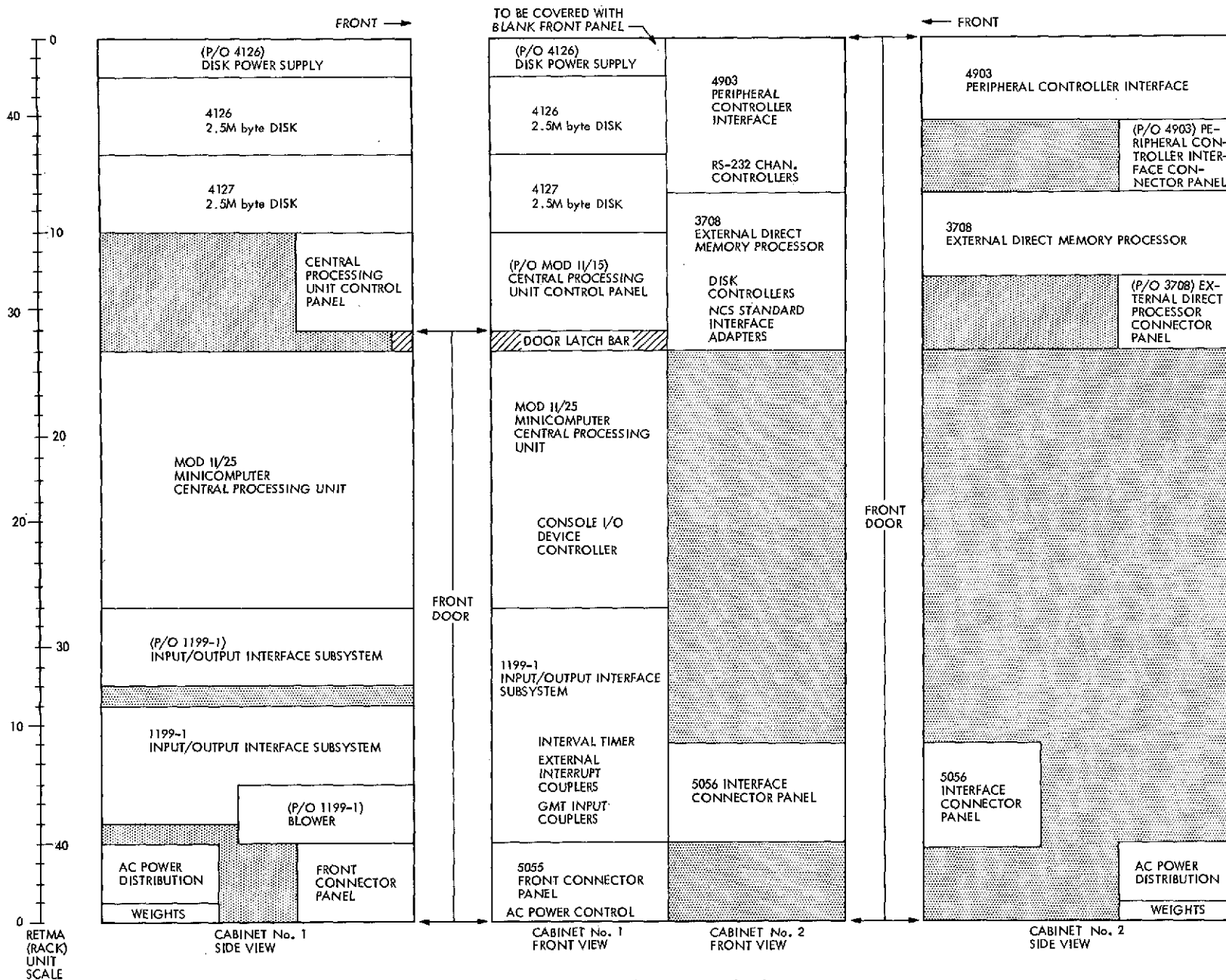


Fig. 3. Minicomputer system Configuration 6 block diagram



PART NUMBERS SHOWN HAVE BEEN ASSIGNED BY MODCOMP.
 CABINET No. 1 - JPL PART No. 9336147-92. CABINET No. 2 - JPL PART No. 9336147-93.
 ALL CABINETS EQUIPPED WITH FULL REAR DOORS. ALL DOORS, FRONT AND REAR, HINGE ON RIGHT SIDE OF DOOR.

Fig. 4. Cabinet assembly layout, minicomputer system Configurations 1 through 5

Network Control System Block I and Block II Software

S. E. Friesema
DSN Data Systems Development Section

The Network Control System (NCS) software implementation for Block I and Block II involves two distinct multicomputer systems. NCS Block I is a three-computer system; NCS Block II is a five-computer system. While completely separate, these two systems will operationally complement each other to provide required NCS operational support until NCS Block III is implemented. Both systems are presently designed and coded and are under NCS testing. NCS Block I will be available for operational testing July 1, 1974. This will not include the capabilities for sequence of events generation, and tracking predicts generation. Both programs are scheduled for operation at a later date. NCS Block II will be available for operational testing in early September 1974.

I. Introduction

The Network Control System (NCS) software development is divided into three major implementations, Block I, Block II, and Block III. This report will describe software implementation status for Block I and Block II.

The Network Control System Block I is basically a three-computer system implemented to:

- (1) Receive and provide accountability for high-speed data blocks (HSDBs) transmitted by Deep Space Stations (DSSs) to the Jet Propulsion Laboratory (JPL).
- (2) Transmit and display command data utilized in the configuration and control of DSSs.
- (3) Format and transmit to selected DSSs:
 - (a) Sequence of events (SOE) files.
 - (b) Seven-day schedules.
 - (c) Tracking predict data.
 - (d) Telemetry predict data.
- (4) Generate for formatting:
 - (a) Seven-day schedules.
 - (b) Sequence of events.
 - (c) Tracking predict data.

- (5) Provide printer dump of selected data being transmitted by the DSSs to JPL and from NCS to the DSSs. This includes wideband data being received in either 1200- or 2400-bit block size.

The NCS Block II is a five-computer system implemented to:

- (1) Receive and provide accountability for high-speed data blocks transmitted by Deep Space Stations to JPL.
- (2) Provide sufficient HSDB data analysis to assure meaningful displays for operational support in the areas of telemetry, tracking, command, and monitor.
- (3) Provide operational status of NCS Block II to a level that will readily identify major system operational problems.

The NCS Block I hardware configuration is shown by the simplified block diagram in Fig. 1. For a more detailed description of NCS Block I hardware configuration see Ref. 1. The NCS Block II hardware configuration is shown by the simplified block diagram in Fig. 2.

II. Block I NCS: System Operation and Software Capabilities

Six high-speed data lines are linked through the Ground Communications Facility (GCF) to the PDP-8 communications processor. All data, and Block I status information, are transferred via a 50-kb wideband data line to the Sigma-5 (Σ -5) real-time processor. Wideband data are received on a seventh channel by the PDP-8. Wideband blocks are multiplexed with regular high-speed data when a wideband data dump request is made. This is done by an operator at either Block I real-time cathode ray tube/keyboard (CRT/KB) display unit.

If the prime PDP-8 fails, the backup PDP-8 may be connected to the real-time Sigma-5 (B) or the backup PDP-8 and Sigma-5 (A) may become the new real-time string. If Sigma-5 (B) fails, either PDP-8 may be connected to Sigma-5 (A) as the new real-time system.

The formatting and generation of data are accomplished on whichever Sigma-5 is designated the non-real-time processor. After data blocks are formatted for transmission and recorded on 9-track magnetic tape, the recorded file or files are loaded on the real-time Sigma-5. The transmission blocks are stored on the real-time Sigma-5 disk until required for transmission. Files being

transmitted, or, in the case of command data, single blocks, are transferred to the PDP-8 via the 50-kb data line and transmitted to the proper high-speed data channel. No wideband data blocks are transmitted in Block I or Block II.

The real-time Sigma-5 peripherals are utilized as follows:

- (1) Only the 9-track magnetic tape units are used. They are used to load files for transmission. Initially, one of the 9-track units is used to load the program or, in the case when recovery is impossible from the disk, to reload the program for reinitialization.
- (2) The line printers provide dumps of high-speed data and wideband data blocks. Command blocks are output in special formats. Special summary requests result in accountability printouts.
- (3) The card reader is not used with the real-time system software.
- (4) The teletype (TTY) devices provide a low-speed log of system performance and operator control.
- (5) The CRT/KB consoles are the dynamic display points. Two formats are available to the operator. One is for real-time accountability and status. The second shows transmission file status. All operator inputs are typed on these keyboards. No entries are made via the TTY.
- (6) The disk is used to store transmission files and maintain recovery files.

The non-real-time peripherals are used as in a normal batch processing environment. The CRT/KB and the communication link to the PDP-8 are not utilized. For a more detailed description of the data processing features of NCS Block I see Ref. 2.

The software module diagram for the PDP-8 internal interface is shown in Fig. 3. The Sigma-5 real-time software module diagram and all existing interfaces are shown in Fig. 4. The non-real-time module structure is shown in Fig. 5. For a detailed description of these modules see Ref. 3.

III. Block I NCS Status

The PDP-8 software has been operating in its basic form in Block I, Phase I and Phase II. The Block I, Phase III version allows both 1200- and 2400-WBD-block

dumps and is ready for acceptance testing and transfer to operations.

The Block I, Phase III real-time Sigma-5 software is functionally complete and tested. All Block I real-time capabilities are ready for acceptance testing with Phase III. This includes all real-time transmission capabilities, with extensions of long-term storage for high-speed transmission data to 5000 blocks from 3000 blocks in Phase I and Phase II.

The Block I, Phase III non-real-time system is ready for acceptance testing. All Block I functional capabilities exist except:

- (1) SOE generation.
- (2) Tracking predicts generation.

The SOE generation program interface has been under evaluation by DSN operations, DSN systems, and NCS implementation personnel. Design of the SOE program is underway, and transfer to operations is scheduled for early November.

The tracking predicts generation program is being implemented by the Tracking and Orbit Determination Section, Section 391. When the Sigma-5 version of the program is available, NCS implementation engineers will help integrate the program into the present non-real-time system.

IV. Block II NCS: System Operation and Software Capabilities

Six high-speed data lines are linked through the Ground Communications Facility (GCF) to the NCS Ground Communications Processor (GCP). The GCP then distributes the high-speed data blocks, via the Star Switch Controller (SSC), to the Real-Time Monitors (RTMs). This distribution is DSS subsystem oriented. There are four

RTMs, tracking, telemetry, monitor, and command. All four RTMs are receive-only subsystems. No data blocks are transmitted from NCS Block II.

The RTM peripherals are utilized as follows:

- (1) Character printer/keyboard (CP/KB). This unit provides a running diagnostic record of subsystem activity.
- (2) Cathode ray tube/keyboard (CRT/KB). These units, two per subsystem, are the active display devices. The keyboards provide for operator control of subsystem activity. Active alarm conditions are displayed at the CRT/KB.
- (3) Low-speed printer (LSP). The low-speed printer is actually another (CP/KB) used to log command activity. The Block II command RTM will log all incoming command blocks including confirmation data.

The GCP software module diagram is shown in Fig. 6. The generalized Real-Time Monitor (RTM) software module diagram is shown in Fig. 7. Detailed descriptions of how these elements function may be found in Ref. 4.

V. Block II NCS Status

The detailed design has been completed and approved for NCS Block II. The GCP has been receiving and distributing data over the SSC since May 1, 1974. Integration of the command and monitor RTMs was begun May 17, 1974. Test high-speed data blocks were transferred via the GCP to the monitor subsystem on June 7, 1974. Tracking and telemetry RTMs are scheduled for integration the first week in July. Both these subsystems are considerably more complex than the monitor or command RTMs. Integration should be accomplished smoothly since common modules and system interfaces will have been integrated and verified well before that time. Acceptance testing should be completed in early September 1974.

References

1. Frey, W. C., "Network Control System Development," in *The Deep Space Network Progress Report*, Technical Report 32-1526, Vol. XV, pp. 167-176. Jet Propulsion Laboratory, Pasadena, Calif., June 15, 1973.
2. Renzetti, N.A., "Data Processing Capabilities of the Network Operations Control Center As Implemented by Block I Network Control System Project," DSN Capabilities Document 890-39, Jet Propulsion Laboratory, Pasadena, Calif., June 1, 1974 (an internal document).
3. Block I Detailed Design Document, Phase III, Network Control System (NCS), SD509758, Jet Propulsion Laboratory, Pasadena, Calif. (an internal document).
4. Network Control System Block II, Baseline Detailed Specifications, ES509271, Rev. A, April 25, 1974 (an internal document).

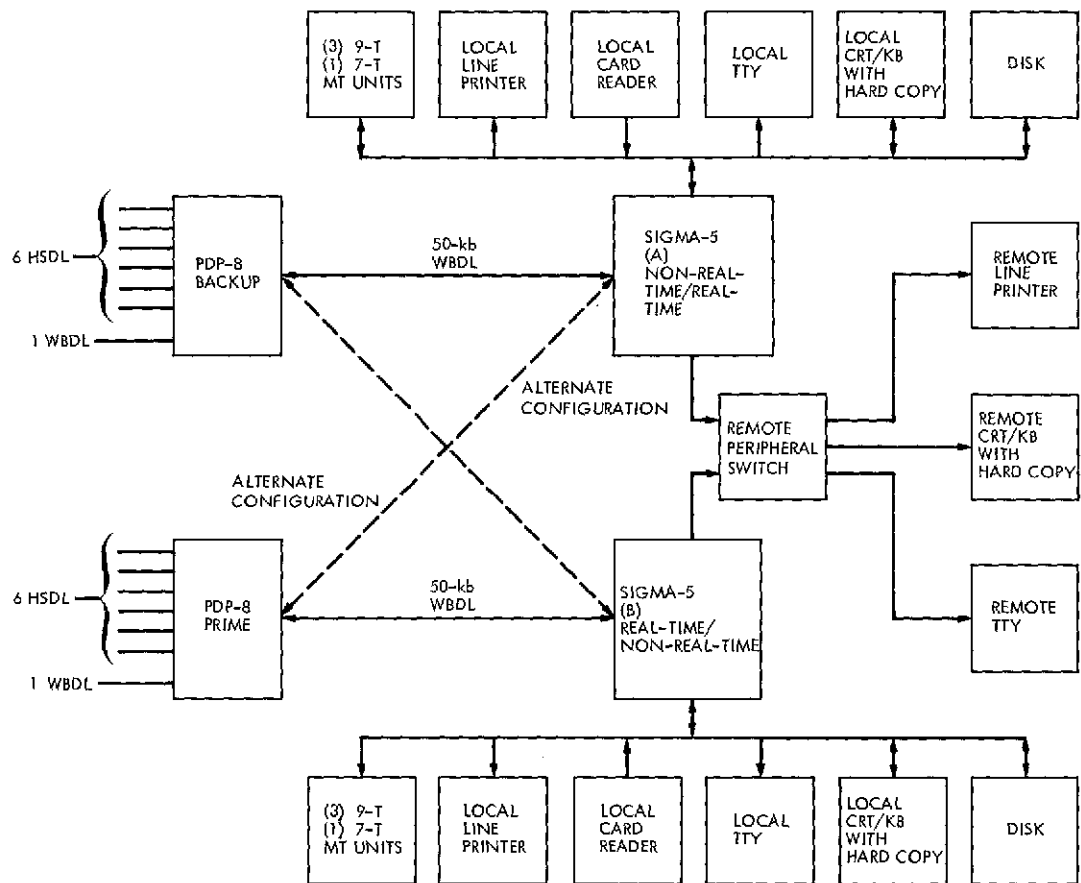


Fig. 1. Network Control System, Block I configuration

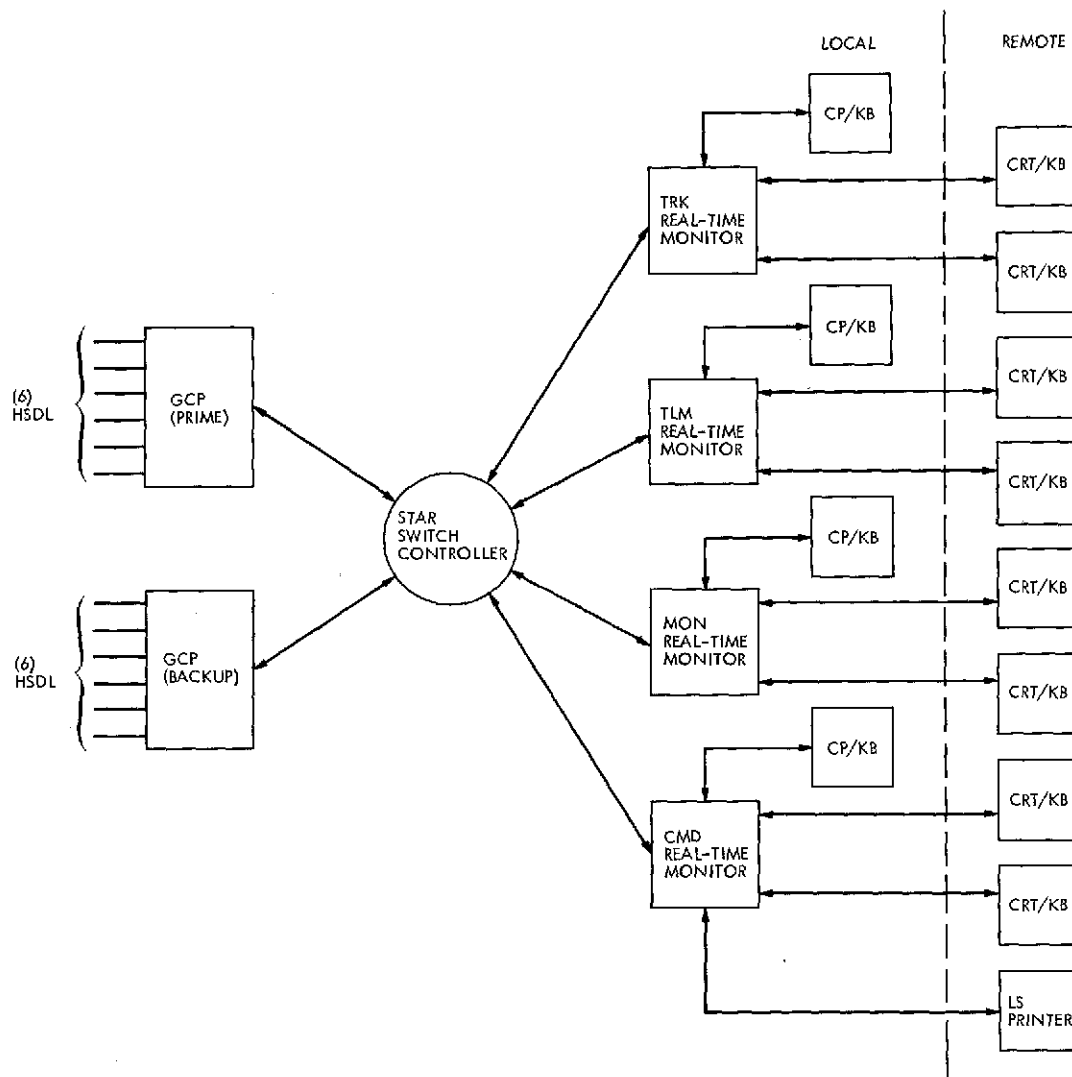


Fig. 2. Network Control System, Block II configuration

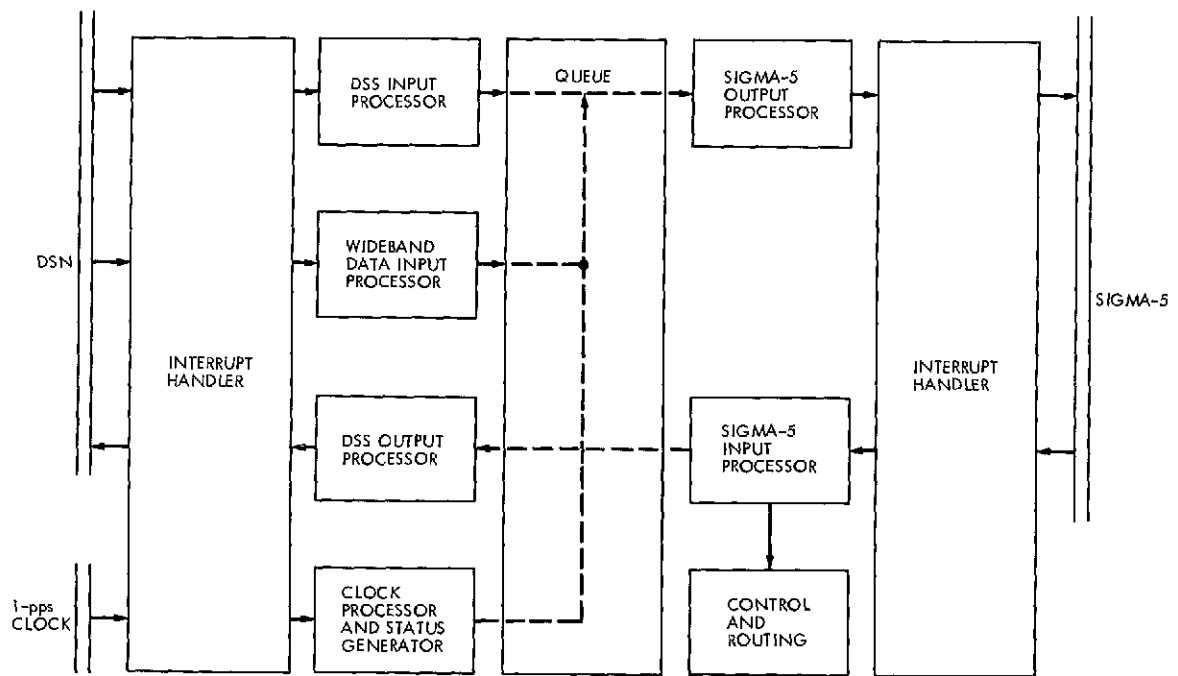


Fig. 3. Network Control System, Block I, PDP-8 software module diagram



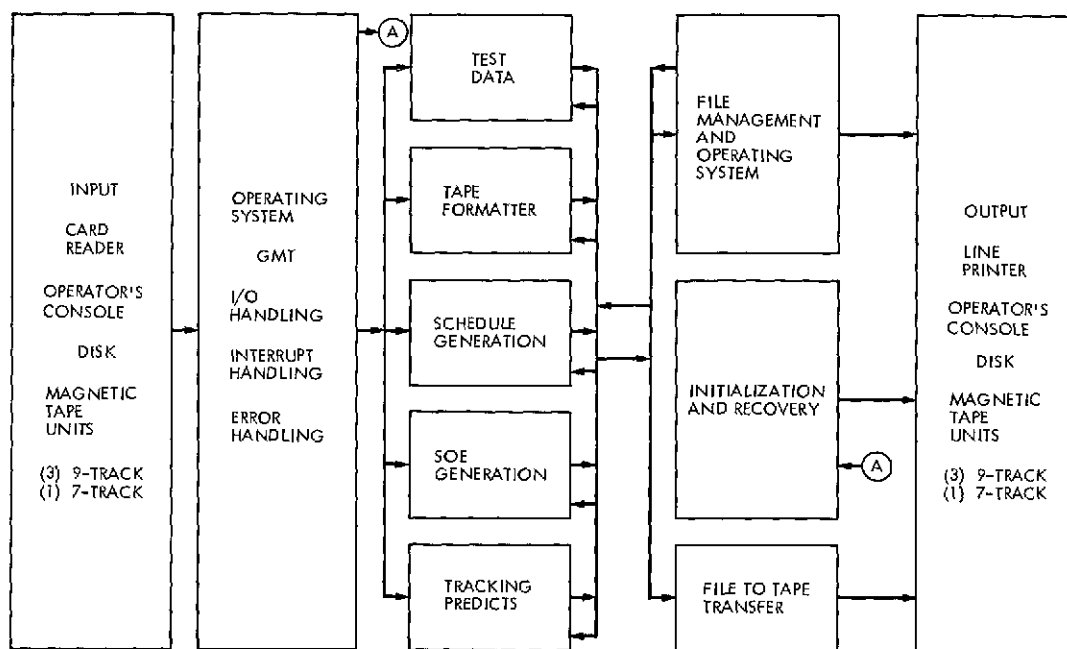


Fig. 5. Network Control System, Block I, Sigma-5 non-real-time software module diagram

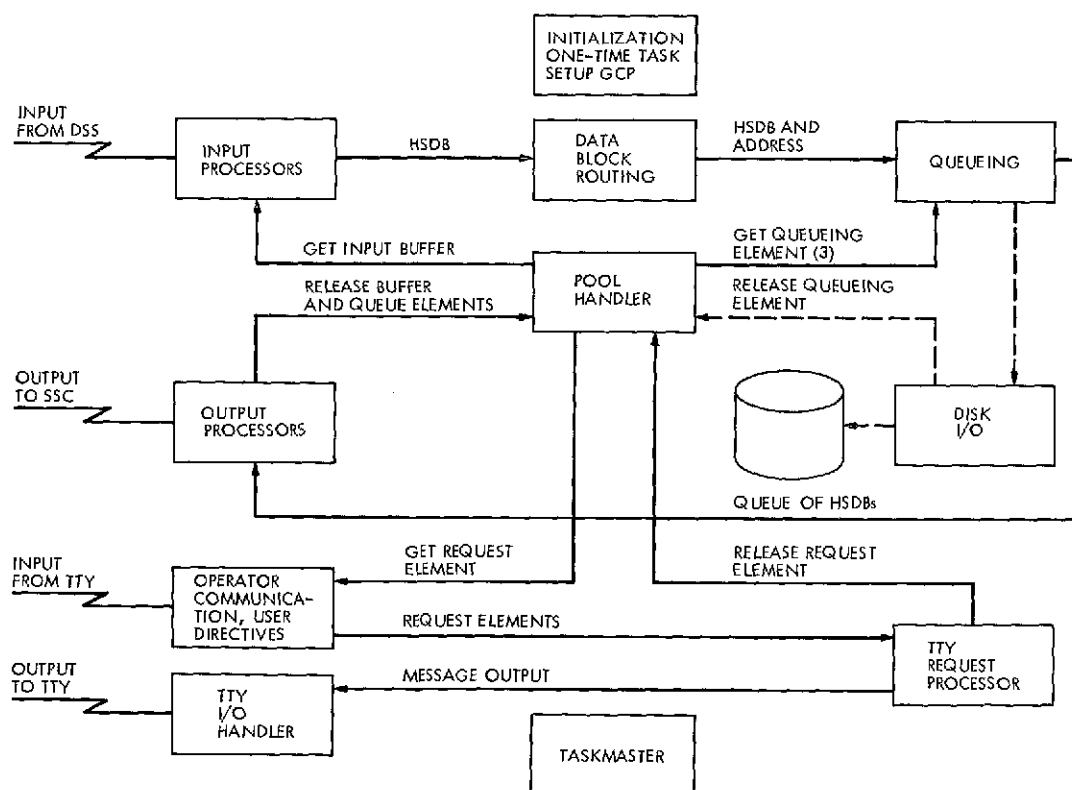


Fig. 6. Network Control System, Block II, GCP software module diagram

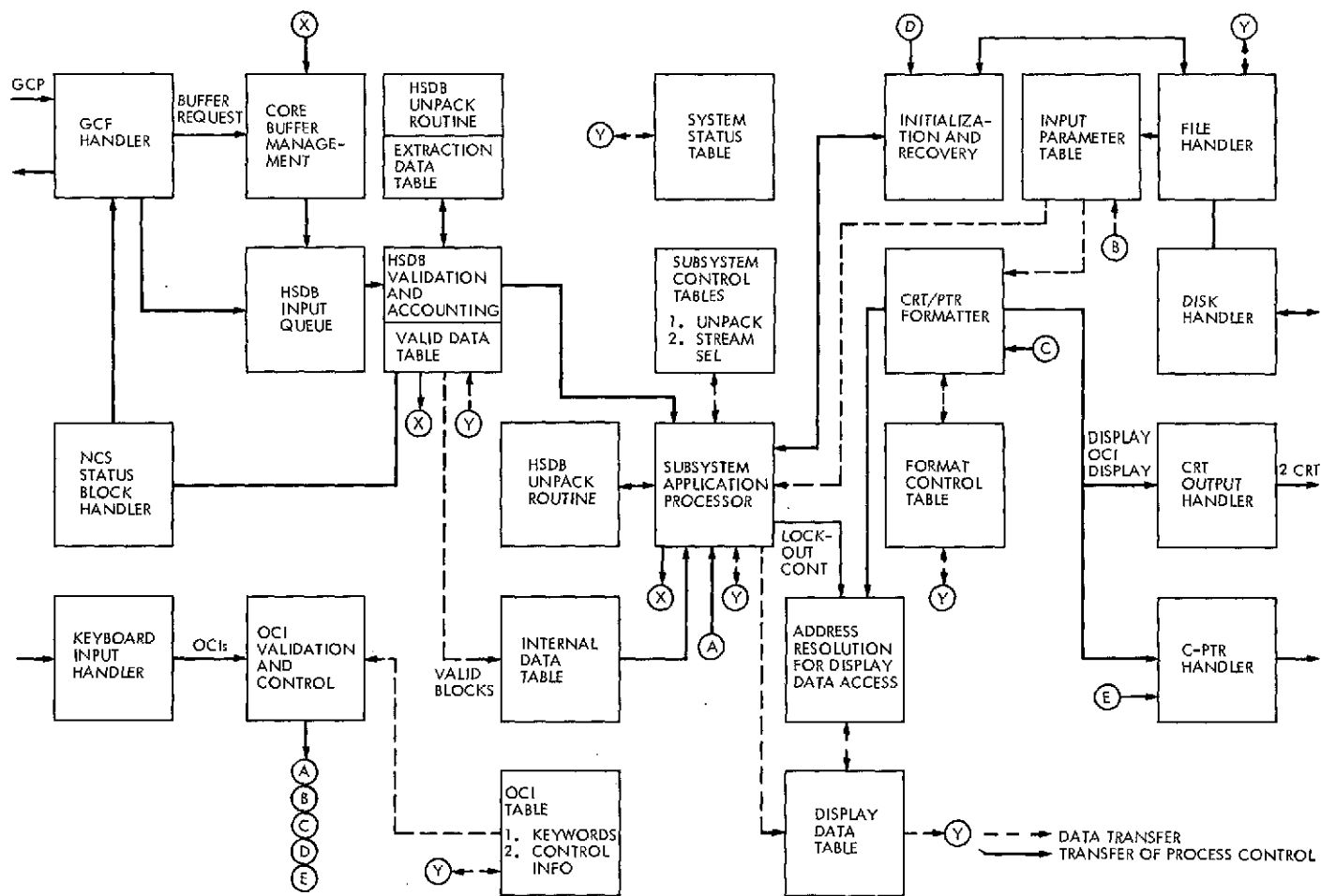


Fig. 7. Network Control System, Block II, real-time monitor software module diagram

Faraday Rotation Experiment

A. L. Price

R. F. Systems Development Section

Very high frequency polarimeters, working in conjunction with the Applications Technology Satellites, form a useful tool for monitoring ionospheric weather conditions. This article describes the installation of two such polarimeters at DSS 13.

Two new Faraday rotation tracking systems have been installed at DSS 13. These systems, often called polarimeters, working in conjunction with the Applications Technology Satellites at 136.35 MHz, provide information for the measurement of columnar electron content of the ionosphere. This installation replaces one which has been in service at DSS 13 since 1969. The purpose of this installation, aside from continued data collection, is to evaluate the performance and reliability of each system. This will lead to the selection of one system for use at the 64-m antenna stations in the DSN as part of the DSS Technical Facilities Subsystem. The polarimeters in use are the Teledyne Micronetics, Model 6501B, Faraday Polarization Tracking System, and the Aldi Research Corporation, Model 2000, VHF Polarimeter. Each polarimeter consists of an antenna system and a receiver.

Data collection and recording equipment are shared by both polarimeters.

Each antenna system is comprised of a pair of geometrically orthogonal, linearly polarized antennas mounted on reinforced concrete pads about 50 m from the DSS 13 operations building. Each antenna is located to have an unobstructed view of the Applications Technology Satellites (Table 1). While the antennas are very similar, they do differ mechanically. The Teledyne antenna (Fig. 1) can be positioned in azimuth and elevation in fixed 5-deg steps and has a positive lock in each position. The antenna is not counterbalanced, however, and cannot be positioned by one person. The Aldi antenna (Fig. 2) is counterbalanced, provides infinite pointing resolution, and is held in position by a friction clamp arrangement. Some

mechanical fabrication was needed with both systems for the installation of antenna-mounted components. The antennas are connected to the receivers with cabling 70 m in length. The Teledyne system requires two coaxial cables only; the Aldi requires one coaxial cable and one multiconductor cable.

Published specifications for each receiver indicate that the performance of each should be similar. Operation of each receiver is also very similar and quite simple. The designs differ somewhat but basically each receiver provides a method of electronically producing the effect of antenna rotation to produce a modulation envelope on the received signal. It is this modulation envelope, when detected, filtered, and compared with the modulating reference signal, that forms the basis for polarization angle measurement. One significant difference between the receivers is apparent. The Aldi system uses a radio frequency pre-amplifier mounted at the antenna and could suffer less from antenna-to-receiver cabling loss. Both receivers were installed in the same standard equipment cabinet which also houses the laboratory-furnished recording equipment (Fig. 3).

The recording equipment consists of a signal conditioning portion, a time code generator, a digital recorder, a paper tape punch, and two dual-channel analog chart recorders. The chart recorders provide a real-time indication of system performance as well as a permanent record. A punched tape and digital recorder printout

make up the remainder of the recorded data. Two outputs from each receiver are presently being recorded. The receiver outputs are calibrated on a daily basis, and the recorded data are sent to the laboratory at regular intervals for data reduction. In addition to the recorded data, a daily log of receiver tuning adjustments, relative signal strengths, and any system changes or malfunctions is maintained.

To provide a basis for fair evaluation of both systems, the manufacturer's installation, calibration, and operation instructions were followed as carefully as possible. The only deviations were in the case of omissions or mistakes in the instructions.

Operation of both systems, to date, has been good except on two occasions. The first resulted from the Aldi system's antenna being blown out of position in azimuth during a windstorm. On the other occasion, while tracking the Applications Technology Satellite Number 5 (ATS-5), the received signal strength from the satellite dropped to a level where the Teledyne system would not operate properly. The Aldi system continued normally although the output was obviously noisier. No other failures of any kind have been encountered.

At the present time, both systems are tracking ATS-1, which provides more than adequate signal strength for both systems.

Table 1. Antenna pointing coordinates

ATS	Azimuth, deg	Elevation, deg
1	232	40
3	119	25
5	162	48

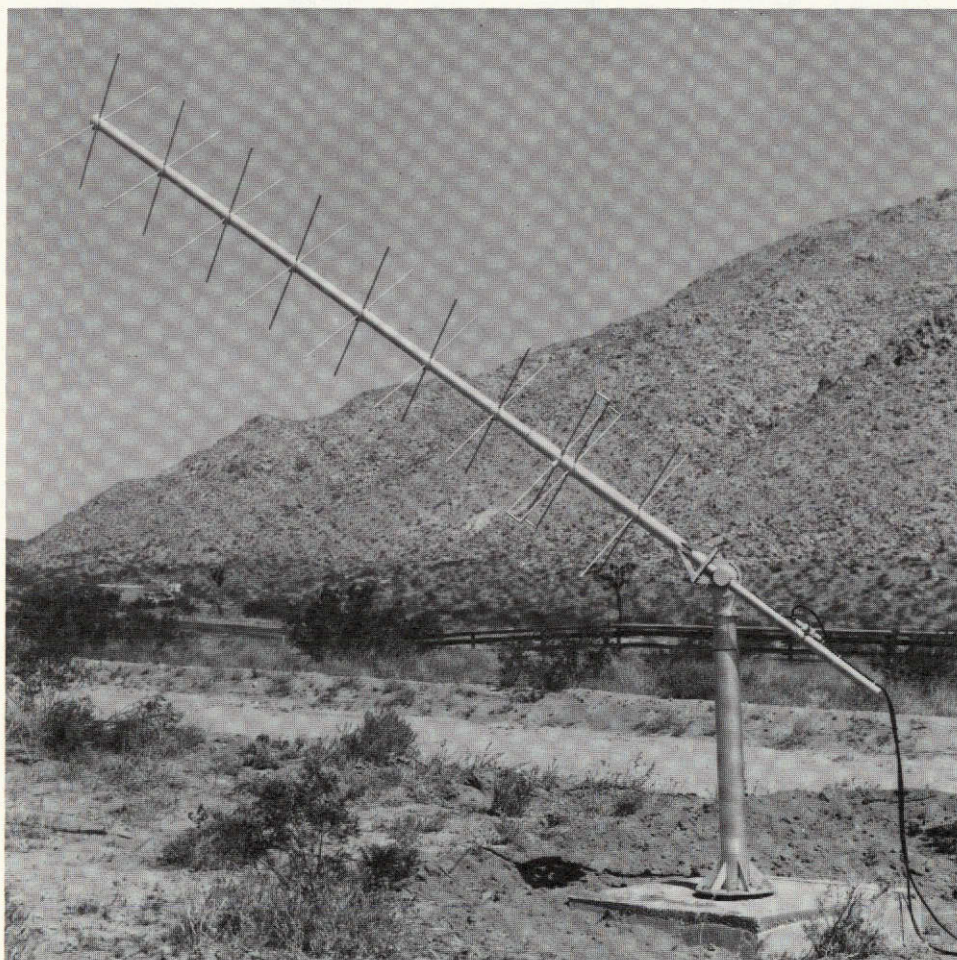


Fig. 1. Teledyne antenna installation

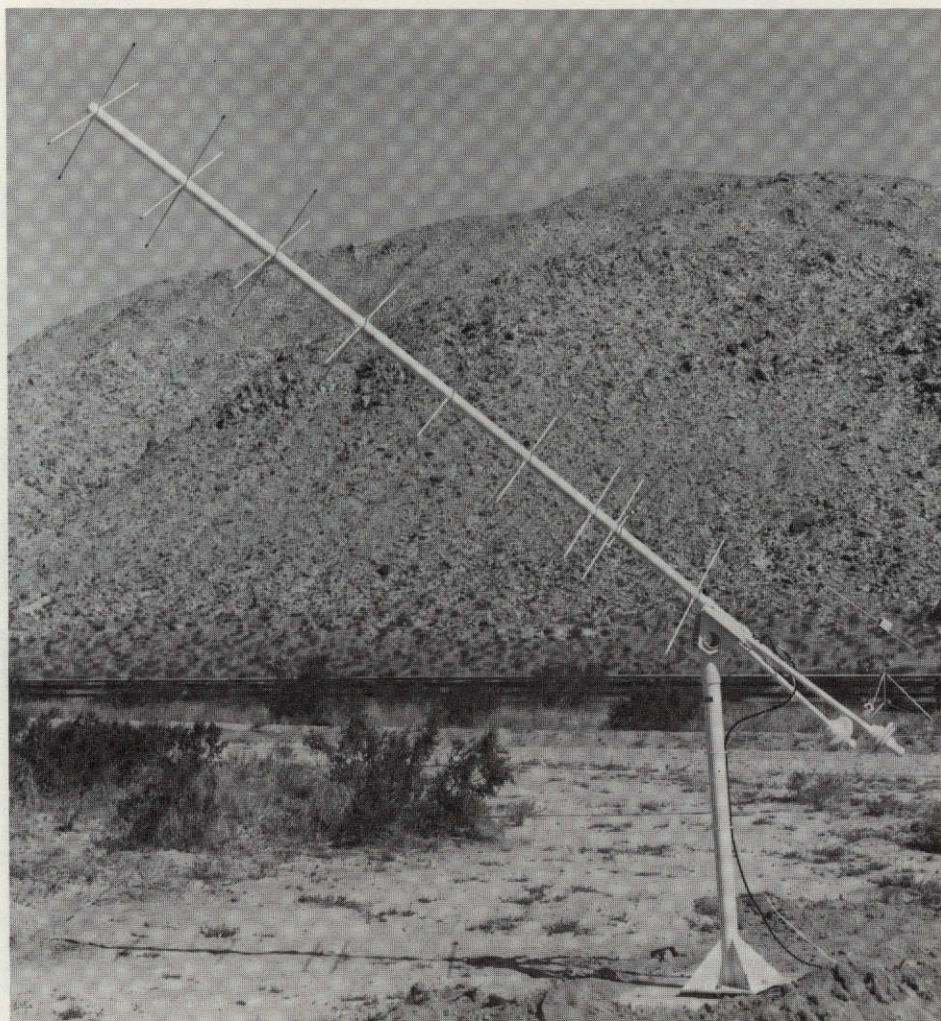


Fig. 2. Aldi antenna installation

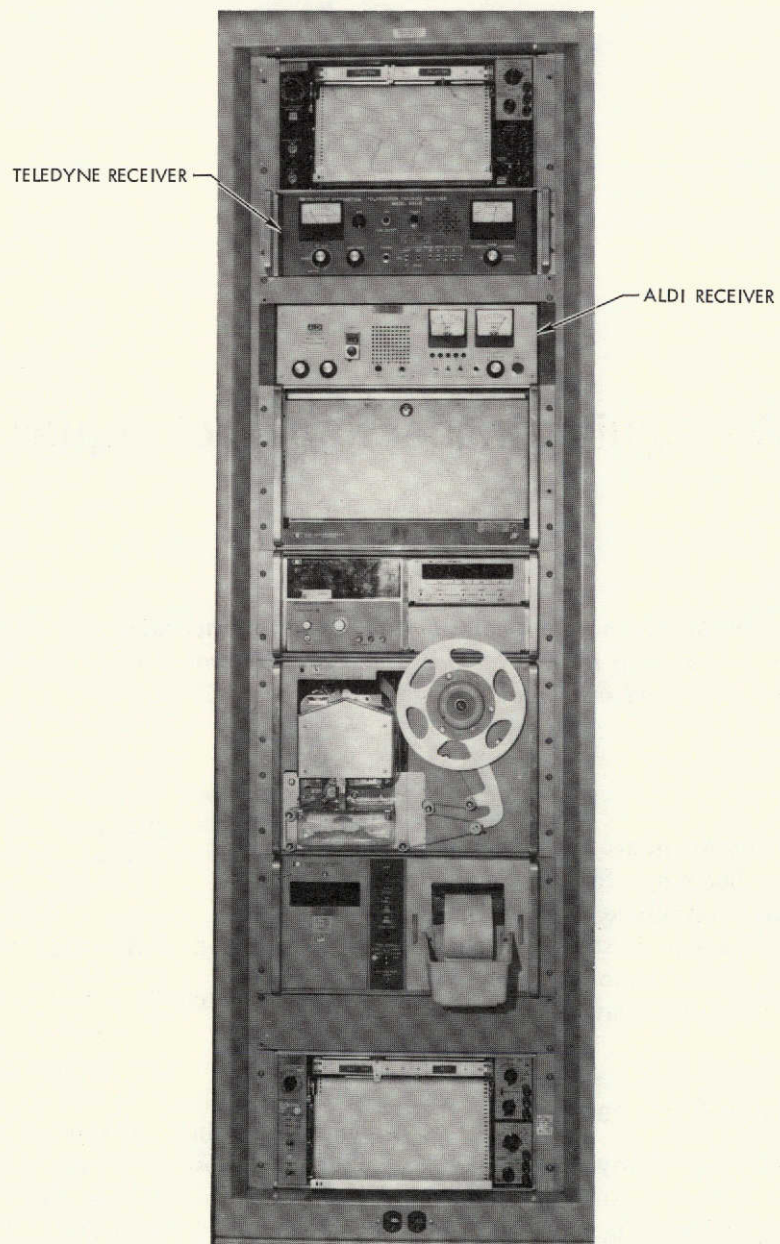


Fig. 3. Receiver and recording equipment installation

Waveguide Inspection Techniques

J. R. Loreman
R. F. Systems Development Section

Because of the demonstrated contribution of certain waveguide internal flaws to system noise and high transmitter back power, an improved inspection is being performed on S-band waveguide using a new precision borescope.

I. Introduction

Discussions with JPL Quality Assurance have led to the procurement of a precision borescope for the detailed internal inspection of S-band waveguide. It is expected that improved inspection of waveguide stock will eliminate failures of finished waveguide assemblies which have been traced to certain internal surface flaws.

II. Description of Precision Borescope

The borescope consists of a power-driven carriage, on which the component to be inspected can be positioned, and a control head. The control head includes the controls for linear positioning of the work piece and the illumination of the borescope probe. The probe located at the end of the support column is angularly positioned manually (Figs. 1 and 2). A polaroid photograph of the borescope's field of view can be made with integral photographic equipment. Magnification can be continuously varied from $7\frac{1}{2}$ to 40 times. Figure 3 shows an inspector operating the borescope while inspecting S-band copper

waveguide stock. The calibration provided on the support tube and the angular position indicator enable accurate location of internal flaws.

III. Results of Initial Use of Borescope

Approximately 20 meters of S-band copper waveguide stock has been inspected prior to being used for the fabrication of water-cooled S-band high-power waveguide assemblies. The waveguide stock was cleaned by a nonetching chemical process in order to eliminate dirt and allow close inspection of the internal surface. Two categories of mechanical flaws which have caused waveguide arcing in the past were detected. These mechanical flaws are the swaging of loose metal into the internal wall of the waveguide during the extrusion process (Fig. 4) and voids or spaces which break through the internal waveguide surface. In addition, surface ripples and various deposits and chemical discolorizations were detected. These additional defects have not been identified with respect to the failure of waveguide components. The inspection has prevented defective portions of the wave-

guide stock from being included in finished waveguide assemblies.

IV. Future Plans

All waveguide stock which is to be incorporated into high-power S-band waveguide for use in the DSN will

be inspected with the borescope. Waveguide stock containing flaws will be eliminated or identified to prevent these flaws being included in finished high-power S-band waveguide assemblies. In addition, a program of evaluation will be carried out to identify all types of internal variations with respect to waveguide component performance.

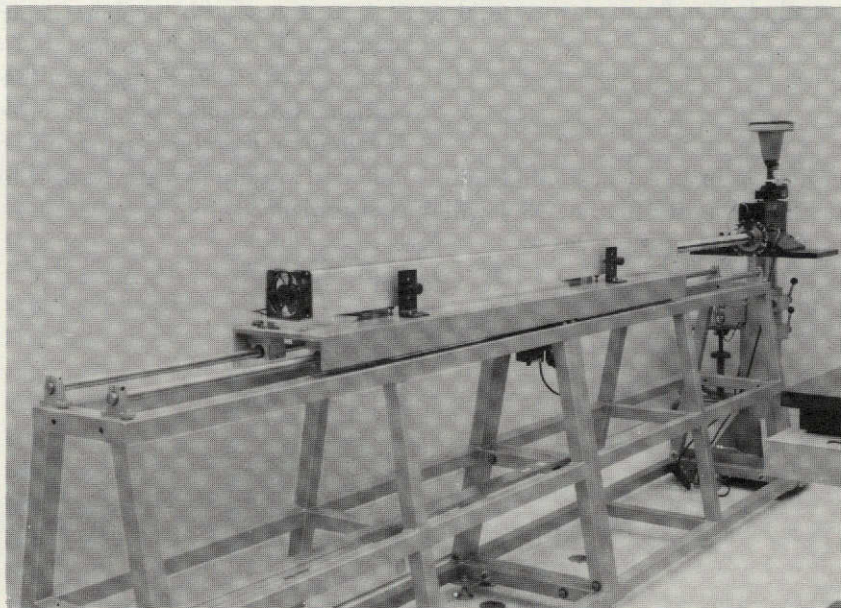


Fig. 1. Precision borescope showing carriage, waveguide to be inspected, and control head

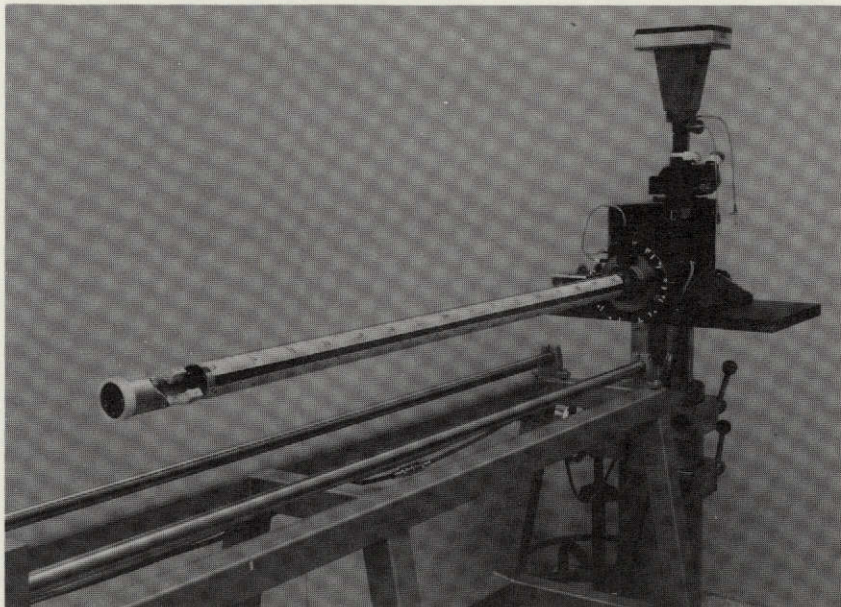


Fig. 2. Control head showing probe (at left), calibrated tube and angular position indicator, and camera

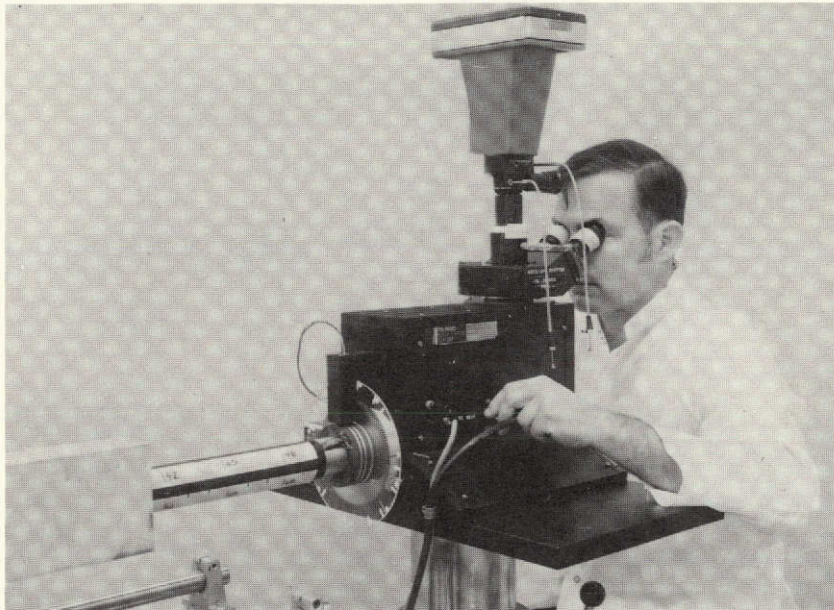


Fig. 3. Operation of precision borescope

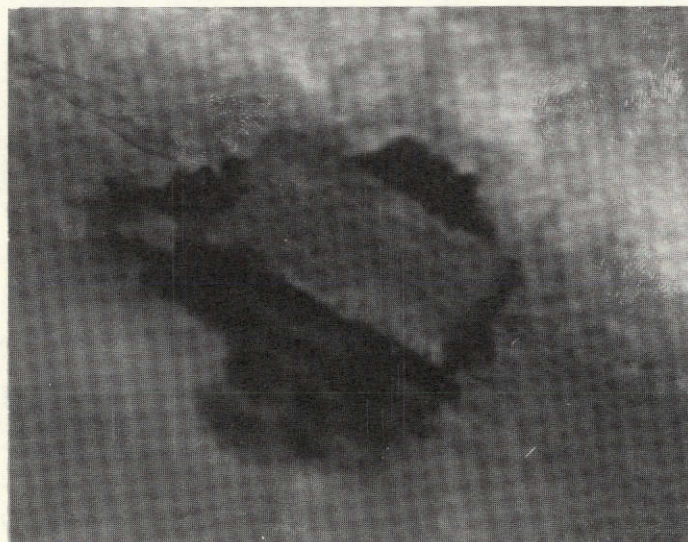


Fig. 4. Mechanical flaw (swaging of loose material into internal surface)

Telemetry and Command Multiple-Mission Software (Model C)

V. D. Jones
DSN Data Systems Development Section

This article gives the status of the Deep Space Station Telemetry and Command operational software dedicated to the support of the Pioneer (10 and 11), Helios, Viking, and Extended Mariner Venus/Mercury missions. New application programs have been written and integrated with the existing executive. Model C retains the telemetry capabilities of Models A and B and utilizes the DSN Mark III-74 Command System (command redesign module). Additional functions have been added to support the Viking mission.

I. Introduction

Model C of the Telemetry and Command Subsystem (TCD) software has been implemented and will support JPL deep space missions through 1975. The multi-mission capability was accomplished by developing many specialized or mission-dependent program elements (data sets). Combinations of these data sets may be integrated to operate in a specific environment (TCD computers) and in a predetermined manner, e.g., control and monitor the Command Modulator Assembly (CMA) for command rate of 8 bits/s. The TCD computers used are the XDS 920 and the Interdata Model 4.

II. Major Categories and Support Software

The basic software categories (modules) are supervisor (executive), command telemetry, and 9-track Digital Original Data Record (DODR) replay. Each module usually consists of many data sets and must perform a dedicated function after integration:

- (1) *Supervisor (EXEC)*. This module performs the nonreal-time task of loading and link-editing all data sets required to do a specific job, viz., high-rate telemetry, low-rate telemetry, etc. EXEC also performs the real-time function of scheduling out-

bound high-speed data blocks, periodic transfers to monitor, DODR logging, local alarms, and initial processing of all input messages.

- (2) *Command.* This module is dedicated to controlling and monitoring the CMA. Model C features one and only one mission-independent command element. Its capabilities are frequency-shift keying (FSK) tone at 1 bit/s, phase-shift keying (PSK)/pseudo-noise (PN) at 1 bit/s, coherent and non-coherent PSK at 8 bits/s maximum.
- (3) *Telemetry.* Subsets from the inventory of telemetry routines are integrated in accordance with mission-related directives specified by the user. Newly acquired data are assembled by this module for transmission to the user in real time. Telemetry-related hardware assemblies are monitored and controlled and their status is recorded in Ground Communications Facility (GCF) images and monitor messages. Local alarms are generated whenever manual intervention is required. Model C telemetry capabilities are outlined in Table 1.
- (4) *9-Track DODR Replay.* This module is considered to be a nonreal-time function and allows the user to selectively replay 9-track tapes logged by the high-rate telemetry channel. Present capabilities include time interval selection, user-dependent code type (UDT), and data-dependent code type (DDT) selections and the option to transmit over GCF lines at a fixed interval, viz., one block per second or at the line rate.

Support software has been developed (and improved) to perform the following functions:

- (1) *Program Tape Maintenance.* A system was developed to delete, add, or alter data sets from the TCD system tape. The system tape is a 7-track digital magnetic tape written by the XDS 920 at a density of 200 bits/2.54 cm (200 bits/in.).
- (2) *Punched Paper Tape and Edit Routine.* Prepares paper tape with input messages for subsequent processing by the (TCP resident) executive. The input messages are mission directives defining such variables as telemetry bit rate, format, command format, configuration(s), and so forth.

- (3) *Bootstrap Loader.* Bootload (on punched paper tape) loads controller (EXEC) from the system tape.

III. Real-Time Operation

After a collection of data sets has been loaded by the supervisor, the newly loaded software becomes an interrupt-driven system with a priority subprogram queue (PSQ) structure. The executive monitors the PSQ and will transfer control to a specific subprogram as a result of a real-time event. This event may be an interrupt or a directive in the form of a manual input message.

IV. Mission-Dependent Data Sets

The software was implemented by developing mission-oriented segments and integrating with a basic nucleus. Each project has been provided with a set of input directives which the operator can use to select specific subsets of routines. Corresponding to each configuration directive is a "configuration list" which is processed by the executive. Each mission has its own data base containing parameters such as the bit rate for high-rate telemetry, abort return address in the command module, etc. Each mission also has its own GCF block formatter in order to meet the DSN/MCCC interface requirements (820-13).

V. Summary

Mission-dependent routines (data sets) may be specified in the configuration table portion of the supervisor. New application programs have been written and integrated with the existing executive. Model A has been used successfully as a flight support instrument for MVM'73. Model B was released with Command System redesign and software central to the support of the Pioneer and Helios Projects. Model B has undergone extensive acceptance testing and successful compatibility testing with the Helios spacecraft. Model C, which is being released, retains the telemetry capabilities of Models A and B plus the command redesign module. Additional functions have been added in order to support the Viking mission, and Model C is now in the final stages of acceptance testing.

Table 1. Telemetry capabilities

TCD computer	Function	Mission and bit rate constraints
XDS 920	Low-rate bit synchronization	MVM'73, Viking 8.33, 33.33 bits/s
ID4, XDS 920	Medium-rate block decoding	MVM'73, Viking 250, 490, 500, 1000, 2000, 2450 bits/s
ID4, XDS 920	Processing of medium- (low-) rate uncoded data	MVM'73, Viking 8.333, 33.333, 250, 500, 1000, 2000 bits/s
ID4, XDS 920	Sequential decoding (192, 384-bit frames) and processing of uncoded data	Pioneer 8 16, 32, 64, 128, 256, 512, 1024, 2048 bits/s
ID4, XDS 920	Sequential decoding (1152-bit frames)	HELIOS Bit rates same as Pioneer
ID4, XDS 920	Processing of uncoded data for Helios	HELIOS Bit rates same as Pioneer
ID4, XDS 920	Processing of high-rate block decoded or uncoded data	MVM'73, Viking Coded: all MVM and Viking rates Uncoded: 250, 500, 1000, 2000, 4000, 8000, 1176000 bits/s

An Interrupt Timing Simulation

V. D. Jones and R. L. Schwartz
DSN Data Systems Development Section

This article describes a timing simulator written in ANSI FORTRAN. The program was developed to aid in the location of timing anomalies in existing interrupt-driven software and to assist in the design of new real-time programs.

I. Introduction

The timing simulation is designed to simulate the real-time processing of internal and external interrupts of both an asynchronous and synchronous nature as well as a series of subprograms that are to be executed as a result of executing an interrupt processing routine.

In order to make use of the simulation, information must be known as to the exact structure and hierarchy of the processing system. The relative priority as well as the duration and frequency of the different routines must also be known.

The simulation handles virtually any system consisting of a supervisory loop with asynchronous and synchronous interrupts and a subprogram queue structure. When all information concerning the system has been given to the program, the simulation of the interrupt handling will occur. Various statistics and state snapshots are available.

A brief timing study of the effect of a 20-character per second Remote Output Teletype on the Viking Telemetry

and Command Processor (TCP) using the XDS 920 computer is provided as an example.

II. Overview

The simulator accepts as input data mnemonics which represent Primary Interrupts (PINs), Clock Interrupts (CLKs), and subprograms in a priority queue (PSQ). Priorities, durations, and interval times (not for all inputs) are given (in number of cycles) and the handling of the interrupts is simulated.

At the beginning of each cycle, every clock is checked to see if its interval has expired.¹ If so, the clock is placed on a push down stack. The primary interrupts are then checked to see if there are any occurrences for that cycle, and, if so, the interrupt is put in the stack. The stack is then sorted according to the priority of each interrupt. At

¹In actuality, a computation is done to determine the next cycle at which a change occurs, and all necessary counters are incremented to that value, eliminating the execution of needless cycles.

this point, the duration counter of the highest priority interrupt is updated. If this is the first cycle of the routine, then the elements in the PSQ associated with that interrupt are enabled. When the duration is satisfied, the interrupt is wiped off the top of the stack. If there are no interrupts to process during that cycle, then the highest priority subprogram that is enabled is fetched and put in the stack. When no PSQ entry has been enabled, the program loops in the supervisor (MAIN) waiting for an interrupt to occur.

Additional features include the ability for a PSQ element to queue other PSQ elements or to enable clock interrupts, and for a clock to have a controlling envelope.

A watchdog timer interval may be specified in order to monitor the activity of the program. This gives status of all interrupts and subprograms. Following the final time specified for the simulation, various statistics are given concerning the activity of the interrupts during the run.

III. Structural Elements of Simulation

A. Priority Subprogram Queue (PSQ)

The PSQ routines are those which are executed in the base or noninterrupt status of the machine. They exist in a priority queue and are enabled by clocks, primary interrupts, and other PSQ routines. Each PSQ can either be assigned a priority as with the clocks and primary interrupts, or will be assigned a default priority of zero, with its position in the PSQ table (relative to the top) determining its priority with respect to other PSQs. Each PSQ entry is disabled after execution. The "main loop" routine is a special case of the PSQ type. It is always enabled and has the lowest priority, thus it will only be executed when nothing else is active or pending.

B. Clock (CLK)

The clock routines are periodically enabled as by a cyclic interrupt. They are given priorities which determine their relative importance with respect to the other clocks, primary interrupts, and, in some cases, the PSQs. The higher the number, the higher the priority. Once started, a clock is enabled once each time its interval expires. This is subject to conditions specified below in regard to the envelope and clock flags. A clock may have a random or deterministic start time. For a random start time, a random number between 1 and 255 is assigned. The duration of the clock interrupt handling routine is

also given. When a clock has been enabled and reaches the top of the stack, it is executed. On the first cycle of execution each CLK enables the PSQs associated with it.

C. Primary Interrupt (PIN)

The PIN routines are asynchronous interrupts whose enabling times are given in the input data. When the PIN occurs, it is enabled, and the first cycle of its operation is used to enable all PSQs associated with it. Since it is asynchronous, no envelope control is required. Each PIN has a priority and duration.

D. Envelope (ENV)

Envelopes or ENVs serve to inhibit or permit clock interrupts. If a clock interrupt is controlled by an envelope, an interrupt is only recognized when the envelope is high. A clock can be controlled by at most one envelope, but an envelope may control more than one clock. The waveform of the envelope is similar to that of the clocks. It is started at a time either specified as random or deterministic. Each ENV is given a duration and an interval. Thus, if an envelope is turned on at time t_0 , it will be on until $t_0 + t_d$. It will be off from $t_0 + t_d$ until $t_0 + t_i$, then on from $t_0 + t_i$ until $t_0 + t_i + t_d$, etc.

E. Clock Control Flag (CCF)

Clock control flags or CCFs are controlled by the completion of PSQs. CCFs exist as a simulation feature to allow disabling and enabling of interrupts by subprograms. Clocks may be controlled by more than one PSQ, and a PSQ may control several clocks.

F. ENV-CCF Interaction

The envelopes (ENVs) and the clock control flags (CCFs) are examined, and, if "true," the appropriate clocks will be enabled. If a clock is disabled when it would normally start as the result of interval expiration, it will not start until the interval has expired (again).

IV. Modified Backus Normal Form (BNF) Description of Simulation Input Data

Input editing is structured to process the mnemonics and associated parameters in accordance with the syntax rules given below. The notation is to be interpreted as follows:

- (1) Read the connective "!=" as: "is formed from"

(2) Read the symbol "<X>" as: "the object named X"

shortens the sequence given by:

(3) $\left\{ \cdot \right\}_a^b$ indicates repetition of the set $\left\{ \cdot \right\}$ from a to b inclusive

$\langle X \rangle := p$
 $\langle X \rangle := q$
 $\langle X \rangle := r$

(4) $\left\{ \cdot \right\}_a^a$ indicates repetition of the set $\left\{ \cdot \right\}$ a times

(6) Any string not enclosed in angular brackets (<...>) represent a terminal element, e.g., +, -, RND, \emptyset (blank), \$, etc.

(5) "|" indicates exclusive or; viz. $\langle X \rangle := p|q|r$

$\langle \text{DIGIT} \rangle := 0|1|2|3|4|5|6|7|8|9$

$\langle \text{CHAR} \rangle := A|B|C|D|E|F|G|H|I|J|K|L|M|N|O|P|Q|R|S|T|U|V|W|X|Y|Z$

$\langle \text{DELIMITER} \rangle := ,|\emptyset$

$\langle \text{TERMINATOR} \rangle := \$ \langle \text{NOISE} \rangle$

$\langle \text{NAME} \rangle := \langle \text{CHAR} \rangle \left\{ \langle \text{CHAR} \rangle | \langle \text{DIGIT} \rangle \right\}_0^5 \langle \text{DELIMITER} \rangle$

$\langle \text{NUMBER} \rangle := \left\{ \langle \text{DIGIT} \rangle \right\}_1^8 \langle \text{DELIMITER} \rangle$ (UNLESS NOTED ELSEWHERE)

$\langle \text{NOISE} \rangle := \langle \text{NAME} \rangle | \left\{ \langle \text{NAME} \rangle \langle \text{DELIMITER} \rangle \right\}_0^\infty$

$\langle \text{NUMERIC DATUM} \rangle := \langle \text{NOISE} \rangle \langle \text{NUMBER} \rangle \langle \text{NOISE} \rangle$

$\langle \text{START TIME} \rangle := \langle \text{NUMBER} \rangle | \text{RND} \langle \text{NUMBER} (\leq 255) \rangle | \text{RND}$

$\langle \text{FLAG} \rangle := +|-$

$\langle \text{TFIN} \rangle := \langle \text{NUMERIC DATUM} \rangle$

$\langle \text{PSQ} \rangle := \langle \text{NAME} \rangle \langle \text{NUMBER (DURATION)} \rangle \langle \text{NUMBER (PRIORITY)} \rangle$
 $\left\{ \langle \text{NUMBER (NUMBER OF PSQs)} \rangle \left\{ \langle \text{NAME (PSQ NAME)} \rangle \right\} \right.$
 $\left. \begin{array}{l} \text{NUMBER PSQs} \} 1 \\ \text{NUMBER PSQs} \} 0 \end{array} \right.$

NOTE: A PSQ may call only those PSQs already input.

$\langle \text{MAIN LOOP} \rangle := \langle \text{NUMERIC DATUM} \rangle$

$\langle \text{WATCHDOG} \rangle := \langle \text{NUMERIC DATUM} \rangle$

$\langle \text{CLOCK} \rangle := \langle \text{NAME} \rangle \langle \text{NUMBER (PRIORITY)} \rangle \langle \text{NUMBER (INTERVAL)} \rangle$
 $\langle \text{NUMBER (DURATION)} \rangle \langle \text{NUMBER (NUMBER PSQs ENABLED)} \rangle >$
 $\langle \text{START TIME} \rangle \left\{ \langle \text{NAME (PSQ NAME)} \rangle \right\} \begin{array}{l} \text{NUMBER PSQs} \\ \text{NUMBER PSQs} \end{array}$
 $\left\{ + \langle \text{NUMBER (NUMBER PSQs ENABLED)} \rangle \right.$
 $\left. \left\{ \langle \text{NAME (PSQ NAME)} \rangle \right\} \begin{array}{l} \text{NUMBER PSQs} \} n \\ \text{NUMBER PSQs} \} 0 \end{array} \right.$

NOTE: "NUMBER OF PSQs ENABLED" reflects the number on that card. Continuation lines contain a separate count. $0 \leq n = \text{total number PSQs enabled} \leq 21$.

NOTE: $0 \leq \text{NUMBER CLOCKS CONTROLLED} \leq 25$

$$\langle \text{PINTIME} \rangle := \left\{ \langle \text{NUMERIC DATUM} \rangle \right\}_{0}^{25}$$
$$\begin{aligned} \langle \text{DATA SETUP} \rangle &:= \langle \text{TFIN} \rangle \langle \text{TERMINATOR} \rangle \left\{ \langle \text{PSQ} \rangle \right\}_0^{30} \langle \text{TERMINATOR} \rangle \\ &\quad \langle \text{MAIN LOOP} \rangle \langle \text{WATCHDOG} \rangle \left\{ \langle \text{CLOCK} \rangle \right\}_0^{25} \langle \text{TERMINATOR} \rangle \\ &\quad \left\{ \langle \text{ENVELOPE} \rangle \right\}_0^{25} \langle \text{TERMINATOR} \rangle \left\{ \langle \text{ISR} \rangle \langle \text{PINTIME} \rangle \right\}_0^{25} \\ &\quad \langle \text{TERMINATOR} \rangle \left\{ \langle \text{CLOCK FLAG} \rangle \right\}_0^{25} \langle \text{TERMINATOR} \rangle \end{aligned}$$

Channel 1 trap (C1TRPA) which takes roughly twice as long during acquisition and to the processing of GCF blocks and the message processor done by the GCFBLK and MSGPRC subprograms. Despite the MSTAT overrun, status was still completed approximately every 315 milliseconds.

During tracking the overrun of MSTAT was less severe, with an overrun only occurring 25% of the time yielding a completed module status update approximately every 130 milliseconds.

An overrun of MSTAT was not caused to any large extent by the addition of the 20-cps teletype but was caused by the increased activity of the Channel 1 trap during acquisition and the long execution time for MSGPRC and GCFBLK (approximately 120 milliseconds).

If the module status is desired more frequently than every 315 milliseconds during acquisition and every 130 milliseconds during tracking, it is suggested that the MSGPRC and GCFBLK subprograms be segmented into four smaller blocks to allow the executive to check for enabled subprograms of higher priority between segment execution.

VI. Program Usage

The program (written in ANSI FORTRAN) takes approximately 14K of memory (7K for instruction bank, 7K for data bank). See the Timing Simulation Descriptive Document (Ref. 1) for a complete description including operating instructions for the UNIVAC 1108 and the XEROX SIGMA 5, and a description of how to construct a simulation given an interrupt processing system.

Reference

1. Schwartz, R., *An Interrupt Timing Simulation*, IOM 3384-74-013, Mar. 8, 1974 (JPL internal document).

Bibliography

- Jones, V. D., "Telemetry and Command Multiple-Mission Software (Model A)," in *The Deep Space Network Progress Report*, Technical Report 32-1526, Vol. XVIII, pp. 163-166, Jet Propulsion Laboratory, Pasadena, Calif., Dec. 15, 1973.
- Schwartz, R., *Viking Remote Output Teletype Timing Analysis*, IOM 3384-74-012, Mar. 1, 1974 (JPL internal document).

```

*INPUT DATA FOR VIKING TELEMETRY AND COMMAND SIMULATION
*
*
TFIN 500000
$
*
*PSQ DURATION
-----
C2FRM 438
C1FRM 538
S1STAT 20
B1STAT 20
S2STAT 20
TMAGC 125
MSTAT 500
SSCON 500
SSCON1 663
DSGEN 250
DDCON 250
DDCON1 413
SNCAL 163
LOMSG 50
BDCON 125
BDCON1 288
C1CON 62
GCFBLK 16625
GCF2 14375
MSGPRC 13413
TYPEIN 15375
TYPMEM 50
TVER 250
$
*
MAIN 3125
WCHD6 500000
*CLKS Prio INT DUR # STRT PSQS ENABLED
-----
PPS1 10 125000 125 6 5 TMAGC SSCON DDCON BDCON C1CON MSGPRC
BITST 18 31250 725 0 16384
SYMIR 17 31250 1438 0 20290
CMAEOM 16 750000 13 0 10
* THIS IS FOR 2000 BPS
I2DDA1 11 58500 125 0 4754
I2DDA2 12 14624 125 0 5676
I1DDA1 13 58500 1200 1 9081 C2FRM
* CHANNEL 3 16000 BPS HIGH RATE
I1DDA2 14 11364 125 0 12382
PPS10 15 12500 375 1 5 MSTAT
C1TRPA 22 938 425 0 1
C1TRPT 22 938 250 0 1
C1TRP1 22 157658 10 1 204500 C1FRM
SEC30 10 3750000 10 4 3750005 SSCON1 DDCON1 BDCON1 DSGEN
+ 3
S1STAT S2STAT B1STAT
HSII 25 625 50 0 256
*
HSII6 25 625000 10 1 31526 GCFBLK
HSOI 24 625 50 0 1
* ROINT 20 CPS
ROINT 11 6250 100 0 5
$
*
*ENV INT DUR # STRT CLOCKS CONTROLLED
-----
ENV1 3625100 3625100 1 5 PPS1
ENV3 500000 157584 1 1 C1TRPA
ENV4 500000 500000 2 157600 C1TRPT HSOI
$
*
*PIN Prio DUR # PSQS ENABLED
-----
EORS 26 20 3 TYPEIN TYPMEM TVER
13767 4283230
CSU 27 100 1 GCF2
29767 6404000
$
*
*EOD

```

Fig. 1. Sample input data for Viking telemetry and command simulation

*****END OF CYCLE 500000*****																									
STACK																									
PRIORITY	NAME	STACK TIME																							
22	C1TRPT	DELTA	TOTAL																						
-1	MAIN	3107	88540																						
CLOCK																									
PRIOR	INTV	TIME	E/D	DUR.	T	START	COUNT	ENV NO.	NAME																
10	125000	124995	0	125	0	5	4	1	PPS1	1.															
18	31250	14866	0	725	0	16384	16	0	BITSRT	2.															
17	31250	10960	0	1438	0	20290	16	0	SYMIR	3.															
16	750000	499990	0	13	0	10	1	0	CMAEOW	4.															
11	58500	27246	0	125	0	4754	9	0	I2DDA1	5.															
12	14624	11732	0	125	0	5676	34	0	I2DDA2	6.															
13	58500	22919	0	1200	0	9081	9	0	I1DDA1	7.															
14	11364	10330	0	125	0	12382	43	0	I1DDA2	8.															
15	12500	12495	0	375	0	5	40	0	PPS10	9.															
22	938	45	0	425	0	1	169	2	C1TRPA	10.															
22	938	45	-1	250	45	1	365	3	C1TRPT	11.															
22	157658	137842	0	10	0	204500	2	0	C1TRP1	12.															
10	3750000	0	0	10	0	3750005	0	0	SEC30	13.															
25	625	369	0	50	0	256	800	0	HS11	14.															
25	625000	468474	0	10	0	31526	1	0	HS11G	15.															
24	625	624	0	50	0	1	547	3	HS01	16.															
11	6250	6245	0	100	0	5	80	0	ROINT	17.															
ENVELOPE DATA																									
ENV	INTERVAL	TIME	DUR	T	START	ENV	E/D																		
1.	ENV1	3825100	499994	3625100	499994	5	-1																		
2.	ENV3	500000	499998	157584	0	1	0																		
3.	ENV4	500000	342399	500000	342399	157600	-1																		
CLOCK FLAGS																									
CLK	1.	2.	3.	4.	5.	6.	7.	8.	9.	10.	11.	12.	13.	14.	15.	16.	17.	18.	19.	20.	21.	22.	23.	24.	25.
FLAG	0	0	0	0	0	0	0	0	0	0	0	0	0	0	0	0	0	0	0	0	0	0	0	0	0
STATE	0	0	0	0	0	0	0	0	0	0	0	0	0	0	0	0	0	0	0	0	0	0	0	0	0
ISR																									
PRIOR	COUNT	DUR.	T	NAME																					
26	1	20	0	EORS																					
27	1	100	0	CSU																					
PS0																									
PRIOR	E/D	COUNT	DUR.	T	NAME																				
0	0	9	438	0	C2FRM	1.																			
0	0	2	538	0	C1FRM	2.																			
0	0	0	20	0	S1STAT	3.																			
0	0	0	20	0	B1STAT	4.																			
0	0	0	20	0	S2STAT	5.																			
0	0	4	125	0	TMAGC	6.																			
0	0	25	500	0	MSTAT	7.																			
0	0	4	500	0	SSCON	8.																			
0	0	0	663	0	SSCON1	9.																			
0	0	0	250	0	DSGEN	10.																			
0	0	4	250	0	DDCON	11.																			
0	0	0	413	0	DDCON1	12.																			
0	0	0	163	0	SNCAL	13.																			
0	0	0	50	0	LOMSG	14.																			
0	0	4	125	0	BDCON	15.																			
0	0	0	288	0	BDCON1	16.																			
0	0	4	62	0	CICON	17.																			
0	0	1	16625	0	GCFBLK	18.																			
0	0	1	14375	0	GCF2	19.																			
0	0	4	13413	0	MSGPRC	20.																			
0	0	1	15375	0	TYPEIN	21.																			
0	0	1	50	0	TYPMEM	22.																			
0	0	1	250	0	TVER	23.																			
-1	0	22	3125	18	MAIN	24.																			
*****TFINAL SIGNED*****																									
SUBPROGRAM MSTAT OVERUN 37.50 % OF TIME																									
CLOCK STATISTICS																									
NAME	MEAN TIME BEFORE COMPLETION																								
PPS1	2111.																								
BITSRT	1375.																								
SYMIR	2689.																								
CMAEOW	481.																								
I2DDA1	441.																								
I2DDA2	613.																								
I1DDA1	3217.																								
I1DDA2	506.																								
PPS10	693.																								
C1TRPA	451.																								
C1TRPT	300.																								
C1TRP1	207.																								
HS11	50.																								
HS11G	41.																								
HS01	50.																								
ROINT	781.																								

Fig. 2. Sample output of Viking telemetry and command model

S-Band/X-Band Doppler Two-Way Nonlinear Jitter Analysis Using Simplified Series-Expansion Techniques

R. C. Bunce
Network Operations Office

Using a simplified nonlinear approach by Yuen together with simplified series expressions to obtain the nonlinear values for Alpha, Gamma, and Sigma, a full program was developed that outputs estimated two-way jitter in degrees as a function of ground and spacecraft signal-level margin above design point. Required modified ("hyperbolic") Bessel functions were calculated individually, rather than by recursion, with the "defining" series to reduce the error. Results were replaced by linear approximation when the series was no longer feasible, well into the "linear range." As an experiment, and to establish feasibility of the entire model, programming was done entirely on the table calculator (four card-sides; about 1700 steps).

I. Introduction

The S-band/X-band (S/X) doppler jitter experienced by DSN stations to date has been small, once hardware problems were identified and resolved. However, as signal levels decrease in the future, both spacecraft and ground margins may drop into the range where thermal noise contributions are a significant parameter. The jitter am-

plitude in this region is not well documented nor understood, because the large S/X multiplier in the spacecraft drastically alters the model from that of the S-band/S-band (S/S) case. Modified linear results were first described in Ref. 1, where an unusual "bottoming-out" of jitter at medium margins was predicted. Reference 1 did *not* use the recently established " $\frac{1}{2}$ factor" on linear σ^2 , so predicted jitter was much larger.¹ In order to deter-

¹The term "margin," as used in this analysis, is simply the ratio of signal power to the noise power in the loop at its design-point bandwidth, or $2BL_0$. By "conventional" theory (now proven obsolete), this would also be the point where linear analysis, by former criteria, would yield a variance of unity. The original program (and Ref. 1) was based on this assumption, which leads to expected jitter values larger than the data normally exhibit. New theory has demonstrated that variance at "design point," calculated by linear methods, is only one-half that formerly used, yielding a factor of $\sqrt{2}$ improvement in sigma. This latter number was subsequently incorporated into the subject program, and all results are based on it. Values are therefore somewhat less than those of Ref. 1, although direct comparison is not possible because of bandwidth differences. Results agreed, at several "check points," with those of J. H. Yuen (Ref. 2 and associated program), within 2 deg. Differences in the calculation of "GAMMA" could account for this.

mine the effects shown in Ref. 1 more accurately, a nonlinear model was subsequently written and programmed, using simplifications suggested by J. H. Yuen (Ref. 2). This paper describes the model, its derivation, and presents and discusses results. It is planned that the model will be used as the basis for S/X doppler system testing in the DSN.

II. Doppler Phase Jitter: A Definition

Doppler is a ground frequency measure yielding an estimate of the difference between the transmitted and received frequencies, the former appropriately translated and biased so that the difference can be reduced to give an estimate of spacecraft velocity (among other things).

The frequency is a cycle count (resolved to 10^{-5} cycle) divided by a counting period, with appropriate time-tag. The data are "curve-fit," and a frequency standard deviation from the curve, or "doppler frequency noise" is calculated for operational use.

Simultaneously, the entire cycle count over a sample period is cumulatively recorded, and differenced each sample period with the previous count. The difference, each sample point, is the true phase change during the period plus the sum of noise displacements at the instants of sampling. This latter figure is instantaneous doppler phase jitter (ϕ_T), and its standard deviation is the measure that the subject program estimates as a function of ground and spacecraft margin. The square of σ_T , or $(\sigma_T)^2$, is the doppler phase jitter variance, or "phase noise," a relative power with respect to the carrier.

As with frequency jitter, ϕ_T data cannot be read directly, but must be differenced from a "curve fit," since true cumulative phase is a variable with spacecraft distance. The data reduction program deals with discrete samples, which I describe here as total phase differences:

$$\hat{\phi}_n(t_n) = \{[\phi_M(t_n) - \phi_C(t_n)] - [\phi_M(t_{n-\tau}) - \phi_C(t_{n-\tau})]\} \quad (1)$$

where

$\phi_M(t_n)$ = cumulative total phase measure to t_n

$\phi_C(t_n)$ = cumulative "curve fit" total phase measure to t_n

$t_n, t_{n-\tau}$ = time to n th and $(n + \tau)$ th sample and τ = sample period

$\hat{\phi}_n(t_n)$ = the n th estimate of phase displacement from "true phase," of which ϕ_C is the cumulative estimate.

$\hat{\phi}_n$ can have other forms than Eq. (1); I show it as a sample expression only. The ground processing, however, no matter how mechanized, yields a measure of $\hat{\phi}_n(t)$ and, after appropriate processing of a large number of such samples, calculates the sigma and variance of this quantity. This is well covered in the literature, and will not be repeated here. The result as stated is $\hat{\sigma}_T$ or $(\hat{\sigma}_T)^2$, and the model developed here is to predict this parameter for S/X band (Mariner Venus/Mercury Mission) application.

III. Phase Jitter Model: General Form

Refer to Fig. 1. The final model output $\hat{\sigma}_T$ consists of two components, a fixed "system" contribution, and the X-band receiver total contribution. The latter has two components also, one of which is modified from a "linear sum" to a nonlinear form; this is a more accurate representation, particularly at small ground margins. The notations on Fig. 1 have the preliminary definitions:

$$\left. \begin{aligned} \hat{\sigma}_T^2 &= \sigma_{RT}^2 + \sigma_S^2 \\ \sigma_{RT}^2 &= (G\sigma_U^2) + (\sigma_{NL})^2 \\ \sigma_{NL}^2 &= F(\rho) \\ \rho &= 1/[\sigma_{RT}^2 + K(G\sigma_{R1})^2] \\ \sigma_U^2 &= (G\sigma_U)^2 + (G\sigma_{R1})^2 \end{aligned} \right\} \quad (2)$$

where (all σ in radians except as expressed otherwise)

$\hat{\sigma}_T^2$ = total predicted jitter variance (converted to degrees for actual program output)

σ_S^2 = composite variance of all fixed (and considered fixed) system sources, such as doppler extractor references (from standards and exciter), 1 pulse/s, counter resolver, receiver VCO residual, etc. For this model $\sigma_S = 6$ deg, which was computed earlier for the linear model.

σ_{RT} = total jitter contributed by X-band receiver

$G = 880/221$, the spacecraft X/S multiplier

σ_U = uplink jitter arising from the exciter frequency sources and multipliers. The spectrum is not well defined, but the jitter is specified as "less than 8 deg in a 3-Hz loop." This will be insignificant by comparison to thermal noise at weak signal levels. A "fixed" value of 2 deg was selected, and treated as a residual, in this

model. Since σ_U is multiplied by G , the rms total of σ_U and σ_S is about 10 deg.

σ_{NL} = composite nonlinear contribution of both receivers

$F(\rho) = \sigma_{NL}$ = function that converts the linear receiver calculations to nonlinear results

ρ = "system" signal-to-noise (S/N), as defined by J. H. Yuen (Ref. 2)

σ_{R_1} = spacecraft total receiver loop output jitter (S-band) due to "white" (gaussian) input noise

σ_{R_2} = same as σ_{R_1} , but for ground X-band receiver

K = a variable multiplier on the spacecraft noise output spectrum to account for filtering of this spectrum by the ground receiver

σ_T = "path" jitter, as present on the down-link prior to reception and filtering. It would be the ground receiver output at very strong signals, if the bandwidth was quite large and the system very low in noise.

If only strong signals were present, without significant thermal noise, this would end the model:

$$\sigma_{R_1}, \sigma_{R_2} \rightarrow 0, \quad \rho \rightarrow \infty, \quad F(\rho) \rightarrow 0$$

For the strong signal model:

$$\sigma_T = \left[\sigma_S^2 + \left(\frac{880}{221} \sigma_U \right)^2 \right]^{1/2} \approx 10 \text{ deg} \quad (3)$$

This is the lower bound for σ_T . As receiver noise contributions begin to be significant, the functions become more sophisticated, as described in the next section.

IV. Phase Jitter Model: Detailed Expressions

The functions σ_{R_1} , σ_{R_2} , K , and (finally) ρ and σ_{NL} depend on the two receiver bandwidths and noise spectral density. Assuming conventional design point definition and damping ($r_0 = 2$), as well as second-order loops containing band-pass filters and limiters (the Block IV/Mariner spacecraft mechanization), the signal levels may be expressed as a margin above design point, initially in dB, but convertible to a power ratio. For this program, the following fixed input parameters were used:

- (1) Spacecraft design point loop bandwidth = $2 BL_0$
S/C = 18 Hz.
- (2) Spacecraft predetection bandwidth = BC S/C = 5000 Hz.
- (3) Ground design point loop bandwidth = $2 BL_0$
GND = 10 Hz.
- (4) Ground predetection bandwidth = BC GND = 2000 Hz.

Although the program was designed for arbitrary bandwidth and spacecraft margin, with ground margin running from 0 to 50 dB in 2-dB steps, spacecraft margin inputs of 15, 17, 20, 25, and 40 dB were processed. Indicating any margin by the notation "dB," and using the modifier "S/C" or "GND" for spacecraft/ground receiver when necessary (as for bandwidths above), the definitions and expressions in Table 1 complete the program preliminary description.

In Table 1, the functions (4) through (10) are straightforward and together with (2) define the entire model in detail. The series (9) and (10) were not, of course, carried to an infinite number of terms; the simplified form of (9), whose integral form was determined as valid by Yuen (Ref. 2), also requires comment. It was found that (10) was accurate to better than 2×10^{-6} , for small angles at the limit of machine capability, and that (9) followed to better than 5×10^{-6} for jitter angles down to about 8 deg, where linear theory was adequate. This approach is not only simplified, but, if necessary, could be programmed easily in DSN field software. A detailed error analysis of the series in (9) and (10) is covered in Ref. 5.

V. Results and Conclusions

Program results are plotted on Fig. 2. The "dip down" in jitter at moderate signal levels, resulting from the large S/X multiplier, showed even more strongly than the analysis with linear theory (Ref. 1). This was due in part to the different input bandwidths, chosen to agree with hardware of the current mission.

The decreasing jitter with decreasing ground margin is attributed to the parameter K , which reflects the narrowing ground bandwidth. This bandwidth reduction "filters" the spacecraft noise, but little ground noise is generated "by comparison." The jitter eventually "bottoms out," then climbs rapidly near design point as the ground noise becomes significant.

It is evident that tracking will be impossible when the spacecraft margin drops below 20 dB, for jitter will never reach tracking levels. Meanwhile, expect jitter levels to improve before they get worse; a rather new phenomenon.

Parameters from Ref. 6 were also programmed (favored values) to confirm results of that memo. Spacecraft margin of 36.3 dB and ground $2 BL_0$ of 3 Hz ($BC = 200$ Hz) were entered, and the X-band receiver jitter at a ground margin of 36.6 dB was interpolated. The input numbers agree with expected conditions when the

100-kW transmitter is used, together with aided tracking (3-Hz loop) on the ground, as covered in Ref. 6. The result, also shown on Fig. 2 (designated point), was 2.88 deg, even below that of the predicted value of 4 deg.

All results shown in Fig. 2 are without residual contribution. If σ_U is set at 2 deg, and the 6 deg of σ_s is also contributed, a minimum residual of about 10 deg occurs, of which 6 deg is "outside" the loop. An expression for adding these contributions to σ_{NL} is given in Fig. 2, resulting in the total expected jitter.

References

1. Bunce, R. C., *S-Band/X-Band Two-Way Doppler Jitter*, IOM 421E-74-073, Apr. 4, 1974 (JPL internal document).
2. Yuen, J. H., *On Coherent Two-Way Doppler Phase Probability Distribution*, IOM 3395-72-81, June 27, 1972 (JPL internal document).
3. Lindsey, W. C., and Simon, M. K., *Telecommunication Systems Engineering*, Prentice-Hall, Inc., Englewood Cliffs, N. J., 1973.
4. *Standard Math Tables*, Edition 17, Chemical Rubber Co., Cleveland, Ohio, 1969.
5. Bunce, R. C., *S-Band/X-Band Two-Way Doppler Jitter, Non-Linear Model*, IOM 421E-74-085, Apr. 26, 1974 (JPL internal document).
6. Brunn, L., *Doppler Phase and Ranging Performance at M_e Using the 100 KW Transmitter*, IOM 3396-73-300, Oct. 22, 1973 (JPL internal document).

Table 1. Detailed expressions for S/X doppler jitter

$$\left. \begin{aligned} |\text{margin}| = M &= 10^{(\text{dB}/10)} & G &= 880/221 \\ \text{predetection S/N ratio} &= A = (2 BL_o/BC) \cdot M \\ A_o &= (2 BL_o/BC) \\ \text{design point loop bandwidth ratio} &= \xi = (2 BL_o S/C)/(2 BL_o \text{ GND}) \end{aligned} \right\} \quad (4)$$

$$\left. \begin{aligned} \text{jitter variance} \\ \text{(either receiver)} \end{aligned} \right\} = \sigma_k^2 = \frac{1}{2M} \left[\frac{1}{3} + \frac{2}{3} \frac{\alpha}{\alpha_o} \right] \Gamma_p \quad (5)$$

$$\left. \begin{aligned} \alpha(A) &= \sqrt{\frac{\pi}{4}} A e^{-A/2} \left[I_0\left(\frac{A}{2}\right) + I_1\left(\frac{A}{2}\right) \right] \\ \alpha_o &= \alpha(A_o) \quad (\text{Ref. 3, p. 50}) \end{aligned} \right\} \quad (6)$$

$$\left. \begin{aligned} \Gamma_p(A) &= \frac{1 - e^{-A}}{\frac{\pi}{4} A e^{-A} \left[I_0\left(\frac{A}{2}\right) + I_1\left(\frac{A}{2}\right) \right]^2 \left[1 + \left(\frac{3.448}{\pi} - 1 \right) \exp \left[-A \left(1 - \frac{\pi}{4} \right) \right] \right]} \\ & \quad (\text{Ref. 3, p. 52; inexact}) \end{aligned} \right\} \quad (7)$$

Solving yields:

$$\left. \begin{aligned} K\sigma_{k_1}^2 &= \frac{1}{4\pi M} \int_{-\infty}^{\infty} |H_1(j\omega) H_2(j\omega)|^2 d\omega \\ H_1(s), H_2(s) &= S/C, \text{ GND loop transfer functions} \\ K &= \left[\frac{K_1}{2 + K_1} \right] \left[\frac{K_1(2 + K_1) + 2(K_1 + K_2 + 2)(\xi + \xi^2) + K_2(2 + K_2)\xi^3}{K_1^2 + 2K_1\xi + 2(K_1 + K_2 - 2K_1K_2)\xi^2 + 2K_2\xi^3 + K_2^2\xi^4} \right] \\ K_1 &= [\alpha_o/\alpha] S/C \quad K_2 = [\alpha_o/\alpha] \text{ GND} \quad (\text{Ref. 3, p. 100}) \end{aligned} \right\} \quad (8)$$

$$\left. \begin{aligned} \sigma_{NL} &= \frac{1}{2\pi} \int_{-\pi}^{\pi} \phi^2 \frac{\exp[\rho \cos \phi]}{I_0(\rho)} d\phi \quad (\text{modulo } 2\pi) \\ & \quad \{ \rho = 1/[\sigma_{k_1}^2 + K(G\sigma_{R_2})^2] \} \\ &= \frac{\pi^2}{3} + 4 \sum_{N=1}^{\infty} (-1)^N \cdot \frac{1}{N^2} \cdot \frac{I_N(\rho)}{I_0(\rho)} \quad (\text{Ref. 2}) \end{aligned} \right\} \quad (9)$$

$$\left. \begin{aligned} I_N(x) &= \left(\frac{x}{2} \right)^N \sum_{M=0}^{\infty} \frac{\left(\frac{x}{2} \right)^{2M}}{(M)!(M+N)!} \\ & \quad (\text{Ref. 4; defining series for } I_N(x)) \end{aligned} \right\} \quad (10)$$

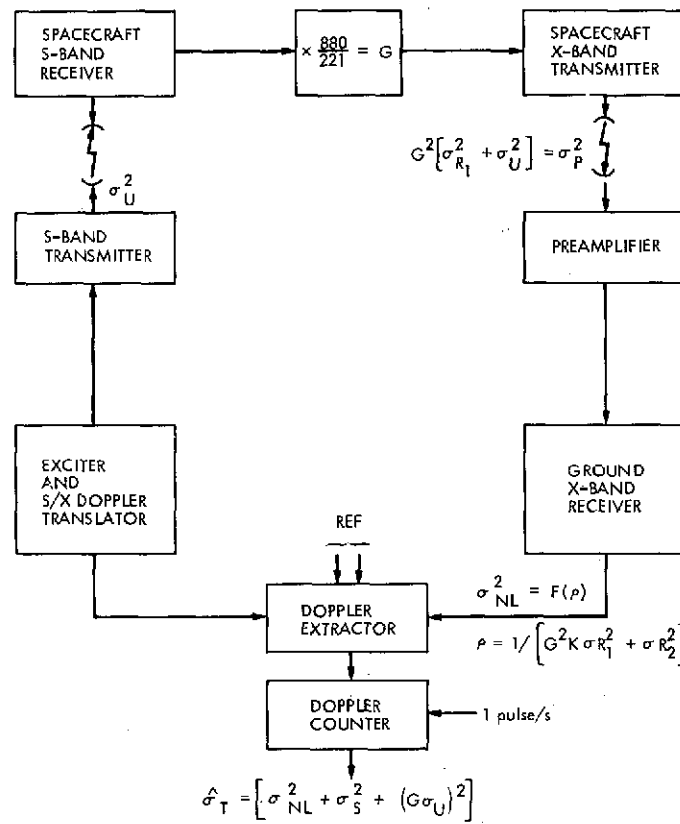


Fig. 1. S/X two-way doppler model diagram

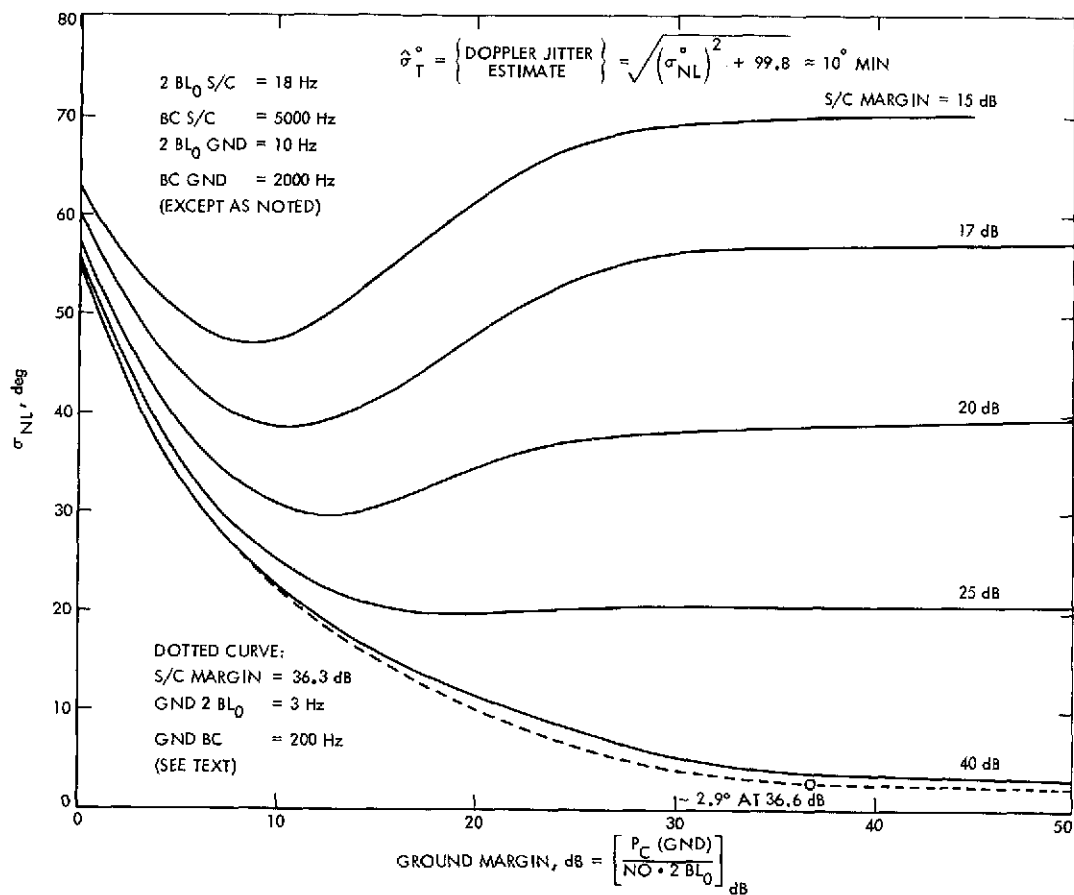


Fig. 2. Ground X-band receiver output jitter, degrees (nonlinear) vs ground and spacecraft margin

A Re-Examination of the AGC Calibration Procedure

G. L. Stevens
Network Operations

In this article a re-examination of automatic gain control (AGC) calibration errors was made to determine if an improvement in reported spacecraft carrier power could be obtained by modifying the signal level tracking calibration procedure. The calibration errors (as a function of the number of independently obtained calibration points) were evaluated to determine if a new AGC calibration procedure using 15 independent calibration points should be adopted. Results of this study indicate that the improvement in calibration accuracy is insignificant and would not warrant a new calibration procedure requiring considerably more time and effort.

I. Introduction

At present, DSN Standard Test Procedure No. 853-51 4A-07 Rev. B is used to calibrate the receiver automatic gain control (AGC) voltage vs the received carrier power so that the digital instrumentation subsystem (DIS), telemetry and command processor (TCP), and the voice report all yield an accurate estimation of the received spacecraft carrier power. Fifteen power-level/AGC voltage pairs covering a 30-dB range are used in the calibration. The test transmitter output signal level is adjusted for the desired calibration levels using the Y-factor method.

The Y-factor detector assembly is used to adjust signal levels for only five of the 15 calibration points. After a

given Y-factor is set, the AGC voltage is measured with the integrating digital voltmeter. Then, the next two calibration signal levels are created by incrementing the test transmitter step attenuator (10 dB per step). This technique produces three calibration points for each of the five Y-factors, representing a significant saving in time and effort. This technique has the disadvantage that the signal level error associated with each Y-factor will bias three of the 15 calibration points in the same direction. Certainly there would be an improvement in the AGC calibration accuracy if 15 uncorrelated calibration points were obtained by using 15 independent Y-factors. The purpose of this study was to determine whether the degree of improvement in calibration accuracy would warrant changing the new signal level calibration procedure (Ref. 1).

II. Method of Evaluation

The method used to determine the AGC calibration errors (as a function of the number of independent Y-factors used) is an extension of an approach by Lesh (Ref. 2). I refer the reader to this article for background material and definitions, instead of duplicating that work here.

To incorporate the effects of Y-factor errors on the calibration accuracy, it is necessary to modify the covariance matrix of the coefficient estimation error G . The covariance matrix is used with the expression

$$E \left\{ \frac{(y - \hat{y})^2}{x} \right\} = g_{11} + 2g_{12}x + [2g_{13} + g_{22}]x^2 + 2[g_{23} + g_{14}]x^3 + [2g_{24} + g_{33}]x^4 + 2g_{34}x^5 + g_{44}x^6 \quad (1)$$

to calculate the mean square error between the fitted third-degree equation and the "ideal" third-degree model.

The covariance matrix calculation involves a column vector α whose elements are the signal power errors as mapped from the noisy AGC voltage through the third-degree polynomial. It is necessary to add another column vector whose elements are the errors in the test transmitter signal level. Major factors contributing to the errors in the test transmitter signal levels include (Ref. 3):

- (1) The resettability and nonlinearity of the AIL precision attenuator in the Y-factor detector assembly.
- (2) The operator's ability to "eyeball average" the strip chart recorder trace and to duplicate that average by adjusting the test transmitter output level.
- (3) The test transmitter CW power stability during the Y-factor measurement.
- (4) Errors in the system parameters which are incorporated in the Y-factor calculations (Ref. 4). These parameters include system operating temperature, test transmitter reference step attenuator (PAD) value, and the Y-factor detector assembly uncorrected filter bandwidth and gain factor. These four parameters are periodically measured to verify/re-establish their values.

The total error in each Y-factor will result in a test transmitter signal level error at each of the 15 calibration points. It is assumed that the calibration signal level

error is a zero mean gaussian random variable. These signal power errors are arranged in a column vector:

$$\beta = \begin{bmatrix} \beta_1 \\ \beta_2 \\ \vdots \\ \beta_{15} \end{bmatrix} \quad (2)$$

It is assumed that the signal power errors resulting from independent applications of Y-factors will be uncorrelated and we can say

$$E \{ \beta_i \beta_j \} = 0 \quad (3)$$

for i, j belonging to different Y-factors. Now that we have defined the vector β and given the vector α we can compute

$$E \{ [\alpha + \beta][\alpha + \beta]^T \} \quad (4)$$

Expanding this term we get

$$E \{ [\alpha + \beta][\alpha + \beta]^T \} = E \{ \alpha \alpha^T \} + E \{ \alpha \beta^T \} + E \{ \alpha^T \beta \} + E \{ \beta \beta^T \} \quad (5)$$

where the elements of the matrix $E \{ \alpha \alpha^T \}$ have the values

$$E \{ \alpha_i \alpha_j \} = (a_2 + 3a_3 x_i)(a_2 + 3a_3 x_j) \sigma_i^2 \sigma_j^2 \quad (6)$$

for $i \neq j$, and for $i = j$,

$$E \{ \alpha_i^2 \} = (a_1 + 2a_2 x_i + 3a_3 x_i^2)^2 \sigma_i^2 + 3[(a_2 + 3a_3 x_i)^2 + 2a_3(a_1 + 2a_2 x_i + 3a_3 x_i^2)](\sigma_i^2)^2 + 15a_3^2(\sigma_i^2)^2 \quad (7)$$

Let us define the matrix $C = [C_{ij}]$; $i, j = 1, 2, \dots, 15$, where

$$C_{ij} = E \{ \alpha_i \alpha_j \} \quad (8)$$

Expanding the second term in Eq. (4) gives

$$E \{ \alpha \beta^T \} = E \begin{bmatrix} \alpha_1 \beta_1 & \alpha_1 \beta_2 & \cdots & \alpha_1 \beta_{15} \\ \alpha_2 \beta_1 & \alpha_2 \beta_2 & \cdots & \alpha_2 \beta_{15} \\ \vdots & \vdots & \ddots & \vdots \\ \alpha_{15} \beta_1 & \alpha_{15} \beta_2 & \cdots & \alpha_{15} \beta_{15} \end{bmatrix} \quad (9)$$

We can say that

$$E \{ \alpha \beta^T \} = 0 \quad (10)$$

since every element of the matrix $E \{ \alpha \beta^T \}$ is equal to the expected value of the product of two independent random variables, one of which is zero mean.

Looking at the third term of Eq. (4) we can see that

$$E \{ \alpha^T \beta \} = 0 \quad (11)$$

for the same reason as above.

Expanding the fourth term of Eq. (4) gives

$$E \{ \beta \beta^T \} = E \begin{bmatrix} \beta_1^2 & \beta_1 \beta_2 & \beta_1 \beta_3 & \cdots & \beta_1 \beta_{15} \\ \beta_2 \beta_1 & \beta_2^2 & \beta_2 \beta_3 & \cdots & \beta_2 \beta_{15} \\ \beta_3 \beta_1 & \beta_3 \beta_2 & \beta_3^2 & \cdots & \beta_3 \beta_{15} \\ \vdots & \vdots & \vdots & \ddots & \vdots \\ \beta_{15} \beta_1 & \beta_{15} \beta_2 & \beta_{15} \beta_3 & \cdots & \beta_{15}^2 \end{bmatrix} \quad (12)$$

Let us first consider the case where we have 15 independent β 's, i.e., a calibration procedure using 15 independent Y-factors. For those elements where $i \neq j$

$$E \{ \beta_i \beta_j \} = 0 \quad (13)$$

because those elements are the expected values of the products of uncorrelated zero-mean random variables.

For the elements on the principal diagonal ($i = j$)

$$E \{ \beta_i^2 \} = \sigma_i^2 \quad (14)$$

where σ_i^2 is the variance of the signal power error produced by the i th Y-factor.

If we define the matrix $D = [D_{ij}]$; $i, j = 1, 2, \dots, 15$, where

$$D_{ij} = E \{ \beta_i \beta_j \} \quad (15)$$

then the final form of the covariance matrix for 15 independent Y-factors is

$$G = (X^T X)^{-1} X^T (C + D) X (X^T X)^{-1} \quad (16)$$

Now consider the case where we have only five independent values for β and each value is triply used such that

$$\beta_i = \beta_{i+5} = \beta_{i+10}$$

and

$$\beta_j = \beta_{j+5} = \beta_{j+10}$$

for $i, j = 1, 2, 3, 4, 5$. This yields no change in the first three terms of Eq. (4). The fourth term, however, is no longer a diagonal matrix. Correlation between signal power errors results in some additional nonzero elements in this matrix.

Consider the elements

$$E \{ \beta_i \beta_j \} \quad i, j = 1, 2, 3, 4, 5$$

of the matrix $E \{ \beta \beta^T \}$ whose elements are

For $|i - j| = 0, 5, 10$

$$E \{ \beta_i \beta_j \} = E \{ \beta_i^2 \} = \sigma_i^2 \quad r = 1, 2, 3, 4, 5$$

$$\text{and } \sigma_r^2 = \sigma_{r+5}^2 = \sigma_{r+10}^2 \quad (17)$$

For $|i - j| \neq 0, 5, 10$

$$E \{ \beta_i \beta_j \} = E \{ \beta_i \} E \{ \beta_j \} = 0 \quad (18)$$

If we define the matrix $D^* = [D_{ij}^*]$; $i, j = 1, 2, \dots, 15$

$$D_{ij}^* = E \{ \beta_i \beta_j \} \quad (19)$$

then the final form of the covariance matrix for five independent Y-factors is

$$G = (X^T X)^{-1} X^T (C + D^*) X (X^T X)^{-1} \quad (20)$$

III. Calculations

An existing FORTRAN computer program was modified to include the calibration errors introduced by the Y-factor method. To determine the DIS computer calibration errors, calibration data from five stations were compiled. Each data set consisted of 15 signal power/AGC voltage pairs as well as the variance for each value of voltage.

It was desired to evaluate the degree of improvement in calibration accuracy which would result from setting up 15 instead of five independent Y-factors. The quantity which best indicates the calibration accuracy is the integral mean square error defined by:

$$I = \frac{1}{x_u - x_v} \int_{x_v}^{x_u} E \{ (y - \hat{y})^2 / x \} dx \quad (21)$$

This quantity represents an averaged value for the calibration error over the 30-dB calibration range. It was computed for each of the five stations, using Y-factor rms errors of 0.0 dB, 0.3 dB, and 1.0 dB. These five data sets were averaged and then the integral root mean square calibration errors (in dB) were calculated and recorded in Table 1.

IV. Conclusion

The purpose of this study was to determine if a significant improvement in the AGC calibration accuracy could be obtained by increasing the number of independent Y-factors used in the calibration procedure from five to 15. Using 15 independent Y-factors, the theoretical decrease in the standard deviation of the DIS estimation error is on the order of 0.002 dB, given a Y-factor rms error of 0.3 dB. For a Y-factor rms error of 1.0 dB, the decrease in the standard deviation of the DIS estimation error is about 0.008 dB.

This small theoretical improvement in the DIS calibration accuracy is insignificant. Also, the time requirement for the calibration would be considerably greater if 15 independent Y-factors were used.

References

1. *Signal Level Tracking Procedure*, DSIF Standard Test Procedure 853-51 4A-07, Rev. B. Jet Propulsion Laboratory, Pasadena, Calif., July 1, 1973 (an internal document).
2. Lesh, J., "Carrier Power Estimation Accuracy," in *The Deep Space Network Progress Report*, Technical Report 32-1526, Vol. IX, pp. 207-217, Jet Propulsion Laboratory, Pasadena, Calif., June 15, 1972.
3. Stelzried, C. T., *Precision Power Measurements of Spacecraft CW Signal Power With Microwave Noise Standards*, Technical Report 32-1066, pp. 2-15. Jet Propulsion Laboratory, Pasadena, Calif., Feb. 15, 1968.
4. *Y-Factor Computer Program DOI-5343-SP-B, DSIF Support Program*. Jet Propulsion Laboratory, Pasadena, Calif., Sept. 9, 1972 (an internal document).

Table 1. Comparison of integral root mean square calibration errors (in dB) as a function of the number of independent Y-factors set up in the calibration procedure (degree of curve fit = 3; $-132 \text{ dBm} \geq P_s \geq -160 \text{ dBm}$)

Number of independent Y-factors	Y-factor rms error = 0.0dB		Y-factor rms error = 0.3dB		Y-factor rms error = 1.0dB	
15 independent Y-factors	0.0129	Narrow AGC BW	0.145	Narrow AGC BW	0.480	Narrow AGC BW
	0.0270	Medium AGC BW	0.147	Medium AGC BW	0.481	Medium AGC BW
	0.0312	Wide AGC BW	0.147	Wide AGC BW	0.481	Wide AGC BW
5 independent Y-factors (used to generate 15 calibration points) ^a	0.0129	Narrow AGC BW	0.147	Narrow AGC BW	0.487	Narrow AGC BW
	0.0270	Medium AGC BW	0.148	Medium AGC BW	0.488	Medium AGC BW
	0.0312	Wide AGC BW	0.149	Wide AGC BW	0.489	Wide AGC BW

^aPresent method of calibration.

Tracking Operations During the Mariner 10 Mercury Encounter

A. L. Berman and G. L. Spradlin
Network Operations Office

Tracking operations during the Mariner 10 Mercury encounter were quite smooth and highly successful. Contributing factors included a lack of any substantial Mercurian atmosphere and, hence, signal refraction, relatively small gravitational perturbation of the spacecraft by Mercury, and a great deal more experience with the Block IV S- and X-band receivers and the digitally controlled oscillators. This report describes the pre-encounter planning and subsequent analysis of tracking operations during the Mariner 10 Mercury encounter phase.

I. Introduction

On March 29, 1974, at 20:46:31.9 GMT (spacecraft time), the Mariner 10 spacecraft reached closest approach to the planet Mercury. This encounter was simultaneously visible to both the Goldstone and the Australian complexes, thus allowing prime participation by two 64-meter Deep Space Stations (DSSs)—DSS 14 and DSS 43. A successful Mercury encounter was the foremost goal of the Mariner Venus/Mercury mission, and was the focal point of intense interest since it would be the first “close-up” examination of the heretofore little-known planet Mercury. Significant configuration at the DSS during Mercury encounter included the Block IV S- and X-band receivers at DSS 14 and the digitally controlled oscillators (DCOs) and open-loop receivers at both DSS 14 and DSS 43. A combination of circumstances resulted in this encounter being relatively uncomplicated from a tracking operations standpoint, these being:

- (1) Mercury has essentially no atmosphere, thereby greatly reducing the signal refraction and the corresponding uncertainties in the doppler at, and times of, enter and exit occultation.
- (2) The mass of Mercury is relatively small, thereby inducing only a small perturbation in the near-encounter doppler.
- (3) Although the Block IV receivers and the DCOs were relatively new, considerable operational experience with them had been obtained in the previous 4-6 months, and especially during the critical Jupiter and Venus encounter phases (see Refs. 1 and 2).

The above augured well for generally successful tracking operations during the Mercury encounter, and, indeed, this was the case.

II. Uplink Tuning Strategy

The initial uplink strategy chosen by the Radio Science/Occultation Team was to have the spacecraft in the two-way mode at both enter and exit occultations. More specifically, it was hoped that acquisition of the uplink at exit occultation could be effected within 2 seconds of the actual spacecraft emergence. The only possible way to accomplish this goal would be to hit the spacecraft receiver with (very close to) the receiver best lock frequency (which with doppler accounted for = XA) at the time of emergence. Factored into the probability of success of this attempt were the uncertainties in doppler at, and time of, emergence and uncertainty in the spacecraft nominal (no doppler) best lock frequency. Additional spacecraft receiver data received and analyzed by the Radio Science/Occultation Team at approximately encounter minus 24 hours indicated substantial possibility that the uplink acquisition plan at emergence would not succeed, and therefore an uplink acquisition "insurance" sweep, which had been proposed some weeks earlier by the DSN Network Operations Analysis Group, was adopted and scheduled at approximately exit occultation plus 7 minutes. The final uplink tuning strategy, seen in Fig. 1, was as follows:

- (1) Spacecraft to enter occultation in the two-way mode with ground transmitted frequency (TSF) to be equal to predicted XA at enter occultation.
- (2) During occultation, ground transmitter to be snapped to a TSF equal to predicted XA of exit occultation.
- (3) Approximately 7 minutes after exit occultation, the ground transmitter to be swept approximately ± 45 Hz (at VCO level) about predicted XA.

The effects of uplink tuning as seen in the downlink two-way doppler are presented in Fig. 2. The values used for enter and exit transmitted frequency (= predicted XA) were, respectively:

$$(XA_P)_{EN} = 22.0161180 \text{ MHz}$$

$$(XA_P)_{EX} = 22.0160820 \text{ MHz}$$

Analysis of Probe Ephemeris Tape (PET) N802 ("best" post-encounter PET) shows the actual XAs to be:

$$(XA_A)_{EN} = 22.0161197 \text{ MHz}$$

$$(XA_A)_{EX} = 22.0160813 \text{ MHz}$$

yielding a difference between transmitted and actual (trajectory difference only) of:

$$\Delta XA_{EN} = (XA_A - XA_P)_{EN} = +1.7 \text{ Hz}$$

$$\Delta XA_{EX} = (XA_A - XA_P)_{EX} = -0.7 \text{ Hz}$$

Based on the above (trajectory) differences, one would expect that the attempt to acquire the uplink quickly and without tuning would have a high probability of success. The best trajectory estimates of the occultation times (PET N802) were:

$$\text{Enter occultation} = 20:56:12 \text{ GMT}$$

$$\text{Exit occultation} = 21:07:33 \text{ GMT}$$

Substantiating the above are the event times as recorded by the open-loop receivers (and supplied by Dr. A. Kliore, Section 391):

$$\text{Enter occultation} = 20:56:11.69 \text{ GMT}$$

$$\text{Exit occultation} = 21:07:33.03 \text{ GMT}$$

$$\text{One-way/two-way transition} = 21:07:43.55 \text{ GMT}$$

It is therefore concluded that the uplink was acquired approximately $10\frac{1}{2}$ seconds after emergence of the spacecraft. Although this acquisition time exceeded the goal of a 2-second acquisition considerably, it very adequately fulfilled the broader goal of locking the uplink quickly and without tuning.

III. Accuracy of Pre-encounter Orbit Determination Solutions as Regards Tracking Operations Planning

Because of the planned attempt to acquire the uplink at exit occultation without tuning, it was particularly desirable to know the enter and exit occultation XAs to the highest degree possible. Figures 3 and 4, respectively, show the enter and exit occultation XAs versus time. The various PETs shown were received over the last several weeks prior to encounter and in the following chronological order:

PET Number C180

C496

C617

C618 {actually used for the encounter}

N802 {"best" post-encounter solution}

In Ref. 2, it was suggested that the practice of holding off the selection of final critical phase tracking operations parameters (event times and frequencies) until a final orbit determination solution is received in the last hours before an encounter is unwarranted and risks operational errors due to hasty implementation. Similarly these data substantiate that conclusion as there is no clear-cut progression in accuracy (to the actual) among the PETs received.

IV. Ground Receiver Operations at Exit Occultation

As in the two previous critical phase encounters (Pioneer 10-Jupiter and Mariner Venus/Mercury-Venus; see Refs. 1 and 2), it was decided that the DCOs would be used in the ACQUISITION MODE (ACQ MODE). The sweep rate selected was ± 1000 hertz/second (S-band), in combination with the following:

Tracking loop bandwidth = 152 Hz (Block III)
 100 Hz (Block IV)
Sweep range = ± 2000 Hz (DSS 14, S-band)
 ± 3000 Hz (DSS 43, S-band)

At both stations the Block III backup receiver was swept for one-way, while all other receivers were swept for two-way (DSS 14) or three-way (DSS 43). During the approximately $10\frac{1}{2}$ seconds of one-way data following exit occultation and prior to uplink acquisition, neither backup Block III receiver locked (note that these data were recorded on the open-loop receivers). However, both prime S-band receivers at DSS 14 and DSS 43 locked to the two-way (DSS 14) or three-way (DSS 43) downlink at the very first time possible. Figures 5 and 6 show the exit occultation acquisitions for DSS 14 and DSS 43, respectively. As can be seen in each case, ground receiver lock was achieved at the very first zero (predicted doppler) crossing after the two-way/three-way downlink signal appearance (21:07:43.55 GMT). One interesting point of note is that the receiver VCO stays shorted continuously during the ACQ MODE on the Block IV receiver, but drifts during the ACQ MODE on the Block III receiver; this is clearly seen in Fig. 5

(Block IV) versus that seen in Fig. 6 (Block III). The linear drift seen in Fig. 5 is that due to doppler.

V. Summary of Key Spacecraft and Ground Events at the DSS During the Mercury Encounter Phase

Table 1 provides a summary of important spacecraft and DSS events (all in ground received time) during the Mercury encounter occultation phase.

VI. Summary of Tracking Operations During the Mercury Encounter Phase

Tracking operations during Mercury encounter were extremely smooth and resulted in a highly successful encounter. Factors which simplified and contributed to the success of tracking operations were:

- (1) Lack of any substantial Mercurian atmosphere.
- (2) Small gravitational effect of Mercury on the spacecraft.
- (3) Far greater experience with the DCOs and Block IV S- and X-band receiver operations than in the previous planetary encounters.

The most difficult operation was the attempt to acquire the uplink almost immediately upon exit with no tuning, and, although the most optimally desired goal of a 2-second or less acquisition was not met, the broader goal of a very rapid acquisition of the uplink with no tuning was very soundly fulfilled.

References

1. Berman, A. L., "Tracking Operations During the Pioneer 10 Encounter," in *The Deep Space Network Progress Report 42-20*, pp. 190-195, Jet Propulsion Laboratory, Pasadena, Calif., Apr. 15, 1974.
2. Berman, A. L., and Spradlin, G. L., "Tracking Operations During the Mariner 10 Venus Encounter," in *The Deep Space Network Progress Report 42-21*, pp. 95-107, Jet Propulsion Laboratory, Pasadena, Calif., June 15, 1974.

Table 1. Spacecraft and DSS events during Mercury encounter occultation phase

Event	Ground received time (Mar. 29, 1974), GMT
Enter occultation	20:56:11.69
DSS 43 drop lock	20:56:12
DSS 14 S-band Block IV drop lock	20:56:12
DSS 14 X-band Block IV drop lock	20:56:12
Exit occultation one-way	21:07:33.03
Downlink one-way to two-way	21:07:43.55
DSS 43 acquire downlink	21:07:46
DSS 14 S-band Block IV acquire downlink	21:07:46
DSS 14 X-band Block IV acquire downlink	21:09:56

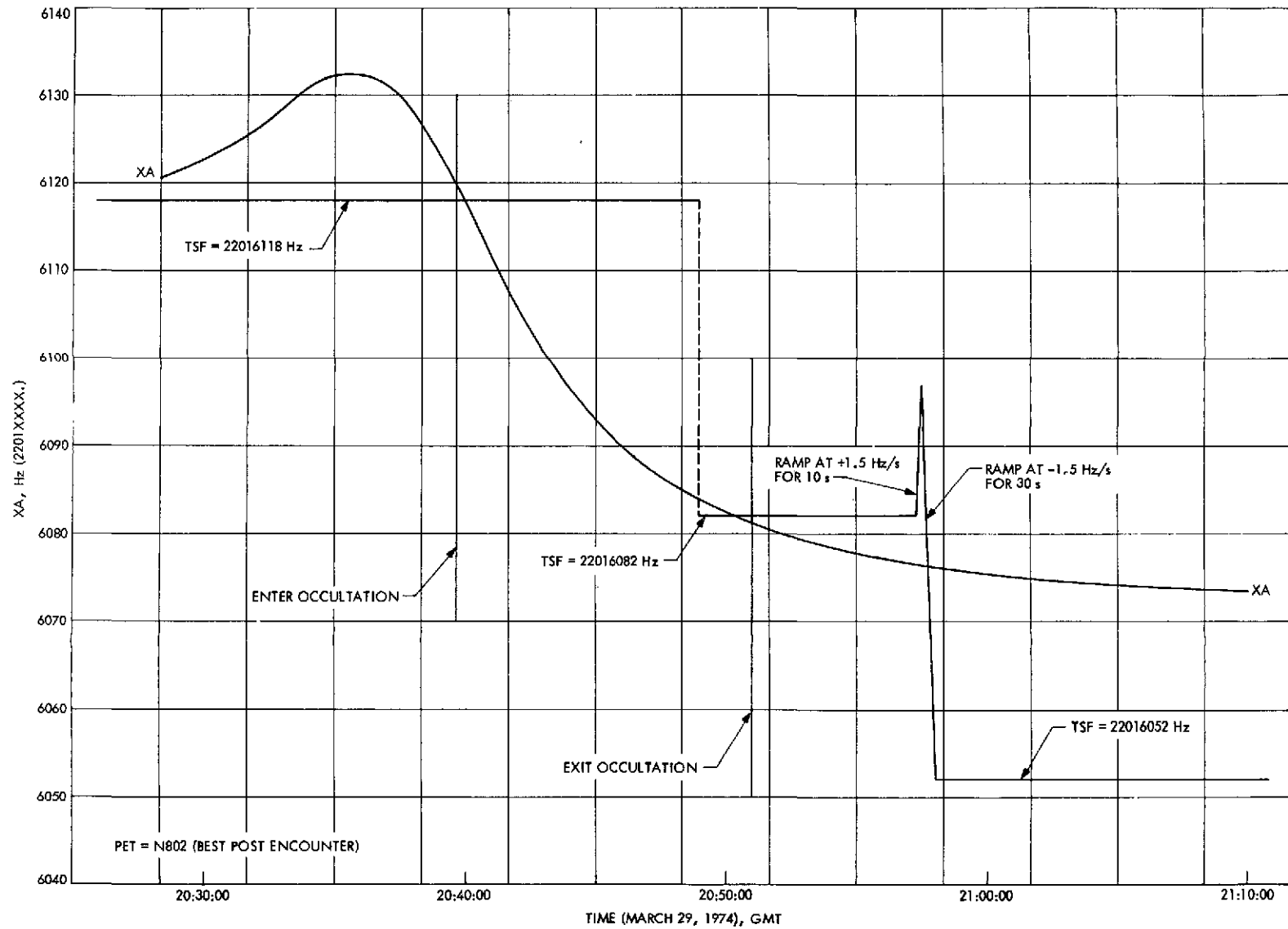


Fig. 1. XA and exciter tuning pattern for Mercury encounter (DSS 14)

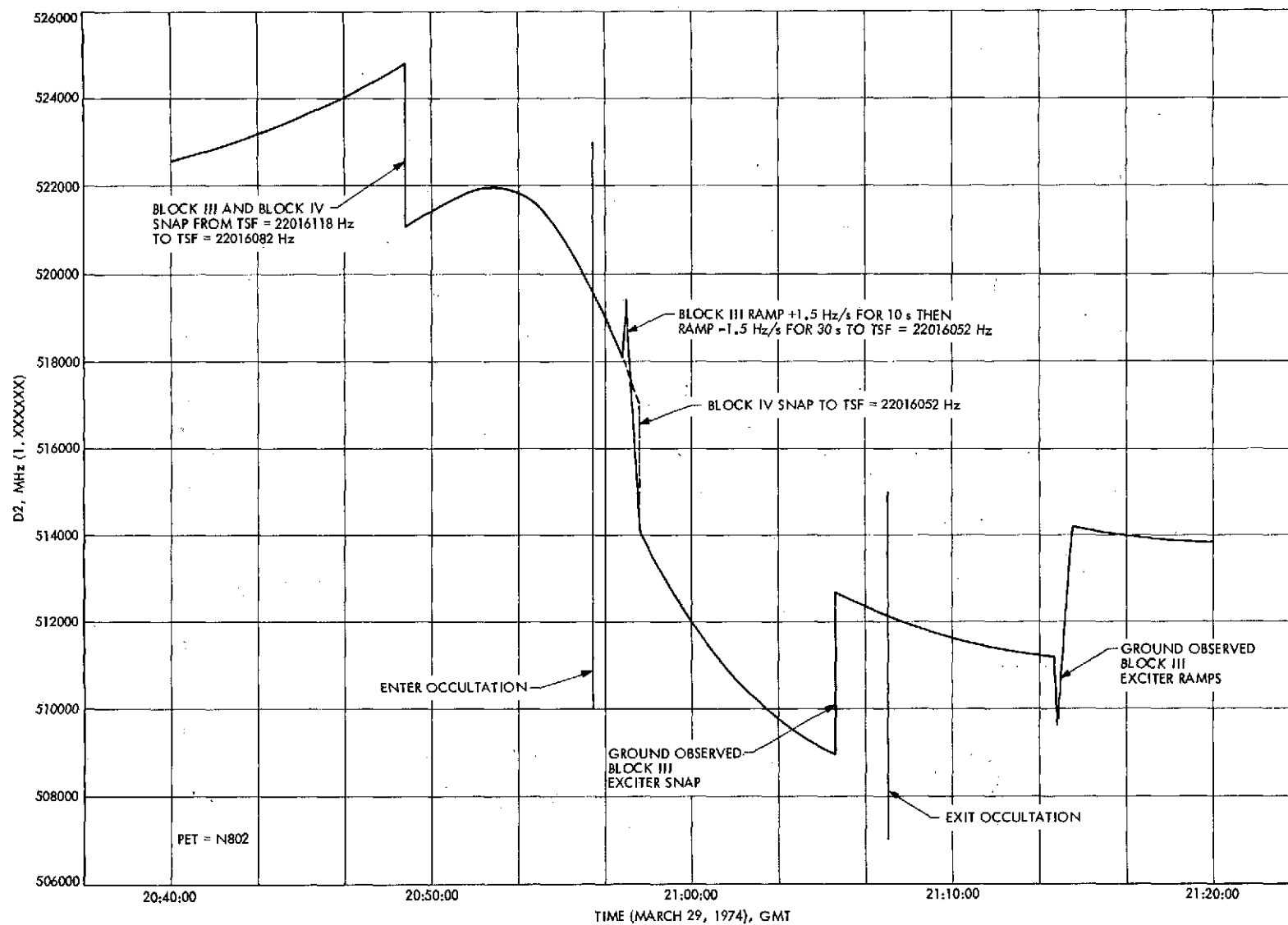


Fig. 2. S-band D2 at Mercury encounter (DSS 14)

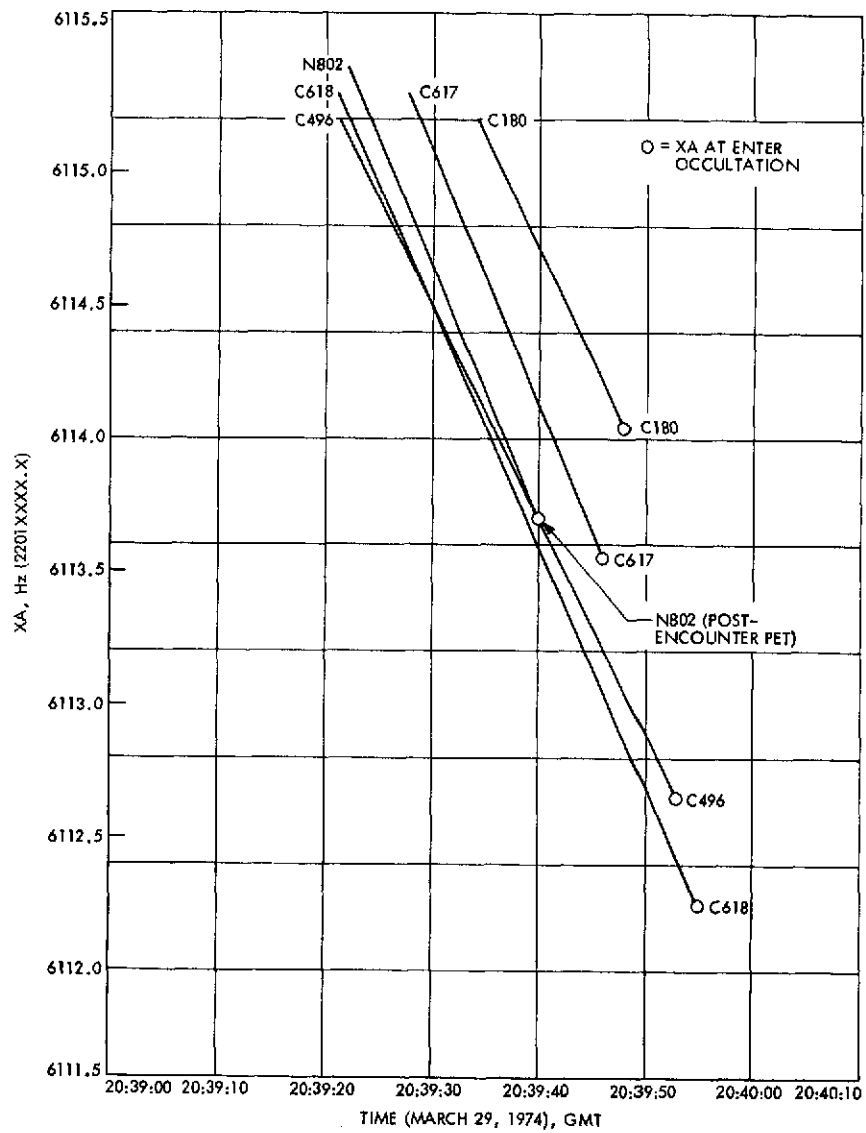


Fig. 3. Enter occultation XA for pre-Mercury encounter orbital solutions

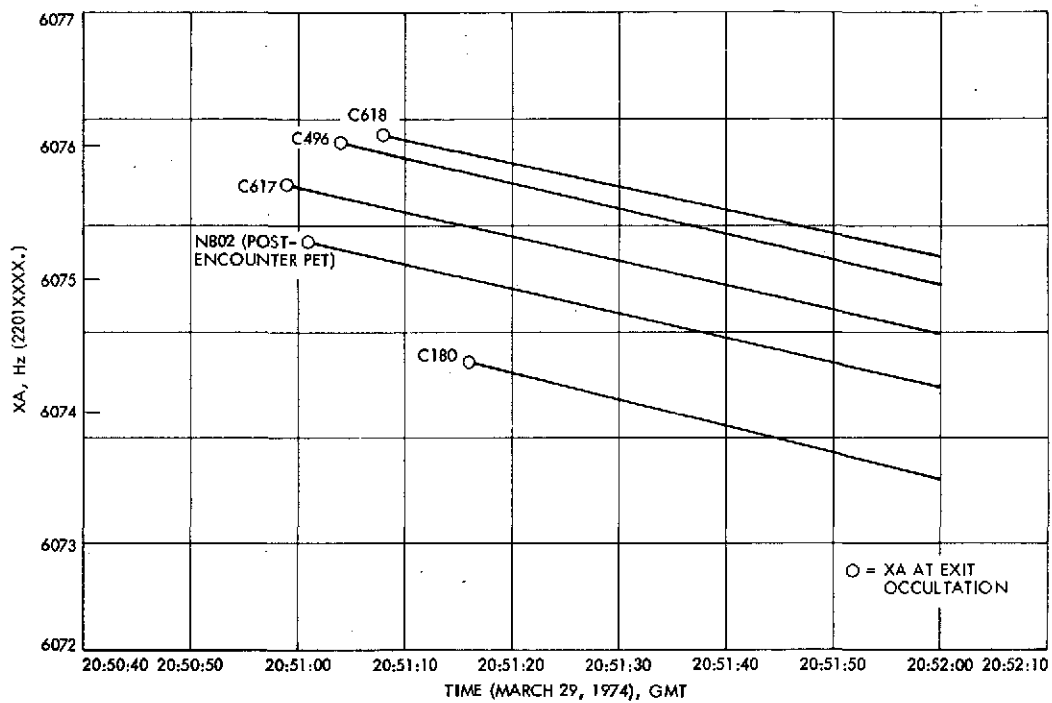


Fig. 4. Exit occultation XA for pre-Mercury encounter orbital solutions

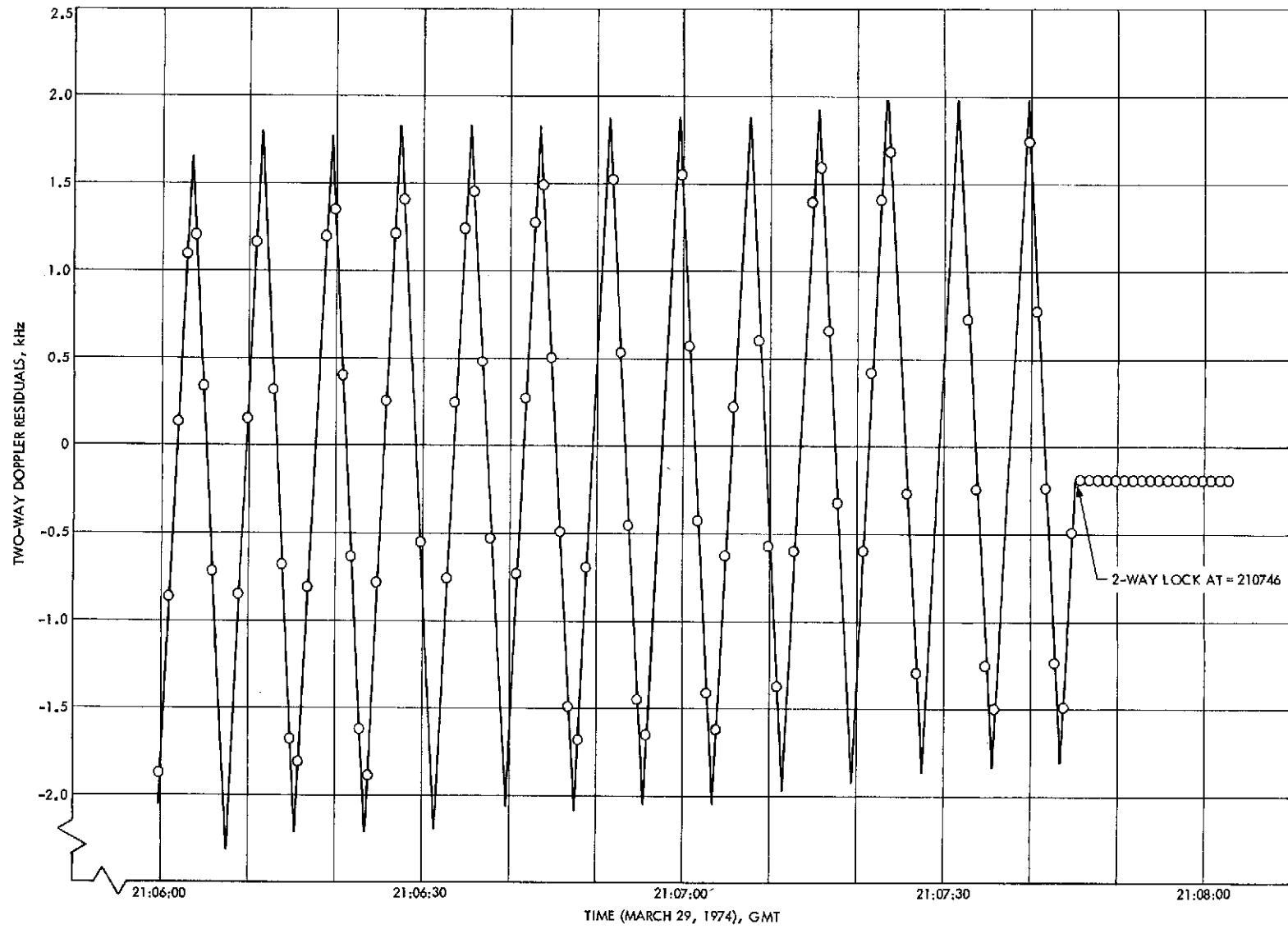


Fig. 5. Acquisition tuning pattern for Mercury exit occultation (DSS 14 Block IV S-band receiver)

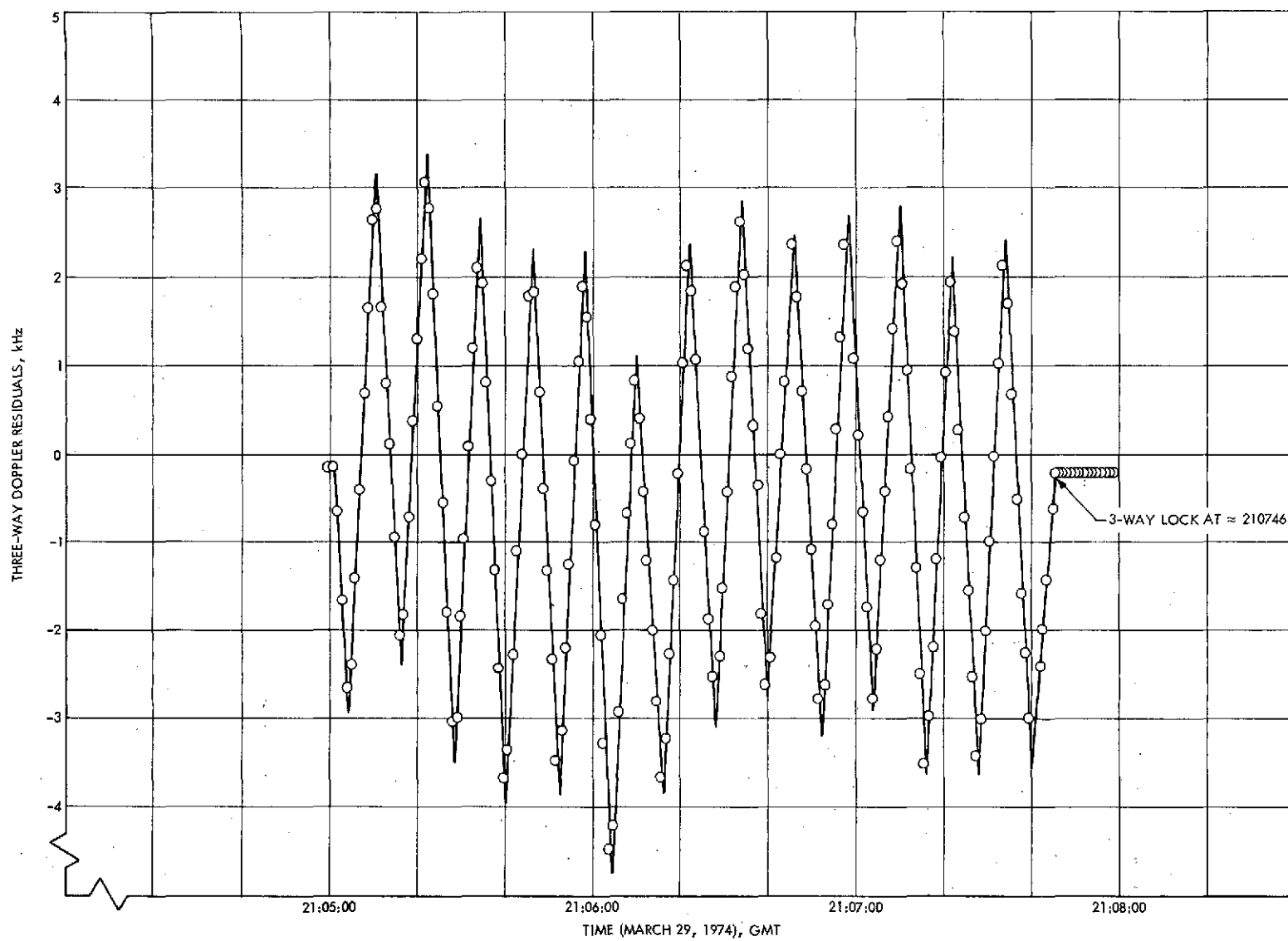


Fig. 6. Acquisition tuning pattern for Mercury exit occultation (DSS 43)

Bibliography

- Anderson, J. D., Null, G. W., and Thornton, C. T., *The Evaluation of Certain Astronomical Constants from the Radio Tracking of Mariner II*, Technical Report 32-476, Jet Propulsion Laboratory, Pasadena, Calif., reprinted from *Progr. Astronaut. Aeronaut.*, Vol. 14, 1964.
- Anderson, J. D., *Determination of the Masses of the Moon and Venus and the Astronomical Unit from Radio Tracking Data of the Mariner II Spacecraft*, Technical Report 32-816, Jet Propulsion Laboratory, Pasadena, Calif., July 1, 1967.
- Anderson, J. D., et al., "The Radius of Venus as Determined by Planetary Radar and Mariner V Radio Tracking Data," *J. Atmos. Sci.*, pp. 1171-1174, Sept. 25, 1968.
- Anderson, J. D., and Hilt, D. E., "Improvement of Astronomical Constants and Ephemerides from Pioneer Radio Tracking Data," *AIAA J.*, Vol. 7, No. 6, pp. 1048-1054, June 1969.
- Anderson, J. D., "Determination of Astrodynamic Constants and a Test of the General Relativistic Time Delay With S-Band Range and Doppler Data From Mariners 6 and 7," *Space Research*, Vol. XI, pp. 105-112, Akademie-Verlag, Berlin, 1971.
- Barnum, P. W., et al., *Tracking and Data System Support for the Mariner Mars 1971 Mission: Orbit Insertion Through End of Primary Mission*, Technical Memorandum 33-523, Vol. III, Jet Propulsion Laboratory, Pasadena, Calif., May 15, 1973.
- Barnum, P. W., and Renzetti, N. A., *Tracking and Data System Support for the Mariner Mars 1971 Mission: Extended Mission Operations*, Technical Memorandum 33-523, Vol. IV, Jet Propulsion Laboratory, Pasadena, Calif., Dec. 15, 1973.
- Bathker, D. A., *Radio-Frequency Performance of an 85-ft Ground Antenna: X-Band*, Technical Report 32-1300, Jet Propulsion Laboratory, Pasadena, Calif., July 1, 1968.
- Bathker, D. A., *Radio Frequency Performance of a 210-ft Ground Antenna: X-Band*, Technical Report 32-1417, Jet Propulsion Laboratory, Pasadena, Calif., Dec. 15, 1969.
- Bathker, D. A., *Predicted and Measured Power Density Description of a Large Ground Microwave System*, Technical Memorandum 33-433, Jet Propulsion Laboratory, Pasadena, Calif., Apr. 15, 1971.
- Baumgartner, W. S., *High-Power CW Radar Transmitter*, Technical Report 32-656, Jet Propulsion Laboratory, Pasadena, Calif., Sept. 1, 1964.
- Berman, A. L., *Tracking System Data Analysis Report, Ranger VII Final Report*, Technical Report 32-719, Jet Propulsion Laboratory, Pasadena, Calif., June 1, 1965.
- Biber, K. W., and Whittlesey, A. C., *Description and Analysis of 890-MHz Noise-Measuring Equipment*, Technical Report 32-898, Jet Propulsion Laboratory, Pasadena, Calif., Mar. 31, 1966.
- Brockman, M. H., and Posner, E. C., *Power Requirements for Deep-Space Telecommunication Links*, Technical Report 32-1395, Jet Propulsion Labora-

- tory, Pasadena, Calif., reprinted from *IEEE Spectrum*, Vol. 6, No. 3, pp. 95-99, Mar. 1969.
- Bunce, R. C., *Unified S-Band Receiver-Exciter Subsystem*, Technical Report 32-809, Jet Propulsion Laboratory, Pasadena, Calif., Sept. 15, 1968.
- Butman, S., "A General Formulation of Linear Feedback Communication Systems with Solutions," *IEEE Trans. Inform. Theor.*, Vol. IT-15, No. 3, pp. 392-400, May 1969.
- Butman, S., "Rate Distortion Over Band-Limited Feedback Channels," *IEEE Trans. Inform. Theor.*, Vol. IT-17, No. 1, pp. 110-112, Jan. 1971.
- Butman, S., and Timor, U., "Interplex—An Efficient Multichannel PSK/PM Telemetry System", *IEEE Trans. Commun.*, Vol. COM-20, No. 3, pp. 415-419, June 1972.
- Cain, D. L., and Hamilton, T. W., *Determination of Tracking Station Locations by Doppler and Range Measurements to an Earth Satellite*, Technical Report 32-534, Jet Propulsion Laboratory, Pasadena, Calif., Feb. 1, 1964.
- Carey, C. N., and Sjogren, W. L., *Gravitational Inconsistency in the Lunar Theory: Confirmation by Radio Tracking*, Technical Report 32-1290, Pt. II, Jet Propulsion Laboratory, Pasadena, Calif., reprinted from *Science*, Vol. 160, No. 3830, pp. 875-876, May 24, 1968.
- Carpenter, R. L., *Study of Venus by CW Radar—1964 Results*, Technical Report 32-963, Jet Propulsion Laboratory, Pasadena, Calif., reprinted from *Astron. J.*, Vol. 71, No. 2, pp. 142-152, Mar. 1966.
- Chadwick, H. D., and Springett, J. C., "The Design of a Low Data Rate MSFK Communication System," *IEEE Trans. Commun. Technol.*, Vol. COM-18, No. 6, pp. 740-750, Dec. 1970.
- Chaney, W. D., *Final Mariner II Tracking System Data Analysis Report*, Technical Report 32-727, Jet Propulsion Laboratory, Pasadena, Calif., Sept. 1, 1965.
- Charles, F. J., and Lindsey, W. C., *Some Analytical and Experimental Phase-Locked Loop Results for Low Signal-to-Noise Ratios*, Technical Report 32-1027, Jet Propulsion Laboratory, Pasadena, Calif., reprinted from *Proc. IEEE*, Vol. 54, No. 9, pp. 1152-1166, Sept. 1966.
- Clark, B. G., et al., "High Resolution Observations of Compact Radio Sources at 13 cm," *Astrophys. J.*, Vol. 161, pp. 803-809, Sept. 1970.
- Clauss, R. C., et al., *Total System Noise Temperature: 15°K*, Technical Report 32-691, Jet Propulsion Laboratory, Pasadena, Calif., Nov. 1964.
- Clauss, R. C., *A 2388-Mc Two-Cavity Maser for Planetary Radar*, Technical Report 32-583, Jet Propulsion Laboratory, Pasadena, Calif., reprinted from *Microwave J.*, Vol. 8, pp. 74-77, May 1965.
- Clauss, R. C., *A Traveling Wave Maser for Deep Space Communication at 2295 and 2388 MHz*, Technical Report 32-1072, Jet Propulsion Laboratory, Pasadena, Calif., Feb. 15, 1967.
- Cohen, M. H., et al., "Compact Radio Source in the Nucleus of M87," *Astrophys. J.*, Vol. 158, No. 2, Pt. 2, pp. L83-L85, Nov. 1969.

- Coyner, J. V., Jr., *Radial Rib Antenna Surface Deviation Analysis Program*, Technical Memorandum 33-518, Jet Propulsion Laboratory, Pasadena, Calif., Dec. 15, 1971.
- Curkendall, D. W., and McReynolds, S. R., "A Simplified Approach for Determining the Information Content of Radio Tracking Data," *J. Spacecraft Rockets*, Vol. 6, No. 5, pp. 520-525, May 1969.
- Curkendall, D. W., and Stephenson, R. R., "Earthbased Tracking and Orbit Determination—Backbone of the Planetary Navigation System," *Astronaut. Aeronaut.*, Vol. 7, No. 5, pp. 30-36, May 1970.
- Curkendall, D. W., "Planetary Navigation: The New Challenges," *Astronaut. Aeronaut.*, Vol. 7, No. 5, pp. 26-29, May 1970.
- "The Deep Space Network—An Instrument for Radio Navigation for the Mariner Mission to Mars—1969," *Proceedings of the Second International Conference of STM and AERA*, Reidel Publishing Company, Holland, May 1969.
- Description of the Deep Space Network Operational Capabilities as of January 1, 1966*, Technical Memorandum 33-255, Jet Propulsion Laboratory, Pasadena, Calif., July 1, 1966.
- Didday, R. L., and Lindsey, W. C., *Subcarrier Tracking Methods and Communication System Design*, Technical Report 32-1317, Jet Propulsion Laboratory, Pasadena, Calif., reprinted from *IEEE Trans. Commun. Technol.*, Vol. COM-16, No. 4, pp. 541-550, Aug. 1968.
- Downs, G. S., and Reichley, P. E., "Observations of Interstellar Scintillations of Pulsar Signals at 2388 MHz," *Astrophys. J.*, Vol. 163, No. 1, Pt. 2, pp. L11-L16, Jan. 1971.
- Downs, G. S., et al., "Mars Radar Observation, A Preliminary Report," *Science*, Vol. 174, No. 4016, pp. 1324-1327, Dec. 24, 1971.
- Easterling, M., *Methods for Obtaining Velocity and Range Information from CW Radars*, Technical Report 32-657, Jet Propulsion Laboratory, Pasadena, Calif., Sept. 1, 1964.
- Easterling, M., and Goldstein, R., *The Effect of the Interplanetary Medium on S-Band Telecommunications*, Technical Report 32-825, Jet Propulsion Laboratory, Pasadena, Calif., Sept. 1, 1965.
- Efron, L., and Solloway, C. B., *Proceedings of the Conference on Scientific Applications of Radio and Radar Tracking in the Space Program*, Technical Report 32-1475, Jet Propulsion Laboratory, Pasadena, Calif., July 1, 1970.
- Esposito, P. B., and Wong, S. K., "Geocentric Gravitational Constant Determined from Mariner 9 Radio Tracking Data," paper presented at the International Symposium on Earth Gravity Models (American Geophysical Union, NASA), St. Louis, Aug. 1972.
- Fjeldbo, G., Kliore, A. J., and Seidel, B. L., "Bistatic Radar Measurements of the Surface of Mars with Mariner 1969," *Icarus*, Vol. 16, No. 3, pp. 502-508, June 1972.
- Fjeldbo, G., and Eshleman, V. R., "Radio Occultation Measurements and Interpretations," in *The Atmospheres of Venus and Mars*, p. 225, Gordon and Breach, Science Publishers, Inc., New York, N.Y., 1968.

- Flanagan, F. M., et al., *Deep Space Network Support of the Manned Space Flight Network for Apollo: 1962-1968*, Technical Memorandum 33-452, Vol. I, Jet Propulsion Laboratory, Pasadena, Calif., July 1970.
- Flanagan, F. M., et al., *Deep Space Network Support of the Manned Space Flight Network for Apollo: 1969-1970*, Technical Memorandum 33-452, Vol. II, Jet Propulsion Laboratory, Pasadena, Calif., May 1, 1971.
- Fredricksen, H., *Error Correction for Deep Space Network Teletype Circuits*, Technical Report 32-1275, Jet Propulsion Laboratory, Pasadena, Calif., June 1, 1968.
- Georgevic, R. M., *Mathematical Model of the Solar Radiation Force and Torques Acting on the Components of a Spacecraft*, Technical Memorandum 33-494, Jet Propulsion Laboratory, Pasadena, Calif., Oct. 1, 1971.
- Goldstein, R., Stevens, R., and Victor, W. K., *Radar Exploration of Venus: Goldstone Observatory Report for October-December 1962*, Technical Report 32-396, Jet Propulsion Laboratory, Pasadena, Calif., Mar. 1, 1965.
- Goldstein, R. M., *The Analysis of Uncooperative Radar Targets*, Technical Report 32-658, Jet Propulsion Laboratory, Pasadena, Calif., Sept. 1, 1964.
- Goldstein, R. M., et al., *The Superior Conjunction of Mariner V*, Technical Report 32-1092, Jet Propulsion Laboratory, Pasadena, Calif., Apr. 1, 1967.
- Goldstein, R. M., "Radar Time-of-Flight Measurements to Venus," *Astron. J.*, Vol. 73, No. 9, Aug. 1968.
- Goldstein, R. M., et al., "Preliminary Radar Results of Mars," *Radio Sci.*, Vol. 5, No. 2, pp. 475-478, Feb. 1970.
- Goldstein, R. M., and Rumsey, H., "A Radar Snapshot of Venus," *Science*, Vol. 169, Sept. 1970.
- Goldstein, R. M., "Radar Observations of Mercury," *Astron. J.*, Vol. 76, No. 10, pp. 1152-1154, Dec. 1971.
- Gordon, H. J., et al., *The Mariner 6 and 7 Flight Paths and Their Determination From Tracking Data*, Technical Memorandum 33-469, Jet Propulsion Laboratory, Pasadena, Calif., Dec. 1, 1970.
- Gottlieb, P., et al., "Lunar Gravity over Large Craters from Apollo 12 Tracking Data," *Science*, Vol. 168, No. 3930, pp. 477-479, Apr. 1970.
- Gray, R. M., and Tausworthe, R. C., "Frequency-Counted Measurements, and Phase Locking to Noise Oscillators," *IEEE Trans. Commun. Technol.*, Vol. COM-19, No. 1, pp. 21-30, Feb. 1971.
- Gubbay, J., et al., "Variations of Small Quasar Components at 2,300 MHz," *Nature*, Vol. 224, No. 5224, pp. 1094-1095, Dec. 1969.
- Gulkis, S., and Gary, B., "Circular Polarization and Total-Flux Measurements of Jupiter at 13.1 cm Wavelength," *Astron. J.*, Vol. 76, No. 1, pp. 12-16, Feb. 1971.
- Hall, J. R., *Tracking and Data System Support for Lunar Orbiter*, Technical Memorandum 33-450, Jet Propulsion Laboratory, Pasadena, Calif., Apr. 1970.
- Hamilton, T. W., et al., *The Ranger IV Flight Path and Its Determination From Tracking Data*, Technical Report 32-345, Jet Propulsion Laboratory, Pasadena, Calif., Sept. 15, 1962.

- Hartop, R. W., *Power Loss Between Arbitrarily Polarized Antennas*, Technical Report 32-457, Jet Propulsion Laboratory, Pasadena, Calif., Sept. 1, 1964.
- Havens, W. F., et al., *Scan Pointing Calibration for the Mariner Mars 1971 Spacecraft*, Technical Memorandum 33-556, Jet Propulsion Laboratory, Pasadena, Calif., Aug. 1, 1972.
- Heftman, K., and Renzetti, N. A., "Data Return Capabilities of the Deep Space Network in the 1970's," AIAA Paper 67-648, *Proceedings of the AIAA Space Program Issues of the 70's Meeting*, Aug. 1967.
- Higa, W. H., *Low-Level Microwave Mixing in Ruby*, Technical Report 32-1016, Jet Propulsion Laboratory, Pasadena, Calif., reprinted from *Proc. IEEE*, Vol. 54, No. 10, p. 1453, Oct. 1966.
- Higa, W. H., "Time Synchronization via Lunar Radar," *Proc. IEEE*, Vol. 60, No. 5, pp. 552-557, May 1972.
- Holmes, J. K., "On a Solution to the Second-Order Phase-Locked Loop," *IEEE Trans. Commun. Technol.*, Vol. COM-18, No. 2, pp. 119-126, Apr. 1970.
- Holmes, J. K., "First Slip Times Versus Static Phase Error Offset for the First and Passive Second-Order Phase-Locked Loop," *IEEE Trans. Commun. Technol.*, Vol. COM-19, No. 2, pp. 234-235, Apr. 1971.
- Holmes, J. K., and Tegnalia, C. R., *Digital Command System Second-Order Subcarrier Tracking Performance*, Technical Report 32-1540, Jet Propulsion Laboratory, Pasadena, Calif., Oct. 1, 1971.
- Holmes, J. K., "Performance of a First Order Transition Sampling Digital Phase-Locked Loop Using Random-Walk Models," *IEEE Trans. Commun.*, Vol. COM-20, No. 2, pp. 119-131, Apr. 1972.
- Hurd, W. J., and Anderson T. O., *Digital Transition Tracking Symbol Synchronizer for Low SNR Coded Systems*, Technical Report 32-1488, Jet Propulsion Laboratory, Pasadena, Calif., reprinted from *IEEE Trans. Commun. Technol.*, Vol. COM-18, No. 2, pp. 141-147, Apr. 1970.
- Jordan, J. F., "Orbit Determination for Powered Flight Space Vehicles on Deep Space Missions," *J. Spacecraft Rockets*, Vol. 6, No. 5, pp. 545-550, May 1969.
- Kellerman, K. I., et al., "High Resolution Observations of Compact Radio Sources at 13 Centimeters," *Astrophys. J.*, Vol. 161, No. 3, pp. 803-809, Sept. 1970.
- Kelly, A. J., *Microwave Probe for Plasma Plumes*, Technical Report 32-625, Jet Propulsion Laboratory, Pasadena, Calif., Feb. 1965.
- Kliore, A., Cain, D. L., and Hamilton, T. W., *Determination of Some Physical Properties of the Atmosphere of Mars from Changes in the Doppler Signal of a Spacecraft on an Earth-Occultation Trajectory*, Technical Report 32-674, Jet Propulsion Laboratory, Pasadena, Calif., Oct. 15, 1964.
- Kliore, A., and Tito, D. A., *Radio Occultation Investigations of the Atmosphere of Mars*, Technical Report 32-1157, Jet Propulsion Laboratory, Pasadena, Calif., reprinted from *J. Spacecraft Rockets*, Vol. 4, No. 5, pp. 578-582, May 1967.
- Kliore, A., "Radio Occultation Measurements of the Atmospheres of Mars and Venus," in *The Atmospheres of Venus and Mars*, edited by J. C. Brandt and M. B. McElrow, p. 205, Gordon and Breach Science Publishers, Inc., New York, N.Y., 1968.

- Kliore, A. J., et al., "Summary of Mariner 6 and 7 Radio Occultation Results on the Atmosphere of Mars," *Space Research*, Vol. XI, pp. 165-175, Akademie-Verlag, Berlin, 1971.
- Kliore, A. J., et al., "Mariner 9 S-Band Martian Occultation Experiment: Initial Results on the Atmosphere and Topography of Mars," *Science*, Vol. 175, No. 4019, pp. 313-317, Jan. 1972.
- Labrum, R. G., et al., *The Surveyor V, VI, and VII Flight Paths and Their Determination from Tracking Data*, Technical Report 32-1302, Jet Propulsion Laboratory, Pasadena, Calif., Dec. 1, 1968.
- Laeser, R. P., et al., *Tracking and Data System Support for the Mariner Mars 1971 Mission: Prelaunch Phase Through First Trajectory Correction Maneuver*, Technical Memorandum 33-523, Vol. I, Jet Propulsion Laboratory, Pasadena, Calif., Mar. 15, 1972.
- Layland, J. W., "On Optimal Signals for Phase-Locked Loops," *IEEE Trans. Commun. Technol.*, Vol. COM-17, No. 5, pp. 526-531, Oct. 1969.
- Layland, J. W., and Lushbaugh, W. A., "A Flexible High-Speed Sequential Decoder for Deep Space Channels," *IEEE Trans. Commun. Technol.*, Vol. COM-19 No. 5, pp. 813-820, Oct. 1971.
- Leavitt, R. K., *The Least-Squares Process of MEDIA for Computing DRVID Calibration Polynomials*, Technical Memorandum 33-542, Jet Propulsion Laboratory, Pasadena, Calif., May 15, 1972.
- Levy, G. S., Ootshi, T. Y., and Seidel, B. L., *Ground Instrumentation for Mariner IV Occultation Experiment*, Technical Report 32-984, Jet Propulsion Laboratory, Pasadena, Calif., Sept. 15, 1966.
- Levy, G. S., et al., *Lunar Range Radiation Patterns of a 210-Foot Antenna at S-Band*, Technical Report 32-1079, Jet Propulsion Laboratory, Pasadena, Calif., reprinted from *IEEE Trans. Antennas Propagation*, Vol. AP-15, No. 2, pp. 311-313, Mar. 1967.
- Levy, G. S., et al., *The Ultra Cone: An Ultra-Low-Noise Space Communication Ground Radio-Frequency System*, Technical Report 32-1340, Jet Propulsion Laboratory, Pasadena, Calif., reprinted from *IEEE Trans. Microwave Theor. Tech.*, Vol. MTT-16, No. 9, pp. 596-602, Sept. 1968.
- Levy, G. S., et al., "Pioneer 6: Measurement of Transient Faraday Rotation Phenomena Observed During Solar Occultation," *Science*, Vol. 166, No. 3905, pp. 596-598, Oct. 1969.
- Lieske, J. H., and Null, G. W., "Icarus and the Determination of Astronomical Constants," *Astron. J.*, Vol. 74, No. 2, Mar. 1969.
- Lieske, J. H., et al., "Simultaneous Solution for the Masses of the Principal Planets from Analysis of Optical Radar and Radio Tracking Data," *Celest. Mech.*, Vol. 4, No. 2, pp. 233-245, Oct. 1971.
- Lindsey, W. C., *Optimum and Suboptimum Frequency Demodulation*, Technical Report 32-637, Jet Propulsion Laboratory, Pasadena, Calif., June 15, 1964.
- Lindsey, W. C., *Improvements to be Realized Through the Use of Block-Coded Communication Systems*, Technical Report 32-947, Jet Propulsion Laboratory, Pasadena, Calif., reprinted from *IEEE Trans. Aerosp. Electron. Syst.*, Vol. AES-2, No. 3, pp. 364-366, May 1966.

- Lindsey, W. C., *Phase-Shift-Keyed Signal Detection with Noisy Reference Signals*, Technical Report 32-968, Jet Propulsion Laboratory, Pasadena, Calif., reprinted from *IEEE Trans. Aerosp. Electron. Syst.*, Vol. AES-2, No. 4, pp. 393-401, July 1966.
- Lindsey, W. C., *A Theory for the Design of One-Way and Two-Way Phase-Coherent Communication Systems: Phase-Coherent Tracking Systems*, Technical Report 32-986, Jet Propulsion Laboratory, Pasadena, Calif., July 15, 1969.
- Lindsey, W. C., *Optimal Design of One-Way and Two-Way Coherent Communication Links*, Technical Report 32-988, Jet Propulsion Laboratory, Pasadena, Calif., reprinted from *IEEE Trans. Commun. Technol.*, Vol. COM-14, No. 4, pp. 418-431, Aug. 1966.
- Lindsey, W. C., and Charles, F. J., *A Model Distribution for the Phase Error in Second-Order Phase-Locked Loops*, Technical Report 32-1017, Jet Propulsion Laboratory, Pasadena, Calif., reprinted from *IEEE Trans. Commun. Technol.*, Vol. COM-14, No. 10, pp. 662-664, Oct. 1966.
- Lindsey, W. C., *Performance of Phase-Coherent Receivers Preceded by Bandpass Limiters*, Technical Report 32-1162, Jet Propulsion Laboratory, Pasadena, Calif., Sept. 15, 1967.
- Lindsey, W. C., "Block Coding for Space Communications," *IEEE Trans. Commun. Technol.*, Vol. COM-17, No. 2, pp. 217-225, Apr. 1969.
- Lindsey, W. C., *Block-Coded Communications*, Technical Report 32-1380, Jet Propulsion Laboratory, Pasadena, Calif., Aug. 15, 1969.
- Lindsey, W. C., *Nonlinear Analysis of Generalized Tracking Systems*, Technical Report 32-1453, Jet Propulsion Laboratory, Pasadena, Calif., reprinted from *Proc. IEEE*, Vol. 57, No. 10, pp. 1705-1722, Oct. 1969.
- Lindsey, W. C., and Simon, M. K., "The Effect of Loop Stress on the Performance of Phase-Coherent Communication Systems", *IEEE Trans. Commun. Technol.*, Vol. COM-18, No. 5, pp. 569-588, Oct. 1970.
- Lindsey, W. C., and Simon, M. K., "Carrier Synchronization and Detection of Polyphase Signals," *IEEE Trans. Commun.*, Vol. COM-20, No. 3, pp. 441-454, June 1972.
- Lorell, J., Anderson, J. D., and Sjogren, W. L., *Characteristics and Format of the Tracking Data to Be Obtained by the NASA Deep Space Instrumentation Facility for Lunar Orbiter*, Technical Memorandum 33-230, Jet Propulsion Laboratory, Pasadena, Calif., June 15, 1965.
- Lorell, J., Sjogren, W. L., and Boggs, D., *Compressed Tracking Data Used for First Iteration in Selenodesy Experiment, Lunar Orbiters I and II*, Technical Memorandum 33-343, Jet Propulsion Laboratory, Pasadena, Calif., May 1, 1967.
- Lorell, J., and Sjogren, W. L., *Lunar Orbiter Data Analysis*, Technical Report 32-1220, Jet Propulsion Laboratory, Pasadena, Calif., Nov. 15, 1967.
- Lorell, J., *Lunar Orbiter Gravity Analysis*, Technical Report 32-1387, Jet Propulsion Laboratory, Pasadena, Calif., June 15, 1969.
- Lorell, J., et al., "Icarus: Celestial Mechanics Experiment for Mariner," *Int. J. Sol. Sys.*, Vol. 12, Jan. 1970.

- Lorell, J., and Laing, P. A., *Compilation of Lunar Orbiter Tracking Data Used for Long-Term Selenodesy*, Technical Memorandum 33-419, Jet Propulsion Laboratory, Pasadena, Calif., Feb. 1, 1970.
- Ludwig, A. C., et al., *Gain Calibration of a Horn Antenna Using Pattern Integration*, Technical Report 32-1572, Jet Propulsion Laboratory, Pasadena, Calif., Oct. 1, 1972.
- Madrid, G. A., et al., *Tracking System Analytic Calibration Activities for the Mariner Mars 1971 Mission*, Technical Report 32-1587, Jet Propulsion Laboratory, Pasadena, Calif., Mar. 1, 1974.
- Martin, D. P., *A Combined Radar-Radiometer With Variable Polarization*, Technical Memorandum 33-570, Jet Propulsion Laboratory, Pasadena, Calif., Oct. 15, 1972.
- McEliece, R. J., *Optimal Communications Nets*, Technical Report 32-697, Jet Propulsion Laboratory, Pasadena, Calif., Apr. 15, 1965.
- McNeal, C. E., *Ranger V Tracking Systems Data Analysis Final Report*, Technical Report 32-702, Jet Propulsion Laboratory, Pasadena, Calif., Apr. 15, 1965.
- Melbourne, W. G., et al., *Constants and Related Information for Astrodynamical Calculations*, Technical Report 32-1306, Jet Propulsion Laboratory, Pasadena, Calif., July 15, 1968.
- Melbourne, W. G., "Planetary Ephemerides," *Astronaut. Aeronaut.*, Vol. 7, No. 5, pp. 38-43, May 1970.
- Miller, L., et al., *The Atlas-Centaur VI Flight Path and Its Determination from Tracking Data*, Technical Report 32-911, Jet Propulsion Laboratory, Pasadena, Calif., Apr. 15, 1966.
- Moyer, T. D., *Mathematical Formulation of the Double-Precision Orbit Determination Program (DPODP)*, Technical Report 32-1527, Jet Propulsion Laboratory, Pasadena, Calif., May 17, 1971.
- Muhleman, D. O., *Relationship Between the System of Astronomical Constants and the Radar Determinations of the Astronomical Unit*, Technical Report 32-477, Jet Propulsion Laboratory, Pasadena, Calif., Jan. 15, 1964.
- Muhleman, D. O., Goldstein, R., and Carpenter, R., *A Review of Radar Astronomy—Parts I, II*, Technical Report 32-824, Jet Propulsion Laboratory, Pasadena, Calif., Jan. 30, 1966, reprinted from *IEEE Spectrum*, Oct. and Nov. 1965.
- Muhleman, D. O., et al., *JPL Radar Range and Doppler Observations of Venus, 1961-1966*, Technical Report 32-1123, Jet Propulsion Laboratory, Pasadena, Calif., July 1, 1968.
- Mulhall, B. D., et al., *Tracking System Analytic Calibration Activities for the Mariner Mars 1969 Mission*, Technical Report 32-1499, Jet Propulsion Laboratory, Pasadena, Calif., Nov. 15, 1970.
- Mulholland, J. D., and Sjogren, W. L., *Lunar Orbiter Ranging Data*, Technical Report 32-1087, Jet Propulsion Laboratory, Pasadena, Calif., reprinted from *Science*, Vol. 155, No. 3758, pp. 74-76, Jan. 6, 1967.

- Mulholland, J. D., *Proceedings of the Symposium on Observation, Analysis and Space Research Applications of the Lunar Motion*, Technical Report 32-1386, Jet Propulsion Laboratory, Pasadena, Calif., Apr. 1969.
- Muller, P. M., and Sjogren, W. L., *Consistency of Lunar Orbiter Residuals With Trajectory and Local Gravity Effects*, Technical Report 32-1307, Jet Propulsion Laboratory, Pasadena, Calif., Sept. 1, 1968.
- Muller, P. M., and Sjogren, W. L., *Mascons: Lunar Mass Concentrations*, Technical Report 32-1339, Jet Propulsion Laboratory, Pasadena, Calif., reprinted from *Science*, Vol. 161, No. 3842, pp. 680-684, Aug. 16, 1968.
- Newburn, R. L., Jr., et al., *Earth-Based Research on the Outer Planets During the Period 1970-1985*, Technical Report 32-1456, Jet Propulsion Laboratory, Pasadena, Calif., Mar. 15, 1970.
- Null, G. W., et al., *Mariner IV Flight Path and Its Determination From Tracking Data*, Technical Report 32-1108, Jet Propulsion Laboratory, Pasadena, Calif., Aug. 1, 1967.
- O'Neil, W. J., et al., *The Surveyor III and Surveyor IV Flight Paths and Their Determination From Tracking Data*, Technical Report 32-1292, Jet Propulsion Laboratory, Pasadena, Calif., Aug. 15, 1968.
- Otoshi, T. Y., *The Effect of Mismatched Components on Microwave Noise-Temperature Calibrations*, Technical Report 32-1345, Jet Propulsion Laboratory, Pasadena, Calif., reprinted from *IEEE Trans. Microwave Theor. Tech.*, Vol. MTT-16, No. 9, pp. 675-686, Sept. 1968.
- Otoshi, T. Y., Stelzried, C. T., and Yates, B. C., "Comparisons of Waveguide Losses Calibrated by the DC Potentiometer, AC Ratio Transformer, and Reflectometer Techniques," *IEEE Trans. Microwave Theor. Tech.*, Vol. MTT-18, No. 7, pp. 406-409, July 1970.
- Otoshi, T. Y., and Stelzried, C. T., "A Precision Compact Rotary Vane Attenuator," *IEEE Trans. Micro. Theor. Technique*, Vol. MTT-19, No. 11, pp. 843-854, Nov. 1971.
- Pease, G. E., et al., *The Mariner V Flight Path and Its Determination From Tracking Data*, Technical Report 32-1363, Jet Propulsion Laboratory, Pasadena, Calif., July 1, 1969.
- Posner, E. C., *Properties of Error-Correcting Codes at Low Signal-to-Noise Ratios*, Technical Report 32-602, Jet Propulsion Laboratory, Pasadena, Calif., June 15, 1964.
- Potter, P. D., *The Design of a Very High Power, Very Low Noise Cassegrain Feed System for a Planetary Radar*, Technical Report 32-653, Jet Propulsion Laboratory, Pasadena, Calif., Aug. 24, 1964.
- Potter, P. D., Merrick, W. D., and Ludwig, A. C., *Large Antenna Apertures and Arrays for Deep Space Communications*, Technical Report 32-848, Jet Propulsion Laboratory, Pasadena, Calif., Nov. 1, 1965.
- Potter, P. D., *A Computer Program for Machine Design of Cassegrain Feed Systems*, Technical Report 32-1202, Jet Propulsion Laboratory, Pasadena, Calif., Dec. 15, 1967.
- Potter, P. D., et al., *A Study of Weather-Dependent Data Links for Deep Space Applications*, Technical Report 32-1392, Jet Propulsion Laboratory, Pasadena, Calif., Oct. 15, 1969.

- Renzetti, N. A., et al., "Radio Tracking Techniques and Performance of the U.S. Deep Space Instrumentation Facility," *Space Research II, Proceedings of the Second International Space Science Symposium*, Florence, Italy, April 1961, North Holland Publishing Company, Amsterdam.
- Renzetti, N. A., and Ostermier, B. J., *Communications with Lunar Probes*, Technical Report 32-148, Jet Propulsion Laboratory, Pasadena, Calif., Aug. 23, 1961.
- Renzetti, N. A., *Tracking and Data Acquisition for Ranger Missions I-V*, Technical Memorandum 33-174, Jet Propulsion Laboratory, Pasadena, Calif., July 1, 1964.
- Renzetti, N. A., *Tracking and Data Acquisition for Ranger Missions VI-IX*, Technical Memorandum 33-275, Jet Propulsion Laboratory, Pasadena, Calif., Sept. 15, 1966.
- Renzetti, N. A., *Tracking and Data Acquisition Support for the Mariner Venus 1962 Mission*, Technical Memorandum 33-212, Jet Propulsion Laboratory, Pasadena, Calif., July 1, 1965.
- Renzetti, N. A., *Tracking and Data Acquisition Report, Mariner Mars 1964 Mission: Near-Earth Trajectory Phase*, Technical Memorandum 33-239, Vol. I, Jet Propulsion Laboratory, Pasadena, Calif., Jan. 1, 1965.
- Renzetti, N. A., *Tracking and Data Acquisition Report, Mariner Mars 1964 Mission: Cruise to Post-Encounter Phase*, Technical Memorandum 33-239, Vol. II, Jet Propulsion Laboratory, Pasadena, Calif., Oct. 1, 1967.
- Renzetti, N. A., *Deep Space Network Support, Atlas/Centaur Missions 1-9*, Technical Memorandum 33-347, Jet Propulsion Laboratory, Pasadena, Calif., Sept. 15, 1967.
- Renzetti, N. A., "Tracking and Data Acquisition System for Mariner Missions," *Proceedings of the Seventh International Symposium on Space Technology and Science*, Tokyo, 1967.
- Renzetti, N. A., *Tracking and Data Acquisition Report, Mariner Mars 1964 Mission: Extended Mission*, Technical Memorandum 33-239, Vol. III, Jet Propulsion Laboratory, Pasadena, Calif., Dec. 1, 1968.
- Renzetti, N. A., and Fearey, J. P., "The Deep Space Network: An Instrument for the Radio Navigation for the Mariner Mission to Mars 1969," *IIInd International Conference on Space Engineering*, Venice, Italy, D. Reidel Publishing Co., Dordrecht, Holland, May 1969.
- Renzetti, N. A., *Tracking and Data System Support for Surveyor: Missions I and II*, Technical Memorandum 33-301, Vol. I, Jet Propulsion Laboratory, Pasadena, Calif., July 15, 1969.
- Renzetti, N. A., *Tracking and Data System Support for Surveyor: Missions III and IV*, Technical Memorandum 33-301, Vol. II, Jet Propulsion Laboratory, Pasadena, Calif., Sept. 1, 1969.
- Renzetti, N. A., *Tracking and Data System Support for Surveyor: Mission V*, Technical Memorandum 33-301, Vol. III, Jet Propulsion Laboratory, Pasadena, Calif., Dec. 1, 1969.
- Renzetti, N. A., *Tracking and Data System Support for Surveyor: Mission VI*, Technical Memorandum 33-301, Vol. IV, Jet Propulsion Laboratory, Pasadena, Calif., Dec. 1, 1969.

- Renzetti, N. A., *Tracking and Data System Support for Surveyor: Mission VII*, Technical Memorandum 33-301, Vol. V, Jet Propulsion Laboratory, Pasadena, Calif., Dec. 1, 1969.
- Renzetti, N. A., *Tracking and Data System Support for the Mariner Venus 67 Mission: Planning Phase Through Midcourse Maneuver*, Technical Memorandum 33-385, Vol. I, Jet Propulsion Laboratory, Pasadena, Calif., Sept. 1, 1969.
- Renzetti, N. A., *Tracking and Data System Support for the Mariner Venus 67 Mission: Midcourse Maneuver Through End of Mission*, Technical Memorandum 33-385, Vol. II, Jet Propulsion Laboratory, Pasadena, Calif., Sept. 1, 1969.
- Renzetti, N. A., *Tracking and Data System Support for the Pioneer Project: Pioneer VI. Prelaunch to End of Nominal Mission*, Technical Memorandum 33-426, Vol. I, Jet Propulsion Laboratory, Pasadena, Calif., Feb. 1, 1970.
- Renzetti, N. A., *Tracking and Data System Support for the Pioneer Project: Pioneer VII. Prelaunch to End of Nominal Mission*, Technical Memorandum 33-426, Vol. II, Jet Propulsion Laboratory, Pasadena, Calif., Apr. 15, 1970.
- Renzetti, N. A., *Tracking and Data System Support for the Pioneer Project: Pioneer VIII. Prelaunch Through May 1968*, Technical Memorandum 33-426, Vol. III, Jet Propulsion Laboratory, Pasadena, Calif., July 15, 1970.
- Renzetti, N. A., *Tracking and Data System Support for the Pioneer Project: Pioneer IX. Prelaunch Through June 1969*, Technical Memorandum 33-426, Vol. IV, Jet Propulsion Laboratory, Pasadena, Calif., Nov. 15, 1970.
- Renzetti, N. A., *Tracking and Data System Support for the Pioneer Project: Pioneer VI. Extended Mission: July 1, 1966-July 1, 1969*, Technical Memorandum 33-426, Vol. V, Jet Propulsion Laboratory, Pasadena, Calif., Feb. 1, 1971.
- Renzetti, N. A., *Tracking and Data System Support for the Pioneer Project: Pioneer VII. Extended Mission: February 24, 1967-July 1, 1968*, Technical Memorandum 33-426, Vol. VI, Jet Propulsion Laboratory, Pasadena, Calif., Apr. 15, 1971.
- Renzetti, N. A., *Tracking and Data System Support for the Pioneer Project: Pioneer VII. Extended Mission: July 1, 1968-July 1, 1969*, Technical Memorandum 33-426, Vol. VII, Jet Propulsion Laboratory, Pasadena, Calif., Apr. 15, 1971.
- Renzetti, N. A., *Tracking and Data System Support for the Pioneer Project: Pioneer VIII. Extended Mission: June 1, 1968-July 1, 1969*, Technical Memorandum 33-426, Vol. VIII, Jet Propulsion Laboratory, Pasadena, Calif., May 1, 1971.
- Renzetti, N. A., *Tracking and Data System Support for the Pioneer Project: Pioneers VI-IX. Extended Missions: July 1, 1969-July 1, 1970*, Technical Memorandum 33-426, Vol. IX, Jet Propulsion Laboratory, Pasadena, Calif., Aug. 15, 1971.
- Renzetti, N. A., and Siegmeth, A. J., *Tracking and Data System Support for the Pioneer Project: Pioneers 6-9. Extended Missions: July 1, 1971-July 1, 1972*, Technical Memorandum 33-426, Vol. XI, Jet Propulsion Laboratory, Pasadena, Calif., May 1, 1973.
- Renzetti, N. A., et al., *Tracking and Data System Support for the Mariner Mars 1969 Mission: Planning Phase Through Midcourse Maneuver*, Technical

- Memorandum 33-474, Vol. I, Jet Propulsion Laboratory, Pasadena, Calif., May 15, 1971.
- Renzetti, N. A., et al., *Tracking and Data System Support for the Mariner Mars 1969 Mission: Midcourse Maneuver Through End of Nominal Mission*, Technical Memorandum 33-474, Vol. II, Jet Propulsion Laboratory, Pasadena, Calif., Sept. 1, 1971.
- Renzetti, N. A., Linnes, K. W., and Taylor, T. M., *Tracking and Data System Support for the Mariner Mars 1969 Mission: Extended Operations Mission*, Technical Memorandum 33-474, Vol. III, Jet Propulsion Laboratory, Pasadena, Calif., Sept. 15, 1971.
- Renzetti, N. A., *A History of the Deep Space Network: From Inception to January 1, 1969*, Technical Report 32-1533, Vol. I, Jet Propulsion Laboratory, Pasadena, Calif., Sept. 1, 1971.
- Rusch, W. V. T., *Phase Error and Associated Cross-Polarization Effects in Cassegrainian-Fed Microwave Antennas*, Technical Report 32-610, Jet Propulsion Laboratory, Pasadena, Calif., May 30, 1965.
- Rusch, W. V. T., and Stelzried, C. T., *Observations of the Lunar Eclipse of December 19, 1964, at a Wavelength of 3.3 MM*, Technical Report 32-1097, Jet Propulsion Laboratory, Pasadena, Calif., reprinted from *Astrophys. J.*, Vol. 148, No. 1, pp. 255-259, Apr. 1967.
- Rusch, W. V. T., *Applications of Two-Dimensional Integral-Equation Theory to Reflector-Antenna Analysis*, Technical Memorandum 33-478, Jet Propulsion Laboratory, Pasadena, Calif., May 1, 1971.
- Sanger, D. K., *Digital Demodulation with Data Subcarrier Tracking*, Technical Report 32-1314, Jet Propulsion Laboratory, Pasadena, Calif., Aug. 1, 1968.
- Siegmeth, A. J., Purdue, R. E., and Ryan, R. E., *Tracking and Data System Support for the Pioneer Project: Pioneers 6-9. Extended Missions: July 1, 1970-July 1, 1971*, Technical Memorandum 33-426, Vol. X, Jet Propulsion Laboratory, Pasadena, Calif., Aug. 15, 1972.
- Siegmeth, A. J., et al., *Tracking and Data System Support for the Pioneer Project: Pioneer 10-Prelaunch Planning Through Second Trajectory Correction December 4, 1969 to April 1, 1972*, Technical Memorandum 33-584, Vol. I, Jet Propulsion Laboratory, Pasadena, Calif., Apr. 1, 1973.
- Simon, M. K., "Nonlinear Analysis of an Absolute Value Type of an Early-Late Gate Bit Synchronizer," *IEEE Trans. Commun. Technol.*, Vol. COM-18, No. 5, pp. 589-596, Oct. 1970.
- Simon, M. K., "Optimization of the Performance of a Digital-Data-Transition Tracking Loop," *IEEE Trans. Commun. Technol.*, Vol. COM-18, No. 5, pp. 686-689, Oct. 1970.
- Simon, M. K., and Lindsey, W. C., "Data-Aided Carrier Tracking Loops," *IEEE Trans. Commun. Technol.*, Vol. COM-19, No. 2, pp. 157-168, Apr. 1971.
- Simon, M. K., "On the Selection of an Optimum Design Point for Phase-Coherent Receivers Employing Bandpass Limiters," *IEEE Trans. Commun.*, Vol. COM-20, No. 2, pp. 210-214, Apr. 1972.
- Simon, M. K., "On the Selection of a Sampling Filter Bandwidth for a Digital Data Detector," *IEEE Trans. Commun.*, Vol. COM-20, No. 3, pp. 438-441, June 1972.

- Sjogren, W. L., et al., *The Ranger V Flight Path and Its Determination From Tracking Data*, Technical Report 32-562, Jet Propulsion Laboratory, Pasadena, Calif., Dec. 6, 1963.
- Sjogren, W. L., et al., *The Ranger VI Flight Path and Its Determination From Tracking Data*, Technical Report 32-605, Jet Propulsion Laboratory, Pasadena, Calif., Dec. 15, 1964.
- Sjogren, W. L., *The Ranger III Flight Path and Its Determination From Tracking Data*, Technical Report 32-563, Jet Propulsion Laboratory, Pasadena, Calif., Sept. 15, 1965.
- Sjogren, W. L., et al., *Physical Constants as Determined From Radio Tracking of the Ranger Lunar Probes*, Technical Report 32-1057, Jet Propulsion Laboratory, Pasadena, Calif., Dec. 30, 1966.
- Sjogren, W. L., *Proceedings of the JPL Seminar on Uncertainties in the Lunar Ephemeris*, Technical Report 32-1247, Jet Propulsion Laboratory, Pasadena, Calif., May 1, 1968.
- Sjogren, W. L., "Lunar Gravity Estimate: Independent Confirmation," *J. Geophys. Res.*, Vol. 76, No. 29, Oct. 10, 1971.
- Sjogren, W. L., et al., "Lunar Gravity via Apollo 14 Doppler Radio Tracking," *Science*, Vol. 175, No. 4018, pp. 165-168, Jan. 14, 1972.
- Slobin, S. D., "Beam Switching Cassegrain Feed System and Its Applications to Microwave and Millimeterwave Radioastronomical Observations," *Rev. Sci. Instr.*, Vol. 41, No. 3, pp. 439-443, Mar. 1970.
- Spier, G. W., *Design and Implementation of Models for the Double Precision Trajectory Program (DPTRAJ)*, Technical Memorandum 33-451, Jet Propulsion Laboratory, Pasadena, Calif., Apr. 15, 1971.
- Springett, J. C., and Simon, M. K., "An Analysis of the Phase Coherent-Incoherent Output of the Bandpass Limiter," *IEEE Trans. Commun. Technol.*, Vol. COM-19, No. 1, pp. 42-49, Feb. 1971.
- Stelzried, C. T., *Post-Amplifier Noise Temperature Contribution in a Low-Noise Receiving System*, Technical Report 32-446, Jet Propulsion Laboratory, Pasadena, Calif., Jan. 1964.
- Stelzried, C. T., Reid, M. S., and Petty, S. M., *A Precision DC-Potentiometer Microwave Insertion-Loss Test Set*, Technical Report 32-887, Jet Propulsion Laboratory, Pasadena, Calif., Mar. 15, 1966.
- Stelzried, C. T., Reid, M. S., and Nixon, D., *Precision Power Measurements of Spacecraft CW Signal With Microwave Noise Standards*, Technical Report 32-1066, Jet Propulsion Laboratory, Pasadena, Calif., Feb. 15, 1968.
- Stelzried, C. T., and Reid, M. S., *Precision Power Measurements of Spacecraft CW Signal Level With Microwave Noise Standards*, Technical Report 32-1070, Jet Propulsion Laboratory, Pasadena, Calif., reprinted from *IEEE Trans. Instrum. Measurement*, Vol. IM-15, No. 4, pp. 318-324, Dec. 1966.
- Stelzried, C. T., and Rusch, W. V. T., *Improved Determination of Atmospheric Opacity From Radio Astronomy Measurements*, Technical Report 32-1115, Jet Propulsion Laboratory, Pasadena, Calif., reprinted from *J. Geophys. Res.*, Vol. 72, No. 9, pp. 2445-2447, May 1, 1967.

- Stelzried, C. T., and Otoshi, T. Y., "Radiometric Evaluation of Antenna-Feed Component Losses," *IEEE Trans. Instrumen. Measurement*, Vol. IM-18, No. 3, pp. 172-183, Sept. 1969.
- Stelzried, C. T., "Precision Microwave Waveguide Loss Calibrations," *IEEE Trans. Instrum. Measurement*, Vol. IM-19, No. 1, pp. 23-25, Feb. 1970.
- Stelzried, C. T., *A Faraday Rotation Measurement of a 13-cm Signal in the Solar Corona*, Technical Report 32-1401, Jet Propulsion Laboratory, Pasadena, Calif., July 15, 1970.
- Stelzried, C. T., et al., "The Quasi-Stationary Coronal Magnetic Field and Electron Density as Determined From a Faraday Rotation Experiment," *Sol. Phys.*, Vol. 14, No. 2, pp. 440-456, Oct. 1970.
- Stelzried, C. T., "Operating Noise-Temperature Calibrations of Low-Noise Receiving Systems," *Microwave J.*, Vol. 14, No. 6, pp. 41-46, 48, June 1971.
- Stelzried, C. T., et al., "Transformation of Received Signal Polarization Angle to the Plane of the Ecliptic," *J. Space. Rock.*, Vol. 9, No. 2, pp. 69-70, Feb. 1972.
- System Capabilities and Development Schedule of the Deep Space Instrumentation Facility 1963-1967*, Technical Memorandum 33-83, Jet Propulsion Laboratory, Pasadena, Calif., Mar. 2, 1962.
- Tardani, P. A., *Madrid Site Selection Report*, Technical Memorandum 33-149, Jet Propulsion Laboratory, Pasadena, Calif., July 17, 1963.
- Tausworthe, R. C., *A Precision Planetary Range-Tracking Radar*, Technical Report 32-779, Jet Propulsion Laboratory, Pasadena, Calif., reprinted from *IEEE Trans. Space Electron. Telem.*, Vol. SET-11, No. 2, pp. 78-85, June 1965.
- Tausworthe, R. C., *Theory and Practical Design of Phase-Locked Receivers*, Technical Report 32-819, Vol. I, Jet Propulsion Laboratory, Pasadena, Calif., Feb. 15, 1966.
- Tausworthe, R., *Cycle Slipping in Phase-Locked Loops*, Technical Report 32-1127, Jet Propulsion Laboratory, Pasadena, Calif., reprinted from *IEEE Trans. Commun. Technol.*, Vol. COM-15, No. 3, pp. 417-421, June 1967.
- Tausworthe, R. C., Easterling, M. F., and Spear, A. J., *A High-Rate Telemetry System for the Mariner Mars 1969 Mission*, Technical Report 32-1354, Jet Propulsion Laboratory, Pasadena, Calif., Apr. 1, 1969.
- Tausworthe, R. C., *DSS Subsystem Implementation by Time-Shared Computer*, Technical Memorandum 33-420, Jet Propulsion Laboratory, Pasadena, Calif., Oct. 1, 1969.
- Tausworthe, R. C., "Convergence of Oscillator Spectral Estimators for Counted-Frequency Measurements," *IEEE Trans. Commun.*, Vol. COM-20, No. 2, pp. 213-217, Apr. 1972.
- Tausworthe, R. C., "Simplified Formula for Mean-Slip Time of Phase-Locked Loops With Steady-State Phase Error," *IEEE Trans. Commun.*, Vol. COM-20, No. 3, pp. 331-337, June 1972.
- Telecommunications Systems Design Techniques Handbook*, Technical Memorandum 33-571, edited by R. E. Edelson, Jet Propulsion Laboratory, Pasadena, Calif., July 15, 1972.
- Textor, G. P., Kelly, L. B., and Kelly, M., *Tracking and Data System Support for the Mariner Mars 1971 Mission: First Trajectory Correction Maneuver Through*

- Orbit Insertion*, Technical Memorandum 33-523, Vol. II, Jet Propulsion Laboratory, Pasadena, Calif., June 15, 1972.
- Thornton, J. H., Jr., *The Surveyor I and Surveyor II Flight Paths and Their Determination From Tracking Data*, Technical Report 32-1285, Jet Propulsion Laboratory, Pasadena, Calif., Aug. 1, 1968.
- Timor, U., "Equivalence of Time-Multiplexed and Frequency-Multiplexed Signals in Digital Communications," *IEEE Trans. Commun.*, Vol. COM-20, No. 3, pp. 435end438, June 1972.
- Titsworth, R. C., *Correlation Properties of Cyclic Sequences*, Technical Report 32-388, Jet Propulsion Laboratory, Pasadena, Calif., July 1, 1963.
- Titsworth, R. C., *Optimal Ranging Codes*, Technical Report 32-411, Jet Propulsion Laboratory, Pasadena, Calif., Apr. 15, 1963.
- "Tracking and Data Acquisition System for Mariner Missions," *Proceedings of the Seventh International Symposium on Space Technology and Science*, Tokyo, May 1967.
- Vegos, C. J., et al., *The Ranger IX Flight Path and Its Determination From Tracking Data*, Technical Report 32-767, Jet Propulsion Laboratory, Pasadena, Calif., Nov. 1, 1968.
- Victor, W. K., Titsworth, R. C., and Rechtin, E., *Telecommunication Aspects of a Manned Mars Mission*, Technical Report 32-501, Jet Propulsion Laboratory, Pasadena, Calif., Aug. 20, 1963.
- Winn, F. B., "Selenographic Location of Surveyor VI," in *Surveyor VI Mission Report: Part II. Science Results*, Technical Report 32-1262, Jet Propulsion Laboratory, Pasadena, Calif., Jan. 10, 1968.
- Winn, F. B., "Post Landing Tracking Data Analysis," in *Surveyor VII Mission Report: Part II. Science Results*, Technical Report 32-1264, Jet Propulsion Laboratory, Pasadena, Calif., Mar. 15, 1968.
- Winn, F. B., "Surveyor Post-Touchdown Analysis of Tracking Data," in *Surveyor Project Final Report: Part II. Science Results*, Technical Report 32-1265, Jet Propulsion Laboratory, Pasadena, Calif., June 15, 1968.
- Winn, F. B., *Surveyor Posttouchdown Analyses of Tracking Data*, NASA SP-184, National Aeronautics and Space Administration, Washington, D.C., p. 369.
- Wollenhaupt, W. R., *Tracking System Data Analysis Report, Ranger 4 Final Report*, Technical Report 32-523, Jet Propulsion Laboratory, Pasadena, Calif., Mar. 1, 1964.
- Wollenhaupt, W. R., et al., *The Ranger VII Flight Path and Its Determination From Tracking Data*, Technical Report 32-694, Jet Propulsion Laboratory, Pasadena, Calif., Dec. 15, 1964.